

Docetaxel uptake and modulation of P-gp-  
mediated docetaxel efflux by tyrosine kinase  
inhibitors in human lung carcinoma  
cell lines.

A thesis submitted for the degree of Ph.D.

by

Denis Collins B.Sc. Hons.

The research work described in this thesis was performed

under the supervision of

Prof. Martin Clynes and Dr. Robert O'Connor

National Institute for Cellular Biotechnology

Dublin City University

Ireland

*I hereby certify that this material, which I now submit for assessment on the programme of study leading to the award of Ph.D. is entirely my own work, that I have exercised reasonable care to ensure that the work is original, and does not to the best of my knowledge breach any law of copyright, and has not been taken from the work of others save and to the extent that such work has been cited and acknowledged within the text of my work.*

Signed: \_\_\_\_\_

ID No.: 51169185

Date: \_\_\_\_\_

## ***Abstract***

Treatment with the taxanes, docetaxel and paclitaxel, can result in the emergence of multi-drug resistance (MDR) mediated by P-gp (MDR-1, ABCB1), which is an effective cellular efflux pump for both agents. This thesis was undertaken to examine the contribution of drug transport mechanisms to chemotherapeutic drug resistance, focussing on docetaxel. Sensitive and resistant NSCLC cell lines were used to model docetaxel transport and examine the ability of three tyrosine kinase inhibitors (TKIs), gefitinib, erlotinib and lapatinib, to circumvent resistance to docetaxel, and other chemotherapeutic agents, arising from P-gp over-expression.

A HPLC – based method was initially employed to quantify docetaxel levels in cells. The very high taxane levels required rendered this method unreliable for prediction of pharmacologically relevant effects. A more sensitive radiolabel-based technique was then developed to examine lower, pharmacologically achievable concentrations (100-500 nM) of docetaxel. The radiolabel-based assay was then applied to examining docetaxel uptake in the DLKP and A549 NSCLC cell lines and docetaxel accumulation and efflux in the P-gp over-expressing A549-Taxol and DLKP-A cell lines.

Passive diffusion is believed to be the mechanism of uptake for docetaxel in most cancer cells due to its lipophilic characteristics. However, evidence was found for an energy-dependent docetaxel uptake mechanism in DLKP and a non-P-gp energy-dependent efflux mechanism in A549. The contribution of the OATP (organic anion transporting polypeptides) family of transporters to docetaxel uptake in A549 could not be discounted. The existence of transporter-mediated docetaxel uptake in NSCLC cells represents an important new factor in determining the sensitivity of cancer cells to docetaxel.

Studies on the TKIs revealed that lapatinib interacted with the ATPase function of P-gp in a manner distinct from gefitinib and erlotinib at clinically achievable concentrations. Lapatinib is most likely a slowly-transported substrate with high affinity for P-gp while erlotinib and gefitinib are most likely transported P-gp substrates. As a result of this, P-gp over-expression may contribute to erlotinib and gefitinib, but not lapatinib, resistance at pharmacological concentrations. Results suggest the three TKIs, particularly lapatinib, have potential clinical utility as MDR modulators capable of augmenting the cytotoxic activity of P-gp substrate chemotherapeutic agents against P-gp positive tumour cells. In addition, each TKI altered EGFR and P-gp protein expression levels.

## *Acknowledgements*

I wish to thank my supervisors Dr. Robert O'Connor and Prof. Martin Clynes, Dr. Finbarr O'Sullivan for his assistance with the laser confocal imaging and Dr. Norma O'Donovan for her assistance with the tyrosine kinase work. The lapatinib study was made possible by GSK and thrived with the support of Prof. John Crown.

From the coveted-key melodrama of the old building to the swipe access modernity of the new, I have had the privileged situation where my work colleagues could also be referred to as my friends. It is also safe to say at one point or another I have hassled everyone for assistance of some kind. Listing all the names would be difficult, and my fear is somebody would be forgotten. I'd like to offer a collective thank you to the all the present members of the Centre, to the many that have left over the years (hopefully not because of my beleaguering) and to friends in the X building, past and present.

There are a number of people that I will name as they were the ones that had to endure my presence most closely, sharing bench space (usually theirs), and basking in the stale smell of beer that accompanied me. On occasion. Alex, Norma, Brigid, Annette, Brendan, Rachel, Kieran and Aoife, there is no need to thank me for enriching your lives. I'm that kinda guy. As for the markers, they were only resting in my lab coat...

For giving me a door from which to keep the wolf, a large thank you with a side order of fries to Noel, Carol, Dave, Frank, Helen, Brigid and Niall. I realise how fortunate I have been to never be short of an offer of lodgings over the last six months. Thank you also to Chris Collins for the helicopter ride. And finally, as big a thank you as can possibly be mustered for my family who helped bear the load throughout the postgrad. This thesis is as much a testament to their support as it is to my endeavour.

The thesis is a record of my scientific enterprises in the N.I.C.B. Not recorded herein are the friendships, Cirque-onian rhythms (kudos Mark, Eric, Paul, Larry, Frank and Leah), relationships (kudos the ladies), Diggers nights (kudos Arthur G.), Sopranos nights (kudos Sean), cups of tea including chat AND digestive biscuit (kudos Cormac) and the highs and lows that this most unpredictable of journeys entailed. While you only get to behold the tome, I also get to keep the memories.

I had hoped to finish with a profound quote to provide inspiration while neatly summarising my Ph.D. experience. Unfortunately, I can't think of any and trawling the net for one that doesn't have any real meaning for me didn't seem right. Instead, inspired by my recent hobo-like existence, hairy dog-like appearance and betraying my televisual heritage while simultaneously heralding the death of intellectualism, I give you *The Littlest Hobo (Abridged)* by Terry Bush and John Crossen.

♪ There's a voice that keeps on calling me. Down the road is where I'll always be. Every stop I make, I'll make a new friend. Can't stay for long, just turn around and I'm gone again. Down this road, that never seems to end, where new adventure lies just around the bend. So if you wanna join me for a while, just grab your hat, come travel light, that's hobo style. There's a world that waiting to unfold, a brand new tale, no-one has ever told, we've journeyed far but you know it won't be long, we're almost there and we've paid our fare with the hobo song. Maybe tomorrow, I'll wanna settle down, until tomorrow, I'll just keep moving on. Maybe tomorrow I'll find what I call home, until tomorrow, you know I'm free to roam. ♪

*To My Family*

*Table of  
Contents*

<b>CHAPTER 1. INTRODUCTION</b>	<b>1</b>
<b>1.1 Lung cancer</b>	<b>2</b>
1.1.1 SCLC	2
1.1.2 NSCLC	2
1.1.3 SCLC treatment	3
1.1.4 NSCLC treatment	3
1.1.5 Chemotherapeutic agents	5
<b>1.2 The Taxanes</b>	<b>7</b>
1.2.1 Taxane mechanism of action	9
1.2.2 Taxane metabolism and pharmacokinetics	11
1.2.3 Taxane resistance	12
<b>1.3 Multi-drug resistance</b>	<b>18</b>
1.3.1 ABC superfamily	18
1.3.2 ABC proteins and MDR	19
1.3.3 ABC proteins associated with taxane resistance	20
1.3.4 Other ABC proteins involved in MDR	26
1.3.5 ABC protein expression in lung tissue	32
<b>1.4 Drug uptake mechanisms</b>	<b>33</b>
1.4.1 Taxane uptake mechanisms	33
1.4.2 SLCO family	34
1.4.3 SLC22 family	35
<b>1.5 EGFR inhibitors in lung cancer</b>	<b>37</b>
1.5.1 Epidermal growth factor receptor (c-ErbB) Family	37
1.5.2 EGFR signalling pathways	38
1.5.3 c-ErbB regulation	39
1.5.4 c-ErbB and cancer	40
1.5.5 Targetted c-ErbB therapies	41
1.5.6 TKIs and ABC transporters	44
<b>1.6 Aims of the thesis</b>	<b>46</b>
<b>CHAPTER 2. MATERIALS AND METHODS</b>	<b>47</b>
<b>2.1 Ultrapure Water</b>	<b>48</b>
<b>2.2 Glassware</b>	<b>48</b>
<b>2.3 Sterilisation Procedures</b>	<b>48</b>
<b>2.4 Preparation of cell culture media</b>	<b>48</b>
<b>2.5 Cells and Cell Culture</b>	<b>49</b>
2.5.1 Subculturing of cell lines	50
2.5.2 Assessment of cell number and viability	52
2.5.3 Cryopreservation of cells	52
2.5.4 Thawing of cryopreserved cells	53
2.5.5 Monitoring of sterility of cell culture solutions	53
2.5.6 Serum batch testing	53
<b>2.6 Mycoplasma analysis of cell lines</b>	<b>54</b>
2.6.1 Indirect staining procedure for <i>Mycoplasma</i> analysis	54
2.6.2 Direct culture procedure for <i>Mycoplasma</i> analysis	54

<b>2.7</b>	<b>Miniaturised <i>in vitro</i> proliferation assays</b>	<b>55</b>
2.7.1	<i>In-vitro</i> proliferation assay experimental procedure	55
2.7.2	Assessment of cell number - Acid Phosphatase assay	57
2.7.3	Assessment of cell number - XTT assay	57
2.7.4	Proliferation assays examining docetaxel accumulation assay conditions	58
2.7.5	Statistical Evaluation	58
<b>2.8</b>	<b>Protein Extraction and Quantification</b>	<b>59</b>
2.8.1	Protein Extraction	59
2.8.2	Protein Quantification	60
<b>2.9</b>	<b>Western Blotting</b>	<b>61</b>
2.9.1	Gel electrophoresis	61
2.9.2	EGFR	62
2.9.3	P-gp/MRP-1	62
2.9.4	Blotting protocol	63
2.9.5	Enhanced chemiluminescence detection	64
<b>2.10</b>	<b>Immunoprecipitation</b>	<b>64</b>
<b>2.11</b>	<b>Laser Scanning Confocal Microscopy (LSCM)</b>	<b>65</b>
<b>2.12</b>	<b>Time course treatments in A549-Taxol</b>	<b>66</b>
2.12.1	EGF treatments	66
2.12.2	TKI treatments	66
<b>2.13</b>	<b>HPLC-based taxane transport assays</b>	<b>67</b>
2.13.1	Taxane accumulation assay in adherent cell lines	67
2.13.2	Taxane accumulation profiles	67
2.13.3	Taxane efflux profiles	68
2.13.4	Taxane accumulation assays involving MDR modulators	68
2.13.5	Taxane accumulation assays in non-adherent cell lines	68
2.13.6	Taxane efflux assay in adherent cell lines	69
2.13.7	HPLC analysis of taxanes	69
2.13.8	HPLC extraction method for the taxanes	70
2.13.9	Preparation of taxane HPLC standards.	71
2.13.10	HPLC analysis of the taxanes	71
<b>2.14</b>	<b>HPLC-based epirubicin transport assays</b>	<b>72</b>
2.14.1	Epirubicin accumulation assays in adherent cell lines	72
2.14.2	Epirubicin efflux assays in adherent cell lines	72
2.14.3	Quantification of epirubicin by HPLC	73
2.14.4	Epirubicin extraction procedure	73
2.14.5	Preparation of epirubicin HPLC standards.	74
2.14.6	HPLC analysis of epirubicin.	75
2.14.7	HPLC data analysis	75
2.14.8	Quantification of epirubicin by mass spectrometry	76
<b>2.15</b>	<b><sup>14</sup>C docetaxel radiolabel assays</b>	<b>76</b>
2.15.1	Standard curve	76
2.15.2	Saturation assay	77
2.15.3	Serum accumulation assay	77
2.15.4	Accumulation assay	78
2.15.5	Time accumulation profile	78
2.15.6	Efflux profile	79
2.15.7	Temperature accumulation assay	79
<b>2.16</b>	<b>ELISAs</b>	<b>80</b>
2.16.1	EGFR	80
2.16.2	Her-2	81

<b>2.17</b>	<b>Determination of cellular ATP levels</b>	<b>83</b>
2.17.1	Reagents	83
2.17.2	Procedure	84
<b>2.18</b>	<b>ATPase Assays</b>	<b>85</b>
2.18.1	ATPase assay materials	86
2.18.2	ATPase assay stock solutions	87
2.18.3	ATPase assay mix	89
2.18.4	Composition of signal	90
2.18.5	ATPase assay controls	91
2.18.6	MDR-transporter ATPase activation assay procedure	94
2.18.7	MDR transporter ATPase inhibition assays	95
2.18.8	Calculation of the specific (sodium orthovanadate-sensitive) MDR transporter ATPase activities	96
2.18.9	Expected MDR transporter ATPase parameters	96

### **CHAPTER 3. HPLC- DETERMINED TAXANE ACCUMULATION AND EFFLUX IN MDR AND SENSITIVE HUMAN LUNG AND LEUKEMIC CELL LINES** **98**

<b>3.1</b>	<b>Introduction</b>	<b>99</b>
<b>3.2</b>	<b>Drug selection and P-gp expression</b>	<b>101</b>
<b>3.3</b>	<b>Optimisation of drug exposure for HPLC analysis</b>	<b>103</b>
<b>3.4</b>	<b>Effects of sulindac on docetaxel accumulation and efflux in the A549 cell line.</b>	<b>106</b>
<b>3.5</b>	<b>Effect of the P-gp inhibitor Elacridar (GF120918) on docetaxel accumulation in A549.</b>	<b>109</b>
<b>3.6</b>	<b>The effect of sodium azide on taxane transport in A549.</b>	<b>111</b>
<b>3.7</b>	<b>The effect of P-gp inhibitors on taxane transport in DLKP.</b>	<b>115</b>
<b>3.8</b>	<b>The effect of ATP inhibitors on docetaxel accumulation in DLKP.</b>	<b>120</b>
<b>3.9</b>	<b>Taxane accumulation and efflux in the multi-drug resistant cell line DLKP-A</b>	<b>122</b>
<b>3.10</b>	<b>The effect of ATP inhibitors on docetaxel transport in DLKP-A</b>	<b>129</b>
<b>3.11</b>	<b>Taxane accumulation in the docetaxel-selected cell line DLKP-TXT.</b>	<b>131</b>
<b>3.12</b>	<b>Taxane accumulation in HL-60 and HL-60 ADR</b>	<b>137</b>
<b>3.13</b>	<b>Summary of HPLC-based method for taxane measurement</b>	<b>141</b>

### **CHAPTER 4. ANALYSIS OF EPIRUBICIN TRANSPORT IN DLKP-A** **143**

<b>4.1</b>	<b>Laser scanning confocal microscopy imaging of epirubicin and paclitaxel.</b>	<b>144</b>
<b>4.2</b>	<b>Epirubicin accumulation and efflux in the multi-drug resistant cell line DLKP-A.</b>	<b>154</b>
<b>4.3</b>	<b>Summary</b>	<b>157</b>

<b>CHAPTER 5. DEVELOPMENT OF A RADIOLABELLED-BASED ASSAY FOR DETERMINATION OF DOCETAXEL ACCUMULATION AND EFFLUX</b>	<b>158</b>
5.1 Introduction	159
5.2 Optimisation of radiolabelled <sup>14</sup> C docetaxel transport assays	160
5.2.1 Scintillation Counter Efficiency	160
5.2.2 Influence of cell number	162
5.2.3 Influence of cell debris	164
5.2.4 Influence of drug adsorption onto plate wells	167
5.2.5 Influence of alterations in medium serum concentration	170
5.3 Comparison of radiolabelled assay and HPLC method for docetaxel measurement.	173
5.4 Summary	184
<b>CHAPTER 6. DOCETAXEL INFLUX IN THE HUMAN LUNG CANCER CELL LINES DLKP AND A549</b>	<b>185</b>
6.1 Introduction	186
6.2 Saturation	188
6.3 Temperature	193
6.4 ATP depletion	196
6.5 The effect of ATP depletion on docetaxel accumulation	201
6.6 OATP inhibitors	206
6.7 Summary	216
<b>CHAPTER 7. TKIS AS MODULATORS OF MULTI-DRUG RESISTANCE</b>	<b>217</b>
7.1 Introduction	218
7.2 Modulation of P-gp by TKIs	219
7.2.1 P-gp, EGFR and Her-2 status of the cell lines	219
7.2.2 Effects of TKIs on P-gp ATPase activity	221
7.2.3 TKI-related increase in docetaxel accumulation in the P-gp-positive DLKP-A cell line	223
7.2.4 Inhibition of docetaxel efflux from the P-gp-positive DLKP-A cell line	226
7.2.5 Increased epirubicin accumulation in the DLKP-A cell line	228
7.2.6 The implications of P-gp modulation by TKIs on cell survival	231
7.2.7 Combination proliferation assays	233
7.2.8 Effects of the P-gp substrate erlotinib and P-gp inhibitor lapatinib on docetaxel accumulation in A549-Taxol	236
7.3 The effects of TKI exposure on P-gp expression in A549-Taxol	238
7.4 The effects of TKIs on EGFR levels	243
7.5 The Effects of TKIs on MRP-1 and BCRP ATPase activity	250
7.6 Summary	255

<b>8.1</b>	<b>HPLC- determined taxane accumulation and efflux in sensitive and MDR human lung and leukemic cell lines</b>	<b>258</b>
8.1.1	Cell lines	258
8.1.2	Optimisation of HPLC timepoints	259
8.1.3	Docetaxel accumulation and efflux in A549	260
8.1.4	The Effects of ATP-depletion on docetaxel accumulation in A549	260
8.1.5	Docetaxel and paclitaxel accumulation in DLKP	261
8.1.6	Docetaxel and paclitaxel transport in DLKP-A	262
8.1.7	Taxane and verapamil proliferation assays in DLKP-A	263
8.1.8	Effect of ATP inhibitors on docetaxel transport in DLKP-A	264
8.1.9	Docetaxel and paclitaxel transport in DLKP-TXT	264
8.1.10	Docetaxel and paclitaxel transport in HL-60	265
8.1.11	Docetaxel and paclitaxel transport in HL-60 ADR	266
8.1.12	Assessment of the HPLC method for taxane quantification	266
<b>8.2</b>	<b>LSCM imaging of epirubicin</b>	<b>267</b>
8.2.1	LSCM imaging of epirubicin in DLKP	267
8.2.2	LSCM of epirubicin in DLKP-A	268
8.2.3	LSCM of epirubicin in DLKP-TXT	268
8.2.4	Laser confocal imaging of Oregon-green paclitaxel in DLKP and A549-Taxol	269
8.2.5	HPLC-based quantification of epirubicin in DLKP-A	269
<b>8.3</b>	<b>Development of a radiolabelled-based assay for determination of docetaxel accumulation and efflux</b>	<b>271</b>
8.3.1	Scintillation counter efficiency and seeding density	271
8.3.2	The presence of cell debris does not quench radioactivity signal	272
8.3.3	Drug adsorption has negligible effect on assay error	272
8.3.4	5% FCS has no effect on <sup>14</sup> C docetaxel accumulation	273
8.3.5	Choice of a standard concentration of <sup>14</sup> C docetaxel for use in DLKP-A efflux assays	273
8.3.6	Calculation of the mass of docetaxel in cells	274
<b>8.4</b>	<b>Comparison of accumulation assays using radiolabel and HPLC techniques</b>	<b>275</b>
8.4.1	Verapamil increased <sup>14</sup> C docetaxel accumulation in DLKP-A and DLKP-TXT	275
8.4.2	Comparison of the accumulation profiles of 100 nM <sup>14</sup> C docetaxel in A549 and A549-Taxol	276
8.4.3	The effects of high extracellular concentrations of docetaxel on efflux profiles in A549 and DLKP	276
8.4.4	Assessment of the radiolabel-based method for docetaxel quantification	278
<b>8.5</b>	<b>A docetaxel uptake mechanism in lung cancer</b>	<b>279</b>
8.5.1	Docetaxel influx in the human lung cancer cell lines DLKP and A549	279
8.5.2	Energy-dependent docetaxel transport	280
8.5.3	<sup>14</sup> C docetaxel accumulation is saturable in DLKP but not A549	280
8.5.4	<sup>14</sup> C docetaxel accumulation is temperature-dependent in A549 and DLKP	281
8.5.5	Depletion of ATP levels by sodium azide, 2-deoxyglucose and antimycin A in A549 and DLKP	282
8.5.6	ATP depletion reduced <sup>14</sup> C docetaxel accumulation in DLKP and increased <sup>14</sup> C docetaxel accumulation in A549	282
8.5.7	Possible docetaxel transport mechanisms in DLKP	283
8.5.8	OATP-mediated docetaxel transport in A549	286
8.5.9	Indocyanine green increases <sup>14</sup> C docetaxel accumulation in A549 and DLKP	287
8.5.10	T <sub>3</sub> and DHEAS increases <sup>14</sup> C docetaxel accumulation in A549	288
8.5.11	ATP-dependent docetaxel transporter in A549	289
8.5.12	Future investigation of cisplatin transport by SLC family members in A549 and DLKP	290
8.5.13	DMSO decreases <sup>14</sup> C docetaxel accumulation	290
<b>8.6</b>	<b>Modulation of P-gp-mediated docetaxel transport</b>	<b>291</b>
8.6.1	Distinct manner of lapatinib's interaction with P-gp	291
8.6.2	Potency of lapatinib in docetaxel combination proliferation and transport assays	292
8.6.3	Lapatinib potentiates epirubicin toxicity and accumulation through inhibition of P-gp	293
8.6.4	IC <sub>50</sub> Determinations in DLKP, DLKP-A, A549 and A549-Taxol	293
8.6.5	Implications of combination proliferation assays	294

8.6.6	Docetaxel accumulation in A549-Taxol	295
8.6.7	Negative effects of TKI P-gp inhibitor	295
8.6.8	Applications of TKIs in combination chemotherapy regimen and as P-gp modulators in the clinic	296
<b>8.7</b>	<b>Possible link between EGFR signalling and P-gp expression</b>	<b>297</b>
8.7.1	EGF treatment reduced EGFR protein levels	299
8.7.2	TKIs increase EGFR levels in A549-Taxol	299
8.7.3	Comparison of ELISAs utilising detection antibodies to intercellular and extracellular EGFR epitopes	301
8.7.4	c-ErbB receptors and P-gp: A more direct association?	301
<b>8.8</b>	<b>TKIs and BCRP and MRP-1</b>	<b>303</b>
8.8.1	BCRP ATPase activity as measured using SB-MXR-M-ATPase membrane preparations	304
8.8.2	Gefitinib, erlotinib and lapatinib stimulate BCRP ATPase activity at low, pharmacologically-relevant, levels	305
8.8.3	Gefitinib, erlotinib and lapatinib have a minor stimulatory effect on MRP-1 ATPase activity	307
8.8.4	The MRP-1 substrate vincristine does not stimulate MRP-1 ATPase activity	308
8.8.5	Sulindac is an activator but not an inhibitor of MRP-1 ATPase activity	308
8.8.6	The possibility of TKI influx mechanisms	309
<b>CHAPTER 9. CONCLUSIONS</b>		<b>310</b>
<b>CHAPTER 10. FUTURE WORK</b>		<b>315</b>
<b>10.1 Docetaxel transport in lung cancer cell lines</b>		<b>316</b>
<b>10.2 Tyrosine kinase inhibitors</b>		<b>317</b>
<b>APPENDIX A</b>		<b>319</b>
<b>APPENDIX B</b>		<b>329</b>
<b>Epirubicin LSCM studies</b>		<b>330</b>
<b>Oregon-green paclitaxel LSCM studies</b>		<b>331</b>
<b>ABBREVIATIONS</b>		<b>332</b>
<b>REFERENCES</b>		<b>334</b>

## ***Chapter 1. Introduction***

## **1.1 Lung cancer**

Lung cancer is the most frequent occurring malignancy in western countries with an incidence of 60 in 100,000 [1]. Smoking is responsible for 80 to 90% of lung cancers. Small cell lung cancer (SCLC) and non-small cell lung cancer (NSCLC) are the two major types of lung cancer. Classification is made based on histological features of the tumour cells. In Europe, an overview of trends since 1960 has shown there has been a levelling off or general fall of lung cancer mortality in men in the last decade excluding Portugal and Romania, while there has been a general increase in cancer mortality in women except in Ireland, the U.K., Denmark and Iceland. The Russian Federation is the only country to register an overall decrease in female lung cancer mortality [2].

### **1.1.1 SCLC**

Small cell lung cancer is an aggressive disease with a median survival of 3 months if left untreated. The proportion of lung cancers that are of the small cell type has decreased in the United States to 13.8% from 17.4% between 1986 and 1998[3]. Tumour extent is described as limited-stage disease (LD) or extensive stage disease (ED) with both stages responding to treatment. LD median survival is 14-20 months with a 20-40% 2-year survival and a 10% 5-year survival rate. ED median survival is 7-10 months and 2-year survival is rare [2]. SCLC has a significant response to chemotherapeutic agents and radiation. 80-90% of LD patients respond to combination chemotherapy with or without radiation [4].

### **1.1.2 NSCLC**

Non-small cell lung cancer accounts for approximately 80% of lung cancers. NSCLC is categorised according to the TNM system (T- Primary tumour size and location, N- regional lymph node invasion status, M- presence of metastases). Depending on its TNM score, the lung cancer is then categorised into stages, Stage I (A or B), Stage II

(A or B), Stage III (A or B) or Stage IV (Table 1) [5]. Patients presenting with early stage, localised disease are considered curatively resectable even though the five year survival rate is 61% for stage IA and 24% for stage IB [1]. The majority of patients therefore suffer a relapse. Unfortunately, 65% present with inoperable stage IIIB or stage IV disease, and the average age is 68 years old, presenting greater problems when trying to minimise treatment related symptoms [6].

The disease stage of NSCLC is of utmost importance in the consideration of treatment, with surgically resectable, locally advanced and metastatic tumours usually considered separately [7].

### **1.1.3 SCLC treatment**

The standard combination therapies for SCLC treatment have been cyclophosphamide- doxorubicin vincristine (CAV), cyclophosphamide, doxorubicin and etoposide (CDE), ifosphamide, carboplatin and etoposide with or without vincristine (ICE±V) and, the increasingly used, and favoured platinum (cisplatin/carboplatin) and etoposide (PE) combinations [2]. Cisplatin-irinotecan is a promising new combination in SCLC treatment [8].

Paclitaxel has been used in a number of trials. A paclitaxel-etoposide-carboplatin (TEC) regimen tested against carboplatin-etoposide-vincristine (CEV) in LD and ED-SCLC patients resulted in a one month increase in median survival for LD-SCLC patients only [9]. Two other trials testing paclitaxel-etoposide-cisplatin (TEP) against platinum (cis or carboplatin)-etoposide (PE) and failed to show enough advantages of this paclitaxel regimen over the existing PE standard to favour its adoption [10].

### **1.1.4 NSCLC treatment**

The platinum drugs, particularly cisplatin, are a mainstay of the chemotherapeutic regimen for NSCLC. Surgery is the best option for (medically operable) early stage NSCLC. The high incidence of recurrence following resection may be attributable to undetectable metastases at diagnosis. This theory has led to numerous trials involving adjuvant chemotherapy and radiotherapy treatments. The efficacy of postoperative

radiotherapy (PORT) in early stage disease is controversial but may still have potential with improved delivery systems [11]. Combined sequential chemoradiotherapy (CTRTR) is also being looked at as an adjuvant therapy, a neo-adjuvant therapy (RT following CT and surgery) and in inoperable advanced Stage III disease [12]. Stage IIIA is generally considered to be the highest stage for which surgery is employed. Unresectable Stage III cancer has traditionally been treated with radiation alone but recently the bi-modal approach of CTRTR has been adopted [13]. Surgical resection and adjuvant platinum-containing chemotherapy has become the optimal treatment strategy for early stage NSCLC [14]. Paclitaxel and carboplatin, and vinorelbine (vinca alkaloid) and cisplatin are two combinations that have shown much promise in this setting [15]. There are a myriad of used, tested and proposed regimens for treating advanced NSCLC. They differ in CT agents combined (although there is constant platinum drug involvement) and use of radiotherapy. Timing options include induction chemotherapy (CT before surgery), adjuvant therapies and sequential or concurrent therapies (adjuvant or neo-adjuvant). Recent and ongoing clinical trials involving the taxanes are creating a significant role for this class of drug in NSCLC treatment. Chu *et al.*, give a comprehensive overview of the taxanes as first line therapy in NSCLC, including a comprehensive review of the major clinical trials and practice guidelines [16].

Recommendations include:

- Paclitaxel and docetaxel combined with cisplatin as one of a number of first line chemotherapy treatment options in NSCLC patients with good performance status
- Carboplatin can be combined with a taxane if cisplatin is not an option.
- A taxane-gemcitabine may be considered in patients with contraindication to both cisplatin and carboplatin.
- Single agent taxane treatment may be considered if combination chemotherapy is deemed inappropriate.

In a study of 52 patients with poor prognosis Stage IIIA N2 NSCLC, the authors concluded that the combination of paclitaxel, carboplatin and gemcitabine was a safe and active regimen [17].

## **1.1.5 Chemotherapeutic agents**

A wide variety of chemotherapeutic agents are used in the treatment of malignancies. They vary in their cellular targets, mechanism of action and types of cancer they are used to treat. The major compounds are classified in Table 1.1.5.1, along with some of the major-ABC resistance proteins they are associated with. The key for the diseases that the chemotherapeutic agents are used to treat listed in Table 1.1.5 is as follows:

**ALL/CLL**- Acute/Chronic lymphocytic leukaemia

**AGL**- acute granulocytic carcinoma

**BC**- breast cancer

**BLC**- bladder cancer

**CC**- colon cancer

**CVC**- cervical cancer

**GC**- genitourinary cancer

**HD**-Hodgkin's disease

**nHD**- non Hodgkin's disease

**HN**- head and neck cancer

**KS**- Kaposi's sarcoma

**LC**- lung cancer

**MM**- multiple myeloma

**NB**- neuroblastoma

**OC**- ovarian cancer

**OS**- osteogenic sarcoma

**PC**- pancreatic cancer

**SC**- stomach cancer

**TC**- testicular cancer

**THC**- thyroid cancer.

**Table 1.1.5.1** Neoplasms are carcinomas unless otherwise stated. Compiled from [18], [19], [20], [21], [22], [23], [24], [25], [26], [27], [28] and [29].

Class	Type of agent	Name	Mechanism of action	Disease	Associated MDR transporter(s)
Alkylating Agents	Nitrogen Mustard	Cyclophosphamide Ifosfamide	DNA cross linkage	ALL, CLL, HD, nHD, MM, BC, OC, LC, NB, CVC, TC	<i>MRP-2, MRP-4</i>
		Melphalan	DNA cross linkage	MM, BC, OC	
Antimetabolites	Folic Acid Analogues	Methotrexate	Folate synthesis inhibition	ALL, BC, HN, LC, OS	<i>MRP-3, MRP-4, MRP-5</i>
	Pyrimidine Analogues	Fluorouracil (5-Fu)	DNA destabilisation	BC, CC, SC, PC, OC, HN	<i>MRP-5, MRP-8</i>
		Gemcitabine	DNA destabilisation	PC, OC	<i>MRP-5</i>
Natural Products	Vinca Alkaloids	Vinblastine	Microtubulintargetted antimitotic	HD, nHD, BC, TC	<i>P-gp, MRP-1, MRP-3</i>
		Vincristine	Microtubin-targetted antimitotic	ALL, NB, HD, nHD, LC	<i>P-gp, MRP-1, MRP-2, MRP-3</i>
	Taxanes	Docetaxel Paclitaxel	Microtubule-targetted antimitotics	OC, BC, LC, HN	<i>P-gp, MRP-2, MRP-7</i>
	Epipodophyllotoxins	Etoposide Teniposide	Topoisomerase II inhibitors	TC, LC, BC, HD, nHD, AGL, KS	<i>P-gp, BCRP, MRP-1, MRP-2, MRP-3</i>
	Camptothecins	Topotecan Irinotecan	Topoisomerase I inhibitors	OC, LC, CC	<i>BCRP, P-gp (T), MRP-1 (I),</i>
	Antibiotics	Daunorubicin	Topoisomerase II inhibitor	AGL, ALL	<i>P-gp, BCRP, MRP-1</i>
		Doxorubicin	Topoisomerase II inhibitor	OS, HD, nHD, AL, BC, GC, THC, LC, SC, NB	<i>P-gp, BCRP, MRP-1</i>
		Epirubicin	Topoisomerase II inhibitor	BC, OC, SC, LC	<i>P-gp, BCRP, MRP-1</i>
Miscellaneous	Platinum Complexes	Carboplatin Cisplatin	DNA cross linkage	TC, OC, BLC, HN, LC, THC, CVC, NB, OS	<i>MRP-2 (Cis), ATP7A, ATP7B</i>
	<i>Anthracenedione</i>	<i>Mitoxantrone</i>	<i>Topoisomerase II inhibitor</i>	<i>AGL, BC, PC</i>	<i>P-gp, BCRP</i>

## 1.2 The Taxanes

Docetaxel and paclitaxel are the most prominent members of the taxane family. Paclitaxel was originally isolated from the bark of the Pacific Yew (*Taxus brevifolia*) while docetaxel is derived from the European Yew (*Taxus baccata*). Both compounds target the microtubules, components of the cell cytoskeleton and essential to the production of the mitotic spindle. Treatment with taxanes results in stabilisation of the microtubules leading to cell cycle arrest in the G2/M phase [30].

Both paclitaxel and docetaxel are widely used in the treatment of ovarian and breast carcinomas and are being adopted as standard therapies for lung, digestive and prostate cancers. Other solid tumours that these drugs have been effective in treating include carcinomas of the head and neck and bladder.

Docetaxel and paclitaxel are similar in structure (Figure 1.2.1), but do have noticeable pharmacological differences. Gligorov and Lotz [31], summarise the major differences.

Docetaxel:

- Exhibits greater uptake into, and slower efflux from, tumour cells (P388, murine leukemia cell line).
- Exhibits greater affinity to the beta-tubulin subunit of microtubules.
- Targets centrosome organisation.
- Acts on cells in the S/G2/M stages of the cell cycle.
- Demonstrates linear pharmacokinetics and no cardiotoxic effects in combination with anthracyclines.

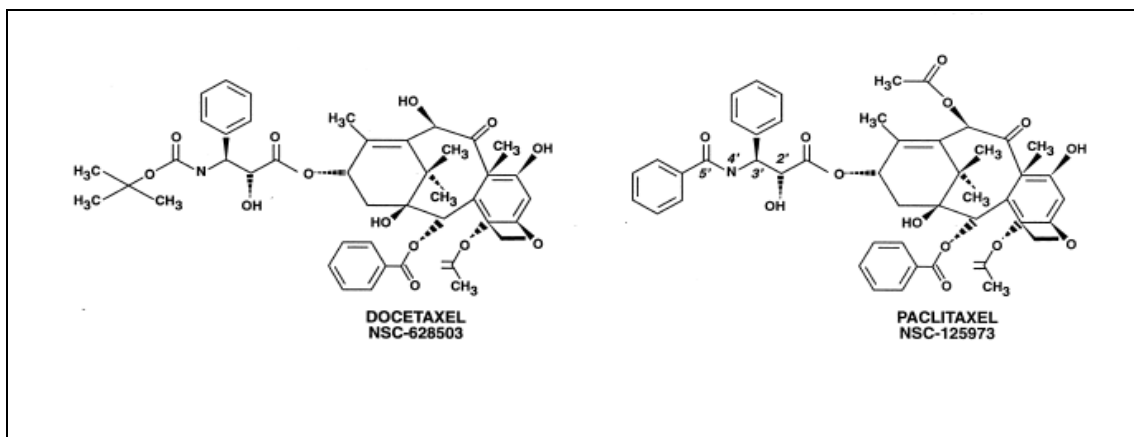
Paclitaxel:

- Targets the mitotic spindle.
- Acts on cells in the G2/M phase of the cell cycle.
- Demonstrates non-linear pharmacokinetics and enhanced cardiotoxicity, especially in combination with the anthracyclines.

The slower efflux of docetaxel could be associated with its greater affinity for beta-tubulin. This affinity also leads to higher intra-cellular concentrations contributing to docetaxel's greater cytotoxicity. There is no definitive evidence explaining the greater uptake of docetaxel in P388 murine leukaemia cells. The ability of the taxanes to arrest cells in the G2/M phase is exploited clinically. This is the cell cycle stage that is most sensitive to radiation. Docetaxel has been used as a radiosensitiser in the clinic and incidentally, the same study also reported anti-tumour immune stimulatory activity of docetaxel, another positive aspect of the use of this drug [32].

Both taxanes cause Bcl-2 phosphorylation leading to apoptosis but the concentration of docetaxel needed to cause apoptosis through Bcl-2 is 100 times less than paclitaxel [33]. Bcl-2 is an anti-apoptotic protein over-expressed in a number of tumours. Paclitaxel increases Raf 1, a serine/threonine protein kinase involved in the MAPK pathway and Bcl-x, leading to decreased levels of Bcl-2 [34].

**Figure 1.2.1** Docetaxel and paclitaxel structure [30]



Given the advantages of docetaxel over paclitaxel listed earlier in this section, it would be assumed that docetaxel is the more potent anti-cancer drug. A head to head study between paclitaxel and docetaxel in metastatic breast cancer did prove that docetaxel was superior to paclitaxel in terms of median overall survival (15.4 vs. 12.7 months), median time to progression (5.7 months v 3.6 months and overall response rate (32% vs. 25%) [35]. Although the incidence of treatment-related hematologic and nonhematologic toxicities was greater for docetaxel than for paclitaxel, the quality-of-life scores were not statistically different between treatment groups over time [35].

The clinical use of docetaxel is more prevalent in Europe than in the U.S., probably related to the geographical location of the development of each drug (docetaxel in Europe, paclitaxel in the U.S.) and the earlier approval of paclitaxel in cancer treatment. Pre-clinical studies of paclitaxel *in vitro* also heavily outway those involving docetaxel, also most likely a function of the aforementioned reasons. The search for factors, such as uptake mechanisms, that would influence docetaxel sensitivity and/or resistance in tumour cells is a major area of study. The existence of such factors and would have important implications for the treatment of cancers like NSCLC with docetaxel.

### **1.2.1 Taxane mechanism of action**

The taxanes are microtubule-interfering agents. Pellegrini and Budman provide a general overview of tubulin dynamics [36]. Tubulin molecules are made up of a heterodimer consisting of alpha- and beta-tubulin subunits. The subunits are arranged head to tail as are the molecules when they join together to form protofilaments. Each microtubule consists of 12 or 13 protofilaments aligned in parallel with the same polarity. There are at least 6 alpha- and beta-tubulin isotypes, differing in their intracellular localisation.

Microtubules have a plus (+) end where there tends to be rapid tubulin assembly and a minus (-) end with slow assembly or even disassembly. The minus end is often anchored at the microtubule-organising centres (MTOCs) with the plus end free in the cytoplasm. GTP and magnesium are required for assembly. Microtubules are continually in a state of dynamic instability, both ends having the ability to switch spontaneously from a growing to a shortening state, dependent on a cycle of GTP hydrolysis and exchange.

Microtubule associated proteins (MAPs) modulate the dynamics at the end of the microtubules. Stabilising MAPs include Tau, MAP1, MAP2, MAP4 and XMAP215 while stathmin, XKCM1, XKIF2 and katanin are regulatory molecules that favour disassembly [36]. Some of these proteins are targets for microtubule interfering agents and may be potential targets for drugs in sensitive or resistant cancers. MAP4, for instance, is phosphorylated by paclitaxel leading to loss of tubulin binding and altered

tubulin function [37]. Paclitaxel resistant cells do not generate phosphorylated MAP4 in response to the drug.

Concentrations of GTP (promotes assembly) and  $\text{Ca}^{2+}$  (inhibits assembly) are other factors that influence the degree of tubulin polymerisation [38].

Docetaxel and paclitaxel share a mutual binding site on the beta tubulin subunit [39]. Docetaxel has a higher affinity for this site and is a more potent tubulin assembly promoter and tubulin stabiliser than paclitaxel [40]. The resulting mitotic arrest triggers the mitotic spindle checkpoint, that induces the mitochondrial permeability transition, releasing pro-death molecules into the cytosol resulting in caspase-dependent apoptosis [38].

As with any other class of drugs, research is ongoing into improving the efficacy of the existing members of the taxane family and producing new more efficacious analogues.

New formulations of paclitaxel and docetaxel are under development to improve delivery, pharmacokinetic properties and reduce drug resistance. Abraxane is paclitaxel formulated as an albumin-bound nanoparticle. This eliminates the cytotoxic solubiliser cremophor EL used in Taxol® improving paclitaxel activity [41]. A formulation of paclitaxel encapsulated in cationic liposomes, to overcome transport associated drug resistance, is now in clinical trials [42]. EGF-conjugated paclitaxel has been generated to provide selectivity for EGFR-expressing tumours is still at the development stage [42]. Enhancement of docetaxel toxicity towards tumour vasculature is being pursued by combination with a monoclonal antibody (3G4). The combination was no more harmful than docetaxel alone and has demonstrated a superior activity in mice bearing orthotopic MDA-MB-435 human breast tumours [43].

BMS-188797 is a new taxane under development. It differs from paclitaxel at the C4 side chain only but it is more active in pre-clinical tumour models. It is now undergoing clinical development [44]. TL-130 is another taxane analogue that was reported to have activity against P-gp-over-expressing cell lines and those containing beta-tubulin mutations [45].

## 1.2.2 Taxane metabolism and pharmacokinetics

The taxanes undergo hepatic oxidative metabolism by the cytochrome P450 family. The majority of the metabolites are excreted in the bile with only 5% excreted renally. Docetaxel is metabolised by the CYP3A4 and CYP3A5 isoenzymes to hydroxydocetaxel and three other minor metabolites. All metabolites are less active than docetaxel [46]. CYP2C8 is the main enzyme involved in metabolising paclitaxel, producing 6- $\alpha$ -hydroxy-paclitaxel. CYP2C8 also oxidises troglitazone and arachidonic acid [47]. Production of the minor secondary metabolite 3-*para*-hydroxyphenyl-paclitaxel is by CYP3A4. Both species can be metabolised further to the dihydroxyl product 6- $\alpha$ -hydroxyl-3-*para*-hydroxyphenyl paclitaxel. The paclitaxel metabolites are less potent than the parent compound, in the case of 6- $\alpha$  hydroxyl paclitaxel 30 times less so [46].

The taxanes are insoluble in aqueous solution. Paclitaxel is formulated in 50% alcohol and 50% cremophor EL while docetaxel is formulated in polysorbate 80 to improve solubility. The drugs are diluted in saline or 5% dextrose-saline for administration.

Docetaxel and paclitaxel are highly bound by plasma proteins (95% paclitaxel, > 95% docetaxel in the bloodstream). The pharmacokinetics of paclitaxel are more complicated than that of docetaxel. Its non-linear disposition and saturable distribution means that dose changes can lead to disproportionate toxicity duration and severity [30]. This leads to difficulties defining the optimal delivery schedule for monotherapy and combinations.

Cremophor EL may contribute to the non-linear kinetics [48]. In contrast, the linear kinetics of docetaxel makes for easier dose optimisation. Toxicity is proportionate to the dose changes and its clearance rate is relatively constant [30].

### 1.2.3 Taxane resistance

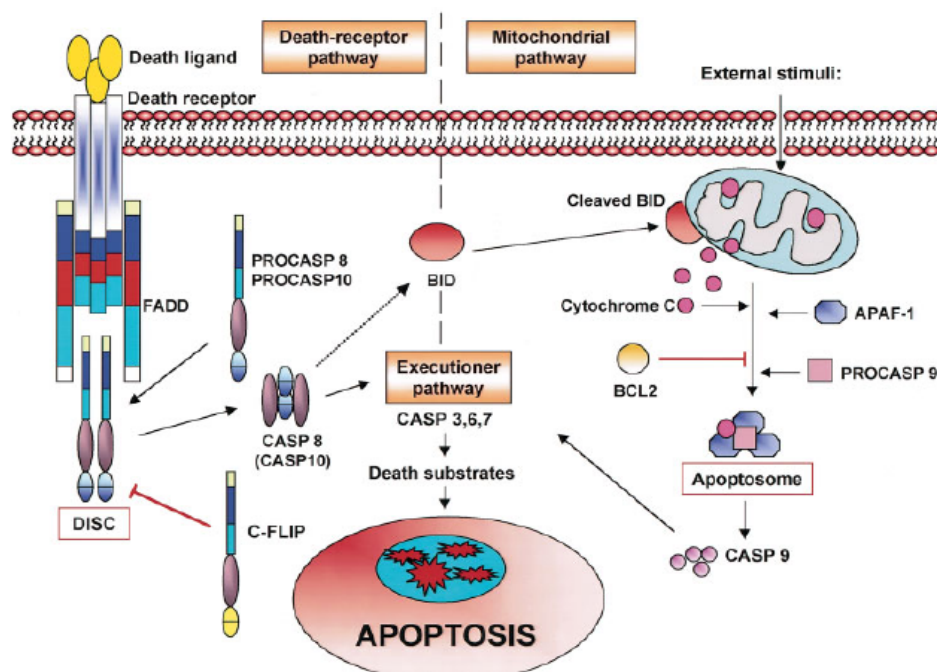
Inherent or acquired, taxane resistance has major clinical consequences. Extensive research has been undertaken in the area and many molecules (and pathways) have been implicated but much of our knowledge remains incomplete. The main contributors to taxane resistance are:

- 1) Changes in regulation of the apoptosis related Bcl-2 family.
- 2) Tubulin mutations.
- 3) Differential expression of tubulin isotypes.
- 4) Changes in other cellular pathways.
- 5) Increased drug efflux by membrane transporters.

#### 1.2.3.1 Apoptosis and taxane resistance

One of the major characteristics of all resistant cells is their ability to avoid apoptosis. A number of apoptosis-related proteins have been examined as potential mediators of taxane resistance. There are two main pathways to apoptosis, extrinsic and mitochondrial. Figure 1.2.3.1.1 gives a basic graphical representation of the two pathways.

**Figure 1.2.3.1.1** Graphical representation of apoptosis pathways. taken from [49].



Death ligands, such as Apo-2L/TRAIL, trigger the extrinsic pathway by binding the cell membrane death receptors DR4 and DR5. This results in the recruitment and assembly of FADD and caspase 8 into a death inducing signalling complex (DISC). Caspase 8 is processed and activated and induces downstream caspases and apoptosis directly or by recruitment of mitochondria related factors[38]. Active caspase 8 cleaves p22BID producing the pro-apoptotic p15 tBID that targets the mitochondria, binding proapoptotic Bax or Bak to trigger mitochondrial loss of prodeath molecules, also known as the mitochondrial permeability transition [38].

Mitotic arrest caused by the taxanes also leads to mitochondrial permeability transition. During this process, the mitochondria secrete pro-death molecules like cytochrome (cyt) c, SMAC, Omi/HtrA2, apoptosis-inducing factor (AIF) and endonuclease G. The released cyt c and dATP bind to Apaf-1 causing its multimerisation. This allows the recruitment of procaspase 9 and procaspase 3 and the processing and activation of caspases 9 and 3 [38]. The Apaf-1/Pro-caspase 9/Pro-caspase 3 complex is termed the “apoptosome”.

Loss of Apaf-1 expression in Apaf-1  $-/-$  mouse embryonic fibroblasts has been shown to confer resistance to paclitaxel- (and etoposide-) induced resistance while ectopic over-expression of Apaf-1 sensitised HL-60 cells to paclitaxel [50].

### ***Bcl-2 family***

Many other apoptosis-related proteins have been shown to have a part to play in taxane resistance. The Bcl-2 family has become a much studied therapeutic target in recent times. The anti-apoptotic Bcl-2 is over-expressed in 70% of breast cancers, 90% of colo-rectal adenocarcinomas and in many other cancers [51]. In the clinic, Bcl-2 expression has correlated with improved response to docetaxel and improved survival [52], [53]. In the oestrogen receptor-expressing breast cancer cell line, MCF-7, Bcl-2 levels were increased after exposure to oestrogen, conferring resistance to paclitaxel-induced apoptosis [54]. An increase of the Bcl-2 to pro-apoptotic Bax ratio was found but there was no increase in the anti-apoptotic Bcl-xL or levels of the drug transport pump P-gp (P-gp, Section 1.3.2.1). Increased Bcl-2 and Bcl-xL levels were also found in paclitaxel-and vincristine- selected HL-60 leukemia cells in addition to P-gp [55].

High expression levels of the pro-apoptotic protein Bim, correlated with susceptibility to paclitaxel-induced apoptosis in a panel of NSCLC cell lines [56]. SiRNA knockdown of Bim has conferred taxane resistance to breast cancer cell lines [38]. This would suggest that down-regulation of Bim could be a factor in NSCLC taxane resistance.

### ***Inhibitors of apoptosis (IAP) family***

The inhibitors of apoptosis (IAP) family include XIAP, cIAP1, cIAP2 and survivin. These proteins inhibit caspase processing and proteolytic activity [38].

Paclitaxel induces apoptosis through down-regulation of XIAP (X-linked inhibitor of apoptosis) and Bcl-2 phosphorylation in NSCLC H460 cells [57]. Inhibition of MEK1/2 potentiates this effect. Docetaxel resistance in epithelial ovarian cancer cells is XIAP-dependent and reversible by phenoxodiol [58]. XIAP is the most potent member of the IAP family considering its ability to suppress apoptosis and inhibit caspases.

Survivin is over-expressed in most human cancers but is not expressed in normal, terminally differentiated adult tissues [59]. Over-expression of survivin inhibits apoptosis and increased survivin levels have been linked to paclitaxel resistance in ovarian cancer cells *in vitro* and in the clinic [60]. Flavopiridol inhibits multiple cyclin dependent kinases including cyclin B-cdk1. This prevents the phosphorylation and accumulation of survivin, enhancing apoptosis. Flavopiridol is in clinical trials combined with the taxanes for treatment of late stage NSCLC [61]. Survivin is of interest in taxane resistance as there is a pronounced upregulation in expression at the G2/M transition of the cell cycle and it forms complexes with centromeres [62].

### ***p53***

p53 is a tumour suppressor protein that acts as a major defence against cancer but has been found to be mutated in 50% of all human cancers [63]. Patients with p53 mutant cancers respond to paclitaxel treatment as well as patients with wild type p53 in NSCLC [64]. Complete loss of p53 function has led to paclitaxel sensitisation in fibroblasts and cisplatin-resistant and -sensitive ovarian cancer cell lines [64], [65]. A

number of indirect explanations have been put forward. Cells with non-functional or mutated p53 no longer have the G1 checkpoint and accumulate in the G2/M phase, a target of mitotic arrest by the taxanes. p21<sup>WAF1/CIP1</sup> which facilitates exit from mitotic arrest is up-regulated by p53. Cells left in mitotic arrest undergo apoptosis. Microtubule associated protein 4 (MAP4), essential for microtubule dynamics is down-regulated by activation of wild-type p53.

MAP4 is down-regulated by activation of wild type p53 [66]. In the absence of functional p53, high levels of MAP4 stabilise microtubules, sensitising cells to paclitaxel. In paclitaxel-resistant A549 cancer cells (found to contain an alpha-tubulin mutation), the stabilising function of MAP4 is inhibited by phosphorylation while the levels of active non-phosphorylated stathmin are increased [67].

### ***1.2.3.2 Tubulin mutations***

Mutations in beta-tubulin resulting in resistance to paclitaxel and decreased microtubule assembly have been described in paclitaxel resistant ovarian cell lines [68]. These mutations cause resistance through altering microtubule dynamics, binding of MAP and motor proteins, rather than through inactivation of the taxane binding site. Beta-tubulin mutations have correlated with poor paclitaxel response and prognosis in stage III and IV NSCLC patients [69].

An increase in microtubule dynamics has been shown to confer paclitaxel resistance to A549 cells selected in paclitaxel. Microtubule dynamics and instability increased with withdrawal of low levels of paclitaxel, blocking A549 cells at the metaphase/anaphase transition [70].

Post-translational modifications to the C-terminal of alpha- and beta- tubulins can also affect binding of structural and motor MAPs including tau, MAP2 and kinesin. The ability of these proteins to interact with the microtubule skeleton *in vitro* is regulated by the levels of polyglutamylation of the alpha- and beta-tubulins [71].

### ***1.2.3.3 Tubulin isotype expression***

Alterations to beta-tubulin isotypes have been found in docetaxel resistant oestrogen-receptor-positive MCF-7 and oestrogen-receptor negative MDA-MB-231 breast cancer cell lines [72]. The MCF-7 docetaxel-resistant cell line exhibited an increase in protein expression of class I, II, II and IV beta-tubulins but there was a different pattern in the MDA-MB-231 docetaxel resistant cells. Only class IV beta tubulin protein levels were increased with class I, II, and III isotype expressions decreasing [72]. Once the IVa and IVb isotypes could be distinguished using RT-PCR, experiments revealed that it was class IVb beta-tubulin not class IVa beta-tubulin, that increased significantly in the docetaxel resistant cells [72].

Paclitaxel-resistant A549 cells showed mRNA increases in beta-tubulin isotypes III and IVa while paclitaxel-resistant ovarian tumour samples showed mRNA increases in isotypes I, III, and IVa [73]. Types III and IVa were barely detectable at the mRNA level in the parent A549 cell lines. A 40-50% downregulation of class III beta tubulin in the paclitaxel resistant A549-T24 cell line was achieved by antisense oligonucleotide treatment and this was associated with a 39% increase in sensitivity to paclitaxel [74]. Two other paclitaxel-selected cell lines, NCIH460 and H69/Txl showed protein increases in alpha-tubulin and actetylated alpha-tubulin respectively [71]. High expression of class III tubulin has been associated with poor prognosis in NSCLC patients receiving a taxane-based therapy [75].

### ***1.2.3.4 Cell pathways associated with taxane resistance***

A number of cell signalling pathway factors continue to emerge in relation to taxane action and resistance.

The MAPKs are a family of serine-threonine kinases activated by diverse stimuli. The three major types are ERK1/2 (extracellular signal-regulated kinases 1/2), the c-JNKs and the p38 kinase [38]. Paclitaxel induces ERK1/2 activities and the downstream transcription factor ELK1. This shows cytotoxic benefit when paclitaxel is combined

with a MAPK kinase inhibitor, especially in tumour cells expressing high levels of Erk1/2 [76].

JNK is activated by paclitaxel in cancer cells through the activation of Ras and/or ASK1 and its involvement in Bcl-2 phosphorylation has been observed [77].

Inhibition of the transcription factor NF-kappaB (by parthenolide) [78] and the heat shock protein, Hsp-90, has been found to sensitise breast cancer cells to paclitaxel [79]. The inhibition of Hsp-90 by LAQ824 also lead to down-regulation of c-Raf, Akt and Her-2. NF-kappaB has been shown to activate MDR1, a well established taxane membrane transporter [80] and regulates expression of the taxane resistance associated proteins, MMP9, Survivin, XIAP, Bcl-2 and COX-2 among others [81]. Constitutively active PI3K/Akt pathway signalling is described in a number of malignancies and has been linked to the multi-drug resistant phenotype [82].

#### ***1.2.3.5 Drug efflux by membrane transporters***

The reduction of intracellular taxane concentrations by membrane transporters is another source of taxane resistance. Three members of the ATP-binding cassette protein (ABC) superfamily of transporters have been implicated in taxane transport and resistance: P-gp (MDR-1, ABCB1), MRP-2 (ABCC2) and MRP-7 (ABCC10).

The multi-drug resistance phenomenon and the aforementioned proteins are explored in greater detail in Section 1.3.2.

### **1.3 Multi-drug resistance**

Clinical drug resistance is a major obstacle in the treatment of all types of cancer. It may be intrinsic, present from first diagnosis and unresponsive to first line chemotherapy, or it may be acquired. Acquired resistance often arises in recurrence of tumours that responded well initially but then display resistance to a broad range of structurally and functionally diverse agents as well as to the drugs they were originally exposed to.

The causes of drug resistance can be divided into two groups, inadequate drug exposure and changes in the cancer cells themselves.

Tumour exposure to chemotherapeutic agents is dependent on a number of factors, mostly physiological. Poor drug bioavailability and distribution, insufficient dosage, increased metabolism and excretion and poor tumour vascularisation all contribute to resistance development.

Transformations within the cancer cell itself include increased drug efflux, decreased drug influx, altered drug distribution, changes in drug detoxification systems and alterations to genes and proteins involved in apoptosis. Other mechanisms include increased tolerance to drug-induced damage to DNA, proteins and/or membranes, altered drug targets and cell cycle regulation [83],[84].

The increased understanding of cellular resistance mechanisms is leading to the development of new targeted cancer therapies.

#### **1.3.1 ABC superfamily**

The ATP-binding cassette (ABC) family of transporters play a major role in the pharmacological behaviour of most drugs in use today. They are the largest family of proteins that bind ATP and use the energy created from ATP hydrolysis to drive transport of various compounds across the cell membrane [85]. The sequence and organisation of a proteins ATP-binding domain (nucleotide-binding domain – NBD) determines its ABC classification and it is central to the ATPase function of the protein. All ATP-binding proteins contain the characteristic Walker A and Walker B motifs in their NBDs. A Walker C motif located upstream of Walker B is the

additional signature element of ABC transporters [86]. The functional protein generally consists of two cytoplasmic NBDs and two transmembrane domains consisting of 6-11 alpha-helices. Substrate specificity is provided by the transmembrane domains and the NBDs transfer energy for substrate transport.

ABC transport is usually uni-directional and involves compounds being moved from the cytoplasm to outside the cell or from the cytoplasm into intracellular bodies. Eukaryotic ABC genes are separated into full transporters, containing two NBDs and two transmembrane domains or half transporters that need to form homo- or heterodimers to function [85].

ABC transporters are highly expressed in intestinal and renal epithelia, hepatocytes, the blood-brain barrier, the blood-CSF (Cerebro-Spinal Fluid) barrier and the blood placental barrier, limiting drug and xenobiotic penetration into the body and into specific cell and tissue compartments [87].

This has major implications for chemotherapeutic agent pharmacokinetics, with drug absorption, distribution, clearance and interactions being influenced strongly by ABC protein expression, affecting the efficacy of these drugs.

### **1.3.2 ABC proteins and MDR**

While altered drug pharmacology is problematic, ABC proteins play a more malevolent role in drug resistance.

Cells exposed to toxic compounds can develop resistance to these agents through a number of mechanisms including changes in intracellular target proteins, increased detoxification and excretion and decreased uptake [19].

In some cases a multi-drug resistant (MDR) phenotype develops, where a cell not only becomes resistant to the initial drug it was exposed to but also a host of other structurally un-related compounds. This is often the case for agents used in cancer chemotherapy, including the taxanes. A number of ABC proteins play a role in MDR by reducing intracellular drug accumulation and increasing drug efflux. Table 1.1.5 gives an account of chemotherapeutic agents and the ABC protein associated with drug resistance for each.

### **1.3.3 ABC proteins associated with taxane resistance**

#### ***1.3.3.1 P-gp (ABCB1, MDR-1)***

P-gp is a 170kDa membrane glycoprotein that is the most studied and best characterised efflux pump in cancer cells. P-gp was first discovered by Juliano and Ling. in 1976 [88]. Chinese Hamster Ovary cells selected for colchicine resistance exhibited cross resistance to a number of amphiphilic compounds. The discovery of increased levels of a membrane bound glycoprotein, named P-glycoprotein, in cells expressing the MDR phenotype followed. The reduced cytotoxicity of these drugs was shown to be related to reduced drug accumulation due to enhanced drug efflux [89].

P-gp has two pairs of six transmembrane alpha-helical domains and two NBDs [90]. The gene maps to chromosome 7 (7q 21.1). P-gp is expressed in many excretory cell types such as kidney, liver, intestine and adrenal gland and in cells at the blood-brain barrier [91, 92].

It is also localised on the apical surface of bronchial and bronchiolar epithelium and the plasma membrane of alveolar macrophages where it is suggested it removes environmental compounds to the lung lumen [93].

P-gp has the capacity to transport the major classes of anti-cancer chemotherapeutic agents out of tumour cells and to affect the pharmacokinetics of these drugs. A summary of the anti-cancer compounds transported by P-gp in their native form is provided in Table 1.3.3.1.1.

**Table 1.3.3.1.1** P-gp substrates transported in native form, taken from [94].

Class	Drug
Taxanes	Docetaxel
	Paclitaxel
Vinca Alkaloids	Vinblastine
	Vincristine
Anthracyclines	Daunorubicin
	Doxorubicin
	Epirubicin
Epipodophyllotoxins	Etoposide
	Teniposide
Anthracenes	Mitoxantrone

### ***P-gp Inhibitors***

Since its discovery, P-gp has been a prime therapeutic target. First generation P-gp inhibitors, such as the calcium channel blocker verapamil and the immunosuppressant cyclosporin A, displayed useful MDR reversal activities *in vitro* and in murine models. The concentrations required, however, were high and often accompanied by increased cytotoxicity [95]. Second generation inhibitors comprise newer analogues of the first generation agents like dexverapamil (less cardiotoxic r-enantiomer of verapamil) and PSC 833 (valsopodar), the non-immunosuppressive analogue of cyclosporin A. These compounds were less cytotoxic and in some cases more potent P-gp modulators but still required micromolar concentrations to be effective. PSC 833 was also an inhibitor of cytochrome P450 3A4, one of the main drug metabolising enzymes in the body [96]. Third generation P-gp modulators have been developed based on structure-activity relationships that exhibit effective MDR reversal concentrations in the nanomolar range. These include GF120918- Elacridar [97], LY 335979- Zosuquidar [98], XR9576- Tariquidar [99], XR9051 [100], OC144-093- Ontogen (ONT-093) [101] and the bi-specific (P-gp and ABCC1) inhibitors, VX-710- Biricodar [102] and VX-853- Timcodar [103].

Combinations of the taxanes and third generation P-gp inhibitors have been promising. Elacridar improved the oral absorption of paclitaxel in mice [104] and has significantly increased systemic exposure to paclitaxel in humans [105]. The combination was well tolerated [105]. A phase I trial has shown zosuquidar to have no adverse effects in combination with docetaxel and a Phase II trial in metastatic breast cancer has been undertaken [106]. Evidence has come to light identifying the tyrosine kinase inhibitors gefitinib and erlotinib as P-gp and BCRP inhibitors [107], [108]. This is covered further in Section 1.5.6.

The clinical significance of P-gp expression is well documented. P-gp expression has been associated with poor clinical response to neo-adjuvant chemotherapy in locally advanced breast cancer and intrinsic P-gp overexpression at diagnosis in acute myeloid leukemia has been found to be a strong predictor of survival [109], [110]. Using immunohistological detection methods, P-gp was found to be present in 11-14% of breast cancer tumours pre-treatment and 30 -43 % of tumours post-treatment [111].

Efforts are under way to find more effective and less cytotoxic MDR modulators.

### ***Cellular Signalling Pathways involved in P-gp regulation***

P-gp expression has been studied extensively in normal and malignant tissues. P-gp is a stress-induced protein and has been shown to be activated by heat shock, irradiation, genotoxic stress, hormones, oncogenes, inflammatory mediators and growth factors such as EGF (epidermal growth factor) [112]. The exact pathway mechanisms involved have yet to be elucidated but many of the taxane-related signalling pathways, such as MAPK, phospholipase c and PI3K, are involved in P-gp regulation.

Activation of phospholipase c (PLC) by a variety of cellular stimuli (doxorubicin exposure, EGF, PDGF) regulates the expression of P-gp and the transcriptional modulation of P-gp by PLC is modulated by the Raf-MAPK (ERK1/ERK2) pathway [113]. JNK, also a member of the MAPK cascade, is activated in response to many stress stimuli and are sometimes referred to as Stress Activated Protein Kinases

(SAPK) [114]. JNK is activated in carcinoma cells by vinblastine, adriamycin and VP-16 resulting in up-regulation of P-gp [115].

A possible mechanism for the involvement of the third MAPK family member has also been suggested. SB203580, a specific inhibitor of the p38-MAPK pathway, reversed P-gp-mediated resistance in murine leukemic L1210/VCR cells [116]. The authors remarked that the mechanism would have to be further investigated but it could be related to P-gp down-regulation.

### ***1.3.3.2 MRP-2 (ABCC2)***

MRP-2 (ABCC2, cMOAT) plays an important role in the membrane transport of a variety of compounds. It is believed to be one of the major transporters determining the pharmacokinetic profile of drugs (involved in hepatic and renal excretion) [117] and plays a role in anti-cancer resistance [118].

Given its importance in drug detoxification it is no surprise that MRP-2 is predominantly expressed at the hepatocyte canalicular membrane [119] and at the apical membrane of human gall bladder epithelial cells [120]. In addition, rat studies have shown low levels of MRP-2 mRNA in the lung, stomach [121] and peripheral blood cells [122]. Loss of MRP-2 activity in humans is responsible for Dubin-Johnson syndrome, a rare hereditary disorder resulting in hyperbilirubinemia [123].

### ***MRP-2 and drug resistance in cancer***

MRP-2 mediates the ATP-dependent transport of various organic anions, including glucuronate, sulfate and glutathione conjugates of endogenous compounds and xenobiotics out of cells. The substrate specificity of MRP-2 (Table 1.3.3.2.1) is very similar to MRP-1 (Section 1.3.4.1), and MRP-2 may also require free glutathione to allow co-transport of some compounds such as vinblastine [124]. Unlike MRP-1, MRP-2 may be capable of transporting glutathione alone without the need for simultaneous co-transport or binding of other compounds [125].

MRP-2 expression in sensitive cell lines has conferred resistance to number of cytotoxic agents, methotrexate, cisplatin, etoposide, vincristine and doxorubicin [124]. Cisplatin-selected (head and neck KB cancer cell line) cancer lines over-express MRP-2 [126] as do hepatocarcinoma cell lines [127] and anti-sense DNA transfected into hepatic cancer cells enhanced drug sensitivity [128]. MRP-2 expression has been found in a range of cancers *in vivo* including breast cancer, lung cancer and acute myeloid leukemias [129], [130], [131]. In a panel of lung cancer cell lines, MRP-2 and MRP-3 expression was almost exclusively found in NSCLC cell lines rather than SCLC cell lines but it was MRP-1 and MRP-3 expression that correlated with resistance to doxorubicin and VP-16 [130].

Docetaxel and paclitaxel are transported by MRP-2 in MRP-2-transfected MDCKII cells and the transport is stimulated by probenecid [132]. This marks MRP-2 as a potential taxane resistance mediator and must increase awareness of possible drug:drug interactions in trials given its role in detoxification.

A role for MRP-2 in NSCLC taxane resistance *in vivo* has not been established as yet.

**Table 1.3.3.2.1** MRP-2 substrates (native or conjugated form), taken from [124].

Class	Drug
Anti-Cancer Drugs	Taxanes [132]
	Cisplatin
	Vinblastine
	Irinotecan
	Topotecan
	Methotrexate
Endogenous Compounds	Bilirubin
	Leukotrienes C4, D4 and E4
	Bile Salts
	Estradiol
	Glutathione

### ***MRP-2 inhibitors***

MRP-2 inhibitors are not particularly specific with many of them inhibiting other transporters such as MRP-1 [133], P-gp [134] or organic anion-transporting polypeptides (OATPs) (rifampicin) (Table 1.3.3.2.2) [135]. Inhibitor interactions are made all the more complicated when you consider their drug dependent effects. Probenecid is an inhibitor of MRP-2-mediated methotrexate transport but it can also stimulate taxane transport [136].

**Table 1.3.3.2.2** MRP-2 inhibitors [124]

Inhibitors
Probenecid
Rifampicin
Cyclosporin A
Glibenclamide
Flavonoids – luteolin, quercetin
Indomethacin
MK571
Azithromycin
Sulindac [137]

### ***1.3.3.3 MRP-7 (ABCC10)***

MRP-7 (ABCC10) is a very recently described addition to the MRP family. It was identified by data-base screening for sequences related to human ABC transporters originally identified by EST analysis [138]. RT/PCR analysis of a number of human tissues revealed the highest transcription levels were in colon, skin and testis [138]. Northern blot experiments failed to produce results in the same tissues inferring low expression rates. Subsequent expression profiling found a splice variant, MRP7A,

expressed in most human tissues with MRP-7 located only in the spleen [139]. Expression of the original MRP-7 [138] and two other unique variants were reported in the human hepatoblastoma cell line HepG2 and prostate cancer cell line CWR22Rv1 [140]. In mice, the highest levels of MRP-7 RNA were found in small intestine, kidney, ovary and testis tissues and there was also lung tissue expression [141].

Membrane vesicle studies have demonstrated transport of the endogenous substrates 17beta-estradiol-(17-beta-D-glucuronide (E<sub>2</sub>17betaG) and leukotriene C<sub>4</sub> by MRP-7 [142]. HEK293 cells ectopically expressing MRP-7 have been used to determine the drug resistance profile of the transporter [143]. MRP-7 confers moderate resistance (2-3 fold) to the vinca alkaloids (vincristine and vinblastine), the anthracycline doxorubicin and paclitaxel. It exhibits its highest activity towards docetaxel (9-13 fold increase). This marks MRP-7 as a potential taxane resistance mediator in cancer.

### **1.3.4 Other ABC proteins involved in MDR**

#### ***1.3.4.1 MRP-1 (ABCC1)***

The multi-drug resistance protein (MRP, ABCC) group is a subset of the ABC family. Other members of ABCC subfamily include the cystic fibrosis transmembrane conductance regulator (CFTR), the sulfonylurea receptors SUR1 and SUR2 and yeast cadmium resistance factor 1 (YCF1) [124].

MRP-1 (ABCC1) was the founding member of the MRP family, first isolated in 1992 [144]. The MRP-1 is a 190 kDa protein consisting of two NBDs and three transmembrane domains, a feature it shares with the MRP-2 (ABCC2), MRP-3 (ABCC3), MRP-6 (ABCC6) and MRP-7 (ABCC10). Other members of the MRP family (MRP-4, MRP-5, MRP-8 and MRP-9) contain two NBDs and two transmembrane domains similar to P-gp [124].

MRP1 is ubiquitously expressed throughout the body, although there are certain organs such as the lungs, kidneys and testes that express relatively high levels of the protein [145]. It is generally localised to the baso-lateral membrane of epithelial cells, which results in MRP1 pumping its substrates into the interstitial space rather than

into an excretory pathway such as the gut or into urine [146], [147]. In the lungs, MRP1 has been implicated in the reaction of this organ to toxicological insult, being expressed at high levels in alveolar macrophages, bronchial epithelium and in cells produced specifically in response to xenobiotics, such as reactive type II pneumocytes [145]. High expression in human and murine testes may point to a possible role in the maintenance of low oestrogen levels in these organs [145].

It has since been characterised as a glutathione and glucuronate pump and resistance factor for anthracyclines, vinca alkaloids, epipodophyllotoxins and camptothecins [148].

Although it has a broad substrate specificity that overlaps with P-gp, it only shares approximately 15% amino acid homology. While P-gp substrates are neutral or mildly positive lipophilic compounds, MRP-1 can transport lipophilic anions and the structurally diverse products of phase II cellular detoxification of hydrophobic xenobiotics (glutathione, sulphate, glucuronate conjugates) and endogenous compounds [148]. This is the major difference between P-gp and MRP-1.

Along with the transport of conjugates, MRP1 can actively co-transport GSH and unmodified vincristine and vinblastine [149]. It is hypothesised that daunorubicin and etoposide are transported in a similar manner [150], [151]. GSH (glutathione) and glucuronate by themselves are not substrates for MRP [152]. The situation where both the GSH-conjugated substrate and the free substrate can be transported can also occur as in the case of the potent cancer carcinogen, aflatoxin B1 [153]. Manipulation of GSH levels can reverse MRP-mediated drug resistance. Depletion of GSH by exposure to buthionine sulfoxamine (BSO) restores drug sensitivity in MRP-expressing cell lines, for example the reversal of a daunorubicin accumulation defect caused by GSH depletion by restoring previous GSH levels [154], [155]. It is possible that drugs that are positively charged or neutral, such as daunorubicin and vincristine, may need GSH to be transported but anionic molecules may not. Evidence for this comes from studies showing the transport of anionic molecules to not be affected by GSH depletion [156]. Methotrexate has been shown to be transported in its native form by MRP-1 [136].

#### **1.3.4.1.1 MRP-1 inhibitors**

Given the similarity between MRP-1 and MRP-2 substrate sets, competitive inhibition by high affinity substrates like leukotriene C<sub>4</sub>, S-decylglutathione and MK571 occurs in both MRP-1 and MRP-2 [157], [158]. More MRP-1 inhibitors include sulfinpyrazone, benzbromerone and probencid [146]. The same inhibitors don't always work for both MRP-1 and MRP-2, even though they have similar substrate specificities. For instance, sulfinpyrazone, an MRP1 inhibitor, does not inhibit the transport of dinitrophenyl S-glutathione by MRP-2 [159].

Non-steroidal anti-inflammatory drugs (NSAIDs) have in recent times become players in the drug resistance arena. A study of the effects of a group of these drugs (indomethacin, sulindac, tolmetin, acemetacin, zomepirac and mefenamic acid) at non-toxic levels illustrated their ability to increase the cytotoxicity of chemotherapeutic agents such as the anthracyclines, VP16 and vincristine in the cell lines HL-60ADR, Cor L23R, DLKP and COR L23P [160]. Sulindac, as a competitive MRP-1 inhibitor, has been the subject of a recent Phase I clinical and pharmacokinetic study in combination with epirubicin in advanced cancer conducted by our group [161].

#### **1.3.4.2 MRP-3 (ABCC3)**

MRP-3, like MRP-1 and MRP-2, is an organic anion transporter [162]. MRP-3 is reported to be expressed mainly in the pancreas, kidney, liver, colon, intestine and adrenal gland [162]. Studies of cloned rat *mrp-3*, suggests it displays a preference for glucuronate conjugates as substrates over glutathione conjugates [163]. Cells expressing the protein are resistant to etoposide, teniposide and short term methotrexate exposure but not other MDR linked drugs [162]. Studies on a murine fibroblast-like cell line retrovirally transduced with MRP-3 cDNA and lacking *mdr1a/b* and *mrp1* showed that when over-expressing MRP-3 these cells were resistant to etoposide and teniposide but not vincristine, doxorubicin and cisplatin [164]. The etoposide resistance was not affected by glutathione depletion. Membrane

vesicles expressing MRP-3 mediated the ATP-dependent transport of etoposide glucuronide, estradiol 17- $\beta$ -D-glucuronide, leukotriene C<sub>4</sub>, dinitrophenyl S-glutathione but not glutathione itself [164].

#### **1.3.4.3 MRP-4 (ABCC4)**

MRP-4 has been found to be expressed in the prostate, testis, ovary, intestine, pancreas and lung tissues [165]. Studies on membrane vesicles prepared from insect cells infected with MRP-4 baculovirus have shown MRP-4 to be specifically associated with the MgATP-dependent transport of cGMP, cAMP, DHEAS and estradiol 17- $\beta$ -D-glucuronide [166]. It was also found that MRP4 is involved in resistance to the anti-cancer purine analogues 6-thioguanine and 6-mercaptopurine and methotrexate [166], [167]. The ability of MRP-4 to transport prostaglandins E<sub>1</sub> and E<sub>2</sub>, mediators of the inflammatory response and over-expressed in some tumours, may suggest a role for MRP-4 in prostaglandin regulation in normal and neoplastic tissue [167]. MRP-4 has been much studied recently as it can function as a cellular efflux pump for the HIV drugs 9-(2-phosphonylmethoxyethyl) adenine PMEA and Azidothymidine monophosphate (AZTMP) in PMEA resistant cells [168].

#### **1.3.4.4 MRP5 (ABCC5)**

MRP-5 is expressed in most normal tissues and is over-expressed in lung, breast colon and pancreatic cancers [169]. Drug transfection studies in drug sensitive cells have shown MRP-5 confers resistance to antifolate drugs such as methotrexate and pemetrexed and to nucleoside –based drugs such as 6- mercaptopurine, 6-thioguanine PMEA, 5-FU and gemcitabine [169]. MRP5 has been shown to be inhibited by sulfapyrazone and benzbromarone but not by probenecid [170].

MRP5 overexpression has produced no prominent resistance to other anti-cancer drugs such as the anthracyclines, vinca alkaloids and epipodophyllotoxins [146].

#### **1.3.4.5 MRP-6 (ABCC6)**

Expression of MRP-6 has been found in the liver and the kidney [165]. Mutations in the MRP-6 gene have been associated with the rare hereditary connective tissue disorder Pseudoxanthoma elasticum [171]. The 3' end of the MRP-6 protein is almost identical to the anthracycline resistance-associated (ARA) protein previously identified in epirubicin-selected leukaemia cells [172]. Studies in membrane vesicles transfected with MRP-6 expression vector have shown that expression of MRP-6 is specifically associated with the transport of glutathione *S*-conjugates but not glucuronate conjugates while MRP-6 transfected cells have shown low levels of resistance to etoposide, tenoposide, doxorubicin and daunorubicin [172].

#### **1.3.4.6 MRP-8 (ABCC11)**

MRP-8 is a lipophilic anion exchanger capable of transporting with a substrate specificity that overlaps with MRP-4 and MRP-5. [142]. A single nucleotide polymorphism in MRP-8 has been shown to determine wet *versus* dry earwax and is the only known physiological role that has been found for MRP-8 [23]. Endogenous transported compounds include LTC<sub>4</sub>, E<sub>2</sub>17BG, DHEAS, and the cyclic nucleotides cAMP, cGMP [142]. MRP-8 mediates resistance to fluoropyrimidines through transport of 5-fluoro-2-deoxyuridine monophosphate, the cytotoxic metabolite of 5-fluorouracil, 5-fluoro-2-deoxyuridine and capecitabine [173].

The substrate range of MRP-9 (ABCC12) is not characterised to date [23].

#### **1.3.4.7 Breast Cancer Resistance Protein (BCRP, ABCG2)**

BCRP is a 70 kDa protein and a more recent addition to MDR transport molecules and is also referred to as MXR (mitoxantrone resistance associated protein), ABCP (Placenta-specific ABC gene) and ABCG2. Identification of the molecule in the anthracycline-selected breast cancer cell line MCF-7/AdrVp led to it being named

BCRP [174]. It later emerged as the prime suspect in the search for a mediator of high mitoxantrone resistance.

The BCRP gene has been mapped to chromosome 4q22 [175]. It seems to be localised mainly to the plasma membrane rather than any intracellular membranes [176]. This does not rule out the possible existence of intracellular BCRP as drug sequestering cytoplasmic vesicles have been observed in the BCRP-over-expressing gastric carcinoma cell line EPG85-257RNOV [177], [178].

BCRP is described as an ABC half-transporter with six transmembrane helices, with the active BCRP transport complex consisting of two half transporters [179]. The phenotype of BCRP resistant cells overlaps with that of classical MDR but is distinct from it. The breast carcinoma cell line MCF-7/BCRPclone8, a BCRP-transfected cell line showed cross-resistance to daunorubicin, doxorubicin, mitoxantrone, SN-38 (active metabolite of irinotecan) and topotecan while retaining sensitivity to cisplatin, paclitaxel and vincristine [174], [180].

The normal physiological role of BCRP is still unknown. In a recent study using two monoclonal antibodies, BXP-34 and BXP-21, high BCRP expression was observed in placental syncytiotrophoblasts, the epithelium of the small intestine and colon, the liver canalicular membrane and in ducts and lobules of the breast [181]. These results point to a role in the placental barrier and a further protective role against xenobiotics in the intestine and liver. There is further evidence that BCRP is involved in cellular homeostatic mechanisms, hypoxic responses and systemic access [182]. This last association is being exploited to improve the pharmacokinetic profiles of BCRP-substrate chemotherapeutic agents when co-administered with a BCRP modulator such as elacridar [182].

The original, specific agent for the reversal of BCRP-dependent is fumitremorgin C [183]. It was isolated from *Asperillus fumigatus* and does not reverse resistance associated with MRP and P-gp [183], [184]. Elacridar, a dual P-gp and BCRP inhibitor, is able to resensitise mitoxantrone-resistant BCRP-expressing cells and is reported as a potent reversal agent of BCRP-mediated resistance to camptothecins [185], [186]. Other modulators of BCRP include tamoxifen, imatinib and the fumitremorgin C analogues, Ko132, Ko134 and Ko143 [182].

### **1.3.5 ABC protein expression in lung tissue**

Many of the ABC transporters, including P-gp, MRP-1 and BCRP, show elevated levels of expression expressed in normal bronchial epithelium [187]. The airways form the first line of defence against inhaled pathogens, pollutants and other toxic agents. The prominent expression of ABC transporters in the lung suggests that they may be central in the protection of the lungs from harmful endogenous and exogenous compounds. There has been conflicting reports for the expression of MRP-2, MRP-3, MRP-4 and MRP-5 in primary bronchial and peripheral epithelial cells [187]. Two studies that examined the levels of P-gp and MRP-1 by RT-PCR in NSCLC cancers revealed 100% expression of MRP-1 in all tumours and 27-43% expression of P-gp [111]. A correlation between current smoking and doxorubicin resistance of NSCLC has been reported, with 42 out of 72 NSCLC smokers expressing P-gp, whereas only 2 out of 22 tumours of non-smokers were P-gp positive [187].

## 1.4 Drug uptake mechanisms

Energy-dependent efflux of chemotherapy drugs is well characterised through the role of the MRP family and P-gp in multi-drug resistance. There are a number of chemotherapy drugs that do not rely solely on passive diffusion for drug entry into cells. Melphalan, the nitrogen mustard derivative of L-phenylalanine, is transported by the L-type amino acid transporter 1 (LAT 1/SLC7A5) system in breast cancer cells [188]. Cisplatin and carboplatin kinetics are linked to human copper transporter 1 (CTR1/SLC31A1) and ATP7B, transporters involved in cellular copper homeostasis [189]. Methotrexate is an anti-metabolite that is transported into the cell by a number of mechanisms, most notably the reduced folate carrier (RFC/SLC19A1) [190]. Anti-cancer nucleoside analogues, such as mercaptopurine and thioguanine, are transported by the equilibrative nucleoside transporter (ENT/SLC29) and concentrative nucleoside transporter (CNT/SLC28) gene groups. [191]. In most cases, as exemplified by melphalan and methotrexate, the existence of an influx mechanism is down to the similarity of the chemotherapy agent to naturally occurring endogenous compounds.

### 1.4.1 Taxane uptake mechanisms

The mechanism by which docetaxel and paclitaxel enter the cell has received relatively little attention as it has been assumed that the lipophilic taxanes enter cells by passive diffusion. Two recent studies have provided evidence for carrier mediated taxane transport. OATP1B3 (organic anion transporting polypeptide 1B3/SLCO1B3/OATP8) is a member of the solute carrier family 21 (SLC21/SLCO) that has exhibited paclitaxel and docetaxel transport in transfected oocytes, a standard approach for analysing a transporter's substrate selectivity [192].

[192]. Using the same experimental procedure, Kobayashi *et al.*, have shown that OAT2 (organic anion transporter 2/SLC22A7), also expressed in the liver, is capable of stimulating uptake of paclitaxel into oocytes [193].

Many of the influx mechanisms identified, including those associated with taxane transport to date, are members of the solute carrier (SLC) superfamily of transporters. As well as the important physiological role as transporters of endogenous substrates, the SLC superfamily plays a major role in systemic drug disposition and mediation of the chemosensitivity and -resistance of cancer cells. Approximately 300 SLC genes have been cloned and organised into 43 families to date [194]. The only documented member of the SLC superfamily shown to transport docetaxel, OATP1B3, is part of the SLCO family [192]. For this reason, the SLCO family became a focus of the investigation into a putative docetaxel uptake mechanism in NSCLC cell lines.

### **1.4.2 SLCO family**

The traditional SLC21 gene and OATP (-A, -B, -C, -8) protein classifications has recently been replaced with a new nomenclature system, OATP/SLCO, based on phylogenetic relationships and chronology of identification [195]. SLCO is used to denote the gene while OATP is used to denote the related protein product. Of the 52 members of the SLCO superfamily found in the human, rat and mouse, 36 have been identified in humans thus far [195]. Their transport mechanism appears to be by sodium-independent anion exchange [196]. This facilitated transport antiporter activity involves coupling the cellular uptake of organic compounds with the efflux of, for example, bicarbonate, glutathione or glutathione-S-conjugates [195]. This system does not directly require or utilise ATP hydrolysis.

OATPs were originally characterised as uptake transporters but some may function primarily as efflux pumps in certain parts of the body [197]. It is likely that the OATP family can mediate bi-directional organic substrate, with the overall directionality of transport dependent on the prevailing substrate gradients [195]. Bidirectional transmembrane BSP transport has been observed in rat Oatp1-expressing HeLa cells and Oatp1-mediated taurocholate/HCO<sub>3</sub> exchange [196].

Expression of a number of OATP family members has been documented in lung tissue. Some OATPs are expressed exclusively in one tissue, such OATP1B1 and OATP1B3 in the liver, while others are expressed in multiple organs, like OATP2B1 (heart, lung, small intestine, kidney, ovary) or the ubiquitously expressed OATP3A1,

OATP2A1 and OATP4A1 [196]. OATP1A2 mRNA expression has been reported in the lung, testis, brain, kidney and liver [196]. While the normal physiological expression of the taxane-transporting OATP1B3 is in the liver, it has been shown to be expressed in various human cancer tissues and cell lines derived from lung, colon, gastric, pancreas, gallbladder and brain cancers [198].

The OATPs mediate the membrane transport of a wide variety of amphipathic organic compounds including bile salts, organic dyes, steroid conjugates, thyroid hormones, numerous drugs and xenobiotic compounds [196]. Endogenous compounds include bile salts (cholate, glycocholate), eicosanoids (prostaglandine E<sub>2</sub>, leukotriene C<sub>4</sub>), hormones and their conjugates (estrone-3-sulfate, E<sub>2</sub>17BG) and bilirubin. Xenobiotic compounds transported include fexofenidine (also a P-gp substrate [199]), methotrexate, pravastatin, digoxin, rifampicin and bromosulfophthalein [196]. The MRP-2 flavonoid substrate epigallocatechin-3-gallate is also an OATP-C substrate [200].

The overlapping of ABC transporter and OATP substrates is no coincidence. OATPs are involved in drug vectoring, transcellular drug transport based on the apical or basolateral expression of transporters. This occurs at areas such as the blood-brain barrier, intestinal and renal epithelia and hepatocytes where the OATPs expressed basolaterally, take drugs into epithelial cells with exporters such as MRP-2 expressed apically to excrete the drug into the lumen [87].

The effect of OATPs on drug disposition and excretion is unquestionable. A role for OATPs in taxane influx (or efflux) in tumours is not implausible due to substrate similarities to recognised taxane transporters, co-expression with these established transporters (MRP-2) in some tissues and documented expression in cancer cells.

### **1.4.3 SLC22 family**

The SLC22 family is divided into two subcategories, OATs (organic anion transporters) and OCTs (organic cation transporters). The OCTs are broad specificity transporters involved in the uptake, excretion and distribution of endogenous organic

cations and cationic xenobiotics [201]. The involvement of OCTs in drug resistance is unknown but they have been shown to transport nucleoside analogues *in vitro* [202]. Although structurally similar, the OATs, in contrast, are involved in the uptake, elimination and distribution of endogenous and exogenous organic anions. There are five human OAT members OAT1 (SLC22A6), OAT2 (SLC22A7), OAT3 (SLC22A8), OAT4 (SLCA11) and URAT1 (SLCA12) [203]. Expression of all members is found in the kidneys except for OAT2, with OAT3 and OAT4 expression also reported in the brain and placenta, respectively [204]. Methotrexate is a substrate for OAT1, OAT3 and OAT4 but not the paclitaxel transporting OAT2 [204], [193]. OAT3 and OAT4 can transport DHEAS while OAT1 can handle NSAID transport [204]. There is no evidence that the OAT family contributes to cancer cell chemosensitivity or resistance *in vivo*.

## **1.5 EGFR inhibitors in lung cancer**

### **1.5.1 Epidermal growth factor receptor (c-ErbB) Family**

The type I receptor tyrosine kinases are a family of transmembrane proteins involved in various aspects of cell growth, survival, and differentiation [205]. Members of the family include the EGFR (epidermal growth factor receptor, c-ErbB1), Her-2/neu, (c-ErbB-2), Her-3 (c-ErbB-3), and Her-4 (c-ErbB-4).

The c-ErbB family have been investigated as potential therapeutic targets due to over-expression in a broad variety of cancers. EGFR has been shown to be over-expressed in bladder, breast, head and neck, kidney, non-small cell lung, and prostate cancers, Her-2 is over-expressed in breast, cervix, colon, endometrial, oesophageal, lung, and pancreatic cancers. Her-3 over-expression has been reported in breast, colon, prostate, and stomach malignancies while Her-4 over-expression has been detected in breast cancer and granulosa cell tumours of the ovary [206], [207], [208].

All four proteins share a similar structure; the extracellular domain contains two regions involved in ligand binding and two cysteine rich regions, the transmembrane domain involved in dimerisation between c-ErbB family members and the intracellular domain which contains the tyrosine kinase domain that phosphorylates tyrosine residues on substrate proteins. The cytoplasmic domain also contains a carboxy-terminal tail with tyrosine autophosphorylation sites which link these receptors to proteins containing Src homology and phosphotyrosine-binding domains [209]. Her-2 and Her-3 are exceptions to the rule containing an inactive ligand binding site and an inactive tyrosine kinase domain, respectively.

There are six known endogenous ligands for EGFR: epidermal growth factor (EGF), transforming growth factor- $\alpha$ , amphiregulin, betacellulin, heparin-binding EGF, and epiregulin. Betacellulin, heparin-binding EGF, and epiregulin are also ligands for Her-4. The neuregulin isoforms NRG1 and NRG2 are ligands of Her-3 and Her-4,

low and high affinity receptors respectively, and the NRG3 and NRG4 isoforms are Her-4 ligands [210].

The members of the c-ErbB family can form four homodimers and six heterodimers. Studies show that certain combinations of dimers are preferred. The Her-2/Her-3 dimer, for instance is reported as being a preferred dimer in breast cancer [211]. Her-3 has an active ligand binding domain but requires heterodimerisation with another family member to activate a signalling cascade due to its inactive tyrosine kinase domain. The Her-2 receptor is an orphan receptor with an inactive ligand binding domain that requires heterodimerisation for activation of its tyrosine kinase domain. Heterodimerisation increases the number of cell signalling pathways that can be activated by various ligands.

### **1.5.2 EGFR signalling pathways**

There are some common signalling pathways activated by all c-ErbB family members. All four members of the family have the potential to stimulate the Ras-Raf-MAPK protein kinase signalling cascade. Phospholipase C $\gamma$ , however binds to specific phosphotyrosines of EGFR but not to the other c-ErbB family members, mediating the formation of diacylglycerol and inositol 1,4,5-trisphosphate second messengers. This leads to downstream activation of Akt [212]. Other factors activated by the c-ErbB family include the cytoplasmic tyrosine kinase c-Src, MAP kinase, c-Jun kinase, and signal transducers and activators of transcription (STATs) [210].

The importance of the signalling pathways activated by the EGFR family of receptor tyrosine kinases can be seen by the key role these pathways play in the regulation of normal cellular development as well the critical part they play in a variety of pathophysiological phenomena [210].

The Ras-Raf-MAPK pathway is a major signalling pathway of EGFR and the other members of the c-ErbB family [212], [213]. Activation of Ras initiates a phosphorylation cascade that leads to the activation of the p44/42 mitogen-activated protein kinases (MAPK's), consisting of the extracellular signal-regulated kinases, Erk1 and Erk2, by dual phosphorylation. Erk1/2 then translocates to the nucleus and regulates transcription and cell proliferation. EGF is also capable of activating the

PI3-Kinase/Akt signalling pathway. Akt is involved down-stream of activated PI3-kinase and supervises the balance of apoptosis and cell survival by inhibition of proapoptotic proteins [212]. The Rac/JNK/p38 MAPK signalling cascade is another important EGFR activated pathway [214]. The stress-activated protein kinase (SAPK) p38 MAPK, is induced by growth factors, pro-inflammatory cytokines and non-steroidal anti-inflammatory drugs [215]. EGF signalling through p38 MAPK can exert apoptotic or mitogenic effects dependent on the cell type [216], [217]. The activity ratio of Erk/p38 MAPK may predict whether tumour cells proliferate or enter a state of dormancy *in vivo*. A high Erk/p38 MAPK ratio favours tumour growth, whereas a high p38 MAPK/Erk ratio induces growth arrest indicating that Erk is negatively regulated by p38 MAPK [218]. EGFR-regulated pathways have been extensively implicated in taxane resistance (Section 1.2.3.4) and P-gp regulation (Section 1.3.2).

### **1.5.3 c-ErbB regulation**

Along with activating downstream signalling pathways, ligand binding to plasma membrane receptor tyrosine kinases (RTKs) such as EGFR and Her-2 promotes cellular internalisation of the proteins. Internalisation leads to downregulation of the signal via degradation of the ligand/receptor complex or in the case of EGFR, to further signalling from endosomes [219]. Most RTKs are predominantly localised in regions of the plasma membrane called lipid rafts that may or may not be associated with caveolins [219]. Lipid rafts are more rigid patches of plasma membrane containing a concentration of cholesterol, sphingolipids and phospholipids that are compositionally identical to vesicles known as caveolae but for the absence of a set of proteins known as caveolins [220]. Ligand activation promotes internalisation of RTKs through clathrin-dependent (EGFR, PDGFR (platelet-derived growth factor receptor), IGF-1R (Insulin growth factor-1 receptor)) or –independent (VEGF-R (vascular endothelial growth factor receptor)) pathways [219]. Internalisation commences with the recruitment of vesicular trafficking molecules and the formation of clathrin-coated membrane invaginations around the RTK. Further adapter proteins facilitate the budding of the clathrin-coated vesicle (CCV) and subsequent release from the plasma membrane [219]. The CCV sheds the clathrin coat and fuses with

early endosomes that either recycle the receptors back to the cell surface or sort them to late endosomes for lysosomal and/or proteosomal degradation [219].

#### **1.5.4 c-ErbB and cancer**

The c-ErbB family was first implicated in carcinogenesis in 1984 with the discovery that the transforming element of an oncogenic avian erythroblastosis retrovirus encoded a truncated ortholog of human EGFR [221]. Two years later, Her-2 was isolated from rat glioblastomas as a carcinogen-induced oncogene (*neu*) with a point mutation in its transmembrane domain resulting in ligand-independent homodimerisation and constitutive activation [222]. Irregular activation of the c-ErbB network can occur through a number of mechanisms including receptor overexpression, autocrine production of ligand, gene amplification and mutation.

All four mechanisms have also been documented for the EGF-receptor, EGFR. EGFR over-expression has been documented in a number of cancers including breast cancer, lung cancer and particularly high frequency of over-expression due to gene amplification in gliomas [223], [224, 225]. Recent retrospective analyses have reported EGFR overexpression in 62% of NSCLC cases with its expression correlated to a poor prognosis [226].

Several mutations in EGFR have been reported. EGFRvIII involves the loss of coding sequence for amino acids 6-273 (exons 2-7) and expression has been shown in 39% of NSCLC tumours and 78% of breast cancer tumours [225]. Further somatic EGFR mutations have been identified in NSCLC that lead to hyperactivation of the kinase domain and over-dependence of the cell on the EGFR pathway for survival. In-frame deletions of amino-acids 747–750 in exon 19 account for 45% of these mutations, exon 21 mutations resulting in L858R substitutions account for 40–45% of mutations, and the remaining 10% of mutations involve exon 18 and 20 [226].

The majority of these mutations have been associated with sensitivity to the tyrosine kinase inhibitors gefitinib and erlotinib (see Section 1.5.5.2) but some are associated with acquired tyrosine kinase inhibitor resistance.

Her-2 is found to be over-expressed in a variety of cancers including 20-30% of breast and ovarian cancers due to over-amplification [225]. Her-2 over-expression correlates with therapeutic resistance and poor prognosis in breast cancer [227]. Trastuzumab (Herceptin®) is a Her-2-targetted monoclonal antibody that has achieved significant

success for the treatment of Her-2 positive metastatic breast cancer improving survival by 25% [228]. Over-expression of Her-2 in NSCLC is reported to be between 4 and 27% in NSCLC, depending on the detection method used [229]. A study by Gatzemeier *et al.*, recently showed that 17% of NSCLC patients presented with Her-2 levels of 2+/3+ using the Herceptest method of Her-2 detection and consequent combination therapy with cisplatin/gemcitabine and trastuzumab *versus* cisplatin/gemcitabine alone did not improve any efficacy endpoint [230]. The Herceptest® is a standard method for determining tumour Her-2 levels that uses an immunohistochemical scoring system (0 (no expression) to 3+ (high expression) to rate Her-2 expression relative to known Her-2 over-expressing cell lines. Her-2 overexpression may still provide a target in NSCLC as there is evidence that Her-2 co-operation is required by EGFR and Her-3 in lung tumourigenesis and Her-2 over-expression is related to cisplatin resistance therefore, Her-2 may have potential in combination with EGFR therapies and as a platinum-sensitiser in NSCLC [229].

Less is known about the involvement of Her-3 and Her-4 in NSCLC. Her-3 over-expression has been found in breast, colon, prostate, bladder, oral and gastric cancers while Her-4 has been found to be a target of mutation in lung, gastric, breast and colorectal carcinoma [225]. Activation of Her-3, and subsequently the PI3K/Akt signalling pathway, by the over-expressed MET tyrosine kinase receptor, rather than EGFR, has been associated with TKI inhibition in NSCLC lung cancer cell lines [231].

### **1.5.5 Targetted c-ErbB therapies**

Two approaches have been adopted for inhibition the c-ErbB family, monoclonal antibodies and small molecule tyrosine kinase inhibitors (TKIs). There are disadvantages and advantages to both types of inhibitor. Monoclonal antibodies are highly specific and they block EGFR ligand binding, receptor internalisation and dimerisation and in some cases (IgG<sub>1</sub> isotype), stimulate the immune response [232]. Although TKIs provide a less robust inhibition of EGFR by preventing activation of EGFR signalling pathways by inhibition of c-ErbB kinase activity only, TKIs have better tumour penetration due to their size and they are effective against constitutively active EGFR [232].

### ***1.5.5.1 Monoclonal antibodies***

Cetuximab (Erbix<sup>®</sup>) is a monoclonal human-murine chimeric antibody against EGFR that has been approved for colorectal cancer treatment [232]. Binding of the antibody causes EGFR internalisation and prevents ligand mediated tyrosine kinase phosphorylation resulting in up-regulation of p27KIP1, a decrease in CDK2, cyclins A and E and G1 cell cycle arrest [233]. Phase II trials have been carried out in combination with docetaxel in recurrent NSCLC. This achieved a partial response rate of 28% and a stable disease rate of 17%, survival analysis is ongoing. In chemotherapy naïve, stage IV NSCLC patients, carboplatin and paclitaxel combined with cetuximab produced a response rate of 29%. Both trials were carried out in patients with EGFR positive tumours [234].

Other monoclonal antibodies that are in Phase II and III trials for NSCLC treatment include panitumumab (Vectibix<sup>®</sup>), matuzumab, nimotuzumab (TheraCIM<sup>®</sup>) and zalutumumab (HuMax-EGFr<sup>®</sup>).

### ***1.5.5.2 Small molecule TKIs***

The major EGFR inhibitors approved in the treatment of NSCLC are gefitinib (Iressa<sup>®</sup>, ZD1839) and erlotinib (Tarceva<sup>®</sup>, OSI-774).

#### ***Gefitinib***

Gefitinib is a quinazoline derivative and reversible inhibitor of EGFR [232]. Gefitinib inhibits EGFR phosphorylation with an IC<sub>50</sub> of 27 to 33 nmol/l [235]. Gefitinib also has the ability to inhibit Her-2 phosphorylation but at higher concentrations (Her-2 phosphorylation IC<sub>50</sub> of 3.7 µmol/l) [235].

Gefitinib is approved as a third line monotherapy for the treatment of advanced NSCLC [232]. Gefitinib has achieved modest success as a single agent therapy in lung cancer. It has shown close to a 25% response rate (stable disease, partial and complete responses together) in advanced disease [236]. In one particular study where

gefitinib monotherapy resulted in 15% partial response, those that responded were most likely to have adenocarcinomas of the bronchoalveolar subtype (25% of NSCLC) and to be never-smokers [237]. It was discovered that gefitinib-sensitive patients had EGFR mutations [238], [239]. Analysis of eight trials (86 patients) in this particular sub-population with EGFR mutations found they had produced response rates of between 76 and 92% [240]. One of these studies compared the median survival time of wild type EGFR and mutated EGFR patients and found them to be 7 months and 31 months respectively [241]. The same study also compared responses to gefitinib between never-smokers and smokers in six trials. Never-smokers showed response rates of between 18 and 63% with a 5-18% range in smokers. Mutations of EGFR occur in two major hotspots, multinucleotide in-frame deletions that eliminate four amino acids in exon 19 and point mutations in exon 21 that result in a specific amino acid substitution at position 858 (L858R) [242]. Squamous cell carcinomas can often express higher levels of EGFR than adenocarcinomas but may not have mutations associated with EGFR inhibitor sensitivity [242]. These results suggest gefitinib efficacy can be improved by patient selection based on tumour phenotype and patient history.

Combination studies with gefitinib and chemotherapy agents have been disappointing. Trials of gefitinib combined with gemcitabine and cisplatin with late stage NSCLC, showed no benefit over the gemcitabine and cisplatin alone [243]. A number of reasons have been suggested for this lack of benefit in combination studies. Suboptimal target modulation due to inadequate dosing, antagonism between gefitinib and the chemotherapeutic agents, the same tumour population being sensitive to chemotherapy and gefitinib, and the benefit to some patients being hidden within in the larger population of patients with insensitive tumours have been purported as possible explanations [244].

### ***Erlotinib***

Erlotinib is another quinazoline-derived reversible EGFR inhibitor that has similar activity to gefitinib [232]. Erlotinib inhibits EGFR phosphorylation with an  $IC_{50}$  of 2 nM in kinase assays and an  $IC_{50}$  of 20 nM in intact cells [245]. Erlotinib is capable of inhibiting Her-2 phosphorylation but at higher concentrations  $IC_{50}$  1  $\mu$ M [246].

Erlotinib was found to have a more favourable hazard ratio than gefitinib and has improved median survival of never-smoker patients in combination with chemotherapy (23 months) over chemotherapy and placebo (10 months) [240]. *Pao et al.*, strongly correlated the mutations with never-smoking patients with adenocarcinoma histology, usually with bronchioalveolar carcinoma features and sensitivity to erlotinib as well as to gefitinib [242]. In a phase II trial of erlotinib in bronchioalveolar carcinomas, it achieved 48% response rates in never smoking patients versus 18% in smokers. This has prompted the initiation of a neo-adjuvant erlotinib trial in combination with docetaxel and cisplatin in operable NSCLC [240].

### ***Lapatinib***

Lapatinib (Tykerb ®, GW2016) is the first dual EGFR and Her-2 inhibitor and is currently in phase III clinical trials in breast cancer [247]. Lapatinib is a potent inhibitor of the tyrosine kinase domains of both c-ErbB family members with IC<sub>50</sub> values against purified EGFR and Her-2 of 10.2 and 9.8 nM, respectively [248]. It has shown biologic and clinical activity in EGFR and/or Her-2- overexpressing tumors [249]. Lapatinib-bound EGFR has a unique structure compared to erlotinib-bound EGFR and lapatinib has a slower off-rate of dissociation from EGFR than erlotinib or gefitinib, producing a longer lasting effect on EGFR phosphorylation [250]. Lapatinib is being studied primarily in breast cancer. A phase III trial of lapatinib in combination with capecitabine *versus* capecitabine alone in Her-2 over-expressing refractory advanced or metastatic breast cancer was stopped after the interim analysis such was the favourable increase in median time to progression (8.5 months vs. 4.5 months) [232].

### **1.5.6 TKIs and ABC transporters**

The ability of gefitinib to interact with members of the ABC family of transporters is well established [107], [108], [251], [252]. Studies of gefitinib using *in vitro* assay systems found that gefitinib is most likely a transported substrate of P-gp but an inhibitor of MRP-1 [251]. Gefitinib has been shown to moderately reverse the P-gp-

mediated resistance to paclitaxel and docetaxel in P-gp over-expressing cells [107]. Data suggest that gefitinib is a transported substrate of BCRP at low physiological levels but may act as an inhibitor at higher concentrations [253]. Gefitinib has reversed resistance to topotecan and mitoxantrone in BCRP-over-expressing cell lines [108], [252]. Gefitinib affinity towards BCRP is ten times higher than that for P-gp [251]. Evidence is available from cell transfection studies that erlotinib is also a BCRP substrate [254]. The interaction of erlotinib and lapatinib with other ABC transporters has not been reported.

Modulation of ABC transporters by TKIs has a number of important pharmacokinetic implications for co-administration of ABC protein cytotoxic drugs and TKIs. Inhibition of ABC proteins involved in the absorption and excretion of drugs could lead to increased exposure levels and reduced clearance levels. This can be exploited to increase oral availability of ABC substrate drugs as demonstrated by the increase in the oral bioavailability of BCRP substrate, irinotecan effected by gefitinib in mice [255]. Elevated systemic levels of chemotherapeutic agents could also lead to increased toxicity levels that have to be compensated for by reduction in dosing levels.

The interactions of TKIs with BCRP in particular are further complicated by the existence of more than 40 naturally occurring single-nucleotide polymorphisms (SNPs) in BCRP [182]. HEK293 cells transfected with BCRP containing one of these SNPs, C241A (Q141K), had impaired ability to transport gefitinib and erlotinib [256]. The frequency of this particular allele was also found to vary between ethnic populations with 46% of the Japanese population found to be carriers, with levels in Caucasians averaging 10% and sub-Saharan Africans 1% meaning genotype may influence chemotherapeutic outcome [182].

The ability of TKIs to modulate the major ABC proteins involved in MDR may also signify a role for TKIs in the circumvention of multi-drug resistance in tumours.

This project was undertaken to look at the resistance to docetaxel mediated by transport proteins in NSCLC cell lines. The mechanism of docetaxel uptake in cancer is a poorly studied subject. A docetaxel uptake mechanism, active or passive, could be an important determinant of the sensitivity of tumour cells to this agent. The P-gp-mediated cellular efflux of docetaxel, and many other chemotherapy drugs, greatly

reduces the efficacy of these cytotoxics. The identification of novel, effective and low toxicity compounds to overcome P-gp-mediated drug resistance is a major goal in cancer research. The ability of TKIs, gefitinib, erlotinib and lapatinib to fulfill such a role has not been fully assessed to date.

## **1.6 Aims of the thesis**

The aims of this thesis were to:

- A)** Examine docetaxel uptake in NSCLC cell lines to determine if it is carrier mediated, and if so, if it is active or passive in nature.
  
- B)**
  - (i) Examine the potential of the tyrosine kinase inhibitors, lapatinib, gefitinib and erlotinib, as modulators of P-gp-mediated docetaxel efflux in NSCLC cell lines.
  
  - (ii) Examine the interaction of lapatinib with BCRP and MRP-1.
  
  - (iii) Examine any link between TKI inhibition of EGFR and P-gp expression levels.

## ***Chapter 2. Materials and Methods***

## **2.1 Ultrapure Water**

Ultrapure water, (UHP) was used for the preparation of all media and solutions. This water was purified to a standard of 12-18 M $\Omega$  / cm resistance by a reverse osmosis system (Millipore Milli-RO 10 Plus, Elgastat UHP).

## **2.2 Glassware**

The solutions utilised in the various stages of cell culture were stored in sterile glass bottles. All sterile bottles and other glassware required for cell culture related applications were prepared as follows: glassware and lids were soaked in a 2% solution of RBS-25 (AGB Scientific) for 1 hour. They were cleaned and rinsed in tap water. The glassware was then washed in an industrial dishwasher, using Neodisher detergent and rinsed twice with UHP. The materials were finally sterilised by autoclaving as described in Section 2.3.

## **2.3 Sterilisation Procedures**

All thermostable solutions, water and glassware were sterilised by autoclaving at 121<sup>0</sup>C for 20 minutes at 15 p.s.i.. Thermolabile solutions were filtered through 0.22  $\mu$ m sterile filters (Millipore, Millex-GV SLGV025BS). Large volumes, (up to 10 litres) of thermolabile solutions were filter sterilised through a micro-culture bell filter (Gelman, 12158).

## **2.4 Preparation of cell culture media**

The basal media used for cell culture were prepared as follows: 10X medium was added to sterile UHP water, buffered with HEPES (N-(2-Hydroxyethyl) piperazine-N-(2-ethanesulfonic acid)) and NaHCO<sub>3</sub> as required and adjusted to pH 7.5 using sterile 1.5 N NaOH or 1.5 N HCL. The media was then filtered through sterile 0.22  $\mu$ m bell filters (Gelman, 12158) and stored in sterile 500 ml bottles at 4°C. Sterility checks were performed on each bottle of media by inoculating samples of the media on to Colombia blood agar plates (Oxoid, CM217), Thioglycollate broths (Oxoid, CM173)

and Sabouraud dextrose (Oxoid, CM217) and incubating the plates at 37<sup>0</sup>C and 25<sup>0</sup>C. These tests facilitated the detection of bacteria, fungus and yeast contamination.

Basal medium was then stored at 4<sup>0</sup>C for up to three months. The HEPES buffer was prepared by dissolving 23.8 g HEPES in 80 ml UHP water and this solution was sterilised by autoclaving. 5 ml of sterile 5N NaOH was then added to give a final volume of 100 ml. NaHCO<sub>3</sub> was prepared by dissolving 7.5 g in 100 ml UHP water followed by autoclaving. Complete media was then prepared as follows: supplements of 2 mM L-glutamine (Gibco, 11140-0350) and 5% foetal calf serum (Sigma, F-7524) were, in the majority of cases, added to volumes of 100 ml basal media. 1ml 100X non-essential amino acids (Gibco, 11140-035) and 100 mM sodium pyruvate (Gibco, 11360-035) were also added to MEM. Complete media were maintained at 4<sup>0</sup>C for a maximum of 1 week.

## **2.5 Cells and Cell Culture**

All cell culture work was carried out in a class II laminar air-flow cabinet. All experiments involving cytotoxic compounds were conducted in a cytogard laminar air-flow cabinet (Gelman Sciences, CG series). Before and after use the laminar air-flow cabinet was cleaned with 70% industrial methylated spirits (IMS). Any items brought into the cabinet were also cleaned with IMS. At any time, only one cell line was used in the cabinet and upon completion of work with any given cell line the cabinet was allowed to clear for at least 15 minutes so as to eliminate any possibilities of cross- contamination between the various cell lines. The cabinet was cleaned weekly with industrial disinfectants (Virkon or TEGO) and these disinfectants were alternated every month. Details pertaining to the cell lines used for the experiments detailed in this thesis are provided in Table 2.5.1. All cells were incubated at 37<sup>0</sup>C and, where required, in an atmosphere of 5% CO<sub>2</sub>. Cells were fed with fresh media or subcultured (see section 2.5.1) every 2-3 days in order to maintain active cell growth. All of the cell lines listed in Table 2.5.1, except for HL-60 and HL60-ADR, are adherent cell lines. HL-60 and HL60ADR cells were grown in suspension in vented 75cm<sup>2</sup> flasks (Costar, 3276) at 37<sup>0</sup>C in an atmosphere of 5% CO<sub>2</sub> in RPMI 1640 media (Gibco, 52400-025) containing 10 % serum.

### **2.5.1 Subculturing of cell lines**

The waste cell culture medium was removed from the tissue culture flask and discarded into a sterile bottle. The flask was then rinsed out with 1 ml of trypsin/EDTA solution (0.25% trypsin (Gibco, 043-05090), 0.01% EDTA (Sigma, E9884) solution in PBS (Oxoid, BRI4a)) to ensure the removal of any residual media. 5 ml of trypsin was added to the flask, which was then incubated at 37<sup>0</sup>C, for approximately 5 minutes, until all of the cells detached from the inside surface of the flask. The trypsin was neutralised by adding an equal volume of complete media to the flask. The cell suspension was removed from the flask and placed in a sterile universal container (Sterilin, 128a) and centrifuged at 1000 r.p.m. for 5 minutes. The supernatant was then discarded from the universal and the pellet was suspended in complete medium. A cell count was performed and an aliquot of cells was used to reseed a flask at the required density. Medium requirements for each cell line used in the project are given in Table 2.5.1.1.

**Table 2.5.1.1** Description, medium requirements and source of cell lines. ATCC = American Tissue Culture Collection, NCTCC = National Cell and Tissue Culture Centre and ECACC= European Collection of Cell Cultures

Cell line	Medium	FCS(%)	Cell type	Source
A549	DMEM/Ham's F12 1:1	5	Human lung adenocarcinoma NSCLC cell line	ATCC
A549-Taxol	DMEM/Ham's F12 1:1	5	Taxol-resistant variant of A549 selected by Dr. Laura Breen	NCTCC
DLKP	DMEM/Ham's F12 1:1	5	Human lung squamous carcinoma NSCLC	NCTCC
DLKP-A	DMEM/Ham's F12 1:1	5	Adriamycin-resistant variant of DLKP selected by Alice Redmond	NCTCC
DLKP-TXT	DMEM/Ham's F12 1:1	5	Taxotere-resistant variant of DLKP selected by Dr. Yizheng Liang	NCTCC
DLKP- Mitox	DMEM/Ham's F12 1:1	5	Mitoxantrone-resistant variant of DLKP selected by Dr. Yizheng Liang	NCTCC
DMS 53	RPMI 1640	10	Human lung SCLC cell line	ECACC
DMS-Taxol	RPMI 1640	10	Taxol-resistant variant of DMS-53 selected by Dr. Lisa Murphy	NCTCC
DMS- Taxotere	RPMI 1640	10	Taxotere-resistant variant of DMS- 53 selected by Dr. Lisa Murphy	NCTCC
HL-60	RPMI 1640	10	Human leukemic cell line	Melvin Centre, KSU
HL-60ADR	RPMI 1640	10	Adriamycin-resistant variant of HL- 60	Melvin Centre, KSU
SK-MES-1	MEM	10	Squamous cell lung carcinoma cell line	ATCC
SK-Taxol	MEM	10	Taxol-resistant variant of SK-MES- 1 selected by Dr. Lisa Murphy	NCTCC
SK-Taxotere	MEM	10	Taxotere-resistant variant of SK- MES-1 selected by Dr. Lisa Murphy	NCTCC

### **2.5.2 Assessment of cell number and viability**

Cells were trypsinised, pelleted and resuspended in medium. An aliquot of the cell suspension was then added to trypan blue (Gibco, 525) at a ratio of 5:1.

The mixture was incubated for 3 minutes at room temperature. A 10  $\mu$ l aliquot of the mixture was then applied to the chamber of a glass coverslip enclosed haemocytometer.

Cells in the 16 squares of the four grids of the chamber were counted. The average cell numbers per 16 squares were multiplied by a factor of  $10^4$  and the relevant dilution factor to determine the number of cells per ml in the original cell suspension.

Non-viable cells stained blue, while viable cells excluded the trypan blue dye as their membrane remained intact, and remained unstained. On this basis, % viability could be calculated.

### **2.5.3 Cryopreservation of cells**

Cells for cryopreservation were harvested in the log phase of growth and counted as described in Section 2.5.2.

Cell pellets were resuspended in a suitable volume of serum. An equal volume of a 10 % DMSO/serum solution was added dropwise to the cell suspension resulting in a final DMSO concentration of 5%.

A total volume of 1ml of this suspension (which should contain approximately  $7 \times 10^6$  cells) was then placed in cryovials (Greiner, 122278).

These vials were then placed in the vapour phase of a liquid nitrogen container, which was equivalent to a temperature of  $-80^{\circ}\text{C}$ .

After a period of three hours, vials were removed from the vapour phase and transferred to the liquid phase for storage ( $-196^{\circ}\text{C}$ ).

#### **2.5.4 Thawing of cryopreserved cells**

A volume of 9 ml of fresh growth medium was added to a sterile universal. The cryopreserved cells were removed from the liquid nitrogen and rapidly thawed at 37<sup>0</sup>C. The cells were removed from the vials and transferred to the aliquoted media.

The resulting cell suspension was centrifuged at 1,000 r.p.m. for 5 minutes. The supernatant was removed and the pellet resuspended in fresh culture medium.

An assessment of cell viability on thawing was carried out (Section 2.5.2).

Thawed cells were then added to an appropriately sized tissue culture flask with a suitable volume of growth medium and allowed to attach overnight.

#### **2.5.5 Monitoring of sterility of cell culture solutions**

Sterility testing was performed in the case of all cell culture media and cell culture-related solutions. Samples of prepared basal media were inoculated on to Columbia blood agar plates (Oxoid, CM331), thioglycollate broths (Oxoid, CM173) and Sabouraud dextrose (Oxoid, CM217) and the plates incubated at 37<sup>0</sup>C and 25<sup>0</sup>C. These tests facilitated the detection of bacteria, fungus and yeast contamination. Complete cell culture media were sterility tested at least four days prior to use, using Columbia blood agar.

#### **2.5.6 Serum batch testing**

Batch to batch variation of FCS can result in alterations to cell growth characteristics. In extreme cases this may result in a lack of cell growth or retarded cell growth in more moderate cases. To minimise the impact of FCS inter-batch variability, growth of the cell lines in a range of FCS samples was screened. The FCS most suitable for each cell line was then purchased in bulk to maintain continuity of cell culture conditions. The screening process involved a comparison of the growth of cells in each FCS sample as a percentage of growth of serum with known acceptable growth rate. Logarithmically growing cells were seeded in a 96-well plate (Costar; 3599)

from a single cell suspension at a density of  $10^3$  cells/well in 100  $\mu$ l of medium without FCS. 100  $\mu$ l volumes of medium containing 10% or 20% FCS was added to the 96-well plate, resulting in final dilutions of the FCS to 5% or 10%, respectively. One column of each plate provided a control containing FCS with a known acceptable growth rate. Plates were placed at 37°C in 5% CO<sub>2</sub>, for 5 days, after which growth was assessed by the acid phosphatase method, see Section 2.7.2.

## **2.6 *Mycoplasma* analysis of cell lines**

Cell lines were tested for possible *Mycoplasma* contamination every three months approximately. The protocol used is detailed in the following Sections 2.6.1 and 2.6.2.

### **2.6.1 Indirect staining procedure for *Mycoplasma* analysis**

*Mycoplasma* negative NRK (normal rat kidney fibroblast) cells were used as indicator cells for this analysis. The cells were incubated with a sample volume of supernatant from the cell lines in question and then examined for *Mycoplasma* contamination. A fluorescent Hoechst stain was used in this analysis. The stain binds specifically to DNA and so stains the nucleus of the cell in addition to any *Mycoplasma* present. *Mycoplasma* infection was indicated by fluorescent bodies in the cytoplasm of the NRK cells.

### **2.6.2 Direct culture procedure for *Mycoplasma* analysis**

Direct staining for *Mycoplasma* analysis involved inoculating samples on to a *Mycoplasma* culture broth (Oxoid, CM403). This was supplemented with 16% serum, 0.002% DNA (BDH, 42026), 2  $\mu$ g/ml fungizone (Gibco, 042 05920),  $2 \times 10^3$  units penicillin (Sigma, Pen-3) and 10 ml of a 25% yeast extract solution. Incubation was carried out at 37°C for a period of 48 hours. Samples of this broth were then streaked onto plates of *Mycoplasma* agar base (Oxoid, CM401), which had been supplemented as described above. The plates were incubated for three weeks at 37°C while exposed to CO<sub>2</sub>. The plates were examined microscopically every 7 days. The appearance of small oval shaped colonies indicated the presence of *Mycoplasma* infection.

## **2.7 Miniaturised *in vitro* proliferation assays**

### **2.7.1 *In-vitro* proliferation assay experimental procedure**

Cells in the exponential phase of growth were harvested by trypsinisation as described in Section 2.5.1.

Cell suspensions containing  $1 \times 10^4$  cells/ml were prepared in cell culture medium. Volumes of 100  $\mu$ l/well of these cell suspensions were added to 96-well plates (Costar, 3599) using a multichannel pipette. Plates were agitated gently in order to ensure even dispersion of cells over a given well. Cells were then incubated overnight at 37°C in an atmosphere containing 5% CO<sub>2</sub>.

For IC<sub>50</sub> determinations drug dilutions were prepared at 2X their final concentration in cell culture medium and 100  $\mu$ l volumes of the drug dilutions were added to each well using a multichannel pipette. For combination assays 50  $\mu$ l of the two compounds to be examined were added at a 4X concentration. Plates were then mixed gently.

Cells were incubated for a further 6 days at 37°C and 5% CO<sub>2</sub>. At this point the control wells would have reached approximately 80-90% confluency.

Assessment of cell survival in the presence of drug was determined by the acid phosphatase assay (Section 2.7.2). The concentration of drug which inhibited 50% of cell growth (IC<sub>50</sub> of the drug) was determined from a plot of the % survival (relative to the control cells) versus cytotoxic drug concentration using the Calcsyn ® software package.

**Table 2.7.1** The drugs used in this thesis and their sources.

<b>Drug</b>	<b>MW (g/mol)</b>	<b>Source</b>
Sulindac	356.4	Sigma
Sulindac sulfide	340.4	Sigma
Elacridar (GF120918)	600.1	GSK
Gefitinib	446.9	Sequoia Chemicals
Erlotinib (HCl)	429.9	Sequoia Chemicals
Lapatinib (Ditosylate Monohydrate)	943.5	GSK
Epirubicin*	579.9	SVUH
Adriamycin (Doxorubicin)*	543.5	SVUH
Paclitaxel (Taxol)*	853.9	SVUH
Docetaxel (Taxotere)*	807.8	SVUH
Vincristine* (sulfate)	923.1	SVUH
Oregon-green paclitaxel	1319.3	Molecular Probes
[ <sup>14</sup> C] docetaxel	807.8	American Radiolabelled Chemicals
Cisplatin*	300.1	SVUH
MK571	537.1	Calbiochem
Mitoxantrone*	517.4	SVUH
Verapamil	491.1	Sigma

\* = Clinical formulation

### **2.7.2 Assessment of cell number - Acid Phosphatase assay**

Following the incubation period of 6 days, media was removed from the plates.

Each well on the plate was washed with 100  $\mu$ l PBS. This was then removed and 100  $\mu$ l of freshly prepared phosphatase substrate (10 mM *p*-nitrophenol phosphate (Sigma 104-0) in 0.1 M sodium acetate (Sigma, S8625), 0.1% triton X-100 (BDH, 30632), pH 5.5) was added to each well.

The plates were incubated in the dark at 37<sup>0</sup>C for 2 hours.

The enzymatic reaction was stopped by the addition of 50  $\mu$ l of 1N NaOH.

The plate was read in a dual beam plate reader at 405 nm with a reference wavelength of 620 nm.

### **2.7.3 Assessment of cell number - XTT assay**

The XTT Assay is a non-radioactive means to measure cell viability in non-adherent cell lines. It is based on the fact that viable cells cleave the yellow tetrazolium salt XTT to form an orange formazan dye. Reading with a spectrophotometer then determines differences in cell survival.

75  $\mu$ l of non-adherent cells are seeded at 5 X 10<sup>4</sup> cells/ml in a 96-well plate.

24 hours later, 75  $\mu$ l of drug containing media is added at 2X concentrations to each well for IC<sub>50</sub> determinations. For combination assays using two drugs, drugs are plated at 4X concentrations with 37  $\mu$ l of each drug dilution being added. Every well should contain 150  $\mu$ l.

After 48 hours, 75  $\mu$ l of the XTT labelling mixture is added to each well.

This mixture consists of 5 ml XTT labelling reagent and 100  $\mu$ l of the electron-coupling reagent.

Following 24 hours, the plates are read @ 460 nm on a spectrophotometer.

#### **2.7.4 Proliferation assays examining docetaxel accumulation assay conditions**

Cells were trypsinised from the flask in the exponential phase of growth as described in Section 2.5.1.

Cell suspensions containing  $1 \times 10^4$  cells/ml were prepared in cell culture medium. Volumes of 100  $\mu$ l/well of this cell suspension were added into 96-well plates (Costar, 3599) using a multichannel pipette. Plates were agitated gently in order to ensure even dispersion of cells over a given well. Cells were then incubated overnight at 37°C in an atmosphere containing 5% CO<sub>2</sub>.

The plates were removed from the incubator and the media was removed from each well. Cells were incubated with either verapamil or docetaxel alone or in combination for 90 minutes at 37°C in an atmosphere containing 5% CO<sub>2</sub>.

Following the 90 minute incubation, the media was removed from each plate and each well was washed twice with 100  $\mu$ l warm PBS.

Cells were incubated for a further 6 days at 37°C in an atmosphere containing 5% CO<sub>2</sub>. At this point the control wells would have reached approximately 80-90% confluency. Cell number was assessed using the acid phosphatase assay (Section 2.7.2).

#### **2.7.5 Statistical Evaluation**

Experimental *in vitro* data are presented as a mean  $\pm$  S.D. from three experiments. Levels of significance from these data were calculated using student's *t* test (two-tailed) (Excel®, Microsoft). A p-value of less than 0.05 was considered significant in all statistical testing.

## 2.8 Protein Extraction and Quantification

### 2.8.1 Protein Extraction

Cells were seeded at  $0.5 - 1 \times 10^6$  cells per petridish in 10 ml of medium.

Cells were grown to 80% confluency and fed every 2-3 days if necessary.

Medium was removed and the cells washed with cold PBS, making sure that as little of the PBS as possible was left in the petri-dish.

500  $\mu$ l cold RIPA buffer (R0278, Sigma), 10X protease inhibitors (P2714, Sigma) (50 $\mu$ l per 500  $\mu$ l of buffer) and 100X PMSF (Sigma) (2.5  $\mu$ l per 500  $\mu$ l buffer) were added to the cells.

Following 20 minutes incubation on ice, the lysed cells were removed using a cell scraper if necessary and transferred to a sterile eppendorf.

The sample was passed through a 21-gauge needle a number of times to shear DNA.

The samples were then centrifuged at 14,000 r.p.m. for 5 minutes at 4<sup>0</sup>C.

The resulting supernatant was transferred to sterile eppendorfs in 100  $\mu$ l aliquots and stored at - 20<sup>0</sup>C. Protein concentration was then determined using the BCA assay (Pierce, Cat# 23227).

NOTE: Once the lysis buffer was added to the cells, all steps were carried out on ice.

#### **RIPA Buffer Components:**

150 mM NaCL

1% Igepal CA-630

0.5% sodium deoxycholate

0.1% SDS

50 mM Tris, pH 8.0

#### **Protease inhibitors (10X):**

20 mM AEBSF

10 mM EDTA

1.3 mM Bestatin

140  $\mu$ M E-64

10  $\mu$ M Leupeptin

3  $\mu$ M Aprotinin

## 2.8.2 Protein Quantification

Protein concentration of samples was determined using the BCA assay kit (Pierce Cat# 23227).

The Pierce BCA protein assay is a detergent-compatible formulation based on bicinchoninic acid (BCA) for the colorimetric detection and quantitation of total protein. The method combines the reduction reaction of  $\text{Cu}^{+2}$  to  $\text{Cu}^{+1}$  by protein in an alkaline medium (the Biuret reaction) with highly sensitive and selective colorimetric detection of the cuprous cation ( $\text{Cu}^{+1}$ ) using a reagent containing bicinchoninic acid. The purple coloured reaction product of this assay is formed by the chelation of two molecules of BCA with one cuprous ion. The water-soluble complex exhibits a strong absorbance at 562 nm that is close to linear with increasing protein concentration over a broad working range (20 -2000  $\mu\text{g/ml}$ ).

### **Assay procedure:**

A 2 mg/ml bovine serum albumin (BSA) solution was prepared freshly in protease inhibitor. A protein standard curve was prepared from the BSA stock with dilutions made in protease inhibitor.

The working reagent was prepared by mixing 50 parts of BCA reagent A with 1 part of BCA reagent B. 200  $\mu\text{l}$  of working reagent is required for each well of a 96-well plate used.

25  $\mu\text{l}$  of each standard or unknown sample was pipetted in duplicate onto a 96-well plate. 200  $\mu\text{l}$  of working reagent was added to each well and the plate was mixed thoroughly on a plate shaker for 30 seconds.

The plate was covered and incubated at  $37^{\circ}\text{C}$  for 30 minutes and absorbance was read at 562 nm.

The average 562 nm absorbance of the blank was subtracted from the 562 nm measurements of all other individual standard and unknown replicates

A standard curve was prepared by plotting the average blank corrected 562 nm absorbance for each BSA standard versus its concentration in  $\mu\text{g/ml}$ . The standard curve was then used to determine the protein concentration of each unknown sample.

## 2.9 Western Blotting

### 2.9.1 Gel electrophoresis

Proteins for analysis by Western blotting were resolved using SDS-polyacrylamide gel electrophoresis (SDS-PAGE).

Component	7.5% Gel	10% Gel	Stacking Gel
Acrylamide/bis-acrylamide 30% solution (Sigma A-3574)	3.8 ml	5.07 ml	840 $\mu$ l
Ultra Pure Water	7.3 ml	5.94 ml	2.84 ml
1.5M Tris/HCl buffer pH 8.8 (Biorad 161-0977)	3.75 ml	3.75 ml	N/A
0.5M Tris/HCl Buffer pH 6.8 (Biorad 161-0978)	N/A	N/A	1.25ml
SDS solution 10% (w/v) (Biorad 161-0416)	150 $\mu$ l	150 $\mu$ l	50 $\mu$ l
Ammonium persulphate 10% solution (Sigma A-3678)	60 $\mu$ l	60 $\mu$ l	20 $\mu$ l
TEMED (Sigma T-9281)	10 $\mu$ l	10 $\mu$ l	5 $\mu$ l

**Table 2.9.1.1:** Preparation protocol for SDS-PAGE gels (2 x 0.75 mm gels).

A running gel of required % was prepared according to Table 2.9.1.1.

The running gel was poured gently into a gel cassette and overlaid with a layer of isopropanol.

The gel was allowed to set for approximately 1 hour at room temperature.

A stacking gel was prepared according to Table 2.9.1.1.

The isopropanol was removed from the running gel and the stacking gel poured. A comb was inserted and the stacking gel was allowed to set for an hour. The gel rig was assembled and the tank filled with 1X SDS running buffer. The gel cassette was inserted in the rig and the well comb removed. The wells were washed with running

buffer Samples were loaded and the gel was run at a constant voltage of 100-150V for approximately 90 minutes or until the dye was about 80% of the way down the gel.

### **2.9.2 EGFR**

A 7.5% running gel and stacking gel was prepared as in Section 2.9.1.

Using the data obtained from the protein quantification step, protein samples were prepared with 10-30 µg protein in 15 µl plus 15 µl loading buffer (Sigma S-3401)). Samples were denatured by heating at 95<sup>0</sup>C for 5 minutes then centrifuged briefly and loaded with 30 µl of each sample including 5 µl of standards and molecular weight markers (New England Biolabs P-7708S).

### **2.9.3 P-gp/MRP-1**

A 10% running gel and a stacking gel were prepared as in Section 2.9.1. Protein samples were prepared with 25-50 µg protein in 15 µl plus 15 µl of 2X loading buffer. Positive controls were included by including 25 µg of P-gp-positive control cell extract or 50 µg MRP-1 positive control cell extract. Samples were **NOT** denatured. The gel cassette was inserted in the rig and the well comb removed. The wells were washed with running buffer and loaded with 30 µl of each sample including 5 µl of pre-stained standards and molecular weight markers (New England Biolabs P-7708S). Gel was run as in Section 2.9.1.

## 2.9.4 Blotting protocol

Once electrophoresis was completed, the gel cassette removed from the tank. The glass plates were carefully separated and the stacking gel removed. The gel, PVDF membrane (Boehringer Mannheim, 1722 026)) were equilibrated in transfer buffer (Biorad 161-0734) for 5-10 minutes.

12 pieces of 3 mm filter paper (Whatman) were also soaked in 1X transfer buffer.

The components were then arranged as follows on the cathode of the semi-dry blotter (Bio-Rad): 6 pieces of filter paper, PVDF membrane, gel and the remaining 6 pieces of filter paper. The stack was then rolled gently to remove any air bubbles that would affect transfer.

Protein transfer was carried out at 250 mA for 60 minutes. After completion of the transfer, the position of the standards was marked and the transfer stack disassembled. The transfer process was verified by treating the PVDF membrane with 1% Ponceau solution for approximately 1 minute. Ponceau was then removed through rinsing in water.

The membrane was incubated in 10 ml of blocking solution (5% Marvel) for 2 hours at room temperature. On removal of the blocking solution, the blot was incubated in 10 ml of TBS (Sigma T5912) containing 1% Marvel and primary antibody overnight at 4<sup>0</sup>C on an agitator (Table 2.9.4.1). Primary antibody was removed and three 10 minute washes in 1X TBS containing 0.5% Tween (Sigma, P7949) were carried out at room temperature while shaking.

**Table 2.9.4.1**

Antibody	Cat #	Dilution	Storage
EGFR (Ab-12)	Lab-Vision-MS-400	1:1000	4 <sup>0</sup> C
<i>P-gp (MDR-1 G-1)</i>	<i>Santa Cruz SC-13131 mouse monoclonal</i>	<i>1:200</i>	<i>4<sup>0</sup>C</i>

Secondary antibody (1 in 1000 dilution of anti-mouse IgG peroxidase conjugate (Dako, P0447) in TBS) was then applied for 1 hour at room temperature with agitation. A further three 10 minute washes in 1X TBS-Tween were carried out while shaking.

### **2.9.5 Enhanced chemiluminescence detection**

Note: This procedure was carried out in a darkroom.

The Blot was incubated in ECL solution (Amersham, RPN2109) (1.5 ml solution A + 1.5 ml solution B) to detect bound peroxidase-conjugated secondary antibody for 1 minute.

The membrane was then placed under a sheet of transparent film in a cassette, ensuring all air bubbles were removed.

A sheet of X-ray film (Kodak, X-OMATS) was placed over the membrane and exposed for 5-15 minutes (depending on the signal).

The exposed autoradiographic film was developed for 3 minutes in developer (Kodak, LX-24) then washed in water for 15 seconds and transferred to a fixative (Kodak, FX-40) for 5 minutes.

The film was washed with water for 5-10 minutes and left to dry at room temperature.

The membrane was exposed for a longer or shorter time based on initial signal.

### **2.10 Immunoprecipitation**

500 µg of protein lysate was added to ~ 700-800 µl RIPA buffer, ~900 µl in total in eppendorfs.

3 µg of EGFR IP antibody (EGFR Ab-15 (Neomarkers, MS-665-P)) was then added to each tube and mixed thoroughly by pipetting. Samples are then shaken at 4<sup>0</sup>C for 30 minutes.

50 µl of protein G-agarose beads were added to each tube and mixed thoroughly. Tubes were mixed overnight on a blood mixer at 4<sup>0</sup>C overnight.

Samples were centrifuged at maximum speed for 25 seconds to pellet the protein/bead complex. The majority of the supernatant was aspirated leaving ~ 5 µl. Pellets were

washed with ~ 500-600  $\mu$ l wash buffer (1X cell lysis buffer prepared from 10X cell lysis buffer (Cell Signalling cat #9803) with added 1X PI cocktail, 1X PMSF and 1X sodium orthovanadate) and mixed by inverting 5 times. Samples were centrifuged at maximum speed for 25 seconds and the supernatant removed. The wash step was repeated twice.

The last centrifugation lasted 35 seconds and as much supernatant as possible was removed. 50  $\mu$ l 1.2X sample buffer was added to each sample, followed by a vortex to mix.

The samples were then denatured at 95<sup>0</sup>C for 5 minutes. Samples were stored at -20<sup>0</sup>C and run on gels according to Section 2.9.1.

## **2.11 Laser Scanning Confocal Microscopy (LSCM)**

LSCM was carried out in conjunction with Dr. Finbarr O'Sullivan. Cells were seeded at 1 X 10<sup>5</sup> cells/well on glass coverslip chamber slides (NUNC) 24 hours prior to the experiment and cultured at 37°C and 5% CO<sub>2</sub>. Medium was removed and for epirubicin studies, cells were exposed to 2  $\mu$ M epirubicin alone or in combination with test compound for 120 minutes. Cells containing drug were examined by confocal laser scanning microscopy using a Leica TCS AOBS.

A spectral scan was performed to obtain the optimum excitation and emission wavelengths. The spectral scan was performed for excitation at 458 nm, 476 nm, 488 nm, 496 nm, 514 nm, and 543 nm. Spectral stacks were obtained with a 5 nm step size. Using the stack profile tool in the LSC software the intensity and spectral profile was obtained. Based on this data, epirubicin fluorescence was examined *in situ* by exciting at 514 nm and emitted light between 531-667 nm collected (Em(max) 600 nm).

For study of tubulin, cells were exposed to 1  $\mu$ M Oregon-green paclitaxel (Molecular Probes) for 120 or 180 minutes. Drug was then removed and replaced with medium. Oregon-green paclitaxel was excited at 493 nm with emission at 520 nm.

## **2.12 Time course treatments in A549-Taxol**

### **2.12.1 EGF treatments**

8 ml of a cell suspension containing  $5 \times 10^5$  cells per ml was plated in petridishes and incubated at  $37^{\circ}\text{C}$  for 24 hours. Medium was then removed and protein extracted from one of the petridishes according to the protocol in Section 2.8.1 as a T0 control. The petridishes were divided into four sets of three dishes. Each set of three received 8 ml of FCS-free medium or 10 ng/ml, 50 ng/ml or 100 ng/ml EGF in FCS-free medium and were incubated at  $37^{\circ}\text{C}$ . At 12, 24 and 48 hour timepoints, medium was removed from one of the petridishes in each group of concentrations and the cells washed in ice cold PBS. Protein was extracted according to Section 2.8.1. Samples were stored at  $-20^{\circ}\text{C}$ .

### **2.12.2 TKI treatments**

8 ml of a cell suspension containing  $5 \times 10^5$  cells per ml was plated in petridishes and incubated at  $37^{\circ}\text{C}$  for 24 hours. Medium was then removed and protein extracted from one of the petridishes according to the protocol in Section 2.8.1 as a T0 control. The petridishes were divided into five sets of three dishes. Each set of three dishes received 8 ml of medium, medium and 0.1% DMSO or 2.5, 5 or 10  $\mu\text{M}$  lapatinib/erlotinib (or medium and 0.2% DMSO or 5, 10 or 20  $\mu\text{M}$  gefitinib) and were incubated at  $37^{\circ}\text{C}$ . At 12, 24 and 48 hour timepoints, medium was removed from one of the petridishes in each group of three and the cells washed in ice cold PBS. Protein was extracted according to Section 2.8.1. Samples were stored at  $-20^{\circ}\text{C}$ .

## **2.13 HPLC-based taxane transport assays**

The optimum cell number for these assays was found to be a 75 cm<sup>2</sup> flask at 80% confluency or a final cell number of 3 X 10<sup>6</sup> cells. Each data point was carried out in triplicate flasks.

10 µM docetaxel or 10 µM paclitaxel were determined as the concentrations that gave a sufficient peak/reading through HPLC measurement.

### **2.13.1 Taxane accumulation assay in adherent cell lines**

Cells were seeded in 75 cm<sup>2</sup> flasks at 1 X 10<sup>5</sup> cells per ml in 10 ml of medium. The assay was carried out once the cells have reached 80% confluency (24-48 hours). The medium was removed and replaced with 37<sup>0</sup>C medium containing 10 µM docetaxel or 10 µM paclitaxel for 90 minutes. After incubation, the drug containing medium was removed and the cells were washed in cold PBS. After removal of the PBS, 3 ml trypsin was added to the flasks. When the cells had detached, 3 ml medium was added and the cells transferred to extraction tubes. Samples were then centrifuged at 1000 r.p.m. for 5 minutes. The supernatant was aspirated and 8 ml cold PBS added. 10 µl of each sample was taken for a cell count. Samples were again centrifuged at 1000 r.p.m. for 5 minutes. The supernatant was removed with as much as possible being removed using lint-free wipes. The resulting pellets were frozen and stored at -20<sup>0</sup>C for extraction.

### **2.13.2 Taxane accumulation profiles**

A set of three flasks was set up as in 2.1.1 for each of the timepoints to be examined. Cells were exposed to 10 µM docetaxel for 15, 45, 75, 105 and 135 minutes and the procedure described in 2.1.1 followed.

### **2.13.3 Taxane efflux profiles**

A set of three flasks was set up as in 2.1.1 for each of the timepoints to be examined. Cells were incubated with 10  $\mu\text{M}$  docetaxel for 90 minutes. After 90 minutes the drug containing medium was removed from the cells, the cells were washed with 37<sup>0</sup>C PBS and fresh 37<sup>0</sup>C medium applied. After 15, 45, 75, 105 and 135 minutes medium was removed from a set of three flasks and the cells washed in cold PBS. The cells were then trypsinised, washed and counted as in 2.1.1.

### **2.13.4 Taxane accumulation assays involving MDR modulators**

Cells were prepared as in 2.1.1. A set of three flasks was set up for each MDR modulator to be tested. These flasks were incubated with 10  $\mu\text{M}$  docetaxel or 10  $\mu\text{M}$  paclitaxel combined with each MDR modulator. A control containing 10  $\mu\text{M}$  docetaxel or 10  $\mu\text{M}$  paclitaxel alone was also carried out. The procedure in 2.1.1 was followed. The addition of drug to each set of flasks was staggered by 20 minutes to allow time for each set of flasks to be taken down.

### **2.13.5 Taxane accumulation assays in non-adherent cell lines**

Triplicate flasks containing 10ml of cell suspension with 1 X 10<sup>5</sup> cells per ml were set up as in 2.1.1. The assay commenced 48 hours after cells were seeded. To initiate the assay, a 10ml solution containing a 2X concentration of 10  $\mu\text{M}$  docetaxel or 10  $\mu\text{M}$  paclitaxel plus the compound to be examined was added to the flasks. A 2X concentration of 10  $\mu\text{M}$  docetaxel or 10  $\mu\text{M}$  paclitaxel alone was added to a set of flasks as a control. The addition of drug to each set of flasks was staggered by 20 minutes to allow time for each set of flasks to be taken down. After 90 minutes the cells were pipetted in to a 30 ml sterilin and centrifuged at 1000 r.p.m. for five minutes. The drug containing medium was aspirated and 10 ml cold PBS added to the cells and this suspension transferred to an extraction tube. The cells were centrifuged again and resuspended in 8 ml cold PBS. 10  $\mu\text{l}$  of this suspension was taken to

perform a cell count. Following centrifugation, the PBS was carefully removed and the pellets stored at  $-20^{\circ}\text{C}$  for extraction.

### **2.13.6 Taxane efflux assay in adherent cell lines**

Cells were seeded as described in 2.1.1. Once the cells reached 80% confluency (24-48 hours), the medium was aspirated and replaced with 10 ml pre-warmed  $10\ \mu\text{M}$  docetaxel or  $10\ \mu\text{M}$  paclitaxel and incubated for 90 minutes. The addition of drug to each set of flasks was staggered by 20 minutes to allow time for each set of flasks to be taken down. The drug containing medium is then removed. At this stage a set of control flasks were taken down for extraction. The remaining flasks were washed with pre-warmed PBS and incubated for a further 40 minutes in pre-warmed medium or a concentration of test compound. This medium is then removed and the procedure to produce a cell pellet for extraction as described in 2.1.1 is followed.

### **2.13.7 HPLC analysis of taxanes**

All reagents used were ultrapure and only HPLC-clean glassware and compatible plastics were used.

#### **2.13.7.1 Reagents used**

##### **HPLC mobile phase:**

600 ml of taxane mobile phase containing acetonitrile, 35 mM ammonium acetate buffer (pH 5) and THF (45:50:5) was carried out as follows as follows:

0.809 g of ammonium acetate was weighed out and transferred to a cleaned mobile phase bottle. 300 ml of water was then added and the pH adjusted to 5 with acetic acid.

270 ml of acetonitrile and 30 ml of THF were then added. Mobile phase was used within one week.

**Ammonium acetate buffer. pH 5.0 0.1M:**

To make 50 ml 0.0385 g of ammonium acetate was weighed out. Add 50 ml of water were added and the pH adjusted to 5 with acetic acid. The solution was aliquotted and kept frozen at -20<sup>0</sup>C.

**Internal standard (IS)**

A solution of 10 µg/ml paclitaxel (Taxol ®) or docetaxel (Taxotere ®) was prepared in methanol for each analysis. Docetaxel and paclitaxel can both be analysed by this method and since both give peaks on the HPLC, one is used as the internal standard for the other.

**2.13.8 HPLC extraction method for the taxanes**

The extraction process and HPLC method were adapted from Ciccolini *et al.*, 2001.

The frozen pellet of cells was thawed and resuspended in 200 µl of UHP water.

Each sample had 100 µl of internal standard (I.S.), 2 ml of ethyl acetate (using a glass pipette) and 100 µl of 0.1% formic acid added. The internal standard for docetaxel was 10 ng/ml paclitaxel made up in methanol and *vice versa* for taxol. The samples were mixed on a blood tube mixer for 5 minutes and then centrifuged at 4000 r.p.m. for a further 5 minutes. The samples separated into two layers, the top layer containing the extracted taxane.

The necessary number of glass autosampler tubes was labelled. A glass Pasteur pipette was used to remove approximately 1.1 ml to the appropriate autosampler tube. The autosampler tubes were then transferred to the evaporation apparatus that had already been pre-warmed to 40<sup>0</sup>C. A few drops of water were added into each of the evaporator wells to aid thermal transfer. The extraction solvents were evaporated with a stream of nitrogen gas. Once the solvents were completely evaporated, the autosampler tubes were covered with septae and plastic lids. The samples were then stored at -20<sup>0</sup>C until required for HPLC analysis.

### **2.13.9 Preparation of taxane HPLC standards.**

Standards and samples must be prepared at the same time using the same reagents.

A broad or narrow range of standards was prepared depending on the range of samples required. 100 µl of a solution of blank cells was added to an extraction tube.

All drug samples were made up at 10 X their final concentration in methanol. 100 µl of the 10 X drug concentration was transferred to duplicate extraction tubes already containing the 100 µl of cells. The usual broad range of standards used were 50, 250, 500, 1000, 2500, 5000 and 25000 ng/ml (10 X concentrations). 100 µl of I.S., 100 µl of 0.1% formic acid and 2 ml of ethyl acetate were added to each of the duplicate standard tubes. A control containing 100 µl UHP instead of a 10X concentration of drug and a blank that substituted 200 µl UHP for the I.S. and a 10X concentration of drug were also prepared.

### **2.13.10 HPLC analysis of the taxanes**

The HPLC analysis was carried out on a Beckman System Gold consisting of a 125 Solvent Module, a 166 Detector, a 508 Autosampler, a Prodigy reverse phase column (ODS3 100A 150 x 4.6mm 5 micron) (Phenomenex, UK) and analysed using the 32 Karat Software package. The mobile phase consisted of 0.809g ammonium acetate, pH 8.8 (acetic acid), 300 ml UHP, 270 ml acetonitrile and 30 ml THF and was prepared as in Section 2.13.7.1. The amount of mobile phase required was calculated from the number of samples, the flow rate and the analysis time per sample (10-15 minutes). When ready to analyse the samples, the HPLC was prepared in advance. Mobile phase was run at a flow rate of 1.8 ml/minute for approximately 20 minutes prior to the start of analysis. The UV detector was set to 227 nm.

A system check was performed by injecting a taxane sample in methanol and demonstrating a suitable peak around the expected retention time. A second injection of just mobile phase was run to washout any residue in the needle.

Once the system was ready, the autosampler vials were reconstituted with 80 µl of mobile phase and fully mixed. 50 µl of each sample was injected onto the column using the autosampler.

Analysis started with the standards from lowest concentration to highest, the extraction blank and the control (I.S.) should also be included at the start. A wash vial of mobile phase was inserted between the standards and the samples to avoid cross over.

## **2.14 HPLC-based epirubicin transport assays**

### **2.14.1 Epirubicin accumulation assays in adherent cell lines**

Cells were seeded into 25 cm<sup>2</sup> flasks (Costar, 3375) at 0.5 X 10<sup>6</sup> cells per flask. Cells were incubated for 48 hours, after which time medium was removed and fresh medium containing epirubicin (2 µM) or combinations of both epirubicin and compound of interest were added. Flasks were incubated at 37<sup>0</sup>C for a period of two hours.

### **2.14.2 Epirubicin efflux assays in adherent cell lines**

For efflux studies, the media was removed from all flasks and replaced with fresh media, or media containing test compound as the experiment required after the two-hour incubation. The flasks were returned to the 37<sup>0</sup>C incubator.

At relevant time points the media was removed from the flasks and the flasks washed twice with PBS. Cells were trypsinised as described in Section 2.5.1 and counted as described in Section 2.5.2. Pellets were washed with PBS and frozen at -20<sup>0</sup>C.

### **2.14.3 Quantification of epirubicin by HPLC**

#### **Reagents used:**

##### **Epirubicin mobile phase**

0.854 ml of formic acid was added to 400 ml of ultrapure water. The pH was brought to 3.2 using 1M ammonium formate. 200 ml of acetonitrile was added and the solution was mixed and left to settle for a few hours with the lid tightly closed.

##### **1M Ammonium Formate Buffer**

15.76 g of Formic acid ammonium salt was added to 200 ml of water in a volumetric flask. The pH was adjusted to 8.5 with concentrated ammonia. The volume of the solution was brought to 250 ml with ultra pure water. The solution was aliquoted into 20 ml stocks and frozen at  $-20^{\circ}\text{C}$  in order to keep it fresh.

##### **33% Silver Nitrate (w/v)**

3.3 g of silver nitrate powder was added to a 10 ml universal. Water was then added to the 10 ml mark. The universal was covered in tin foil, as it is light sensitive and kept frozen at  $-20^{\circ}\text{C}$ .

##### **Daunorubicin internal standard**

A 1  $\mu\text{g/ml}$  solution of daunorubicin was made in ultra pure water and covered in tin foil as it is light sensitive.

##### **Epirubicin standards**

Epirubicin standards were made in ultra pure water at 50, 250, 500, 1000, 2,500, 5,000, and 25,000 ng/ml. (these were 10 X concentrations).

### **2.14.4 Epirubicin extraction procedure**

The frozen pellets of cells were thawed and re-suspended in 200  $\mu\text{l}$  of ultra pure water. The cells were transferred to a polypropylene extraction tube. In the case of the epirubicin standards 100  $\mu\text{l}$  of blank cells were added to the extraction tubes. 100  $\mu\text{l}$  of the each 10 X epirubicin standard was added to duplicate tubes.

20 µl of silver nitrate solution, 100 µl of daunorubicin internal standard, 700 µl of ice-cold isopropanol, 100 µl of 1M ammonium formate buffer (pH 8.5) and 1400 µl of chloroform were added to each tube.

The tubes were mixed on a blood mixer for 5 minutes

Following centrifugation at 4000 r.p.m. for 5 minutes, the liquid clarified to two separate layers. The bottom organic layer contained the drug.

1.1 ml of the bottom layer from each tube was removed using a glass Pasteur pipette to an auto sampler tube.

An evaporation apparatus was set up and pre-warmed to 40°C. A few drops of water were added into each evaporating well.

The auto sampling vials were placed into the evaporating wells.

The liquid in each auto sampling tube was evaporated with a stream of nitrogen gas.

When all liquid had evaporated the vials were covered with septae and lids and frozen at -20°C.

#### **2.14.5 Preparation of epirubicin HPLC standards.**

100 µl of a solution of blank cells was added to duplicate extraction tubes. 100 µl of the each 10 X epirubicin standard was added to the tubes containing the 100 µl of cells.

The usual range of standards used were 50, 250, 500, 1000, 2500, 5000 and 25000 ng/ml (10 X concentrations). 20 µl of silver nitrate solution, 100 µl of daunorubicin internal standard, 700 µl of ice-cold isopropanol, 100 µl of 1M ammonium formate buffer (pH 8.5) and 1400 µl of chloroform were added to each tube.

The tubes were mixed on a blood mixer for 5 minutes

Following centrifugation at 4000 r.p.m. for 5 minutes, the liquid clarified in to two separate layers, the bottom layer containing the drug.

A control containing 100 µl UHP instead of a 10 X concentration of drug and a blank that substituted 200 µl UHP for the I.S. and a 10 X concentration of drug were also prepared.

#### **2.14.6 HPLC analysis of epirubicin.**

The HPLC was left at a flow rate of 0.5 ml/minute of mobile phase (see Section 2.14.3.1), flowing over a Prodigy reverse phase column (ODS3 100A, 150 × 4.60 mm, 5 micron) (Phenomemex, UK) for 20 minutes prior to beginning analysis.

The same Beckman System Gold HPLC system with integrated pump, autosampler and UV detector as used with the taxanes was utilised with a Hitachi LaChrom fluorescence detector (L-7480) coupled to the system.

UV measurement was performed at 253 nm and fluorescence measurement at 480 nm excitation and 560 nm emission wavelengths.

Analysis continued as per Section 2.13.10, starting with a system check sample of epirubicin and then doxorubicin.

#### **2.14.7 HPLC data analysis**

The HPLC produced measurements of the areas of each peak in a sample. The area calculation of the software was double checked to make sure that they were accurate. Once the docetaxel and paclitaxel peaks were identified, the data was exported in to Microsoft Excel. A peak area ratio (P.A.R.) was generated for all the samples. This is the area of the paclitaxel, docetaxel or epirubicin peak (whichever is being measured) divided by the area of the I.S. The P.A.R. results for the standards are used to generate a concentration versus P.A.R. curve. The concentrations used were 1 X as only 100 µl of the standard had been included. The reverse plot is used to generate the equation of the line. The formula of the line was then used to convert the P.A.R. of each unknown sample to mass paclitaxel, docetaxel or epirubicin measured in nanograms. The cell counts obtained during the assay were then used to express the result as ng of drug per million cells.

### **2.14.8 Quantification of epirubicin by mass spectrometry**

Cellular levels of epirubicin were quantitated using LC-MS analysis as previously reported [257]. Briefly, 5 ml of cell suspension was seeded into 25cm<sup>2</sup> flasks at 1 X 10<sup>5</sup> cells per ml in triplicate and incubated at 37<sup>0</sup>C for 24 hours. 2 μM epirubicin was added to the medium and the cells were incubated for 2 hours in the presence or absence of test compound. Cells were then washed with ice-cold PBS, trypsinised and cell counts performed. Epirubicin was extracted from the cells using a liquid-liquid extraction method and epirubicin levels were quantitated on an LC –MS system consisting of MDLC (GE Healthcare Life Sciences, Bucks., U. K.) coupled to an LTQ hybrid ion trap mass spectrometer (Thermo Scientific, MA, U.S.A.).

## **2.15 <sup>14</sup>C docetaxel radiolabel assays**

### **2.15.1 Standard curve**

Dilutions of <sup>14</sup>C docetaxel at 0.01, 0.05, 0.1, 0.25, 0.5, 1, 2 and 5 μM were made in 0.1M NaOH. 250 μl of each dilution was added to a scintillation vial containing 3 ml of scintillation fluid. A blank containing 250 μl 1M NaOH was also included. All points were carried out in duplicate. The samples were read on the scintillation counter, producing C.P.M. values.

To examine the effect of cell debris on docetaxel radioactivity, the same standards were prepared in 0.1 M NaOH. Cells were seeded at 1 X 10<sup>5</sup> cells per ml per well in a 24 well-plate. Medium was removed from the cells followed by two washes with cold PBS. Ensuring all PBS was removed from the wells, 250 μl of each duplicate <sup>14</sup>C docetaxel concentration was added to a cell-containing well. The <sup>14</sup>C docetaxel concentrations were mixed thoroughly, transferred to a scintillation vial containing 3 ml scintillation fluid and read on the scintillation counter.

### **2.15.2 Saturation assay**

Each well in a 24-well plate was seeded with 1 ml of cell suspension containing  $1 \times 10^5$  cells per ml. Following a 24 hour incubation at  $37^{\circ}\text{C}$ , medium was removed from the cells. 500  $\mu\text{l}$  of pre-warmed  $^{14}\text{C}$  docetaxel at concentrations of 5, 15, 25, 50, 75, 100, 200, 300, 400 and 500 nM were added to duplicate wells in medium containing 5% FCS. Warm media was added to the four remaining wells that were to be used for cell counts. The cells were incubated with the  $^{14}\text{C}$  docetaxel concentrations for 90 minutes at  $37^{\circ}\text{C}$ . Drug containing medium was aspirated and the cells washed twice in cold PBS. 250  $\mu\text{l}$  of 1M NaOH was added to each well and then transferred to scintillation vials containing 3 mL scintillation fluid to be analysed. Medium was removed from the four remaining wells on the plate, the cells trypsinised and a cell count performed.

### **2.15.3 Serum accumulation assay**

21 wells of four 24-well plates (A, B, C, and D) were seeded with 1 ml of cell suspension containing  $1 \times 10^5$  cells per ml. Following a 24 hour incubation at  $37^{\circ}\text{C}$ , medium was removed from the cells. 100 nM concentrations of  $^{14}\text{C}$  docetaxel were prepared in 0, 1, 5, 50 and 100% FCS with medium. All samples were pre-warmed. 500  $\mu\text{l}$  of these concentrations were applied to each of the plates in triplicate wells. 500  $\mu\text{l}$  of medium was applied to the three wells to be used for cell counts. Drug was removed from plate A after 30 minutes, plate B after 60 minutes, plate C after 90 minutes and plate D after 120 minutes. Each well was washed twice with cold PBS and 250  $\mu\text{l}$  of 1M NaOH was added. Samples were then transferred to scintillation vials containing 3 ml scintillation fluid to be analysed. Medium was removed from the three remaining wells on each plate, the cells trypsinised and a cell count performed.

#### **2.15.4 Accumulation assay**

Each well in a 24-well plate was seeded with 1 ml of cell suspension containing  $1 \times 10^5$  cells per ml. Following a 24 hour incubation at  $37^{\circ}\text{C}$ , medium was removed from the cells. A solution of 2X 100 nM (or 500 nM)  $^{14}\text{C}$  docetaxel was prepared. Three wells received 250  $\mu\text{l}$  medium, 15 wells received the test compound at various concentrations and three wells received the vehicle control. 500  $\mu\text{l}$  medium was placed in the remaining three wells required for cell counts. Triplicate wells allows for a maximum of 5 test compound concentrations. 250  $\mu\text{l}$  2X 100 nM  $^{14}\text{C}$  docetaxel was then added to the 21 test wells. Drug was removed after 90 minutes and each well was washed twice with cold PBS and 250  $\mu\text{l}$  of 1M NaOH was added. Samples were then transferred to scintillation vials containing 3 ml scintillation fluid to be analysed. Medium was removed from the three remaining wells on each plate, the cells trypsinised, and a cell count performed. All medium used in the assay was pre-warmed to  $37^{\circ}\text{C}$ .

#### **2.15.5 Time accumulation profile**

Each well in a 24-well plate was seeded with 1 ml of cell suspension containing  $1 \times 10^5$  cells per ml. Following a 24 hour incubation at  $37^{\circ}\text{C}$ , medium was removed from the cells. 500  $\mu\text{l}$  of 100 nM  $^{14}\text{C}$  docetaxel was added to 20 wells and 500  $\mu\text{l}$  medium to the remaining 4 wells used for cell counts. The plate was incubated at  $37^{\circ}\text{C}$ . At the 10, 30, 50, 70, 90, 110, 130, 150, 170 and 190 minute timepoints, drug was removed from duplicate wells, the cells washed twice in cold PBS and 250  $\mu\text{l}$  1M NaOH added. Samples were then transferred to scintillation vials containing 3 ml scintillation fluid to be analysed. After the 190 minute timepoint, medium was removed from the three remaining wells on each plate, the cells trypsinised, and a cell count performed. All medium used in the assay was pre-warmed to  $37^{\circ}\text{C}$ .

### **2.15.6 Efflux profile**

Each well in a 24-well plate was seeded with 1 ml of cell suspension containing  $1 \times 10^5$  cells per ml. Following a 24 hour incubation at  $37^{\circ}\text{C}$ , medium was removed from the cells. 500  $\mu\text{l}$  of 100 nM  $^{14}\text{C}$  docetaxel was added to 21 wells and 500  $\mu\text{l}$  medium to the remaining 3 wells to be used for cell counts. After 90 minutes, the drug containing medium was aspirated from all 21 wells,  $^{14}\text{C}$  docetaxel levels were examined in 3 of the wells as a control and 500  $\mu\text{l}$  fresh medium was placed on 18 of the wells. At the 10, 20, 40, 60, 80 and 100 minute timepoints drug was removed from triplicate wells, the cells washed twice in cold PBS and 250  $\mu\text{l}$  1M NaOH added. Samples were then transferred to scintillation vials containing 3 ml scintillation fluid to be analysed. After the 100 minute timepoint, medium was removed from the three remaining wells on each plate, the cells trypsinised, and a cell count performed. All medium used in the assay was pre-warmed to  $37^{\circ}\text{C}$ .

### **2.15.7 Temperature accumulation assay**

Four wells of twenty 24-well plates were seeded with 1 ml of cell suspension containing  $1 \times 10^5$  cells per ml. Following a 24 hour incubation at  $37^{\circ}\text{C}$ , medium was removed from the cells. 500  $\mu\text{l}$  was added to 3 of the wells in each plate and 500  $\mu\text{l}$  medium to the remaining well to be used for a cell count. Four plates were placed in an incubator at 0, 27, 37, 41 and  $46^{\circ}\text{C}$ . A plate was taken from each incubator at the 30, 60, 90 and 120 minute timepoints. At each timepoint, drug was removed from triplicate wells, the cells washed twice in cold PBS and 250  $\mu\text{l}$  1M NaOH added. Samples were then transferred to scintillation vials containing 3 ml scintillation fluid to be analysed. Medium was removed from the remaining well on each plate, the cells trypsinised, and a cell count performed. All medium used in the assay was pre-warmed to  $37^{\circ}\text{C}$ .

## **2.16 ELISAs**

Samples were extracted and quantified as in Section 2.8. EGFR levels were examined using developmental sandwich ELISA assay kits, DY231 and DY1854 while Her-2 levels were determined using a rapid format sandwich ELISA kit, QIA10.

### **2.16.1 EGFR**

#### **Extracellular EGFR domain (R&D Systems, DY231)**

This kit utilised antibodies against an extracellular domain of EGFR. The capture antibody (Part 840830) was diluted to the working concentration of 0.8 µg/ml in PBS without carrier protein. A treated 96-well plate (Nunc, 467466 F16 Maxisorp) was coated with 100 µl per well of the diluted capture antibody. The plate was sealed and incubated overnight at room temperature. The following day, each well was aspirated and washed with wash buffer (0.05% Tween in PBS, pH 7.2-7.4), repeating the process two times for a total of three washes. To wash, each well was filled with 400 µl wash buffer using a squirt bottle. Complete removal of liquid at each step was essential for good performance. After the last wash, any remaining wash buffer was removed by inverting the plate and blotting it against clean paper towels. Plates were then blocked by adding 300 µl of reagent diluent to each well (1% BSA in PBS, pH 7.2 to 7.4). The plate was then incubated at room temperature for a minimum of 1 hour, followed by three washes with wash buffer. The plate was then ready for sample addition.

100 µl of sample containing 50 µg of protein or standards (Part 840832, recombinant human EGFR) was added in reagent diluent per well. A seven point standard curve using 2-fold serial dilutions from 2000 pg/ml was used. An adhesive strip was used to cover the plate and it was then incubated for 2 hours at room temperature. Three washes were then repeated as before. 100 µl of the detection antibody (Part 840831, biotinylated goat anti-human EGFR) diluted in reagent diluent to 200 ng/ml was then added to each well. The plate was covered with an adhesive strip and incubated for 2 hours at room temperature. Three washes with wash buffer were carried out as before.

100  $\mu$ l of the working dilution of Streptavidin-HRP (Part 890803) was added to each well. The plate was covered again and left to incubate for 20 minutes at room temperature, avoiding direct light. Wash buffer was used to perform three washes as before. 100  $\mu$ l of substrate solution (R&D Systems, DY999) was added to each well, followed by incubation for 20 minutes at room temperature avoiding direct light. To terminate the reaction, 50  $\mu$ l of stop solution (R&D Systems, DY994) was dispensed to each well. Gentle agitation mixed the solutions and the optical density of each well was read immediately, using a microplate reader set to 450 nm. Wavelength correction was set to 540 nm or 570 nm. EGFR levels were determined from a standard curve plotting absorbance *versus* concentration EGFR (ng/ml). Final EGFR concentration (pg/ $\mu$ g total protein) was calculated from the sample concentration (50  $\mu$ g/100  $\mu$ l).

#### **Intracellular EGFR domain (R&D Systems, DY1854)**

This kit used antibodies detecting the intracellular domain of EGFR. The procedure was the same as that for DY1854 with a number of variations. Samples and standards were diluted in IC Diluent #12 (1% NP-40, 20 mM Tris (pH 8.0), 137 mM NaCl, 10% glycerol, 2 mM EDTA, 1 mM activated sodium orthovanadate). Detection antibody was diluted to a working concentration of 200 ng/ml with IC Diluent # 14 (R&D Systems, DY995), as was the Streptavidin-HRP conjugate. EGFR levels were determined from a standard curve plotting absorbance *versus* concentration EGFR (ng/ml). Final EGFR concentration (pg/ $\mu$ g total protein) was calculated from the sample concentration (50  $\mu$ g/100  $\mu$ l).

### **2.16.2 Her-2**

#### **C-erbB2/c-neu rapid format ELISA kit (Cat# QIA10)**

Samples were prepared as in Section 2.8. The appropriate number of capture antibody pre-coated wells were removed and placed in the well holder. A working solution of wash buffer was prepared by adding 25 ml of the 20 X concentrated solution (provided), to 475 ml of deionized water and mixed well. Lyophilised standard was

reconstituted in dH<sub>2</sub>O to give a concentration of 3 ng/ml by carefully. The reconstituted standard was left sit for 15 minutes at room temperature, with occasional swirling. Excessive agitation of the standard was avoided. Two fold serial dilutions of the standard were made in sample diluent (supplied) to provide the following concentrations: 3, 1.5, 0.75, 0.375, 0.188, and 0 ng/ml. Reconstituted standards were discarded after one use. Samples were diluted with sample diluent (provided) to contain 50 µg protein per 100 µl.

Samples and each of the standard concentrations were added in duplicate by pipetting 100 µl into the appropriate wells using clean pipette tips for each sample.

Wells were covered with a plate sealer and incubated at room temperature for 2 hours. Wells were washed 3 times with 1 X wash buffer making sure each well was filled completely. 100 µl of the detector antibody (provided) was pipetted into each well, covered with a plate sealer and incubated at room temperature for 1 hour.

Wells were washed 3 times with 1 X wash buffer, again making sure each well was filled completely. 500 X Conjugate 1:500 was diluted in conjugate diluent to provide 100 µl of 1 X solution for each sample and standard well. The solution was filtered with a 0.2 µm syringe filter prior to use.

100 µl of the 1 X Conjugate was pipetted into each well, covered with a plate sealer and incubated at room temperature for 30 minutes. Wells were washed 3 times with wash buffer making sure each well was filled completely.

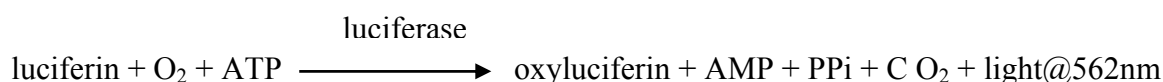
The entire plate was flooded with dH<sub>2</sub>O. Contents of the wells were removed by inverting over a sink and residual dH<sub>2</sub>O by tapping on paper towels.

100 µl of substrate solution (provided) was added to each well and incubated in the dark at room temperature for 30 minutes. The reaction was terminated by addition of 100 µl of stop solution to each well in the same order as the previously added substrate solution.

Absorbance was measured in each well using a spectrophotometric plate reader at dual wavelengths of 450/595 nm (or 450/540 nm). Wells were read within 30 minutes of adding the stop solution. Her-2 levels were determined from a standard curve plotting absorbance *versus* concentration Her-2 (ng/ml). Final Her-2 concentration (pg/µg total protein) was calculated from the sample concentration (50 µg/100 µl).

## 2.17 Determination of cellular ATP levels

Cellular ATP levels were determined using the bio-luminescent luciferase-based Enliten® ATP assay system (Promega, FF2000). The light producing reaction which is catalysed by the luciferase enzyme is given below:



A concentration of 1% trichloroacetic acid (TCA) was used to extract ATP from cells. Application of TCA to living cells disrupts the cell membranes allowing release of cell contents (including ATP) and TCA irreversibly inactivates the enzymes which catalyse ATP conversion reactions. For maximum ATP yield, the pH must be acidic (pH < 1.2) during the extraction procedure. The indicator xylenol blue is included during the extraction procedure to give a visual indication of the pH. A red colour is representative of a pH of less than 1.2. TCA concentrations greater than 0.1% inhibit the luciferase reaction and so samples must be diluted in tris-acetate buffer before determination of the ATP content. This also raised the pH to ~ 7.5, the optimal conditions for the luciferase reaction (xylenol blue- yellow, pH 2.8-8.0). A final concentration of < 0.002% xylenol blue was required for negligible spectrophotometric interference.

**Note:** all efforts were made to ensure minimum contamination by external sources of ATP. Autoclaved tips and glassware, sterile plastics and gloves were used throughout.

### 2.17.1 Reagents

**0.1 M Tris Acetate buffer (with 2 mM EDTA):** 0.372 g of EDTA (Sigma, E6758) was dissolved in 75 ml of dH<sub>2</sub>O by heating. 6.06 g of tris acetate (Sigma, T1258) was then added and dissolved by heating. The solution was allowed to cool and the pH adjusted to 7.75 with acetic acid and made up to 500 ml.

**10% TCA solution (including 4 mM EDTA with 0.002% xylene blue):** 0.149 g EDTA was dissolved in 50 ml dH<sub>2</sub>O by heating. 2 mg of xylene blue (Sigma, 114561) was added and dissolved by heating. Addition of 10 g of trichloroacetic acid (Sigma, T4885) followed and the volume made up to 100 ml with dH<sub>2</sub>O.

### **2.17.2 Procedure**

1 ml of a  $1 \times 10^5$  cells/ml solution were seeded per well of a 24-well plate and incubated overnight at 37°C. Medium was removed and replaced with pre-warmed fresh medium or medium containing ATP depleting agents (sodium azide (Sigma, S8032), 2-deoxyglucose (Sigma, D3179) or antimycin A (Sigma, A8674)). Medium was replaced in wells included for cell counts also. Following incubation, medium was aspirated from the plate and all wells washed with ice-cold PBS. 100 µl of a 1% TCA solution (10 ml 10% TCA solution and 90 ml dH<sub>2</sub>O) was added to each well for 5 minutes, except the wells providing cell counts, to which 500 µl trypsin was added. The presence of a red colour gave confirmation of acidic pH required for ATP extraction. 900 µl of 0.1M Tris Acetate buffer was added to each test well producing a yellow colour (pH~ 8 as required for luciferase reaction). 500 µl medium was added to the cell count wells and the number of cells present determined as in Section 2.5.2. 10 µl of each sample was then transferred to a 96-well luminescence plate already containing 90 µl Tris Acetate buffer per well. Two-fold serial dilutions of the 100 nM ATP standard (Promega FF2000, F203A) to 3.125 nM were prepared in ATP-free water (Promega FF2000, F201A). 100 µl of each standard was pipetted into the 96-well luminescence plate in duplicate. The Enliten luciferase/luciferin agent (Promega FF2000, F120A) was reconstituted in reconstitution buffer (Promega FF2000, F180A). 100 µl of the reconstituted luciferase/luciferin agent was added to each well and the luminescence measured on a Bio-Tek II Synergy HT with a sensitivity setting of 125 and utilising KC<sup>4</sup> Synergy software. A plot of luminescence (RLU, relative luminescence units) *versus* the concentration of the known standards (ng/ml) provided the concentration of the samples. The cell counts were used to convert the values to ng/10,000 cells once the dilution factor was taken into account.

## 2.18 ATPase Assays

The ATPase activity of the human multidrug resistance (MDR) transporter proteins P-gp, MRP-1 and BCRP, was determined using purified membrane vesicles transfected to express high levels of the selected human MDR transporter proteins. The ATPase activity for measuring human P-gp (SB-MDR1-*Sf9*-ATPase) and MRP-1 (SB-MRP1-*Sf9*-ATPase) ATPase activities were performed in membrane vesicles prepared from insect *Sf9* (*Spodoptera frugiperda*) cells, while the wild type BCRP membrane vesicles (SB-MXR-M-ATPase) were prepared from selected mammalian cells. The membrane vesicles and assay protocols related herein were supplied by Solvo Biotechnology (Hungary). The protocol for the BCRP ATPase assay differs slightly from the P-gp and MRP-1 ATPase assay and these differences will be noted throughout.

MDR transporters pump substrates out of the cell by using ATP hydrolysis as an energy source. ATP hydrolysis yields inorganic phosphate (Pi), which can be detected by a simple colorimetric reaction. The amount of Pi liberated by the transporter is proportional to the activity of the transporter.

In the presence of a transported substrate the ATPase activity of the MDR-transporter increases. If a compound is an inhibitor of the transporter, or a slowly transported compound, it will inhibit the MDR-ATPase activity measured in the presence of a stimulating agent. The BCRP ATPase membrane preparations have a higher intrinsic baseline ATPase activity that is activated by some compounds and inhibited by others allowing activation and inhibition studies to be performed directly without the need for a stimulating agent.

The ATPase assays are a modification of the method of Sarkadi *et al.* [258].

## 2.18.1 ATPase assay materials

A list of the compounds required for the ATPase assays, and the individual storage conditions are shown in Table 2.18.1.1

**Table 2.18.1.1** Materials required for the ATPase assays.

Substance	Cat. Number	Storage
<b>Tris-Base</b> (Tris[hydroxymethyl]aminomethane)	Sigma T-1503	RT, >1year
<b>MOPS</b> (3-[N-Morpholino]propanesulfonic acid)	Sigma M-1254	RT, >1year
<b>EGTA</b>	Sigma E-3889	RT, >1year
<b>KCl</b>	Sigma P-9333	RT, >1year
<b>Na-azide</b>	Sigma S-8032	RT, >1year
<b>DTT</b>	Serva 20710	4 °C, >1 year
<b>Ouabain</b>	Sigma O-3125	RT, >1year
<b>SDS</b>	Sigma L-6026	RT, >1year
<b>KH<sub>2</sub>PO<sub>4</sub></b>	Sigma P-5379	RT, >1year
<b>Verapamil</b>	Sigma V-4629	RT, >1year
<b>N-ethylmaleimide (NEM), (for MRP1 studies)</b>	Sigma E-1271	4 °C, >1 year
<b>Glutathione (for MRP1 studies)</b>	Sigma G-4251	4 °C, >1 year
<b>Sulfasalazine (BCRP studies)</b>	Sigma P-7791	RT, >1 year
<b>Hoechst 33342 (BCRP studies)</b>	Sigma B-2261	-20 °C, >1 year
<b>Na-Orthovanadate (Na<sub>3</sub>VO<sub>4</sub>)</b>	Sigma S-6508	RT, >1year
<b>ATP (disodium salt)</b>	Sigma A-2383	-20 °C, >1 year
<b>MgCl<sub>2</sub> (hexahydrate)</b>	Sigma M-2670	RT, >1year
<b>Zinc acetate (dihydrate)</b>	Sigma Z-4540	RT, >1year
<b>Ammonium-molybdate (tetrahydrate)</b>	Sigma A-7302	RT, >1year
<b>Ascorbic acid</b>	Pharaceutical grade	4 °C, >1 year
<b>DMSO</b>	Sigma D-2650	RT, >1year

## 2.18.2 ATPase assay stock solutions

The stock solutions for use in ATPase activation and inhibition assays are given in Table 2.18.2.1 and Table 2.18.2.2. UHP water was used for all dilutions.

**Table 2.18.2.1** Stock solutions for use in the ATPase assays.

<b>Solution</b>	<b>Storage</b>
<b>1.7 M Tris</b> 20.587 g of Tris was dissolved in 100 ml distilled water.	4 °C, >1 year
<b>0.1 M MOPS-Tris</b> 2.09 g of MOPS was dissolved in 90 ml distilled water; the pH was adjusted to 7.0 with 1.7 M Tris (about 2 ml). The solution was brought to 100 ml with distilled water.	4 °C, >1 year
<b>100 mM EGTA-Tris pH 7.0</b> 38.04 mg of EGTA was dissolved in about 10 ml of 1.7 M Tris. 80 ml of distilled water was added and the pH was adjusted to 7.0 with 1.7 M Tris. The solution was brought to 100 ml with distilled water.	4 °C, >1 year
<b>1 M KCl</b> 7.46 g of KCl was dissolved in 100 ml distilled water.	4 °C, >1 year
<b>0.1 M Na-azide</b> 0.65 g of Na-azide was dissolved in 100 ml distilled water.	4 °C, >1 year
<b>0.1 M DTT</b> 0.3086 g of DTT was dissolved in 20 ml distilled water.	-20 °C in small aliquots
<b>10 mM Ouabain</b> 14.6 mg of Ouabain was dissolved in 2 ml distilled water in a glass tube. It was stirred with a glass rod until dissolved.	Prepare fresh
<b>5% SDS</b> 5 g of SDS was dissolved in 100 ml of distilled water.	RT, > 1 year
<b>100 mM KH<sub>2</sub>PO<sub>4</sub></b> 0.1361 g of KH <sub>2</sub> PO <sub>4</sub> was dissolved in 10 ml distilled water.	-20 °C in small aliquots
<b>Phosphate standard solutions</b> 0.5 mM, 1 mM, 2 mM, 4 mM and 8 mM KH <sub>2</sub> PO <sub>4</sub> were prepared from the 100 mM stock in distilled water.	-20 °C in small aliquots

**Table 2.18.2.2** Stock solutions for use in the ATPase assays.

<b>Solution</b>	<b>Storage</b>
<p><b>0.2 M MgATP</b></p> <p>2.2 g of ATP and 0.8 g MgCl<sub>2</sub> were dissolved in 10 ml of distilled water and the pH was adjusted to 7.0 with 1.7 M Tris. The solution was brought to 20 ml with distilled water.</p>	-20 °C in small aliquots
<p><b>2 mM Verapamil (for MDR1 studies)</b></p> <p>A 2 mM stock of Verapamil was made in DMSO.</p>	-20 °C in small aliquots
<p><b>0.5 mM Hoechst 33342 (for MXR studies)</b></p> <p>0.5 mM Hoechst 33342 in DMSO</p>	
<p><b>0.5 mM Sulfasalazine (for MXR studies)</b></p> <p>0.5 mM Sulfasalazine in DMSO</p>	-20 °C in small aliquots
<p><b>60 mM Na-Orthovanadate</b></p> <p>A 60 mM stock of Na-Orthovanadate was made in distilled water.</p>	-20 °C in small aliquots
<p><b>300 mM NEM (for MRP1 studies)</b></p> <p>0.375 g of NEM was dissolved in 10 ml of 0.1 M MOPS-Tris.</p>	-20 °C in small aliquots
<p><b>300 mM Glutathione (for MRP1)</b></p> <p>0.922 g of Glutathione was dissolved in 8 ml distilled water and the pH was adjusted to 6.8 with 10 M NaOH. The solution was brought to 10 ml with distilled water.</p>	-20 °C in small aliquots
<p><b>150 mM NEM-GS (for MRP1)</b></p> <p>300 mM NEM was mixed with 300 mM glutathione in 1:1 ratio.</p>	Prepare fresh
<p><b>15mM Zinc Acetate</b></p> <p>330 mg of Zinc Acetate was dissolved in 100 ml of distilled water.</p>	4 °C, 2 weeks
<p><b>35 mM Ammonium Molybdate in 15 mM Zinc Acetate pH 5.0</b></p> <p>0.864 g of Ammonium Molybdate was dissolved in 15 ml of Zn Acetate and the pH was adjusted to 5.0 with HCl solution. The solution was brought to 20 ml with 15 mM Zn Acetate. This solution was stored in a container wrapped with aluminum foil in the dark.</p>	4 °C, 1 week, dark
<p><b>10% Ascorbic Acid pH 5.0</b></p> <p>1 g Ascorbic Acid was dissolved in 10 ml distilled water and the pH was adjusted to 5.0 with NaOH (prepared freshly).</p>	Prepared freshly

### 2.18.3 ATPase assay mix

The ATPase assay mix was prepared as per Tables 2.18.3.1 and 2.18.3.2. Ouabain and DTT were added freshly before use. The rest of the solutions were pre-mixed and stored at 4<sup>o</sup>C.

DMSO was used as the general solvent in these assays with a final concentration of 2% during the assay. The assays are designed to tolerate up to 2 % of a wide variety of solvents (ethanol, acetonitrile, and methanol) that should be included in all controls instead of DMSO if used.

Some molecules require the presence of glutathione to be transported by MRP-1 and to modulate the ATPase activity of MRP-1 in ATPase assays. For this reason, glutathione was included in the assay mix at a concentration of 2 mM in both MRP-1 activation and inhibition studies in this project.

**Table 2.18.3.1** P-gp and MRP-1 assay mix

<b>Ingredient</b>	<b>Volume (µl)</b>	<b>Final concentration</b>
0.1 M MOPS-TRIS, pH 7.0	5,000	50 mM
1 M KCl	500	50 mM
0.1 M Na-azide	500	5 mM
0.1 M DTT	200	2 mM
100 mM EGTA-TRIS, pH 7.0	10	0.1 mM
Distilled Water	3,790	
Total volume	10,000	

**Table 2.18.3.2** BCRP Assay-mix

<b>Ingredient</b>	<b>Volume (µl)</b>	<b>Final concentration</b>
0.1 M MOPS-TRIS, pH 7.0	5,000	50 mM
1 M KCl	500	50 mM
0.1 M Na-azide	500	5 mM
0.1 M DTT	200	2 mM
100 mM EGTA-TRIS, pH 7.0	10	0.1 mM
10 mM Ouabain	1,000	1 mM
Distilled Water	2,790	
Total volume	10,000	

#### **2.18.4 Composition of signal**

As a result of the relatively complex composition of the assay, transporter activities from OD (optical density/absorbance) values can only be calculated with adequate controls. Therefore, it was important to understand how the different experimental conditions modify the read out (OD, reflecting Pi concentration). The total Pi measured is composed of the following elements:

1. There is some Pi present in the final assay suspension (containing the membranes and ATP). This is mainly due to the contamination of the membranes and ATP with Pi, and some non-enzymatic ATP hydrolysis.
2. Some of the ATPase activities in the membranes are sodium orthovanadate ( $\text{Na}_3\text{VO}_4$ )-insensitive. This is important to determine since the transporter-specific, sodium vanadate-sensitive activity can only be calculated by subtracting this background sodium orthovanadate-insensitive activity. This activity may somewhat vary with membrane stocks, thus including this control in the calculations also decreases inter-assay variability
3. There is a small amount of sodium orthovanadate-sensitive ATPase activity present in the membranes not related to transporter ATPase. This can be assayed

by measuring the sodium orthovanadate-sensitive ATPase activity of a control membrane. This was not done for the ATPase assays in this thesis.

4. The rest of the signal is the transporter specific ATPase activity of the membrane suspension, which is sodium orthovanadate-sensitive. Transporters show some baseline ATPase activity that varies for different transporters and different membrane preparations. Substrates of the transporter stimulate the baseline ATPase activity while inhibitors or slowly transported compounds inhibit the baseline ATPase activity.
5. Some drugs are coloured or might interfere with the assay in any other non-specific way. In order to separate any non-specific effects, test drugs with and without 1.2M sodium orthovanadate were included as control wells.

### **2.18.5 ATPase assay controls**

In order to accurately define the Pi liberated due to sodium orthovanadate-sensitive transporter activity, a number of controls were set up for measuring different elements of the signal. All controls were performed in duplicate.

**Control 1: Assay background control:** 40 µl membrane in assay mix and 40 µl 5% SDS were added to the wells. DMSO (1 µl DMSO/well) was also added because the compounds tested were dissolved in DMSO. The plate was preincubated at 37<sup>0</sup>C for 5 minutes (P-gp and MRP-1) or 32<sup>0</sup>C for 5 minutes (BCRP). 10 µl of 25 mM MgATP was added to the wells and the plate was incubated at 37<sup>0</sup>C (P-gp or MRP-1) or 32<sup>0</sup>C (BCRP) for the requisite time. The colour reaction for inorganic phosphate was developed. This control showed the Pi present in the well without any enzymatic ATP hydrolysis. Control 1 served as a quality check of the components of the assay mix, solvents and the ATP and membrane used.

**Control 2: Sodium orthovanadate-insensitive ATPase activity:** 40 µl membrane in assay mix and 1 µl of 60 mM sodium orthovanadate were added to the wells (final sodium orthovanadate concentration is 1.2 mM). DMSO (1 µl DMSO/well) was

added as the compounds tested were dissolved in DMSO. The plate was preincubated at 37°C for 5 minutes (P-gp and MRP-1) or 32°C for 5 minutes (BCRP). The reaction was started by adding 10 µl of 25 mM MgATP to the wells and the plate was incubated at 37°C (P-gp or MRP-1) or 32°C (BCRP) for the requisite time. The reaction was stopped by adding 40 µl 5% SDS/well at the end of the incubation period and the colour reaction for inorganic phosphate was developed. This control showed the ATPase activity not sensitive to sodium orthovanadate.

**Control 3: Baseline ATPase activity:** 40 µl membrane in assay mix and DMSO (1 µl DMSO/well) were added as the compounds tested were dissolved in DMSO. The plate was preincubated at 37°C for 5 minutes (P-gp and MRP-1) or 32°C for 5 minutes (BCRP). The reaction was started by adding 10 µl of 25 mM MgATP to the wells and the plate was incubated at 37°C (P-gp or MRP-1) or 32°C (BCRP) for the requisite time. The reaction was stopped by adding 40 µl 5% SDS/well at the end of the incubation period and the colour reaction for inorganic phosphate was developed. This control showed the basic level of Pi liberation in the presence of a given membrane, transporter and solvent for the drugs. For obtaining the vanadate-sensitive baseline ATPase activity, Control 2 was subtracted from this value.

**Ctrl 4: Fully activated ATPase activity:** 40 µl membrane in assay mix was added. For the P-gp ATPase assay, 40 µM verapamil was added (1 µl of 2 mM verapamil/well), for the MRP-1 assay, 10 mM NEM-GS was added (3.3 µl of 150 mM NEM-GS/well), and for the BCRP assay, 10 µM sulfasalazine (1 µl of 0.5 mM sulfasalazine/well), to obtain maximum ATPase activity. The plate was preincubated at 37°C for 5 minutes (P-gp and MRP-1) or 32°C for 5 minutes (BCRP). The reaction was started by adding 10 µl of 25 mM MgATP to the wells and the plate was incubated at 37°C (P-gp or MRP-1) or 32°C (BCRP) for the requisite time. The reaction was stopped by adding 40 µl 5% SDS/well at the end of the incubation period and the colour reaction for inorganic phosphate was developed. This control showed the maximum level of Pi liberation in the presence of a given membrane and transporter. For obtaining the full vanadate-sensitive ATPase activity Control 2 was subtracted, for obtaining the drug-stimulated ATPase activity fraction, Control 3 was subtracted.

**Control 5: Inhibited ATPase activity (BCRP only):** 40  $\mu$ l membrane in assay mix was added. 10  $\mu$ M of Hoechst 33342 was added (1  $\mu$ l of 0.5 mM Hoechst 33342/well) to obtain maximum ATPase activity. The plate was preincubated at 32<sup>0</sup>C for 5 min. The reaction was started by adding 10  $\mu$ l of 25 mM MgATP to the wells and the plate was incubated at 32<sup>0</sup>C. The reaction was stopped by adding 40  $\mu$ l 5% SDS/well at the end of the incubation period and the colour reaction for inorganic phosphate was developed. This control showed ATPase activity in the presence of a specific inhibitor of BCRP.

### **2.18.6MDR-transporter ATPase activation assay procedure**

The assay mix was assembled as per Table 2.18.3.1 or Table 2.18.3.2 and kept on ice. The assay components were added to a 96-well plate that was also kept on ice at all times as follows.

A Pi ( $\text{KH}_2\text{PO}_4$ ) calibration series was prepared by adding 10  $\mu\text{l}$  of the phosphate standard solutions (Table 2.18.2.1) per well to 40  $\mu\text{l}$  assay mix (to obtain 5-80 nmoles of Pi/well). 40  $\mu\text{l}$  5% SDS was added to these wells. These were performed in duplicates.

The predetermined membrane protein concentration (5 mg/ml) was used to prepare a 1 mg/ml membrane suspension in the case of P-gp and MRP-1, and a 0.5 mg/ml membrane suspension for BCRP by diluting membranes in the assay mix and mixed well.

40  $\mu\text{l}$  of membrane suspension was added to the desired wells of a 96-well plate (samples and controls) according to Table 2.18.6.1.

Control wells were set up according to Section 2.18.5.

1  $\mu\text{l}$  of 60 mM sodium orthovanadate was added. 1  $\mu\text{l}$  of the required test reagents/drugs in DMSO per well were then added to the membrane suspension.

The plates were then transferred to a 37<sup>0</sup>C (P-gp/MRP-1) or 32<sup>0</sup>C (BCRP) incubator and preincubated for 5 minutes.

A 25 mM MgATP solution was made by diluting the stock ATP solution (0.2 M) in assay mix.

The ATPase reaction was started by the addition of 10  $\mu\text{l}$  of 25 mM MgATP (final MgATP concentration was 5 mM).

The plates were incubated at 37<sup>0</sup>C in an incubator for 20 minutes in the P-gp ATPase assays or 60 minutes for the MRP1 ATPase assay. The plates for the BCRP ATPase assay were incubated at 32<sup>0</sup>C for 40 minutes. The ATPase reaction was stopped by adding 40  $\mu\text{l}$  5% SDS to each well.

The detection reagent was prepared by adding 5 ml of 35 mM ammonium molybdate in 15 mM zinc acetate to 15 ml of the freshly prepared 10% ascorbic acid. This solution was mixed by inverting. 200  $\mu\text{l}$  of detection reagent was added to each well.

The plate was mixed well by shaking the plates thoroughly. The plates were incubated at 37<sup>0</sup>C for 25 minutes, and the OD was read between 630 and 850 nm.

**Table 2.18.6.1** Standard 96-well plate layout used for ATPase assays

	1	2	3	4	5	6	7	8	9	10	11	12
	Calibration		Controls		Test drug A		Test drug A + vanadate		Test drug B		<i>Test drug B + vanadate</i>	
A	0		Control 1		30 $\mu$ M		30 $\mu$ M		30 $\mu$ M		30 $\mu$ M	
B	5 nmol Pi		Control 2		15 $\mu$ M		15 $\mu$ M		15 $\mu$ M		15 $\mu$ M	
C	10 nmol Pi		Control 3		5 $\mu$ M		5 $\mu$ M		5 $\mu$ M		5 $\mu$ M	
D	20 nmol Pi		Control 4		2.5 $\mu$ M		2.5 $\mu$ M		2.5 $\mu$ M		2.5 $\mu$ M	
E	40 nmol Pi				1 $\mu$ M		1 $\mu$ M		1 $\mu$ M		1 $\mu$ M	
F	80 nmol Pi				0.25 $\mu$ M		0.25 $\mu$ M		0.25 $\mu$ M		0.25 $\mu$ M	
G												
H												

### 2.18.7 MDR transporter ATPase inhibition assays

P-gp and MRP-1 inhibition assays were carried out as in Section 2.18.6 with minor adjustments to the protocol.

An excess of an established activator of each MDR transporter was added to provide maximum ATPase activity to study the ATPase inhibitory effects of test compounds.

For P-gp inhibition assays, 25  $\mu$ l of 2 mM verapamil per ml (40  $\mu$ M final concentration) was added to the membrane suspension AFTER a volume of membrane suspension was removed for the Controls.

For MRP-1 inhibition assays, 82.5  $\mu$ l of 150 mM NEM-GS per ml (10 mM final concentration) was added to the membrane suspension AFTER a volume of membrane suspension was removed for the Controls. The assay then proceeded as for the activation assays.

A BCRP inhibition assay was not performed as inhibition of the naturally active basal level of BCRP ATPase activity could be determined directly without the use of a

stimulating agent. However, a fifth control (Section 2.18.5) was included to determine the maximal inhibited ATPase activity and the assay carried out as in Section 2.18.6.

### **2.18.8 Calculation of the specific (sodium orthovanadate-sensitive) MDR transporter ATPase activities**

The average OD values of the duplicate calibration curve and controls were calculated. A calibration curve using the calibration curve OD values and the amount of Pi ( $\text{KH}_2\text{PO}_4$ ) used (nmol/well) was set up.

The average OD values of the samples tested were also calculated. The nanomoles of Pi liberated in the controls and in the samples were calculated by using the calibration curve.

The Pi liberated in Control 2 was subtracted from Pi liberated in Control 3. This gave the baseline sodium orthovanadate-sensitive ATPase activity.

The Pi liberated in Control 2 from was subtracted from the Pi liberated in Control 4. This gave the fully activated sodium orthovanadate-sensitive transporter ATPase activity.

The Pi values determined in the presence of sodium orthovanadate were subtracted from the Pi values measured without sodium orthovanadate for each compound examined. This gave the sodium orthovanadate-sensitive transporter ATPase activity for each drug and drug concentration assayed.

The  $\text{Na}_3\text{VO}_4$ -sensitive transporter ATPase activity was calculated in terms of Pi liberated/mg membrane protein/min. To do this the nmol/well were divided by the amount of membrane protein in each well and the time of incubation in minutes.

### **2.18.9 Expected MDR transporter ATPase parameters**

The expected parameters for ATPase activity as supplied by Solvo Biotechnology were as follows. The typical sodium orthovanadate-sensitive ATPase activity of P-gp-containing *Sf9* cell membranes (measured under the above described conditions) was 8-16 nmoles Pi/mg membrane protein/min. This activity increased to 35-60 nmoles Pi/mg membrane protein/min in the presence of 20-40  $\mu\text{M}$  verapamil. The nmoles Pi/mg membrane ATPase activity of the MRP-1 membranes was significantly lower

for MRP-1. The basal ATPase activity was 3-6 nmoles Pi/mg membrane protein/min, stimulated to 9-18 nmoles Pi/mg membrane protein/min in the presence of 10 mM NEM-GS. The BCRP membranes were expected to have a baseline activity of 5-10 nmoles Pi/mg membrane protein/min, a maximal activity of 15-25 nmoles Pi/mg membrane protein/min and an inhibited activity of 0-3 nmoles Pi/mg membrane protein/min.

***Chapter 3. HPLC- determined taxane accumulation  
and efflux in MDR and sensitive human lung and  
leukemic cell lines***

### **3.1 Introduction**

To study taxane transport effectively, a sufficiently sensitive method to measure changes in taxane levels in multi-drug resistant and sensitive cell lines was required. Our group had used high performance liquid chromatography (HPLC) to measure levels of the anthracyclines successfully in the past [160]. On developing a HPLC-based procedure for taxane measurement, a number of issues were identified.

To establish the basic parameters of taxane transport, docetaxel and paclitaxel accumulation were examined in a panel of non-small cell lung cancer (NSCLC) cell lines. The sensitive adenocarcinoma cell line, A549, and squamous cell, DLKP, cell line were chosen along with the drug resistant DLKP-A (high P-gp over-expression) and DLKP-TXT (low P-gp expression).

The HL-60s cell line was utilised to compare docetaxel and paclitaxel transport in a cell line devoid of major efflux transporter activity. Taxane transport was also examined in the drug-resistant, MRP-1 over-expressing, variant, HL-60 ADR, to investigate if MRP-1 expression changed taxane accumulation.

The effects of potent P-gp inhibitors on taxane transport in drug resistant cell lines was assessed to define the range of measurement facilitated by the HPLC method within which potential new P-gp inhibitors could be ranked. The assays were also carried out in the sensitive cell lines to provide a negative control and discount the possibility of other taxane efflux mechanisms in these cell lines.

Sulindac was found to be an MRP-1 inhibitor by our group [160]. To explore any possible interactions between sulindac and P-gp and other putative taxane transporters, sulindac was studied in taxane transport assays in all cell lines.

Preliminary studies in A549 and DLKP utilising compounds known to deplete ATP levels were performed to provide an insight into the plausibility of an energy-dependent influx mechanism in lung cancer cells and assess the potential of the HPLC method for quantifying such changes accurately.

HPLC-based analysis was used to examine taxane accumulation and efflux in non-small cell lung cancer (NSCLC) cell lines and two leukaemia cell lines, HL-60 and HL-60ADR. Time-points, cell number and drug concentration were optimised and the assay was then used to examine the influence of P-gp and MRP-1 expression on taxane accumulation. Cyclosporin A, verapamil and the third generation inhibitor, elacridar (GF120918), were used to examine the involvement of P-gp in taxane transport.

### **3.2 Drug selection and P-gp expression**

P-gp expression was analysed in the panel of cell lines by western blot (Figure 3.1.1). P-gp was detected in the taxane selected cell lines, DLKP-TXT (selected with docetaxel by Dr. Yizheng Liang) and A549-Taxol (selected with paclitaxel by Dr. Laura Breen). Significantly elevated levels of P-gp were detected in the doxorubicin (adriamycin)-selected DLKP-A. The DLKP and A549 parent cell lines and the mitoxantrone-selected DLKP-Mitox did not express measurable levels of P-gp by Western blot.

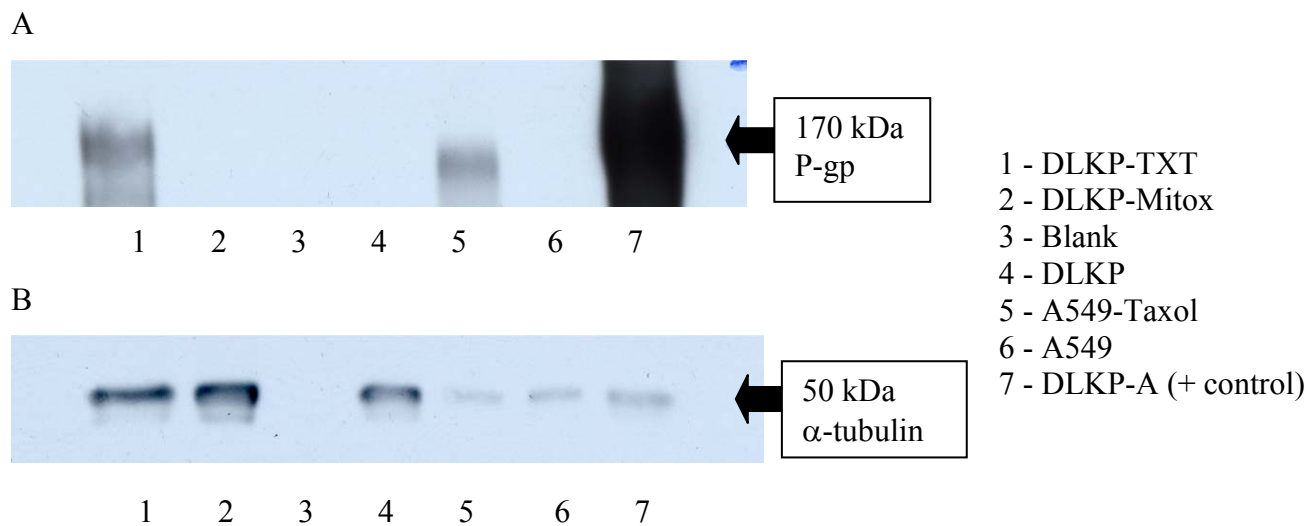


**Figure 3.2.1** Western blot for P-gp (A) in two NSCLC cell lines and drug selected variants. DLKP-TXT was selected with docetaxel, DLKP-Mitox was selected with mitoxantrone and A549-Taxol was selected with paclitaxel (® Taxol). Samples were also blotted for alpha-tubulin expression (B).

### **3.3 Optimisation of drug exposure for HPLC analysis**

Cellular docetaxel accumulation levels were measured in A549 cells exposed to 10  $\mu\text{M}$  docetaxel for various durations up to 140 minutes (Figure 3.3.1). Docetaxel accumulation was found to be gradual. 90 minutes was chosen as a practical time-point that resulted in a measurable mass of docetaxel and would allow observation of differences in docetaxel accumulation.

The efflux profile for docetaxel in A549 cells was measured after exposure to 10  $\mu\text{M}$  docetaxel for 90 minutes (Figure 3.3.2). After the 90 minutes exposure the drug was removed and replaced with fresh medium and efflux was measured at various time-points, up to 140 minutes. 40 minutes was chosen as the time-point for measurement of efflux as the level of docetaxel plateaued within this time.

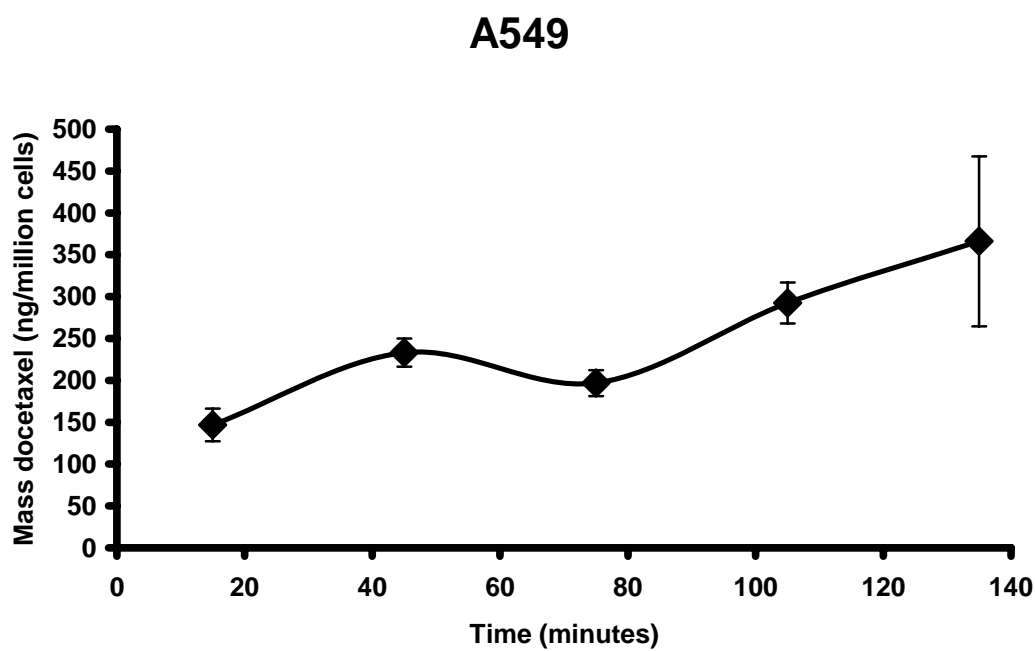


**Figure 3.3.1** HPLC accumulation profile of 10  $\mu\text{M}$  docetaxel over time in A549, measured as the mass of docetaxel (ng) accumulated in  $10^6$  cells. Data are mean  $\pm$  SD calculated on experiments performed in triplicate.

## A549

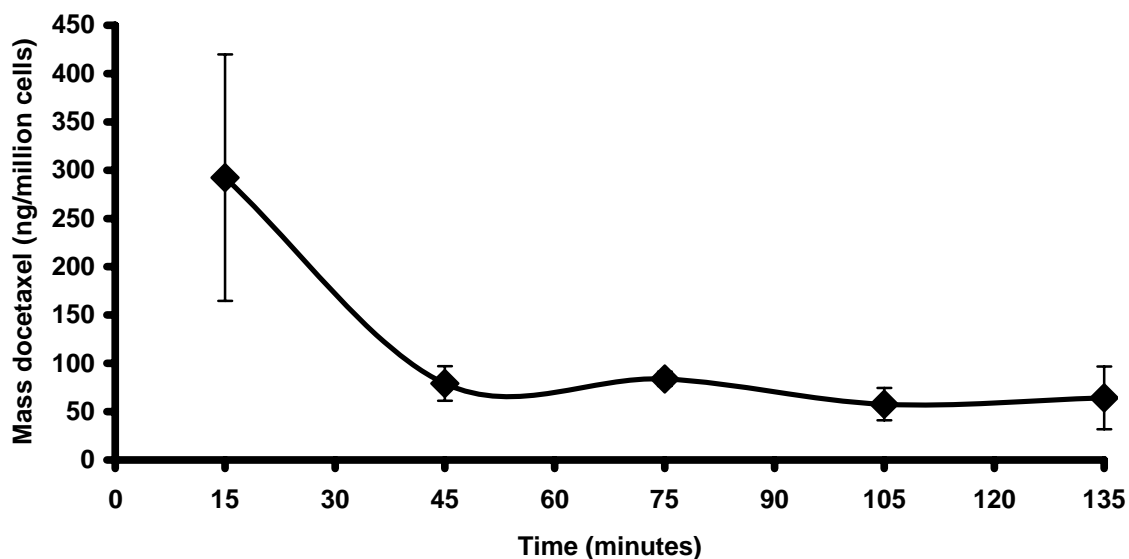


**Figure 3.3.2** Profile of docetaxel efflux from A549 cells after treatment with 10  $\mu$ M docetaxel for 90 minutes. After 90 minutes, the drug was removed and replaced with fresh medium (T0) and the mass of docetaxel retained in the cells was measured at various time-points up to 135 minutes. Data are mean  $\pm$  SD calculated on experiments performed in triplicate.

### **3.4 Effects of sulindac on docetaxel accumulation and efflux in the A549 cell line.**

A549 cells were incubated with 10  $\mu\text{M}$  docetaxel and various concentrations of the MRP-1 inhibitor sulindac for 90 minutes (Figure 3.4.1). 5, 10 and 20  $\mu\text{M}$  sulindac are clinically relevant concentrations. All three concentrations of sulindac had no effect on docetaxel accumulation in this cell line.

To examine the effect of sulindac on docetaxel efflux in the A549 cell line, cells were incubated with 10  $\mu\text{M}$  docetaxel for 90 minutes. The drug was then removed and replaced with medium or varying concentrations of sulindac for 40 minutes (as determined from Figure 3.4.2). 5, 10, and 20  $\mu\text{M}$  sulindac had no significant effect on docetaxel efflux from A549 cells.

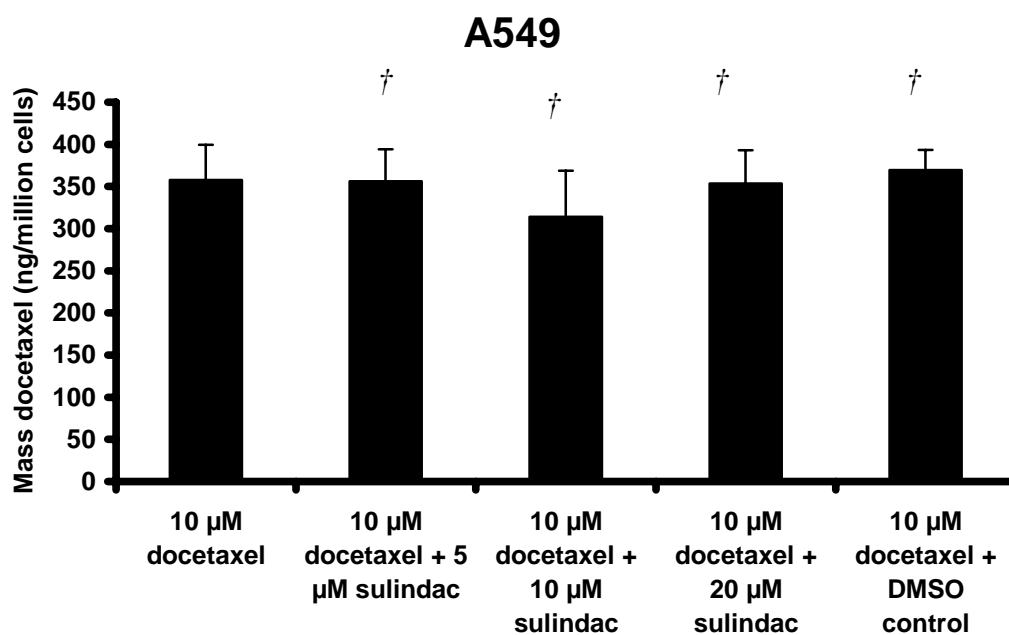


**Figure 3.4.1** Effect of the MRP-1 inhibitor sulindac on the mass of docetaxel (ng) accumulated per million cells in the A549 cell line. Cells were incubated with 10  $\mu$ M docetaxel alone or in combination with 5, 10, or 20  $\mu$ M sulindac for 90 minutes. The control contains the concentration of DMSO vehicle present in 20  $\mu$ M sulindac. Data are mean  $\pm$  SD calculated on experiments performed in triplicate. † not significantly different from control values,  $P > 0.05$  relative to the control (10  $\mu$ M docetaxel alone).

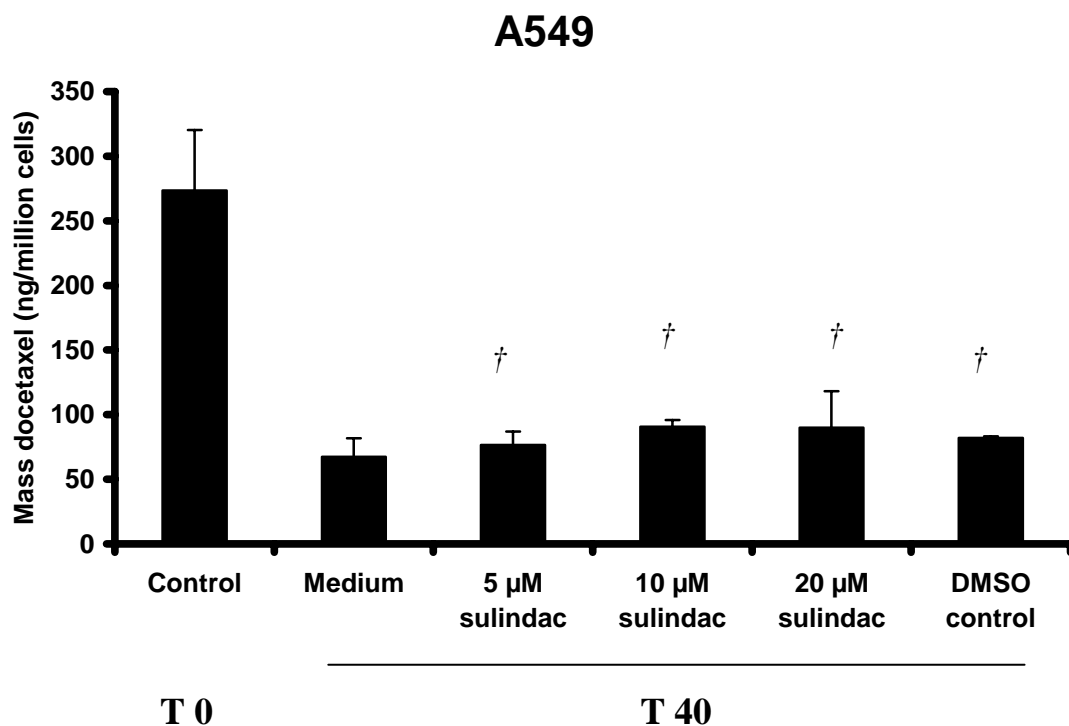


**Figure 3.4.2** The effect of sulindac on docetaxel efflux in A549. Cells were exposed to 10  $\mu$ M docetaxel for 90 minutes (control, T0). Docetaxel was removed and replaced with medium or medium containing sulindac or DMSO control for 40 minutes (T40). The control contained the equivalent amount of DMSO present in 20  $\mu$ M sulindac. Data are mean  $\pm$  SD calculated on experiments performed in triplicate. † not significantly different from the T40 medium control,  $P > 0.05$  relative to the T40 medium control.

### **3.5 Effect of the P-gp inhibitor Elacridar (GF120918) on docetaxel accumulation in A549.**

The mass of docetaxel accumulated in the P-gp-negative A549 cell line was examined in the presence of the P-gp inhibitor elacridar. Cells were incubated with 10  $\mu\text{M}$  docetaxel for 90 minutes. The addition of 2.5, 5 and 10  $\mu\text{M}$  elacridar had no effect on cellular docetaxel levels after 90 minutes (Figure 3.5.1).

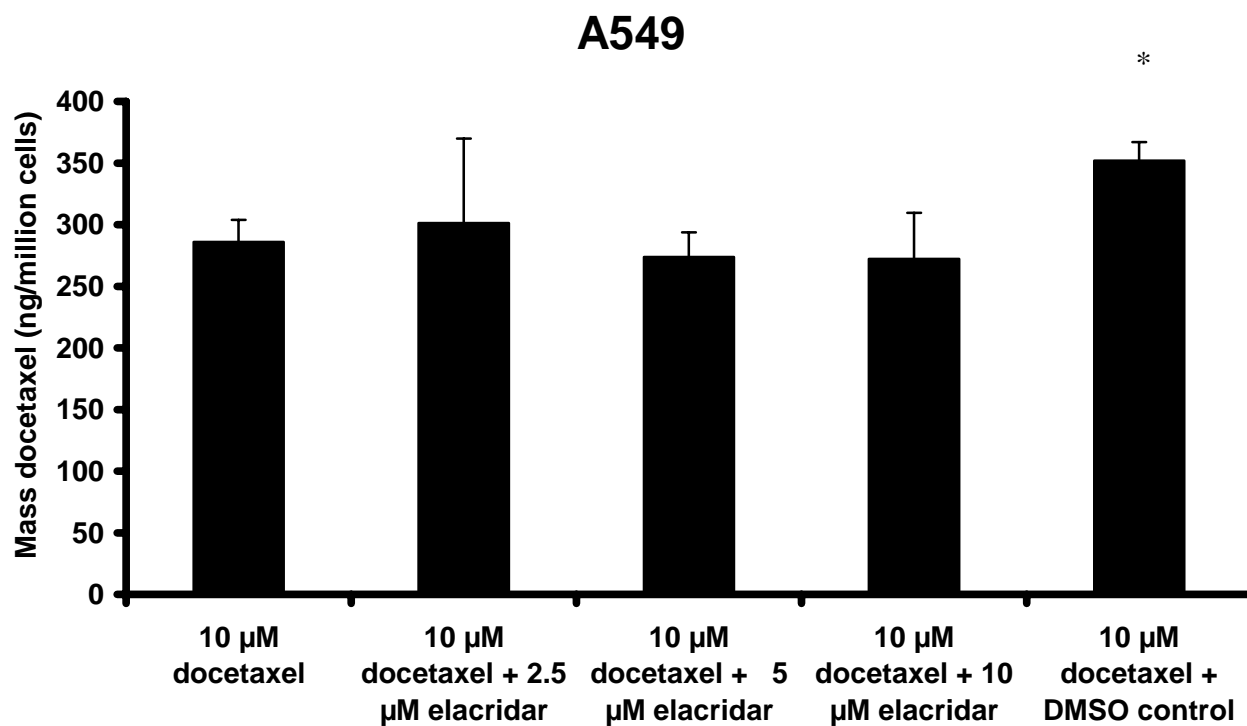


**Figure 3.5.1** A549 cells were incubated with 10  $\mu$ M docetaxel or 10  $\mu$ M docetaxel and a range of elacridar concentrations for 90 minutes. A 0.3% DMSO control was included with an equivalent amount of vehicle as found in 10  $\mu$ M elacridar. Data are mean  $\pm$  SD calculated on experiments performed in triplicate \* significantly different from control (10  $\mu$ M docetaxel).  $P < 0.05$  relative to the control.

### **3.6 The effect of sodium azide on taxane transport in A549.**

One of the aims of this project was to examine the possibility of the existence of an energy-dependent taxane influx mechanism in lung cancer cells. Sodium azide is widely used to deplete ATP levels in cell systems. The effect of a wide range of azide concentrations on docetaxel accumulation was examined in the A549 cell line using glucose-free medium and dialysed serum (serum filtered to remove small molecules < 10,000 MW) , Figure 3.6.1. The presence of sodium azide did not reduce the amount of docetaxel accumulated significantly. A docetaxel accumulation, Figure 3.6.2, and efflux assay, Figure 3.6.3, was then carried out in the presence of 10 mM sodium azide, glucose free medium and dialysed serum to assess the effects of sulindac on taxane transport in conditions with reduced ATP-levels. Sulindac did not significantly affect docetaxel accumulation or efflux in the presence of sodium azide in the A549 cell line.

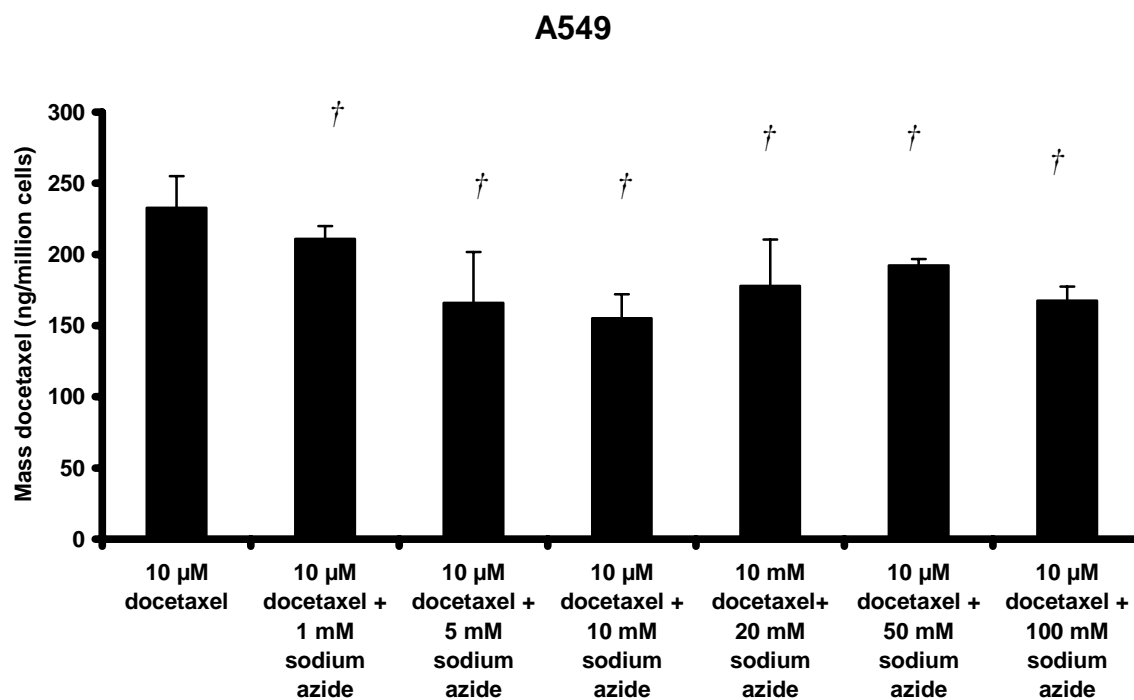


**Figure 3.6.1** A549 cells were incubated with 10  $\mu$ M docetaxel or 10  $\mu$ M docetaxel and a range of sodium azide concentrations for 90 minutes. The assay was carried out in glucose-free DMEM medium containing 5% dialysed serum. Data are mean  $\pm$  SD calculated on experiments performed in duplicate. Sodium azide was dissolved in water. † no significant difference relative to the control (10  $\mu$ M docetaxel),  $P > 0.05$  relative to the control.

### A549

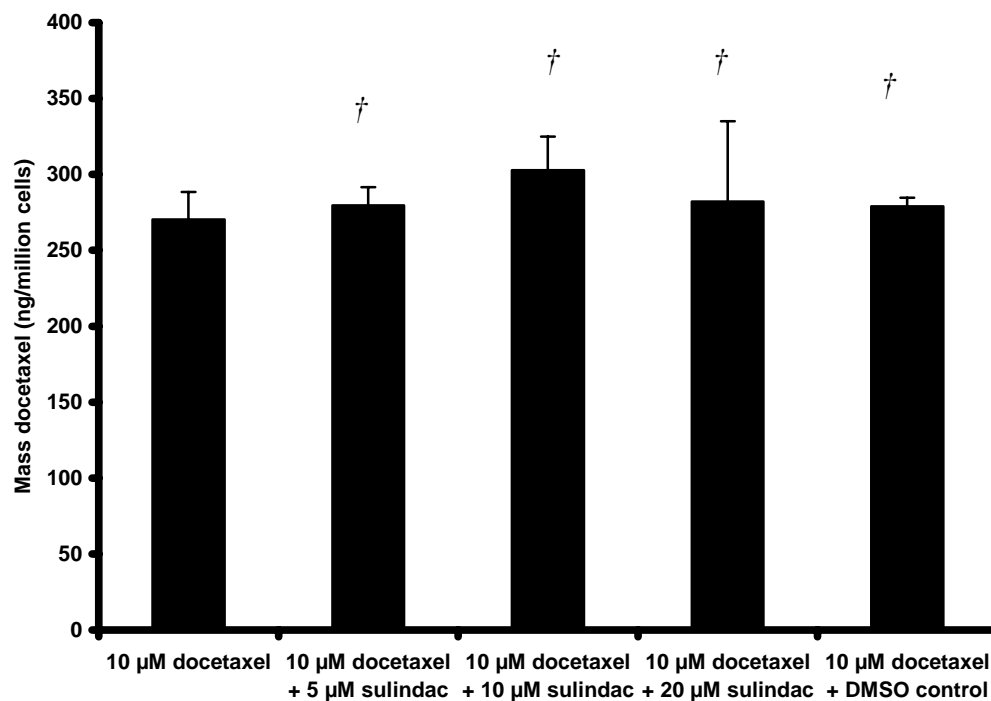


**Figure 3.6.2** The effect of sulindac on docetaxel accumulation in A549 in the presence of 10 mM sodium azide. A549 cells were incubated with 10 µM docetaxel or 10 µM docetaxel and a range of sulindac concentrations for 90 minutes. The assay was carried out in glucose-free DMEM medium containing 5% dialysed serum and 10 mM sodium azide. Sulindac was dissolved in DMSO. Control contained 0.7% DMSO. Data are mean +/- SD calculated on experiments performed in triplicate. † no significant difference relative to the control (10 µM docetaxel),  $P > 0.05$  relative to the control.

## A549

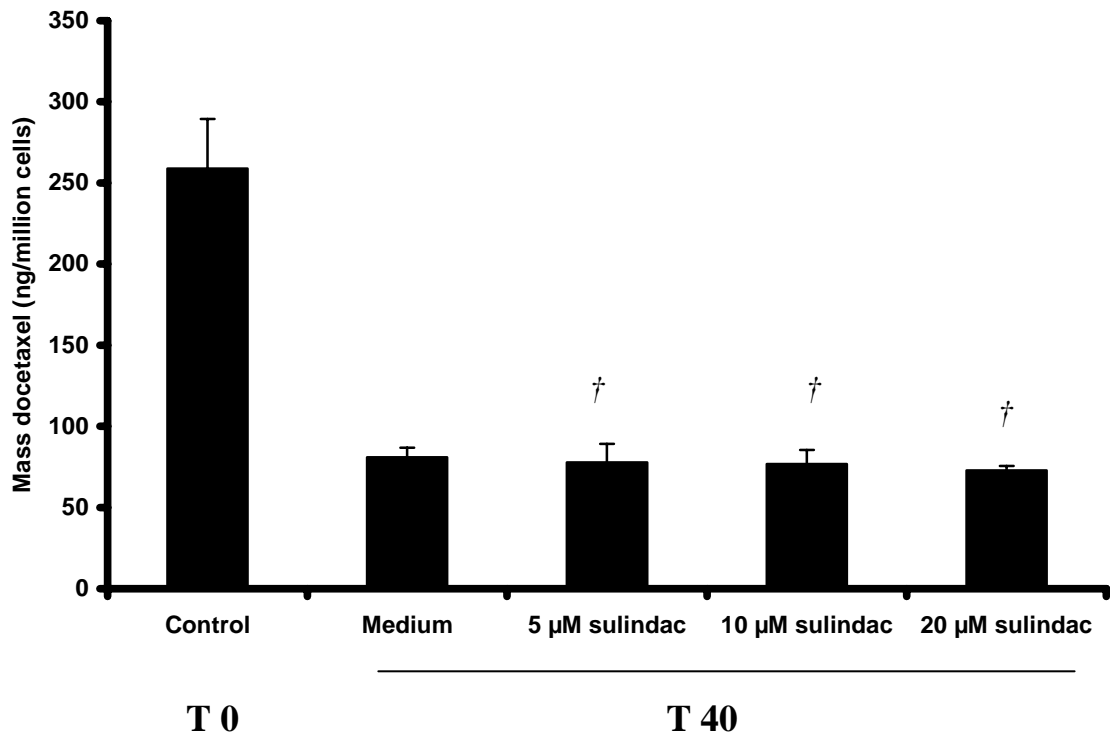


**Figure 3.6.3** The effect of sulindac on docetaxel efflux in A549 in the presence of 10 mM sodium azide. Cells were exposed to 10 µM docetaxel in glucose-free medium (DMEM) for 90 minutes (control, T0). Docetaxel was removed and replaced with glucose-free medium or glucose-free medium containing sulindac for 40 minutes (T40). The DMSO control was omitted as it was shown to have no effect, Figure 3.3.2. Data are mean +/- SD calculated on experiments performed in triplicate.

† no significant difference relative to the control (T40 Medium), P > 0.05 relative to the control.

### **3.7 The effect of P-gp inhibitors on taxane transport in DLKP.**

The DLKP cell line expresses the drug resistance associated MRP-1 efflux pump [160]. Cyclosporin A and verapamil are classic P-gp modulators while elacridar is a third generation non-reversible P-gp inhibitor. A comparison of taxane accumulation in the presence of these inhibitors is shown in Figure 3.7.1. DLKP does not express detectable levels of P-gp (Figure 3.2.1). Approximately four times more docetaxel than paclitaxel was accumulated in this cell line. None of the P-gp inhibitors affected paclitaxel accumulation.

DLKP cells were loaded with docetaxel for 90 minutes. The drug was then removed and the cells were incubated with medium or the P-gp modulators cyclosporin A and verapamil. Cyclosporin A had no effect on docetaxel retention while the effect of verapamil was minute but significant, Figure 3.7.2. Elacridar and sulindac had no significant effect on docetaxel retention, Figure 3.7.3.

A trypan blue cell viability study was carried out in DLKP to ensure the extreme levels of taxanes used in the HPLC assay did not cause direct toxic insult to the cancer cells resulting in necrosis within the time frame of the experiment. Docetaxel, rather than paclitaxel, was chosen for the experiment given its greater toxicity. Cells were grown according to procedure and the percentage cell death determined by the trypan blue method (Section 2.5.2). 10  $\mu$ M docetaxel did not cause a significant increase in dead cells in the accumulation and efflux assays compared to the accumulation assay control (Table 3.7.1).

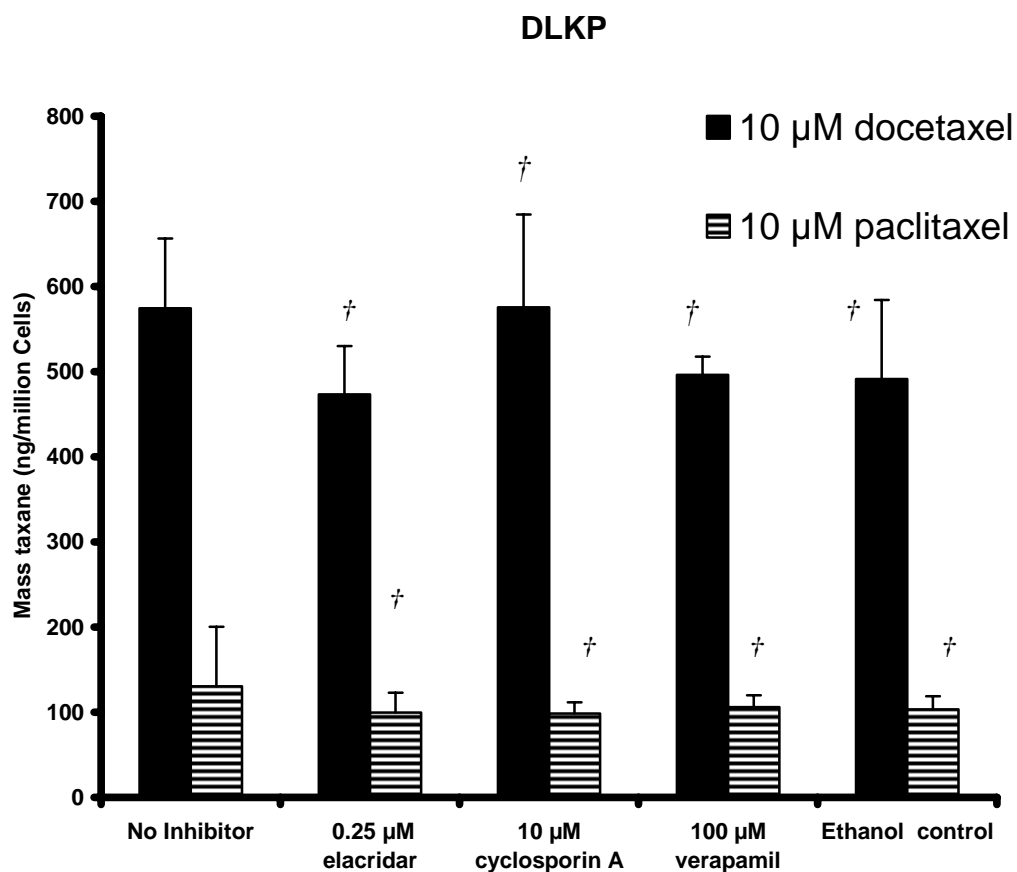


**Figure 3.7.1** Comparison of docetaxel and paclitaxel accumulation in DLKP. Cells were exposed to 10  $\mu$ M docetaxel or paclitaxel for 90 minutes in the presence or absence of inhibitor. The ethanol control is specifically for cyclosporin A. Verapamil is dissolved in water. Elacridar was delivered in DMSO. Data are mean  $\pm$  SD calculated on experiments performed in triplicate. <sup>†</sup> no significant difference relative to the control (No inhibitor),  $P > 0.05$  relative to the control.

## DLKP

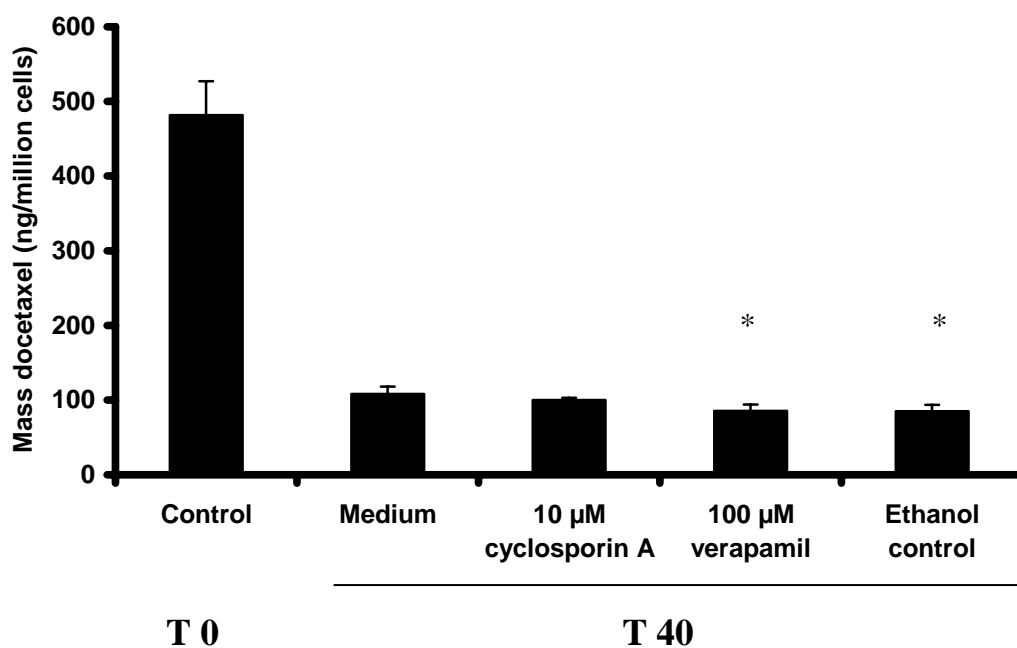


**Figure 3.7.2** Docetaxel efflux assay in DLKP. T0 represents the mass of docetaxel accumulated in DLKP cells exposed to 10 μM docetaxel for 90 Min. T40 represents the mass of docetaxel remaining in the cells 40 minutes after drug removal and in the presence of P-gp inhibitors or medium. DLKP does not express P-gp. Data are mean  $\pm$  SD calculated on experiments performed in triplicate. \* significantly different from the control (T40 Medium),  $P < 0.05$  relative to the control.

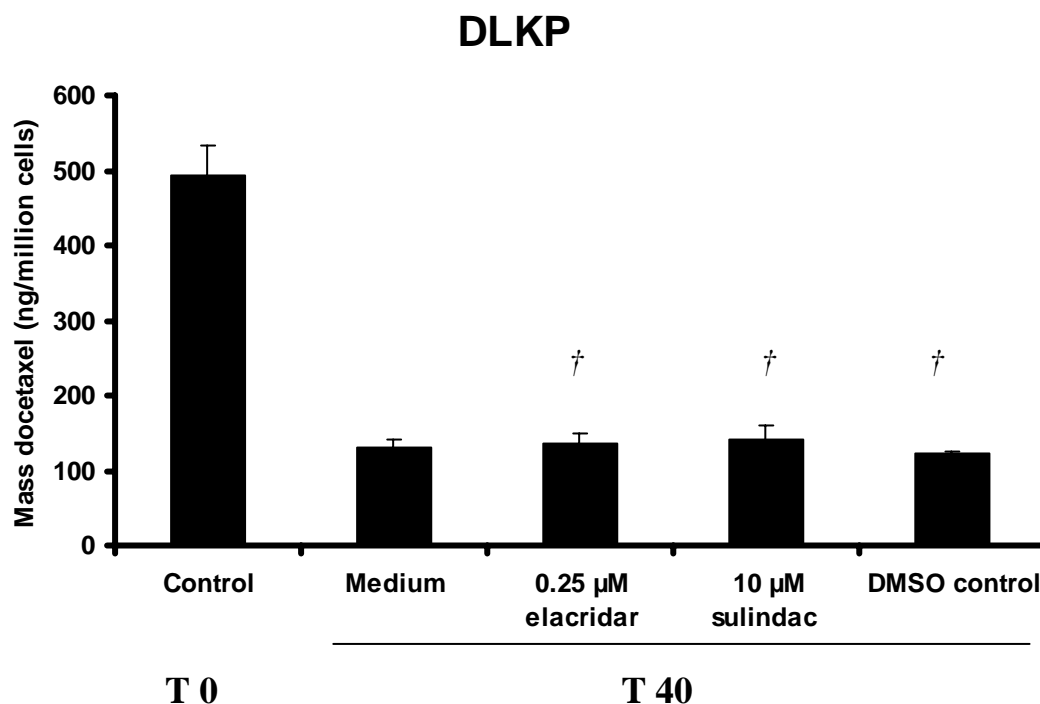


**Figure 3.7.3** Docetaxel efflux assay in DLKP. T0 represents the mass of docetaxel accumulated in DLKP cells exposed to 10  $\mu$ M docetaxel for 90 minutes. T40 represents the mass of docetaxel remaining in the cells 40 minutes after drug removal and in the presence of elacridar, sulindac or medium. DLKP does not express P-gp. Data are mean  $\pm$  SD calculated on experiments performed in triplicate. † no significant difference relative to the control (T40 Medium),  $P > 0.05$  relative to the control.

**Table 3.7.1** Measurement of % dead DLKP cells using the trypan blue method. Four cell counts were taken from duplicate flasks and the total viable and non-viable cell counts averaged to determine % of cells that were dead. † no significant difference,  $P > 0.05$  relative to the control values.

Conditions	% Dead Cells
Accumulation assay control- Medium for 90 minutes	2.96 +/- 0.46
10 $\mu$ M docetaxel in medium for 90 minutes	4.63 +/- 2.09 †
Efflux assay control – loaded with 10 $\mu$ M docetaxel for 90 minutes, drug removed and replaced with medium for 40 minutes	2.68 +/- 0.61 †
Loaded with 10 $\mu$ M docetaxel for 90 minutes, drug removed and replaced with medium containing 0.25 $\mu$ M elacridar for 40 minutes	2.96 +/- 2.06 †

### **3.8 The effect of ATP inhibitors on docetaxel accumulation in DLKP.**

Docetaxel accumulation was examined in the presence of 10 mM sodium azide, 5 mM 2-deoxyglucose and elacridar in the DLKP cell line, Figure 3.8.1. Sodium azide and 2-deoxyglucose are standard agents used to deplete cellular ATP levels. Elacridar was included as a negative control for P-gp activity. Addition of 10 mM sodium azide in glucose-free medium reduced docetaxel accumulation from 284 ng/million cells in the presence of glucose to 148 ng/million cells. The inclusion of 5 mM 2-deoxyglucose with sodium azide did not significantly decrease docetaxel accumulation further compared to sodium azide alone,  $P = 0.18$ . The presence of elacridar had no significant effect on docetaxel accumulation in DLKP.

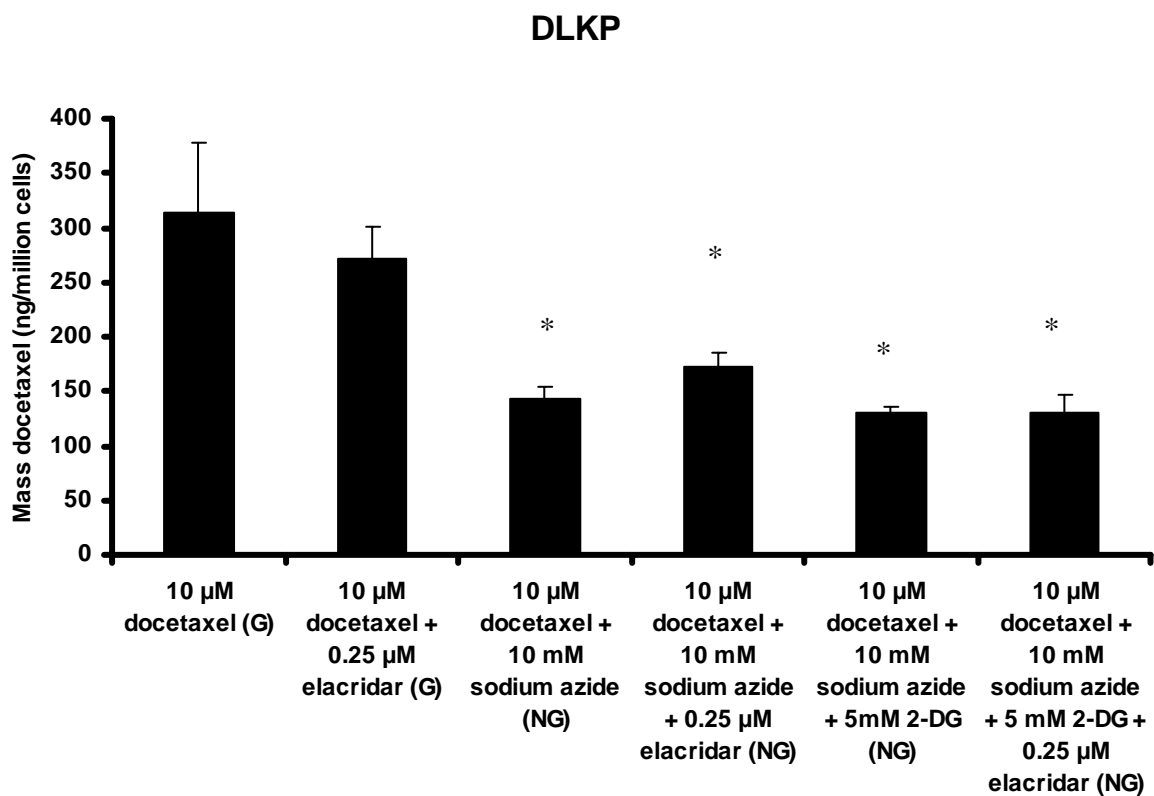


**Figure 3.8.1** DLKP cells were incubated with 10 µM docetaxel or 10 µM docetaxel and various combinations of sodium azide, 2-deoxyglucose and elacridar for 90 minutes. (G) denotes glucose containing DMEM/Ham's F12 supplemented with 5% FCS. (NG) denotes glucose-free DMEM containing 5% dialysed FCS. Sodium azide and 2-deoxyglucose were dissolved in water, elacridar was dissolved in DMSO. Data are mean +/- SD calculated on experiments performed in triplicate. \* significantly different from the control (10 µM docetaxel (G)),  $P < 0.05$  relative to glucose containing control.

### **3.9 Taxane accumulation and efflux in the multi-drug resistant cell line DLKP-A**

DLKP-A is a resistant variant of DLKP created by increasing exposure to adriamycin by Dr. Mary Heenan [259]. The DLKP-A cell line over-expresses P-gp (Figure 3.2.1) and is highly resistant to the taxanes. A comparison of docetaxel and paclitaxel accumulation in this cell line is shown in Figure 3.9.1. Four times more docetaxel than paclitaxel was accumulated in this P-gp over-expressing cell line. Elacridar increased docetaxel and paclitaxel retention 4-fold and 2-fold, respectively. Cyclosporin A increased accumulation of both taxanes approximately 2-fold. Verapamil has no effect on docetaxel levels but a similar affect to cyclosporin A on paclitaxel levels.

Docetaxel and paclitaxel efflux in DLKP-A is shown in Figure 3.9.2. There was approximately six times more docetaxel than paclitaxel accumulated in this cell line after 90 minutes. Elacridar was the only inhibitor that increased docetaxel retention after 40 minutes. Cyclosporin A and verapamil had no effect on docetaxel efflux. Sulindac increased docetaxel efflux but not significantly relevant to the control. All three P-gp inhibitors successfully maintained control levels (T<sub>0</sub>) of paclitaxel.

Cyclosporin A and verapamil are well established P-gp inhibitors. Their poor ability modulating docetaxel accumulation and efflux in the DLKP-A cell line (Figures 3.9.1 and 3.9.2) was not reflected in proliferation assays carried out in this cell line. Verapamil had no effect on docetaxel accumulation or efflux but the combination of docetaxel (37 nM) with verapamil (1, 2 and 10  $\mu$ M) resulted in a concentration-dependent and synergistic increase in toxicity (Figure 3.9.3). All concentrations of verapamil used were below 100  $\mu$ M, the concentration that fails to affect docetaxel and paclitaxel accumulation in the HPLC-based assays in this cell line. Verapamil also potentiated the toxicity of paclitaxel in DLKP-A (Figure 3.9.4), consistent with the HPLC-determined paclitaxel accumulation assay in DLKP-A (Figure 3.9.1).

DLKP-A is highly resistant to the taxanes due to high levels of P-gp over-expression. Verapamil had little effect on docetaxel accumulation and efflux but did modulate paclitaxel levels in these assays. This is reflected in the proliferation assay in Figure 3.9.4. The combination of 10  $\mu$ M verapamil (ten-fold less than the 100  $\mu$ M verapamil concentration used in the HPLC assays) and 58 nM paclitaxel is synergistic in this seven day proliferation assay. The lower levels of verapamil (1 and 2  $\mu$ M) did not potentiate paclitaxel toxicity.

DLKP-A cells were exposed to the HPLC assay conditions of 10  $\mu$ M docetaxel and 100  $\mu$ M verapamil for 90 minutes and then allowed to proliferate for six days. The three concentrations of verapamil used did not increase docetaxel levels over 90 minutes as there was only an additive increase in docetaxel toxicity (Figure 3.9.5).

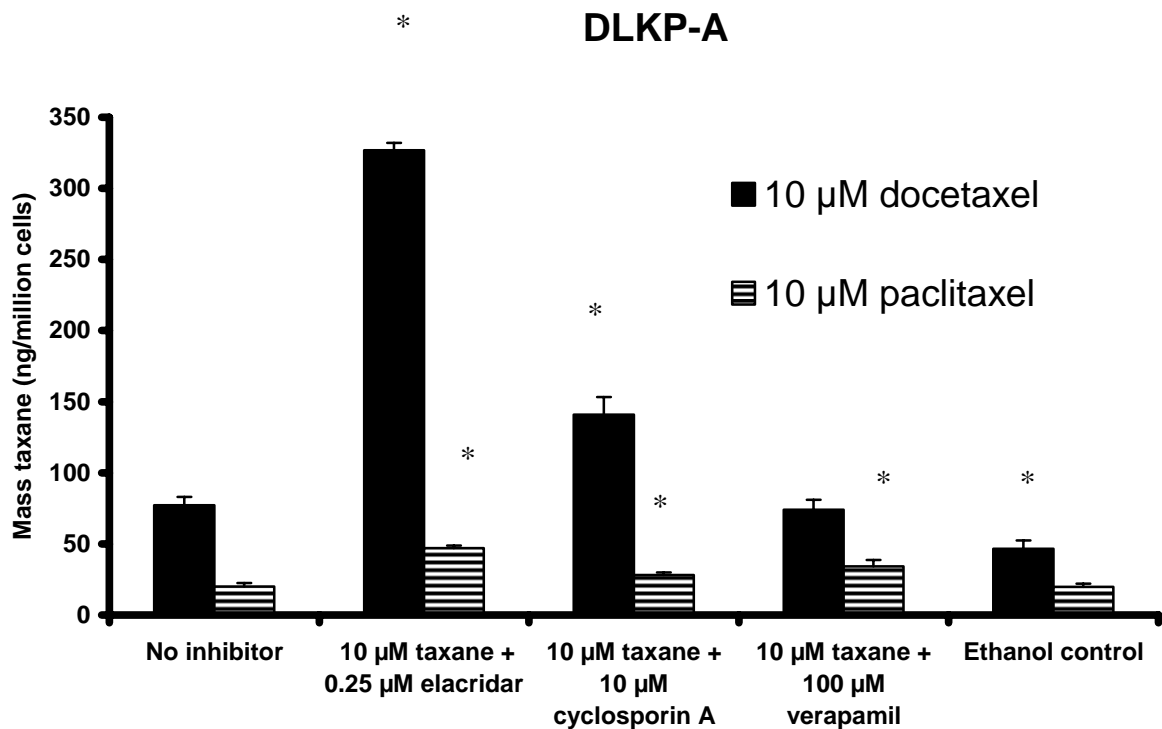


**Figure 3.9.1** Comparison of docetaxel and paclitaxel accumulation in DLKP-A over 90 minutes. The DLKP-A cell line was exposed to 10  $\mu$ M docetaxel or 10  $\mu$ M paclitaxel alone or in the presence of the P-gp modulators, elacridar, cyclosporin A and verapamil. Ethanol is the cyclosporin A delivery vehicle. Verapamil and elacridar were dissolved in water and DMSO respectively. Data are mean  $\pm$  SD calculated on experiments performed in triplicate. \* significantly different from the control (No inhibitor),  $P < 0.05$  relative to control.

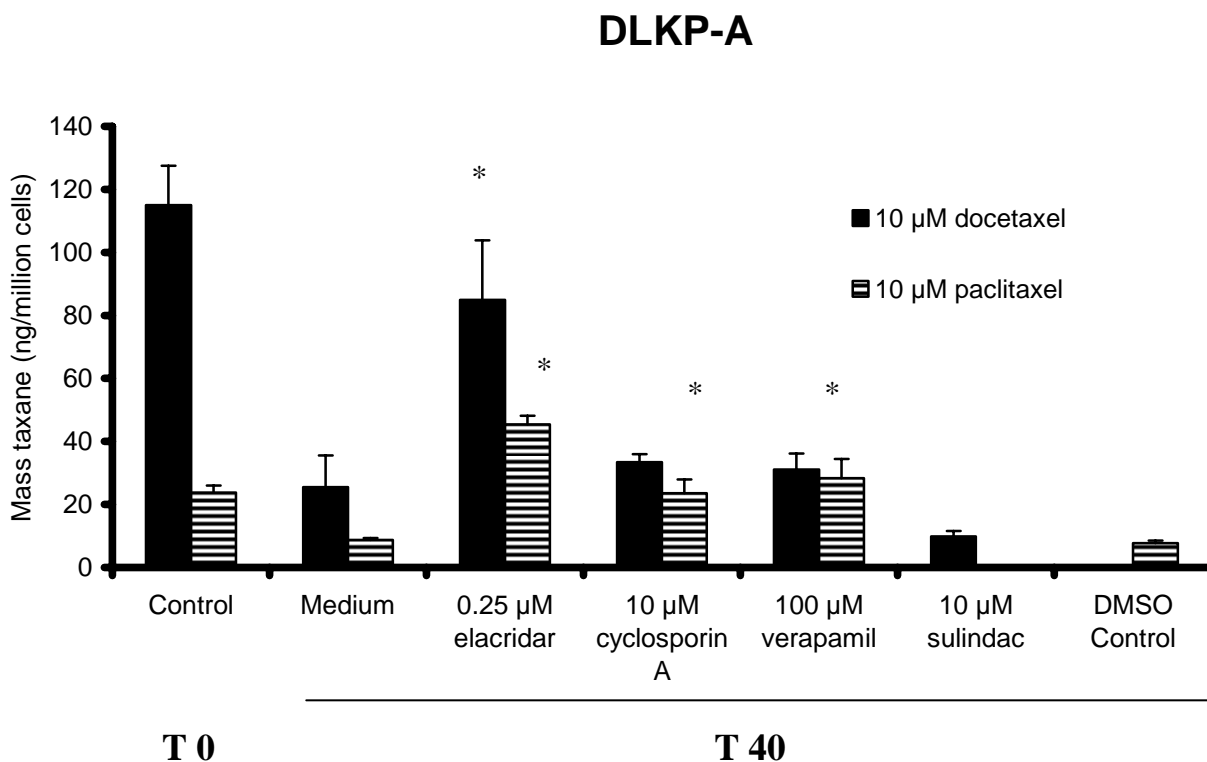


**Figure 3.9.2** Comparison of docetaxel and paclitaxel efflux assays in DLKP-A. The control, T0, represents DLKP-A cells exposed to either 10 μM docetaxel or 10 μM paclitaxel for 90 minutes. The T40 values represent the mass of each taxane remaining in the cells 40 minutes after the taxane was removed and various P-gp inhibitors or sulindac were added. DLKP-A over-expresses P-gp. The DMSO control relates to elacridar. Cyclosporin A, sulindac and verapamil were dissolved in ethanol, DMSO and water, respectively. T40 values for 10 μM sulindac and paclitaxel or a DMSO control for docetaxel were not obtained. Data are mean +/- SD calculated on experiments performed in triplicate. \* significantly different from the control (T40 Medium),  $P < 0.05$  relative to control.

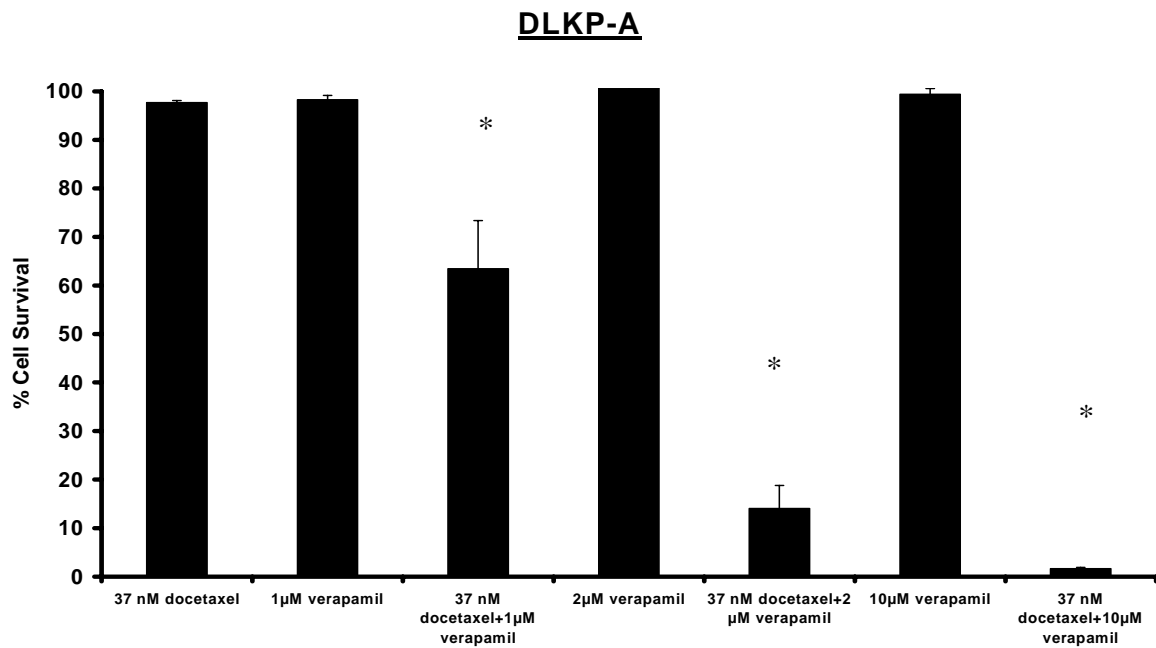


**Figure 3.9.3** Proliferation assay combining 37 nM docetaxel and 1, 2 and 10  $\mu$ M verapamil in DLKP-A. Cells were seeded in 96-well plates 24 hours before application of the drugs and were then allowed to proliferate for a further 6 days. Data are mean  $\pm$  SD calculated on experiments performed in duplicate. \* significantly different from the control (37 nM docetaxel alone),  $P < 0.05$  relative to control.

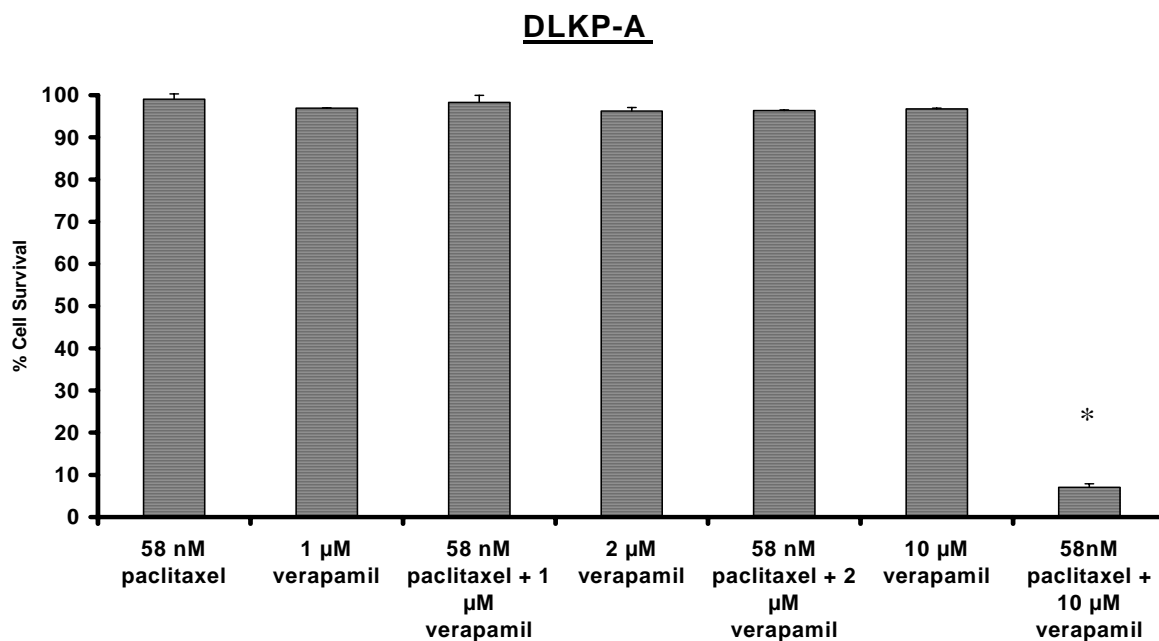


**Figure 3.9.4** Proliferation assay combining 58 nM paclitaxel and verapamil in DLKP-A. Cells were seeded in 96-well plates 24 hours before application of the drugs and were then allowed to proliferate for a further 6 days. Data are mean +/- SD calculated on experiments performed in duplicate. \* significantly different from the control (58 nM paclitaxel alone),  $P < 0.05$  relative to control.

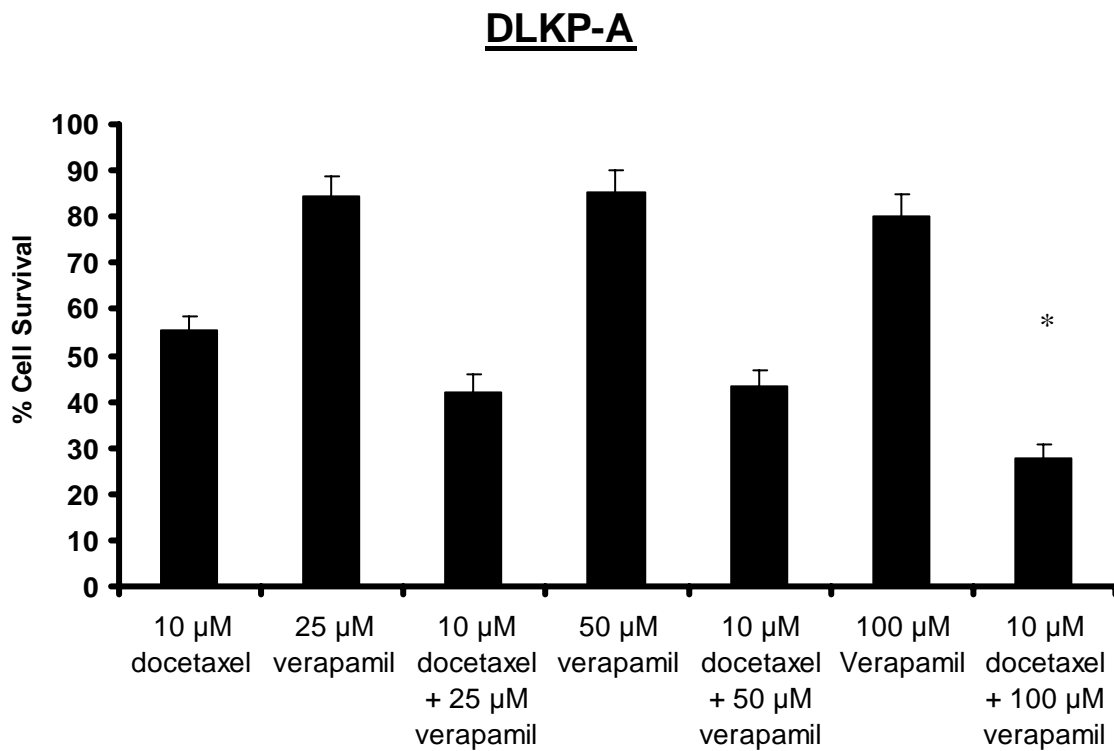


**Figure 3.9.5** Proliferation assay exposing DLKP-A to 10 μM docetaxel and verapamil for 90 minutes. Cells were seeded in 96-well plates 24 hours before application of the drugs for 90 minutes. The drugs were removed and the cells washed. Fresh medium was applied and the cells allowed to proliferate for a further 6 days. Data are mean +/- SD calculated on experiments performed in duplicate.

\* significantly different from the control (10 μM docetaxel alone),  $P < 0.05$  relative to control.

### **3.10 The effect of ATP inhibitors on docetaxel transport in DLKP-A**

Docetaxel accumulation was examined in the presence of 10 mM sodium azide, 10 mM 2-deoxyglucose and elacridar in the DLKP-A cell line, Figure 3.10.1. The combination of sodium azide and 2-deoxyglucose is frequently used to deplete cellular ATP levels. Elacridar was included as a positive control for inhibition of P-gp activity. Addition of 10 mM sodium azide in glucose-free medium increased docetaxel accumulation presumably due to inhibition of P-gp efflux activity by partially decreasing ATP levels. Concurrent treatment with sodium azide and elacridar increased the levels of docetaxel retained further, suggesting a residual P-gp activity inhibited by elacridar. The inclusion of 10 mM 2-deoxyglucose with sodium azide or elacridar with 2-deoxyglucose and sodium azide did not significantly decrease docetaxel accumulation compared to the glucose containing control.

## DLKP-A

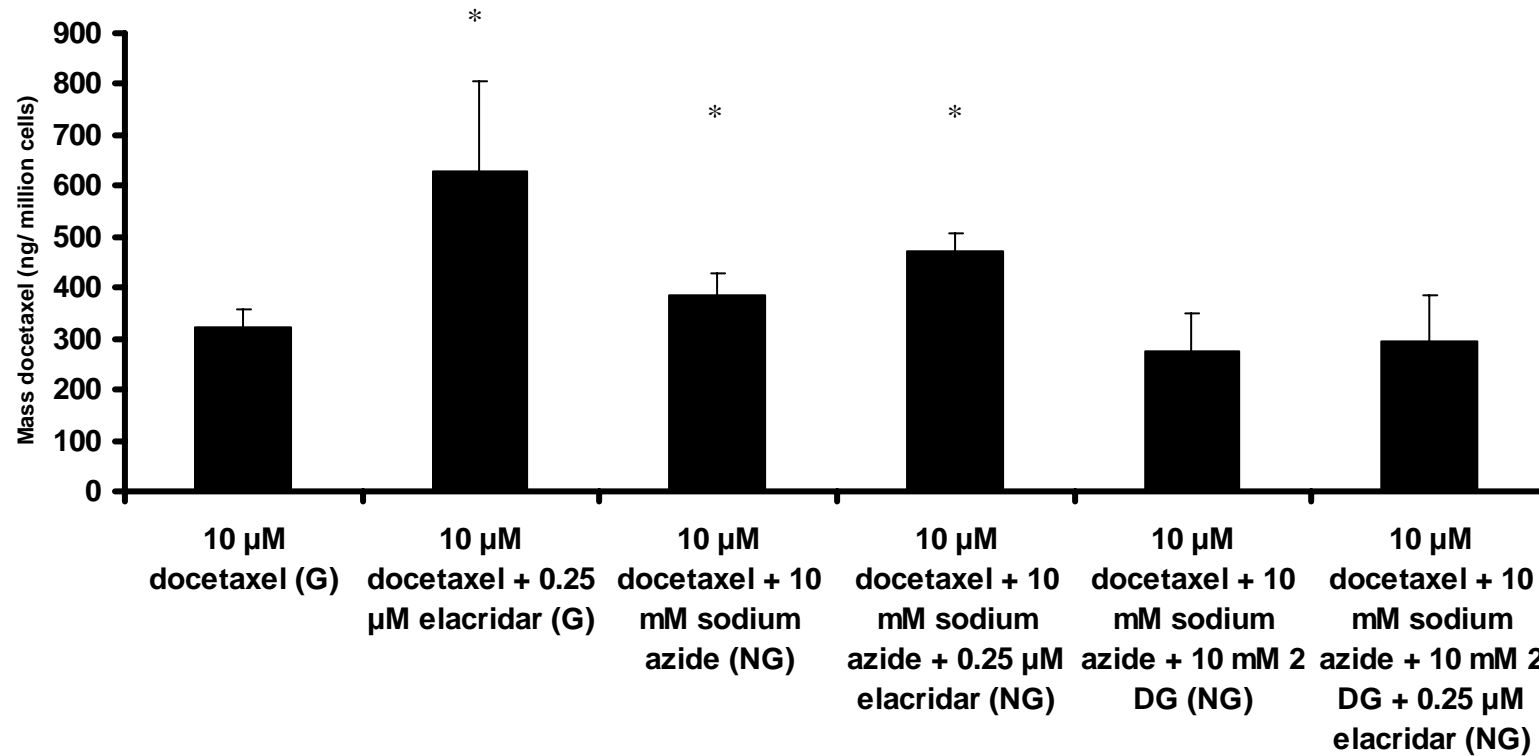


**Figure 3.10.1** DLKP-A cells were incubated with 10  $\mu$ M docetaxel or 10  $\mu$ M docetaxel and various combinations of sodium azide, 2-deoxy glucose and elacridar for 90 minutes. (G) denotes glucose containing DMEM/Ham's F12 supplemented with 5% FCS. (NG) denotes glucose-free DMEM containing 5% dialysed FCS. Sodium azide and 2-deoxyglucose were dissolved in water, elacridar was dissolved in DMSO. Data are mean  $\pm$  SD calculated on experiments performed in triplicate. \* significant,  $P < 0.05$  relative to glucose containing control.

### **3.11 Taxane accumulation in the taxotere-selected cell line DLKP-TXT.**

DLKP-TXT is a docetaxel-selected variant of DLKP that was found to express P-gp (Figure 3.2.1), MRP-1 and BCRP (N.I.C.B. culture collection information, [260]). The amount of paclitaxel accumulated in DLKP-TXT was approximately one third of the amount of docetaxel (Figure 3.11.1). The ratio was closer to 1:4, paclitaxel:docetaxel in DLKP and DLKP-A. In this cell line, cyclosporin A > elacridar > verapamil at increasing docetaxel accumulation but cyclosporin A was the only compound to produce a significant increase (Figure 3.11.1). Although DLKP-TXT expresses P-gp, elacridar did not have as great an effect on taxane accumulation as it did in the DLKP-A cell line. This supports the fact that lower levels of P-gp protein are expressed in DLKP-TXT. Interestingly, sulindac decreased paclitaxel accumulation in this cell line. Elacridar and verapamil minutely increased paclitaxel accumulation, but not significantly.

Verapamil had little effect on paclitaxel and docetaxel accumulation in the P-gp-expressing DLKP-TXT. Verapamil did, however, exhibit a synergistic, concentration-dependent potentiation of docetaxel and paclitaxel toxicity in DLKP-TXT proliferation assays. The toxicity of 1 nM docetaxel (Figure 3.11.2) and 5 nM paclitaxel (Figure 3.11.3) was significantly potentiated by 5, 10 and 20  $\mu$ M verapamil. Higher concentrations of verapamil did not increase docetaxel or paclitaxel retention in DLKP-TXT over 90 minute accumulation assays.

Elacridar is a potent P-gp inhibitor and it increased docetaxel and paclitaxel accumulation in DLKP-TXT by a small margin (Figure 3.11.1). Proliferation assay results show that the lowest concentration tested (0.25  $\mu$ M), the same concentration used in the 90 minute accumulation assay exhibited synergy when combined with docetaxel (Figure 3.11.4) and paclitaxel (Figure 3.11.5).

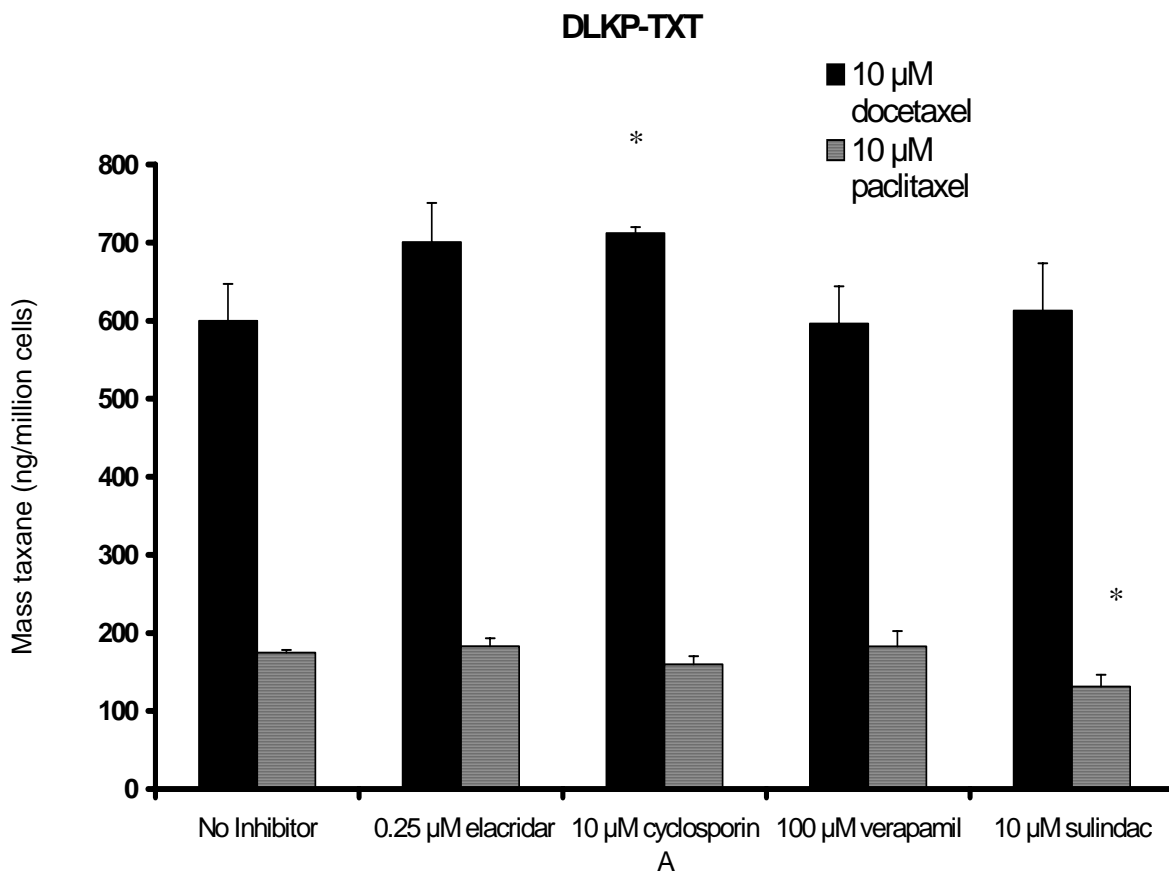


**Figure 3.11.1** Comparison of docetaxel and paclitaxel accumulation in DLKP-TXT. The DLKP-TXT cell line was exposed to 10 μM docetaxel or 10 μM paclitaxel alone, or in combination with the P-gp modulators, elacridar, cyclosporin A and verapamil. Ethanol is the cyclosporin A delivery vehicle. Verapamil and elacridar were dissolved in water and DMSO respectively Data are mean +/- SD calculated on experiments performed in triplicate. \* significantly different from the control (No inhibitor), P < 0.05 relative to respective control.

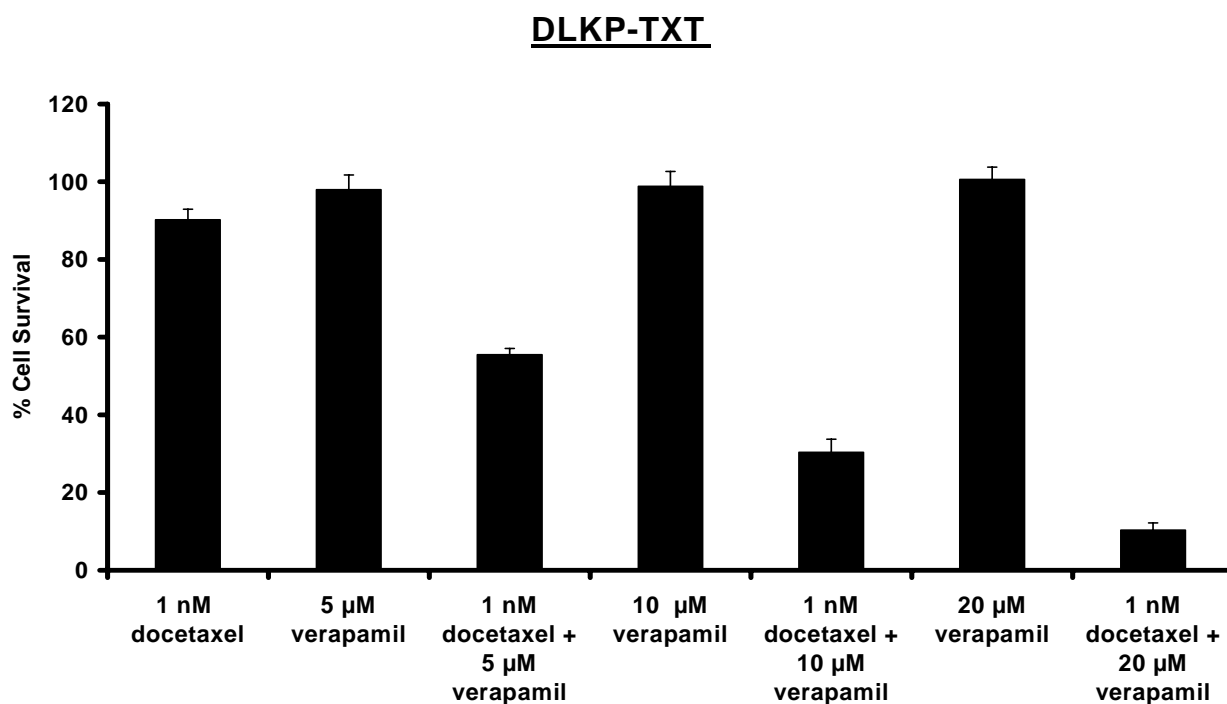


**Figure 3.11.2** Proliferation assay combining docetaxel (1 nM) and verapamil (5, 10, 20  $\mu$ M) in DLKP-TXT. DLKP-TXT expresses P-gp. Verapamil was dissolved in water. This result was obtained from a single determination of eight replicates. Verapamil increased docetaxel toxicity in a concentration-dependent manner.

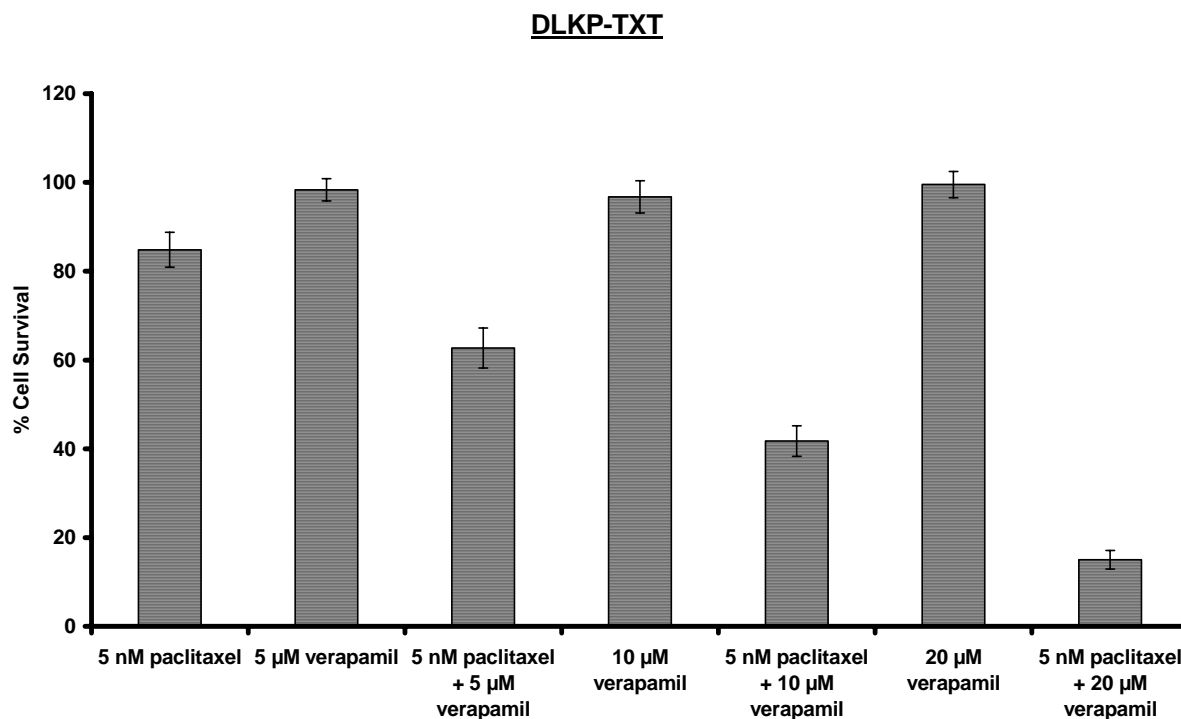


**Figure 3.11.3** Combination toxicity assay 5 nM paclitaxel and verapamil in DLKP-TXT. DLKP-TXT expresses P-gp. Verapamil was dissolved in water. This result was obtained from a single determination of eight replicates. Verapamil increased paclitaxel toxicity in a concentration-dependent manner.

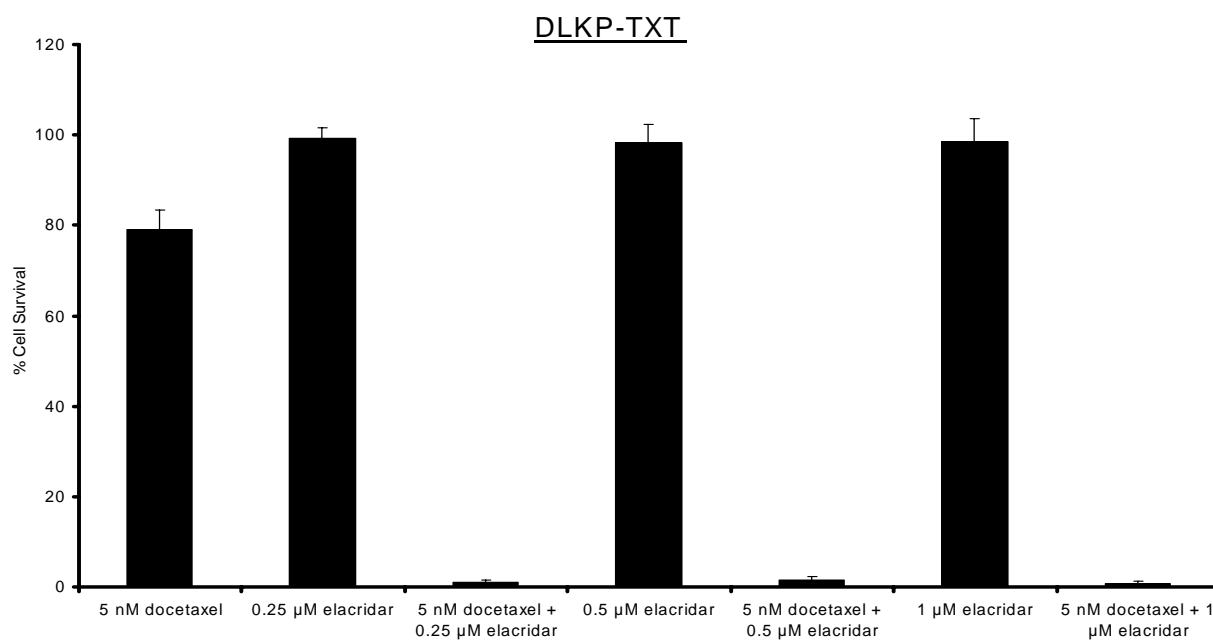


**Figure 3.11.4** Proliferation assay combining 5 nM docetaxel and elacridar in DLKP-TXT. DLKP-TXT expresses P-gp. Elacridar was dissolved in DMSO. This result was obtained from a single determination of eight replicates. The combination of 5 nM docetaxel and elacridar at all concentrations examined was highly synergistic.

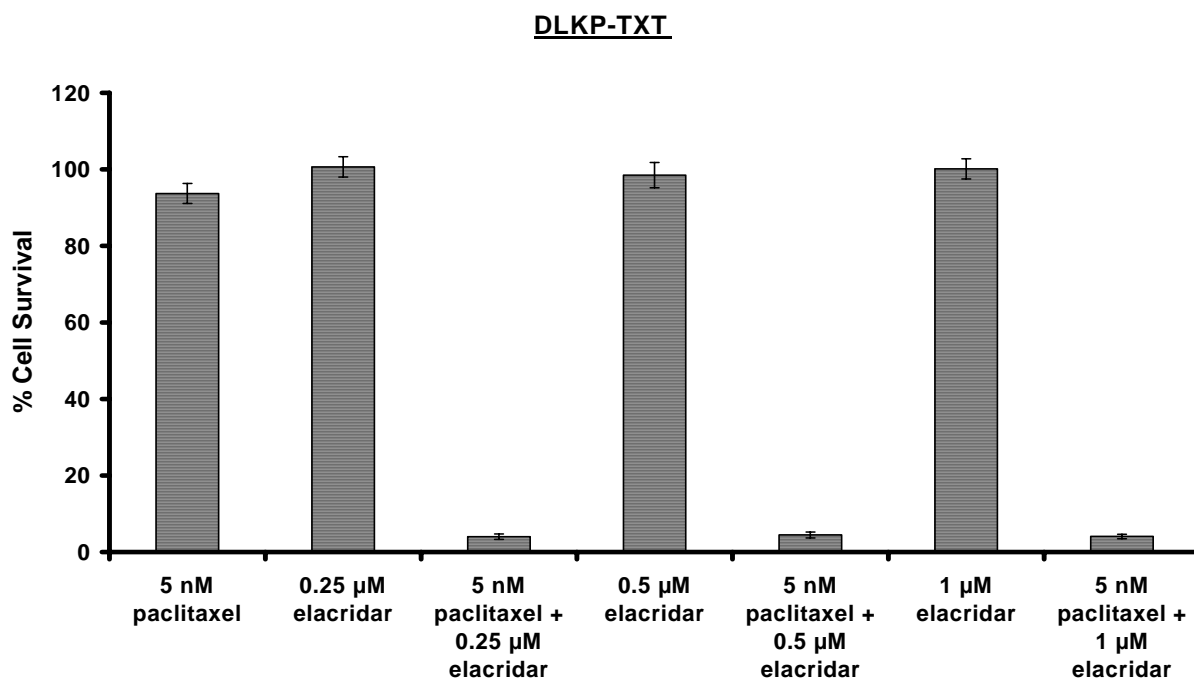


**Figure 3.11.5** Proliferation assay combining 5 nM paclitaxel and elacridar in DLKP-TXT. DLKP-TXT expresses P-gp. This result was obtained from a single determination of eight replicates. Elacridar was dissolved in DMSO. The combinations of 5 nM paclitaxel and elacridar at all concentrations examined was highly synergistic.

### 3.12 Taxane accumulation in HL-60 and HL-60 ADR

HL-60 is a non-adherent human leukemic cell line [261]. HL-60 accumulated approximately 1.2 times the mass of docetaxel than paclitaxel which is much less than the ratio observed in any of the other cell lines examined using the HPLC method, Figure 3.12.1. DLKP-TXT accumulated approximately three times more docetaxel (Figure 3.11.1) and DLKP-A (Figure 3.9.1) and DLKP (Figure 3.7.1), approximately four times more docetaxel than paclitaxel. A direct comparison of the mass of taxanes retained in the HL-60 vs. the DLKP cell lines cannot be made as there is a considerable size difference between these cell lines, the HL-60 cells being smaller than DLKP. The results shown support evidence that HL-60 do not express P-gp. The effect of elacridar on docetaxel accumulation was not significant. More surprising was the significant reduction of accumulation of both taxanes by verapamil. Verapamil is a much less specific pump inhibitor than elacridar and cyclosporin A to a lesser extent. 10  $\mu\text{M}$  sulindac, an inhibitor of MRP-1, had no significant effect with either taxane.

A paclitaxel efflux assay in HL-60 reaffirms that this cell line does not express P-gp (Figure 3.12.2). 9.6% of the accumulated paclitaxel was retained following 40 minutes in drug-free medium. The only significant change in the mass of paclitaxel effluxed was a decrease related to 0.25  $\mu\text{M}$  elacridar. Paclitaxel efflux was unaffected by verapamil or cyclosporin A.

The HL-60ADR cell line is a drug resistant variant of HL-60 created by exposure to adriamycin (doxorubicin), HL-60ADR over-express the MRP-1 drug efflux pump [262]. There was decreased retention of both taxanes in comparison with the HL-60 cell line (Figure 3.12.3). P-gp inhibitors did not have a significant effect on retention of either taxane, bar cyclosporin A, which increased docetaxel accumulation, although not significantly. The MRP-1 inhibitor, sulindac, also had no effect on docetaxel or paclitaxel accumulation. As with HL-60, approximately 1.4 times the amount of docetaxel than paclitaxel was accumulated in this cell line.

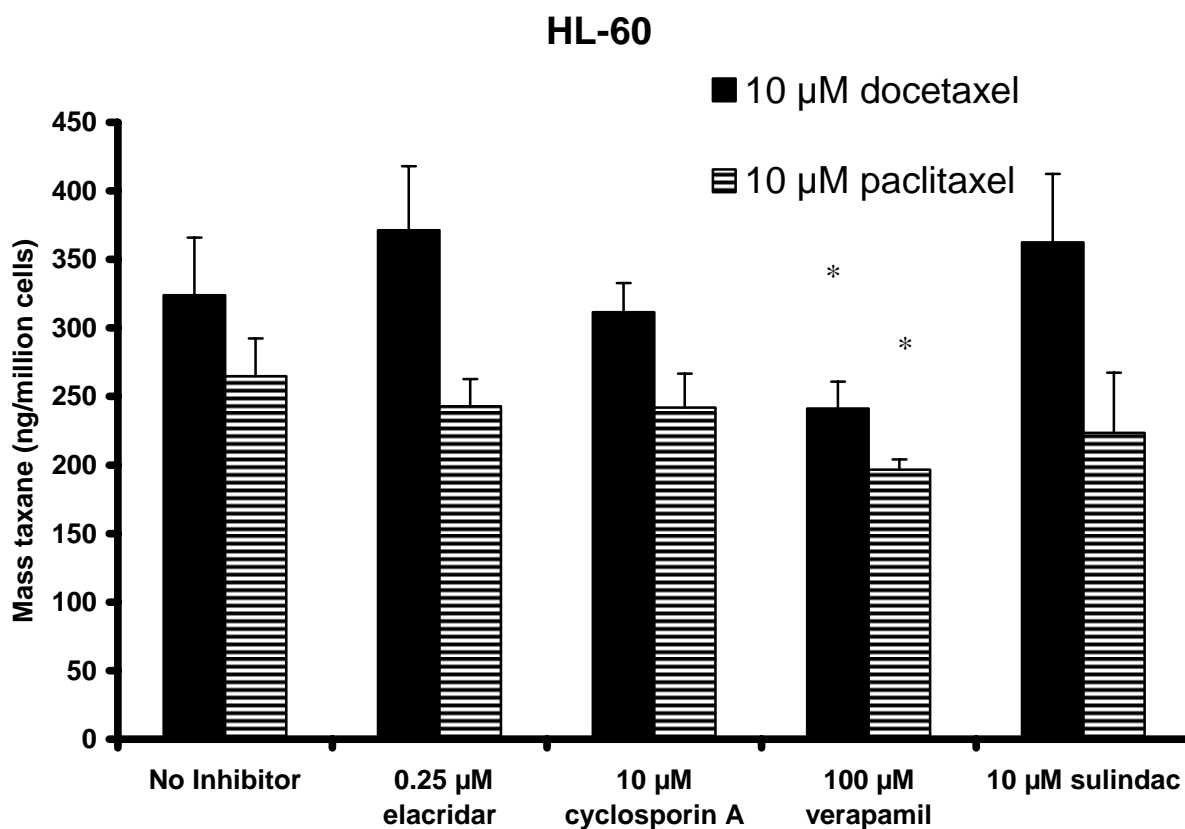


**Figure 3.12.1** Comparison of docetaxel and paclitaxel accumulation in HL-60 over 90 minutes. HL-60 cells were incubated with 10 μM docetaxel or 10 μM paclitaxel alone and in combination with the P-gp modulators elacridar, cyclosporin A and verapamil and the MRP-1 inhibitor sulindac for 90 minutes. Elacridar and sulindac were dissolved in DMSO. Ethanol is the cyclosporin A delivery vehicle. Verapamil was dissolved in water. Vehicle controls have been performed in previous experiments. Data are mean +/- SD calculated on experiments performed in triplicate. \* significantly different from the control (No inhibitor),  $P < 0.05$  relative to control.

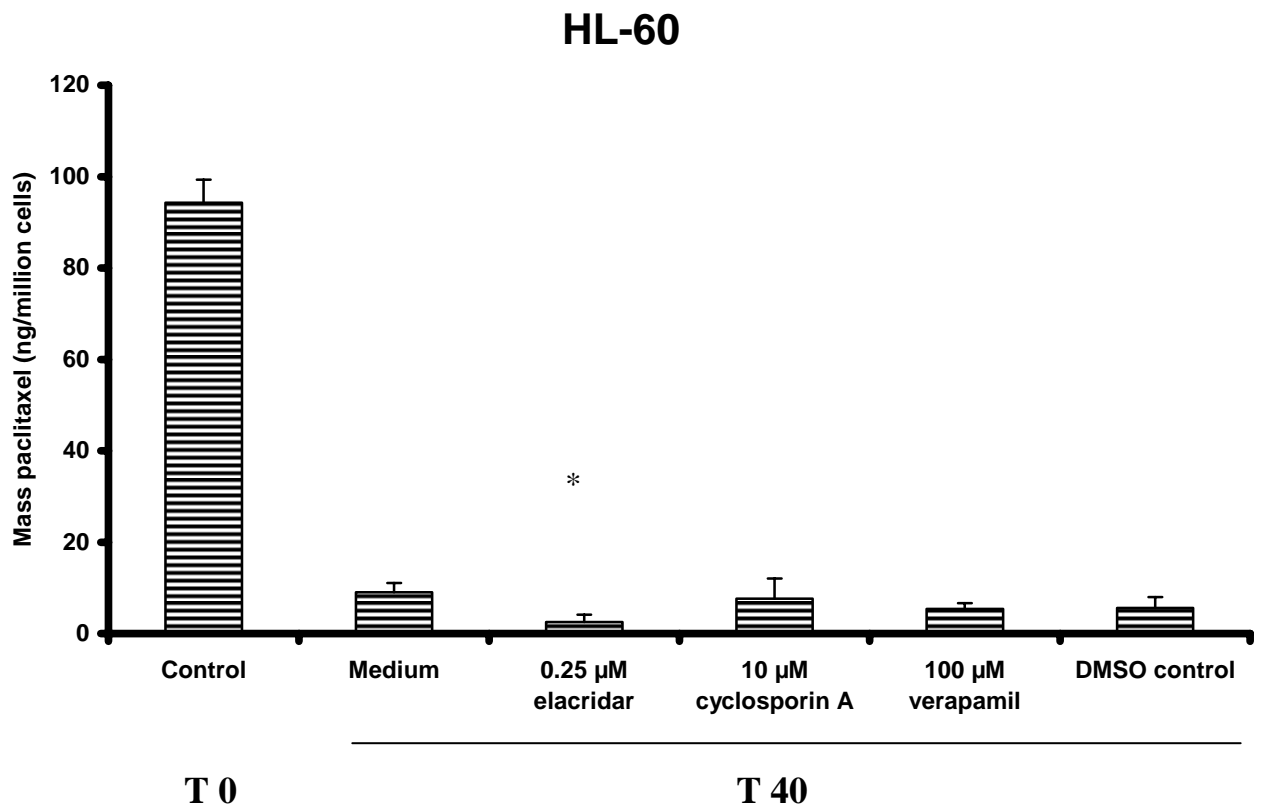


**Figure 3.12.2** Paclitaxel efflux assay in HL-60. The control, T0, represents HL-60 cells exposed to 10  $\mu$ M paclitaxel for 90 minutes. The T40 values represent the mass of paclitaxel remaining in the cells 40 minutes after the paclitaxel was removed and the P-gp inhibitors elacridar, cyclosporin A or verapamil were added. Cyclosporin A, elacridar and verapamil were dissolved in ethanol, DMSO and water, respectively. Vehicle controls have been performed in previous experiments. Data are mean  $\pm$  SD calculated on experiments performed in triplicate. \* significantly different from the control (T40 Medium),  $P < 0.05$  relative to control.

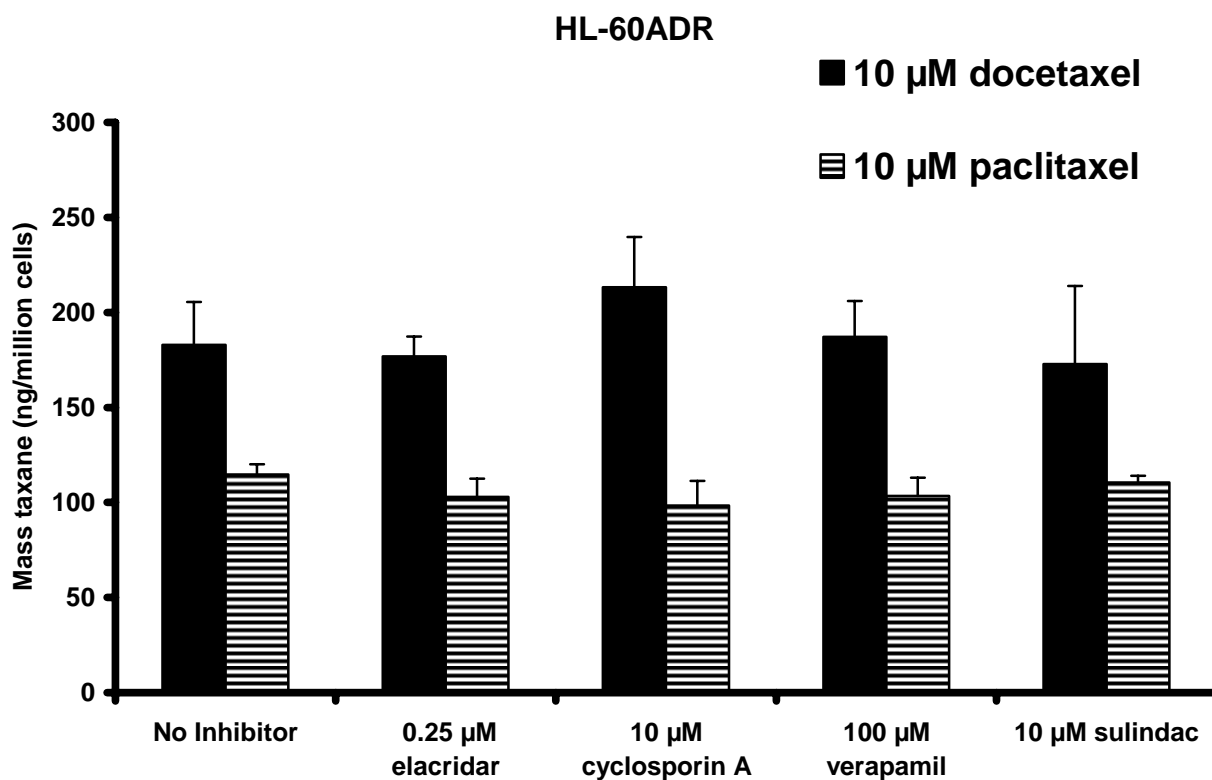


**Figure 3.12.3** Comparison of docetaxel and paclitaxel accumulation in the MRP-1 over-expressing HL-60ADR cell line. HL-60ADR cells were incubated with 10  $\mu$ M docetaxel or 10  $\mu$ M paclitaxel alone and in combination with the P-gp modulators elacridar, cyclosporin A and verapamil and the MRP-1 inhibitor sulindac for 90 minutes. Elacridar and sulindac were dissolved in DMSO. Ethanol was the cyclosporin A delivery vehicle. Verapamil was dissolved in water. Data are mean  $\pm$  SD calculated on experiments performed in triplicate.

### **3.13 Summary of HPLC-based method for taxane measurement**

The HPLC assay proved a number of points. A greater mass of docetaxel than paclitaxel was accumulated in all cell lines examined, corresponding to the more cytotoxic effect of docetaxel in growth assays, although this ratio varied significantly between cell lines. The P-gp inhibitors and the MRP-1 inhibitor, sulindac had no effect on taxane transport in the non-P-gp-expressing cell lines A549 and DLKP. ATP depletion decreased docetaxel accumulation in DLKP but had no significant effect in A549.

In the P-gp-expressing DLKP-A, elacridar was the most potent inhibitor of taxane transport (in accumulation and efflux studies), followed by cyclosporin A. Verapamil did not inhibit docetaxel but did inhibit paclitaxel accumulation and efflux in DLKP-A. Verapamil did, however, exhibit synergistic toxicity with both taxanes in cytotoxicity assays, suggesting an ability to modulate P-gp. ATP depletion increased docetaxel accumulation in this cell line. This effect is examined further in Chapter 6.

DLKP-TXT also expresses P-gp but at lower levels than DLKP-A. The increase in docetaxel accumulation caused by cyclosporin A and elacridar in this cell line was not as dramatic as that seen in DLKP-A. Verapamil had no effect. Combinations of elacridar and verapamil with the taxanes showed equally dramatic synergy in proliferation assays. Verapamil, elacridar and cyclosporin A did not significantly affect paclitaxel accumulation. Interestingly, sulindac decreased paclitaxel levels in this cell line through an unknown mechanism.

The levels of docetaxel and paclitaxel accumulated in HL-60 and HL-60ADR were more similar compared to the other cell lines examined. The decrease in HL-60 docetaxel accumulation related to verapamil was unexpected. Verapamil had a similar effect on paclitaxel accumulation in this cell line. Elacridar treatment resulted in a minor, but significant, increase in paclitaxel efflux from HL-60. None of the inhibitors had a significant effect on docetaxel or paclitaxel accumulation in the MRP-1-over-expressing HL-60ADR.

The studies utilising the HPLC technique for measurement of the taxanes highlighted a number of limitations of the method, generally related to the docetaxel and paclitaxel levels required in the assays.

- 10  $\mu\text{M}$  of docetaxel or paclitaxel is supraphysiological, limiting extrapolation of *in vitro* data to the *in vivo* setting.
- The high concentrations of the taxanes may mask the effects of weaker competitive inhibitors.
- The high concentrations of taxanes may mask the influence of putative uptake mechanisms by saturating any such mechanism. Higher taxane concentrations also increase the contribution of passive diffusion to taxane accumulation.
- The assay protocol was not conducive to high through-put of results.

***Chapter 4. Analysis of epirubicin transport in DLKP-A***

## 4.1 Laser scanning confocal microscopy imaging of epirubicin and paclitaxel.

The anthracycline epirubicin is a P-gp and MRP-1 substrate and therefore P-gp modulators affect epirubicin transport in P-gp-expressing cell lines. Epirubicin is naturally fluorescent and its localisation within cells can be observed by laser confocal microscopy. Taking exposure time (120 minutes) and epirubicin concentration (2  $\mu$ M) from the anthracycline accumulation assay, a spectral scan was performed on DLKP cells exposed to epirubicin for 120 minutes to determine the optimal absorbance (514 nm) and emission (Em Max. 600 nm) wavelengths (Section 2.11). These values were then fixed and used in all epirubicin laser confocal imaging.

Figure 4.1.1 shows detailed laser confocal images of epirubicin accumulation in the DLKP cell line. A single cross section scan revealed epirubicin is not uniformly distributed throughout the nucleus but localises at the nuclear envelope and internal nuclear structures (Figure 4.1.1A). The combination of a number of cross sections (Z-plane stack) provides greater detail on the cytoplasmic epirubicin localisation (Figure 4.1.1B). Numerous, distinct intercellular epirubicin deposits are visible with a definite concentration of drug occurring at the plasma membrane. The plasma membrane and subcellular localisation are displayed with greater clarity in the further magnified image in Figure 4.1.1C.

Figures 4.1.2, 4.1.3 and 4.1.4 are laser confocal microscope images of DLKP, DLKP-A and DLKP-TXT, respectively, exposed to epirubicin alone (A), or in combination with the P-gp modulators elacridar (B), cyclosporin A (C), verapamil (D) or the MRP-1 inhibitor sulindac (E).

The compounds had no effect on epirubicin fluorescence in DLKP at the concentrations used in HPLC-based taxane accumulation and efflux assays (Figure 4.1.2).

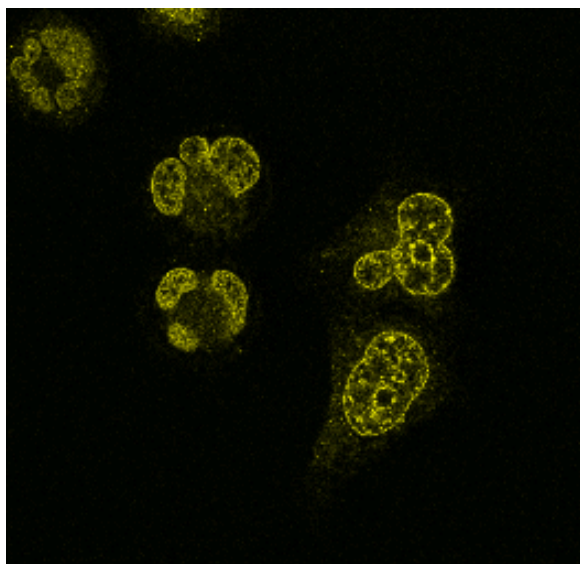
In the P-gp over-expressing DLKP-A, all three P-gp modulators increased nuclear epirubicin fluorescence while the MRP-1 inhibitor sulindac had no effect on nuclear epirubicin fluorescence after a two hour exposure period (Figure 4.1.3).

DLKP-TXT expresses lower levels of P-gp than DLKP-A. The three P-gp modulators do not affect nuclear epirubicin fluorescence compared to the control, Figure 4.1.4. The MRP-1 inhibitor sulindac decreased nuclear fluorescence of epirubicin. Of note with respect to this result is that sulindac also decreased accumulation of paclitaxel, but not docetaxel, in DLKP-TXT (Figure 3.10.1).

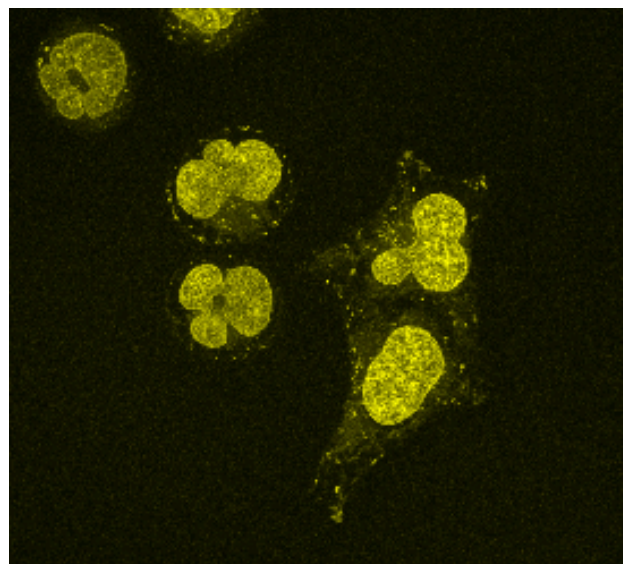
LSCM images of the microtubulin-labelling Oregon-green paclitaxel were obtained in DLKP and A549-Taxol. Over 120 minutes, incubation with 1  $\mu$ M oregon-green paclitaxel gave adequate labelling for visualisation. Tubulin in DLKP had a more localised, centralised distribution (Figure 4.1.5) than the more disperse and homogenous distribution of tubulin in A549-Taxol (Figure 4.1.6). A wide field view of Oregon-green paclitaxel uptake in A549-Taxol revealed inconsistent levels of accumulation within the population (Figure 4.1.7). The nuclei of A549-Taxol cells were devoid of oregon-green paclitaxel fluorescence and a number of cells contained fluorescent oregon-green paclitaxel containing vesicles (Figure 4.1.7). An A549-Taxol cell undergoing mitosis was imaged (Figure 4.1.8). The polarised centromeres and mitotic spindles are clearly visible.

Additional three dimensional imaging of epirubicin and paclitaxel in NSCLC cell lines is provided in Appendix B.

A)



B)



C)

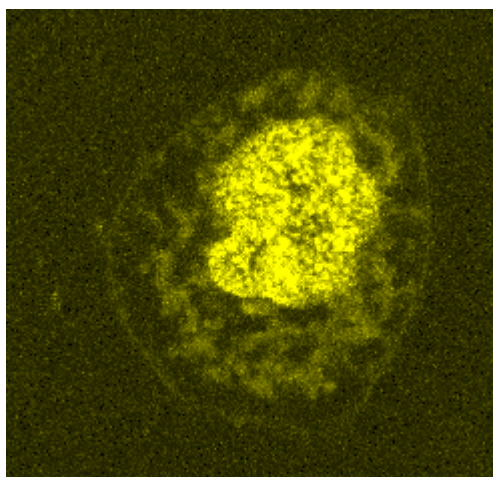
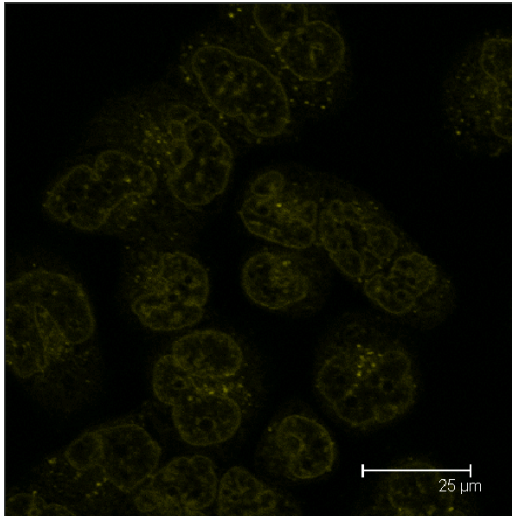
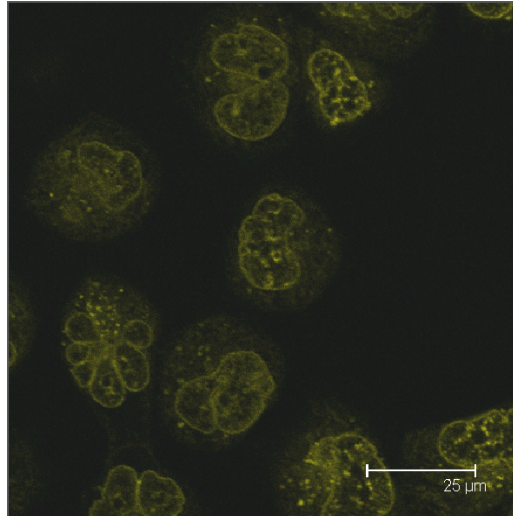


**Figure 4.1.1** DLKP cells were exposed to a concentration of 2  $\mu$ M epirubicin for 2 hours. The drug-containing medium was removed and replaced with drug-free medium. Epirubicin fluorescence was then imaged using a laser confocal microscope. A) A single confocal scan through the Z plane, B) Full projection combining all Z plane scans, C) high magnification single scan of DLKP cell.

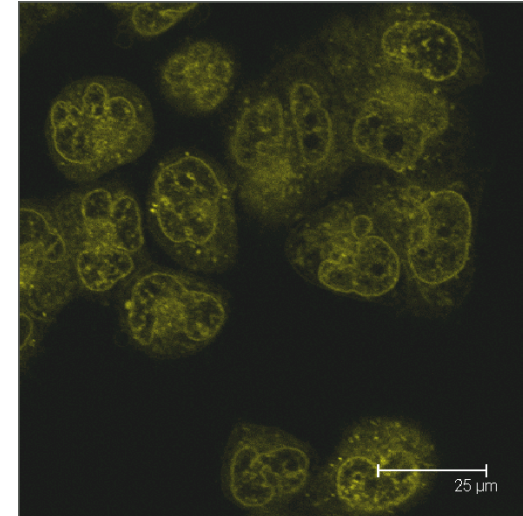
**(A) 2  $\mu$ M epirubicin**



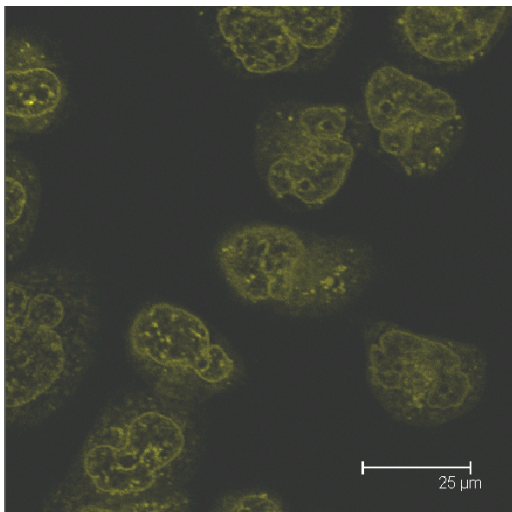
**(B) 2  $\mu$ M epirubicin + 0.25  $\mu$ M elacridar**



**(C) 2  $\mu$ M epirubicin + 10  $\mu$ M cyclosporin A**



**(D) 2  $\mu$ M epirubicin + 100  $\mu$ M verapamil**



**(E) 2  $\mu$ M epirubicin + 10  $\mu$ M sulindac**

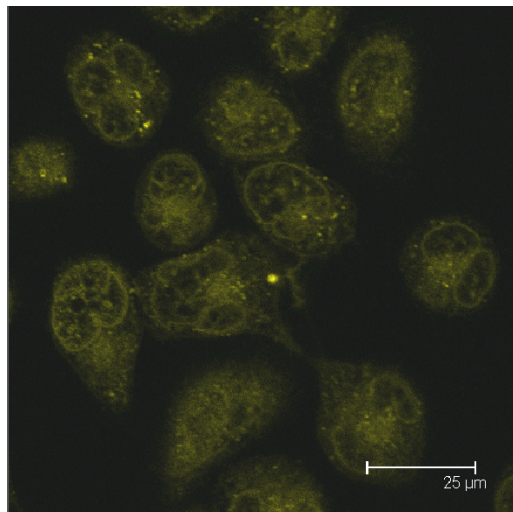
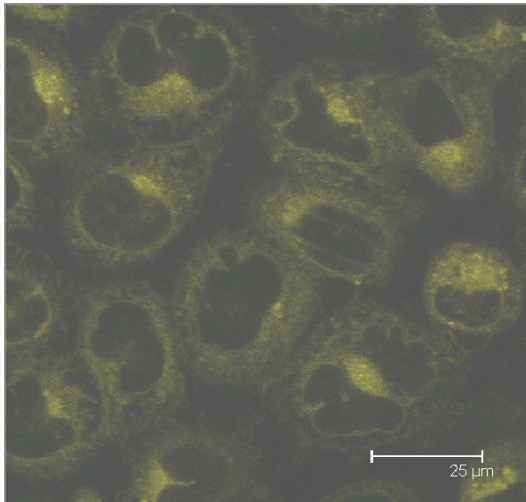
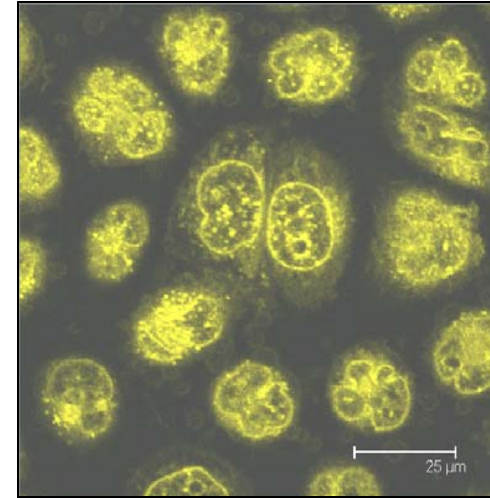
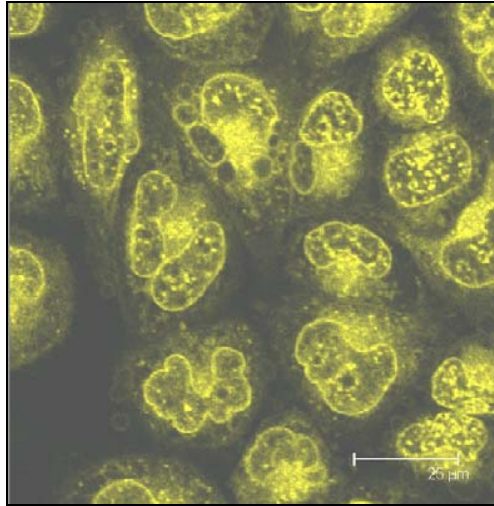


**Figure 4.1.2** DLKP cells were exposed to a concentration of 2  $\mu$ M epirubicin alone or 2  $\mu$ M epirubicin in combination with 0.25  $\mu$ M elacridar, 10  $\mu$ M cyclosporin A, 100  $\mu$ M verapamil or 10  $\mu$ M sulindac for 2 hours. The drug-containing medium was then removed and replaced with drug-free medium. A single scan of epirubicin fluorescence was then imaged using a laser scanning confocal microscope.

**(A) 2  $\mu$ M epirubicin control**



**(B) 2  $\mu$ M epirubicin + 0.25  $\mu$ M elacridar (C) 2  $\mu$ M epirubicin + 10  $\mu$ M cyclosporin A**



**(D) 2  $\mu$ M epirubicin + 100  $\mu$ M verapamil (E) 2  $\mu$ M epirubicin + 10  $\mu$ M sulindac**

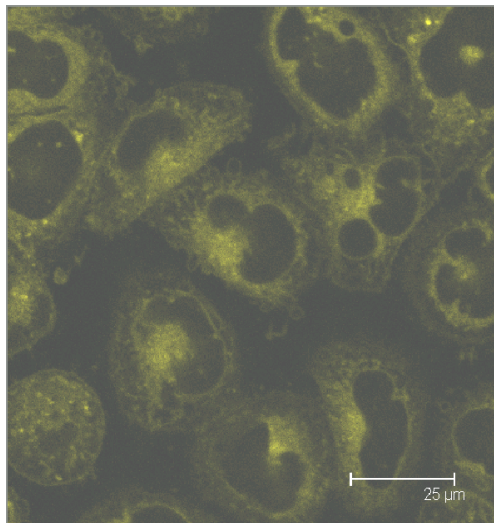
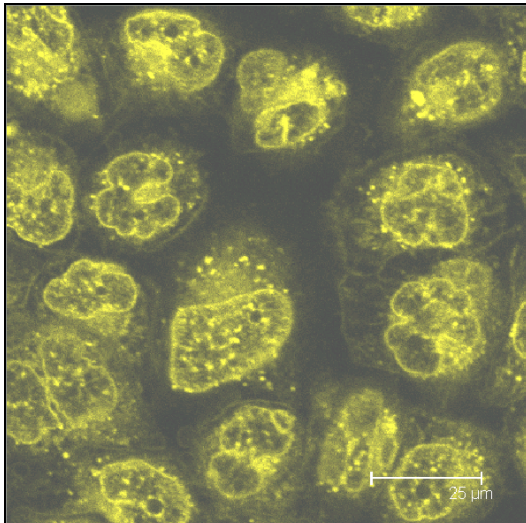
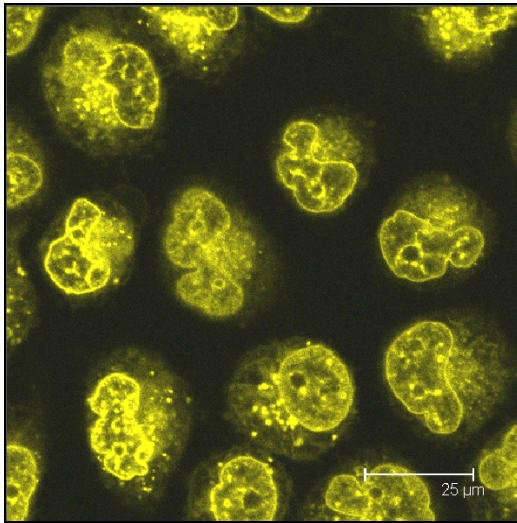
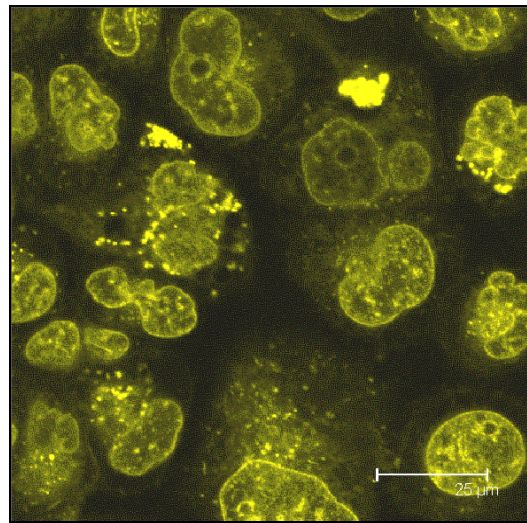


**Figure 4.1.3** DLKP-A cells were exposed to a concentration of 2  $\mu$ M epirubicin alone or 2  $\mu$ M epirubicin in combination with 0.25  $\mu$ M elacridar, 10  $\mu$ M cyclosporin A, 100  $\mu$ M verapamil or 10  $\mu$ M sulindac for 2 hours. The drug-containing medium was then removed and replaced with drug-free medium. A single scan of epirubicin fluorescence was then imaged using a laser scanning confocal microscope.

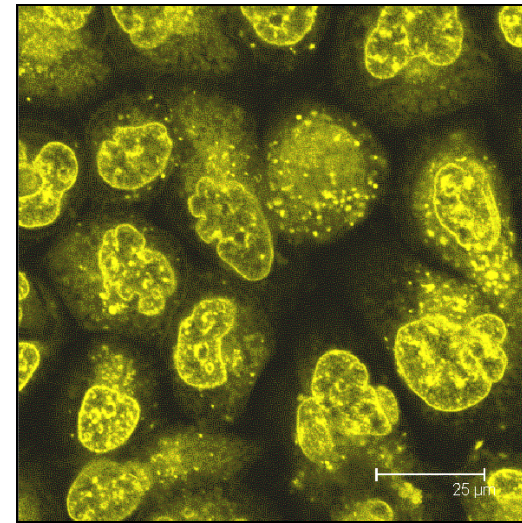
(A) 2  $\mu$ M epirubicin control



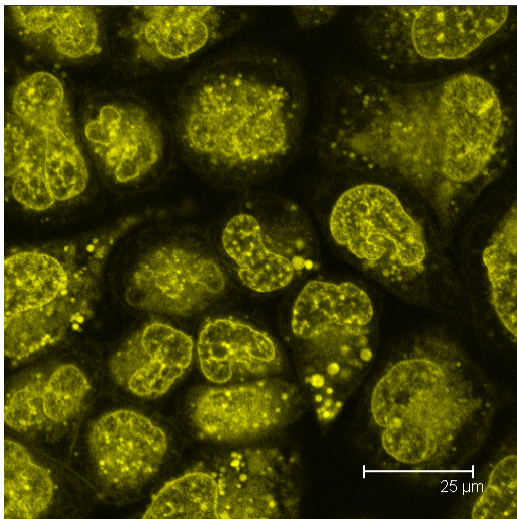
(B) 2  $\mu$ M epirubicin + 0.25  $\mu$ M elacridar



(C) 2  $\mu$ M epirubicin + 10  $\mu$ M cyclosporin A



(D) 2  $\mu$ M epirubicin + 100  $\mu$ M verapamil



(E) 2  $\mu$ M epirubicin + 10  $\mu$ M sulindac

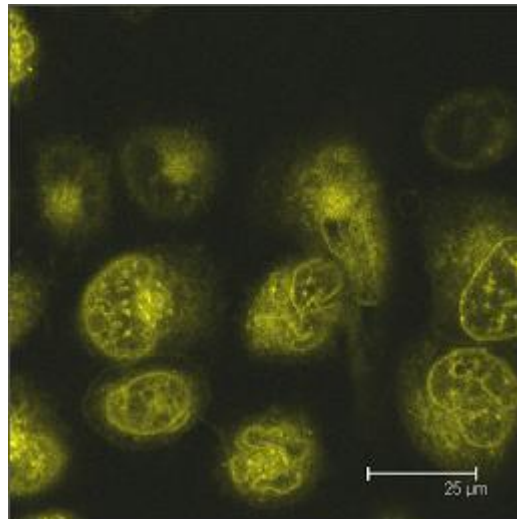


**Figure 4.1.4** DLKP-TXT cells were exposed to a concentration of 2  $\mu$ M epirubicin alone or 2  $\mu$ M epirubicin in combination with 0.25  $\mu$ M elacridar, 10  $\mu$ M cyclosporin A, 100  $\mu$ M verapamil or 10  $\mu$ M sulindac for 2 hours. The drug-containing medium was removed and replaced with drug-free medium. A single scan of epirubicin fluorescence was then imaged using a laser scanning confocal microscope.

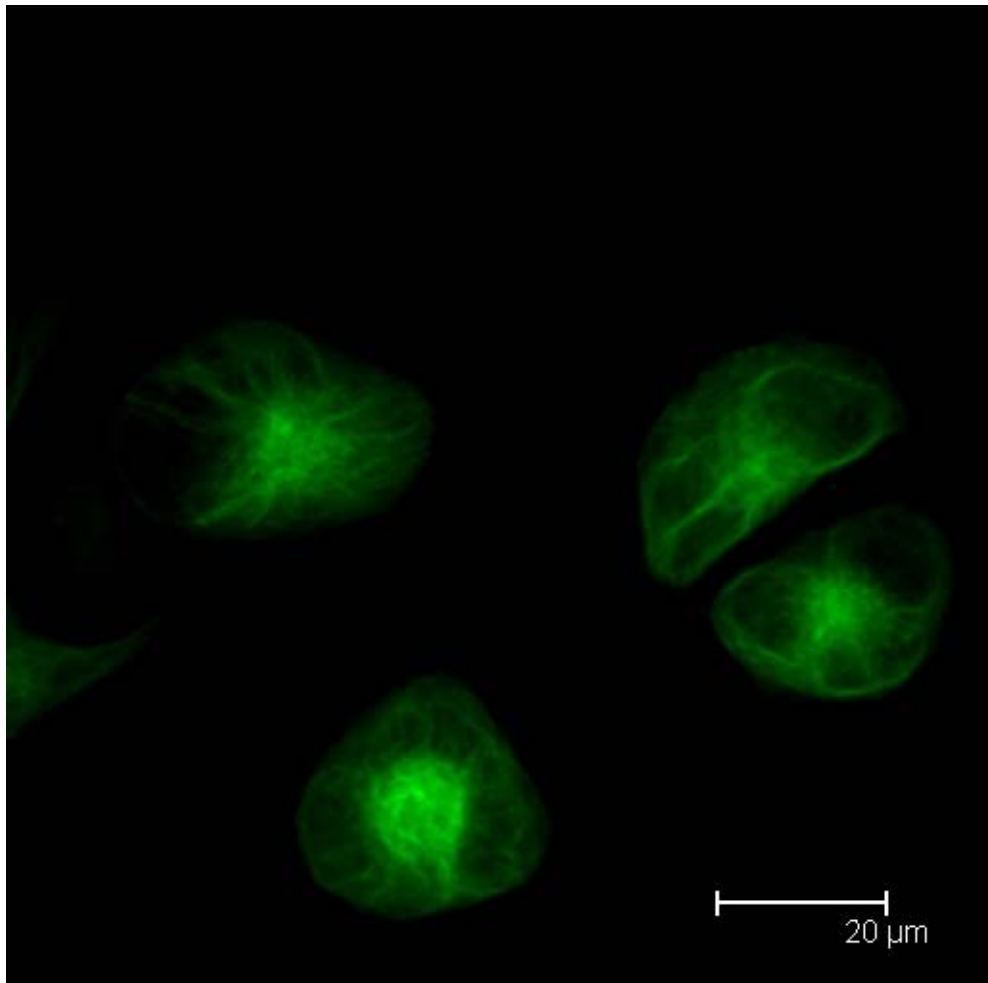


**Figure 4.1.5** DLKP cells were incubated with 1  $\mu\text{M}$  Oregon-green paclitaxel for 3 hours. The drug- containing medium was removed and replaced with drug-free medium. Oregon-green paclitaxel fluorescence was then imaged using a laser scanning confocal microscope. 3-D animations of this image can be found in Appendix B.

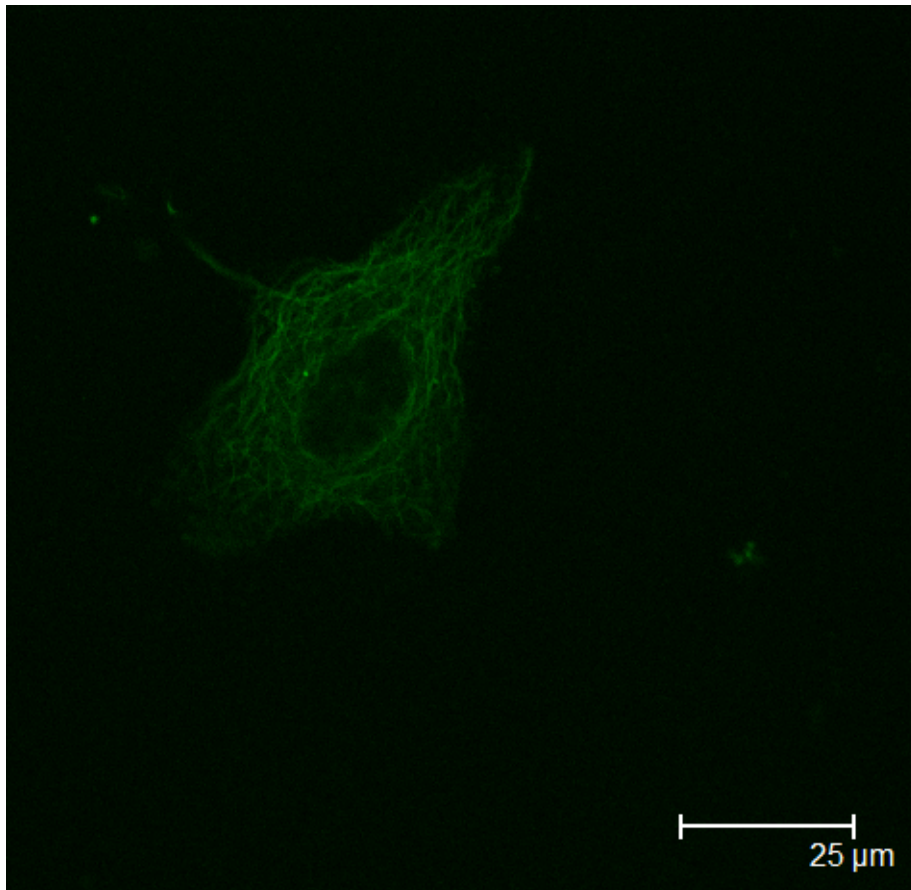


**Figure 4.1.6** A549-Taxol cells were incubated with 1  $\mu$ M Oregon-green paclitaxel for 2 hours. The drug-containing medium was removed and replaced with drug-free medium. Oregon-green paclitaxel fluorescence was then imaged using a laser scanning confocal microscope.

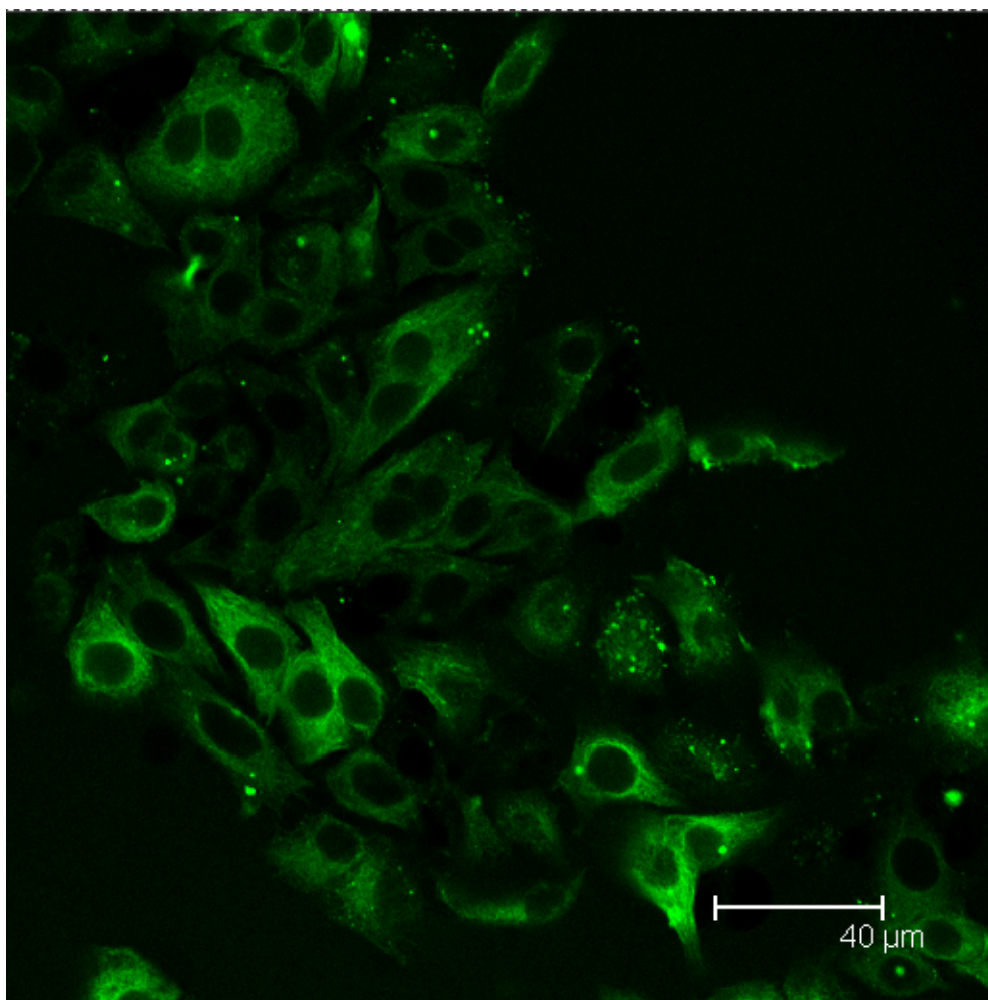


**Figure 4.1.7** A549-Taxol cells were incubated with 1  $\mu$ M Oregon-green paclitaxel for 2 hours. The drug- containing medium was removed and replaced with drug-free medium. Oregon-green paclitaxel fluorescence was then imaged using a laser scanning confocal microscope.

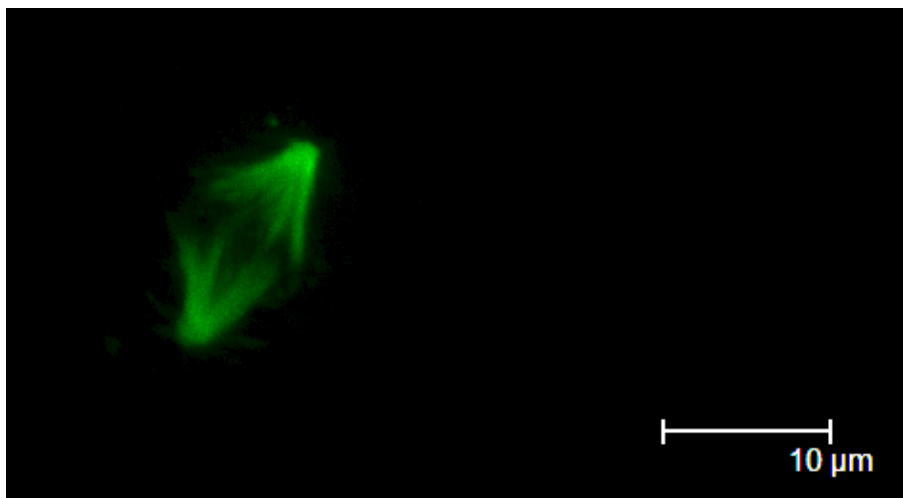


**Figure 4.1.8** A549-Taxol cells were incubated with 1  $\mu\text{M}$  Oregon-green paclitaxel for 2 hours. The drug- containing medium was removed and replaced with drug-free medium. Oregon-green paclitaxel fluorescence was then imaged using a laser scanning confocal microscope.

## **4.2 Epirubicin accumulation and efflux in the multi-drug resistant cell line DLKP-A.**

A previously developed HPLC method for measurement of epirubicin (Materials and Methods) was used to quantify epirubicin levels in DLKP-A in the presence of cyclosporin A, verapamil and elacridar, Figure 4.2.1. All three inhibitors increased epirubicin levels significantly relative to the control. Figure 4.2.2 shows the results of an epirubicin efflux assay in DLKP-A. All three compounds significantly inhibited epirubicin efflux from DLKP-A.

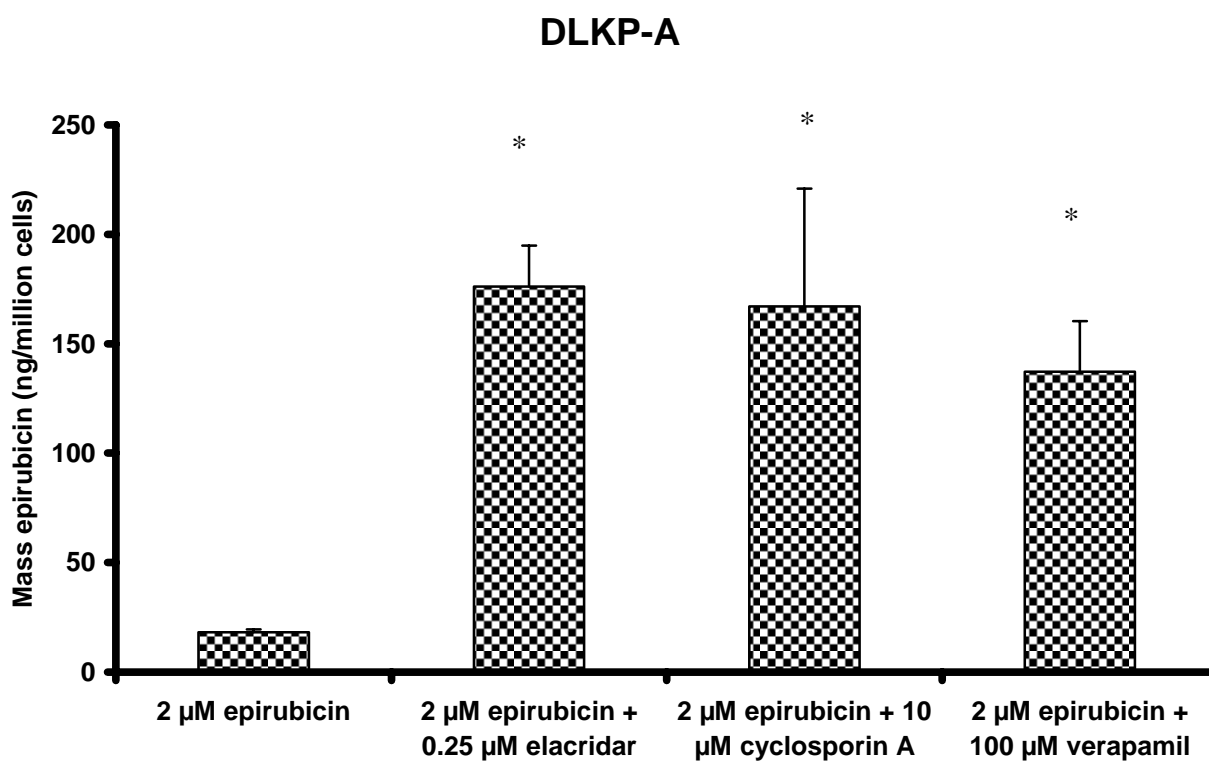


**Figure 4.2.1** Epirubicin accumulation in DLKP-A over 120 minutes. The DLKP-A cell line was exposed to 2  $\mu$ M epirubicin alone or in the presence of the P-gp modulators, elacridar, cyclosporin A and verapamil. Ethanol is the cyclosporin A delivery vehicle. Verapamil and elacridar were dissolved in water and DMSO respectively. Vehicle controls have been performed in previous experiments. Data are mean  $\pm$  SD calculated on experiments performed in triplicate.\* significantly different from the control (2 $\mu$ M epirubicin alone),  $P < 0.05$  relative to control.

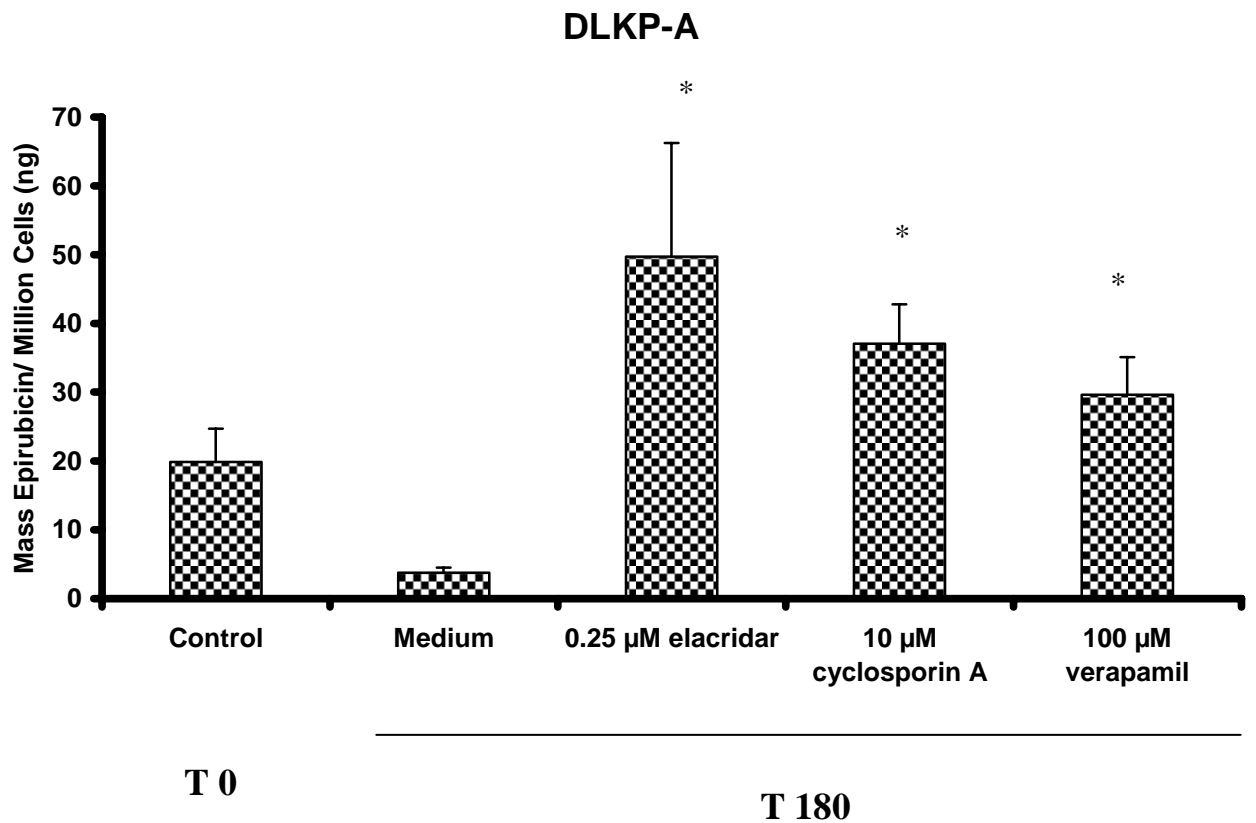


**Figure 4.2.2** Epirubicin efflux assay in DLKP-A. The control, T0, represents DLKP-A cells exposed to 2  $\mu$ M epirubicin for 120 minutes. The T180 values represent the mass of epirubicin remaining in the cells 180 minutes after epirubicin was removed and the P-gp inhibitors elacridar, cyclosporin A or verapamil were added. DLKP-A over-expresses P-gp. Cyclosporin A, elacridar and verapamil were dissolved in ethanol, DMSO and water, respectively. Vehicle controls have been performed in previous experiments. Data are mean  $\pm$  SD calculated on experiments performed in triplicate.

\* significant,  $P < 0.05$  relative to T180 medium control.

### 4.3 Summary

Laser scanning confocal imaging showed:

- The P-gp inhibitors elacridar, cyclosporin A and verapamil and the MRP-1 inhibitor sulindac failed to affect fluorescence of the P-gp substrate, epirubicin, in DLKP.
- Elacridar, cyclosporin A and verapamil, but not sulindac, markedly increased epirubicin fluorescence in DLKP-A.
- There was no change in nuclear epirubicin fluorescence in DLKP-TXT due to elacridar, cyclosporin A or verapamil. Although a subjective observation, fluorescence levels were lower in the presence of sulindac.
- Oregon-green paclitaxel is suitable for visualisation of tubulin in the NSCLC cell lines A549-Taxol and DLKP.

Using a HPLC-based method for quantification, elacridar, cyclosporin A and verapamil increased epirubicin accumulation and inhibited epirubicin efflux in DLKP-A.

The laser scanning confocal microscopy and HPLC results with epirubicin revealed that transport of epirubicin, at the assay concentration of 2  $\mu\text{M}$ , was more sensitive to verapamil and cyclosporin A modulation than docetaxel, at the assay concentration of 10 $\mu\text{M}$ .

***Chapter 5. Development of a radiolabelled-based assay for  
determination of docetaxel accumulation and efflux***

## 5.1 Introduction

To address the limitations ascribed to the HPLC method for taxane measurement (Section 3.13), a more sensitive and efficient analytical technique was required to examine docetaxel transport at pharmacologically relevant concentrations. Two techniques were considered, detection of radiolabelled docetaxel by scintillation counting and mass spectrometry. Circumstances dictated that the mass spectrometry technique would require a lengthy optimisation process and the protocol would be of a similar timespan as the HPLC method.  $^{14}\text{C}$  docetaxel was readily available commercially, relatively safe, stable and able to provide the levels of sensitivity required to confidently assess docetaxel influx and efflux mechanisms.

Once the taxanes are radiolabelled, a liquid scintillation counter can detect much lower taxane amounts than the HPLC method previously employed. To develop this assay, a number of parameters had to be optimised including cell number, medium serum concentration, the minimum drug concentration the cells could be exposed to and the length of time the cells should be exposed to the drug. The scintillation counter efficiency was also determined.

## 5.2 Optimisation of radiolabelled <sup>14</sup>C docetaxel transport assays

### 5.2.1 Scintillation Counter Efficiency

A scintillation counter gives results as counts per minute (C.P.M.). D.P.M., disintegrations per minute, is the theoretical rate of decay of a substance and is always higher than the reported C.P.M. The efficiency depends on the type of counter being used and can be calculated from the following formula:

$$\frac{\text{C.P.M.} - \text{Background}}{\text{D.P.M.}} \times 100$$

A counting device will always give a reading even if there is no radioactivity added to the sample being measured. Natural radiation, cosmic rays and electronic noise all contribute to background radioactivity. The D.P.M. of a radiochemical can be calculated from its specific radioactivity, the number of curies (Ci) or D.P.M. per unit weight. One curie represents  $3.7 \times 10^{10}$  disintegrations per second (D.P.S.) or  $2.22 \times 10^{12}$  D.P.M.

The C.P.M. of a range of <sup>14</sup>C radiolabelled docetaxel concentrations in 0.1M NaOH were measured and the D.P.M. for each calculated to give the % efficiency of the counter for <sup>14</sup>C isotopes, Table 5.2.1.1.

**Table 5.2.1.1** The C.P.M. for a range of docetaxel concentrations were determined and the counter efficiency expressed as a percentage of the theoretical disintegrations per minute.

<b><sup>14</sup>C Docetaxel (μM)</b>	<b>C.P.M (counts per minute)</b>	<b>Minus Background (20 C.P.M.)</b>	<b>Theoretical D.P.M. (disintegrations per minute)</b>	<b>% Efficiency</b>	
0.05	1550	1530	3330	45.95	
0.1	3172	3152	6660	47.33	
0.2	6458	6438	13320	48.33	
0.5	15798	15778	33300	47.38	
0.75	23898	23878	49950	47.80	
1	31715	31695	66600	47.59	
2	63778	63758	133200	47.87	
5	159885	159865	333000	48.01	
7.5	240250	240230	499500	48.09	
10	318026	318006	666000	47.75	
				<b>Average % Efficiency</b>	<b>Average Error</b>
				47.61	0.66

## 5.2.2 Influence of cell number

From previous laboratory practice and literature values, a concentration of  $1 \times 10^5$  cells per ml per 24-well plate well provides a confluent monolayer for the cell lines used after twenty four hours. Maximising the cell number per well is important as it affects the maximum amount of drug that can be accumulated and therefore the minimum drug concentration the cells can be exposed to. Cells were exposed to  $^{14}\text{C}$  docetaxel for 90 minutes, concurrent with the taxane exposure time in the HPLC-based assays (Figure 5.2.2.1). DLKP-A was chosen as it accumulated the lowest levels of docetaxel of the cell lines to be examined because of P-gp over-expression. Increasing the cell seeding density from  $1 \times 10^5$  to  $2 \times 10^5$  cells per ml had no effect on the amount of docetaxel accumulated at the concentrations of  $^{14}\text{C}$  docetaxel tested. A cell seeding density of  $1 \times 10^5$  resulted in a confluent cell monolayer after 24 hours.

## DLKP-A

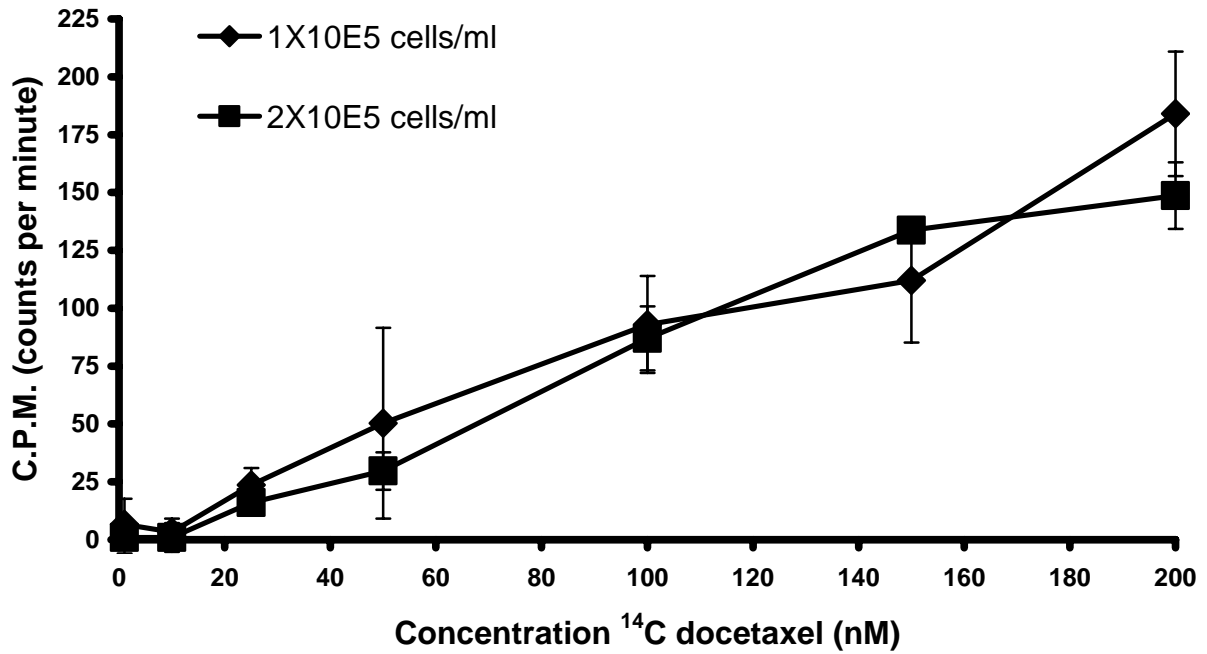


**Figure 5.2.2.1** <sup>14</sup>C docetaxel accumulation assay in DLKP-A. DLKP-A were seeded at 1 X 10<sup>5</sup> or 2 X 10<sup>5</sup> cells per ml in a 24-well plate twenty four hours prior to drug exposure. 1 X 10<sup>5</sup> cells resulted in a confluent monolayer in each well for the assay. Cells were exposed to stated docetaxel concentrations for 90 minutes. Data are mean +/- SD calculated on experiments performed in duplicate.

### **5.2.3 Influence of cell debris**

The samples to be measured contained cell debris that could interfere with counting efficiency. In Figure 5.2.3.1A, the volume of cells added to each sample was equal to the amount present under accumulation/efflux assay conditions. The results indicate that there was negligible quenching of the radiolabelled  $^{14}\text{C}$  docetaxel signal by cell debris.

The C.P.M. values recorded by the liquid scintillation counter are an average of the C.P.M. taken at set intervals over a minute. The lower the C.P.M. of a sample, then the greater the % error. Figure 5.2.3.1B graphs the % error (as calculated by the scintillation counter) for each result against the concentration of docetaxel in the presence and absence of cell debris. The % error is below 5% for concentrations above 0.05  $\mu\text{M}$  and this was deemed acceptable.

### <sup>14</sup>C Docetaxel Std. Curves With and Without Cells

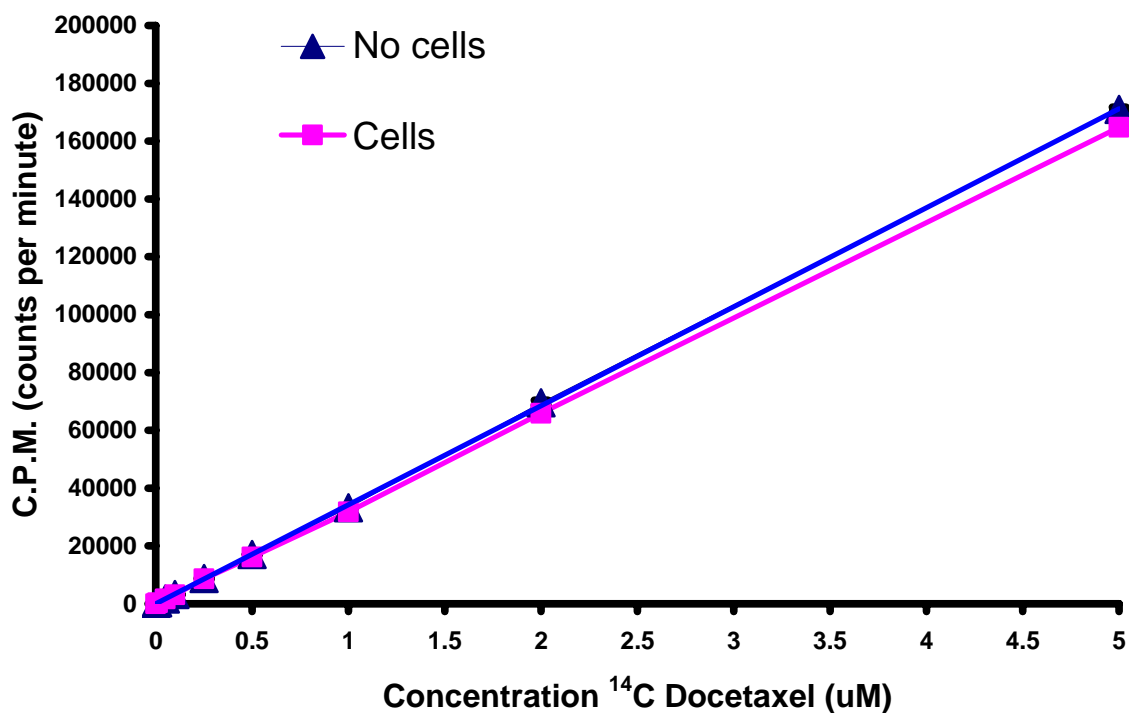


**Figure 5.2.3.1A** Comparison of <sup>14</sup>C docetaxel standard curves in the presence and absence of cells. The blue curve (-▲-) represents the observed C.P.M. for a range of docetaxel concentrations in 0.1M NaOH. The pink curve (-■-) is the same concentrations measured in the presence of cell debris and 0.1M NaOH. Data are mean experiments performed in duplicate.

### Comparison Of % Error Of C.P.M. Reading

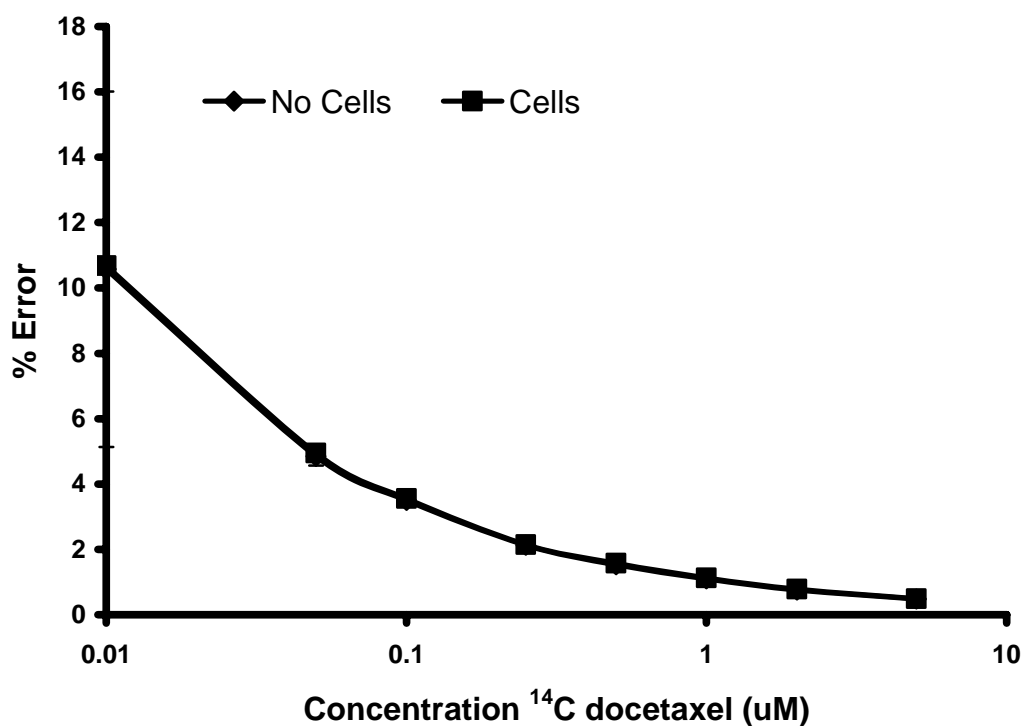


**Figure 5.2.3.1B** The % error in C.P.M. readings plotted against log concentration for the docetaxel standard curves in Figure 5.2.3.1A. % error values were produced by the scintillation counter for each reading. Data are mean experiments performed in duplicate.

#### **5.2.4 Influence of drug adsorption onto plate wells**

A number of wash steps were included in each assay to remove excess drug in the medium and attached to the tissue culture treated plates. To ensure the recorded C.P.M. readings reflected accumulated drug within the cells, a control assay was carried out.

In Figure 5.2.4.1A, the upper trend is the C.P.M. reading of the mass of docetaxel accumulated in 90 minutes over a range of docetaxel concentrations. The lower trend is the drug adsorption control in which the same concentrations of docetaxel were incubated in wells for 90 minutes in the absence of cells. Both experiments were carried out using the same procedure, all data points in duplicate. <sup>14</sup>C docetaxel accumulation was saturable in DLKP. 100 nM applied to the cells for 90 minutes gave a measurable mass of <sup>14</sup>C docetaxel that allowed for increases and decreases in accumulation. The scintillation counter error was also acceptably low. As the values of the registered C.P.M. decrease (Figure 5.2.4.1A), the relatively constant C.P.M. count error acquires a higher % value (Figure 5.2.4.1B). There was negligible loss of docetaxel due to drug adsorption. 100 nM docetaxel is 100 times less than the 10 $\mu$ M used in the HPLC assays.

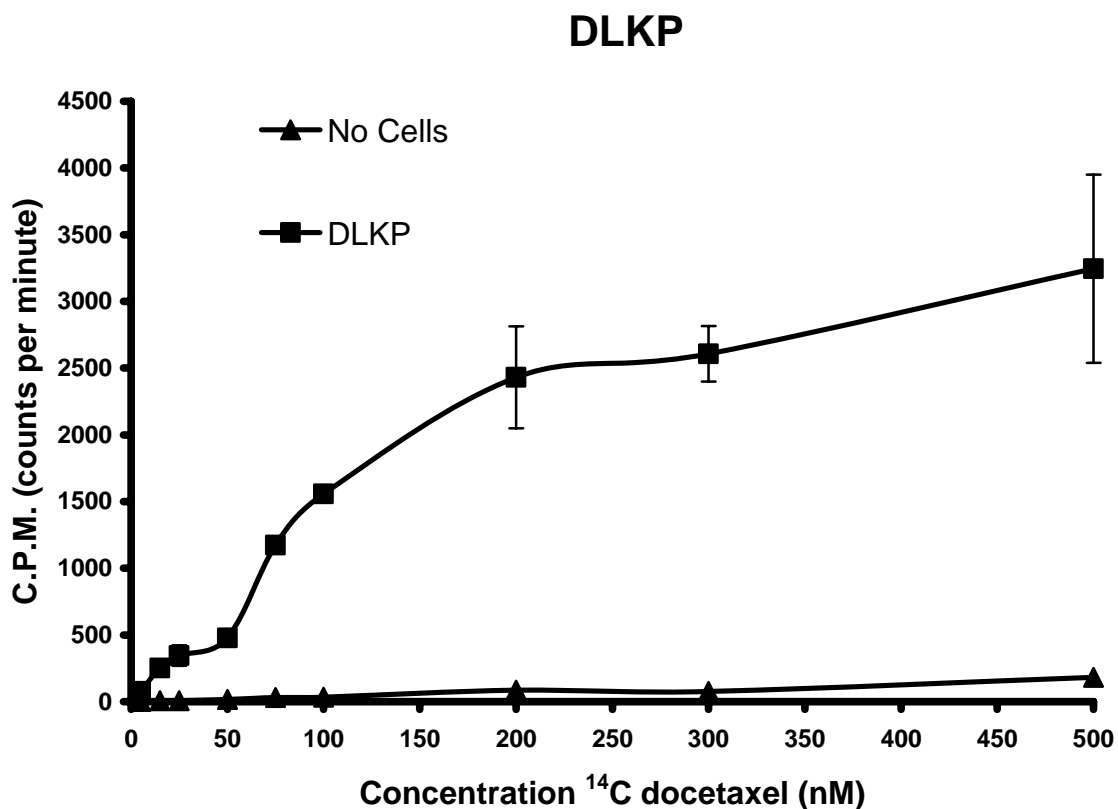


**Figure 5.2.4.1A** Drug adsorption control assay performed with a docetaxel saturation assay in DLKP. The upper trend (-■-) represents a saturation assay carried out in DLKP in a 24 well-plate. Increasing concentrations of <sup>14</sup>C docetaxel were incubated with DLKP for 90 minutes. The lower trend (-▲-) is the same assay carried out in an empty 24-well plate to account for drug adsorption to the plate. Data are mean +/- SD calculated on experiments performed in triplicate.

## DLKP

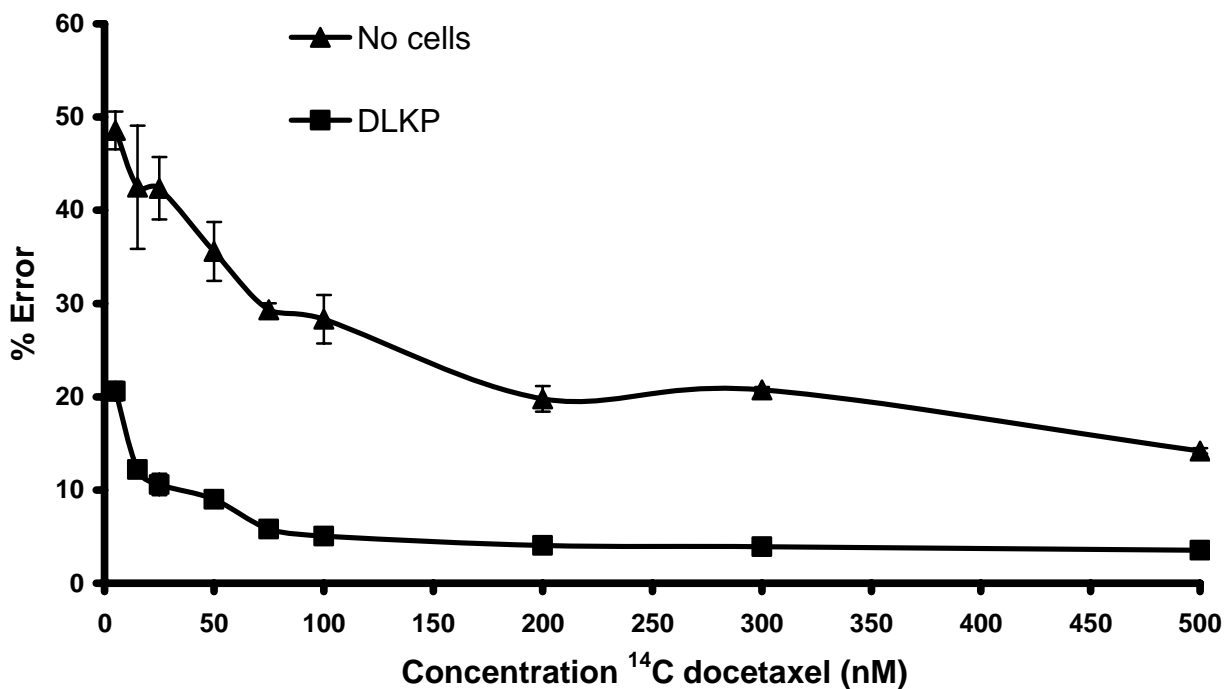


**Figure 5.2.4.1B** A comparison of the C.P.M. error readings for the accumulation assay in Figure 5.1.4.1A. The control (upper trend) demonstrated much higher errors due to lower C.P.M. being registered as there were no cells to retain the <sup>14</sup>C docetaxel within the wells. The lower trend is the error from the accumulation assay performed in the presence of cells. The reading error of 5% for 100 nM is deemed acceptable for this assay. Data are mean +/- SD calculated on experiments performed in duplicate.

### **5.2.5 Influence of alterations in medium serum concentration**

The A549 and DLKP cell lines are generally cultured in 5% foetal calf serum and DMEM/Ham's F12. To investigate the influence of serum concentration on docetaxel accumulation, both A549 (Figure 5.2.5.1) and DLKP cells (Figure 5.2.5.2) were exposed to 100 nM <sup>14</sup>C docetaxel for time periods of 30 to 120 minutes in the presence of a range of serum concentrations. For both cell lines, the higher concentrations of 100% and 50% serum decreased docetaxel accumulation significantly. The lower concentrations of 5, 1 and 0% serum showed little influence on docetaxel accumulation in either cell line.

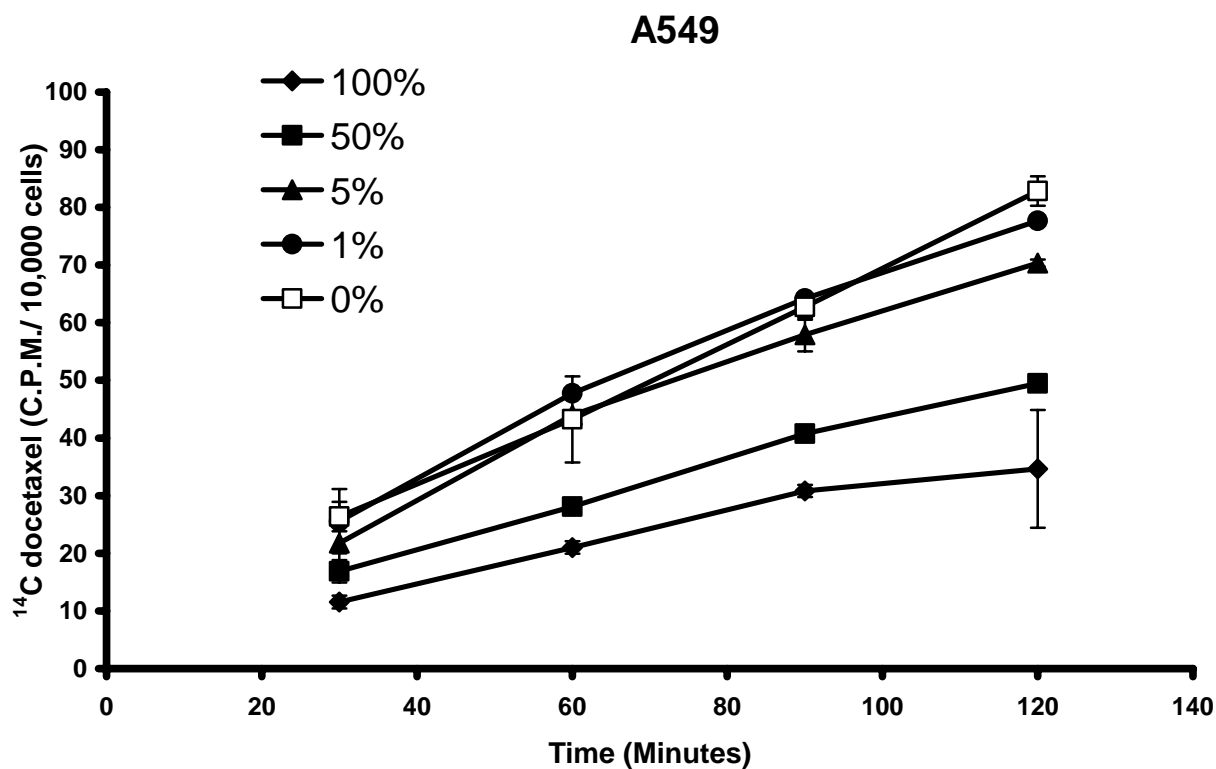


**Figure 5.2.5.1** Effect of medium serum concentration on docetaxel accumulation in A549. Cells were incubated with 100 nM  $^{14}\text{C}$  docetaxel in the presence of 100, 50, 5, 1 and 0% foetal calf serum in DMEM/Ham's F12.  $^{14}\text{C}$  docetaxel accumulation was measured at 30, 60, 90 and 120 minutes for each serum concentration. Data are mean +/- SD calculated on experiments performed in triplicate.

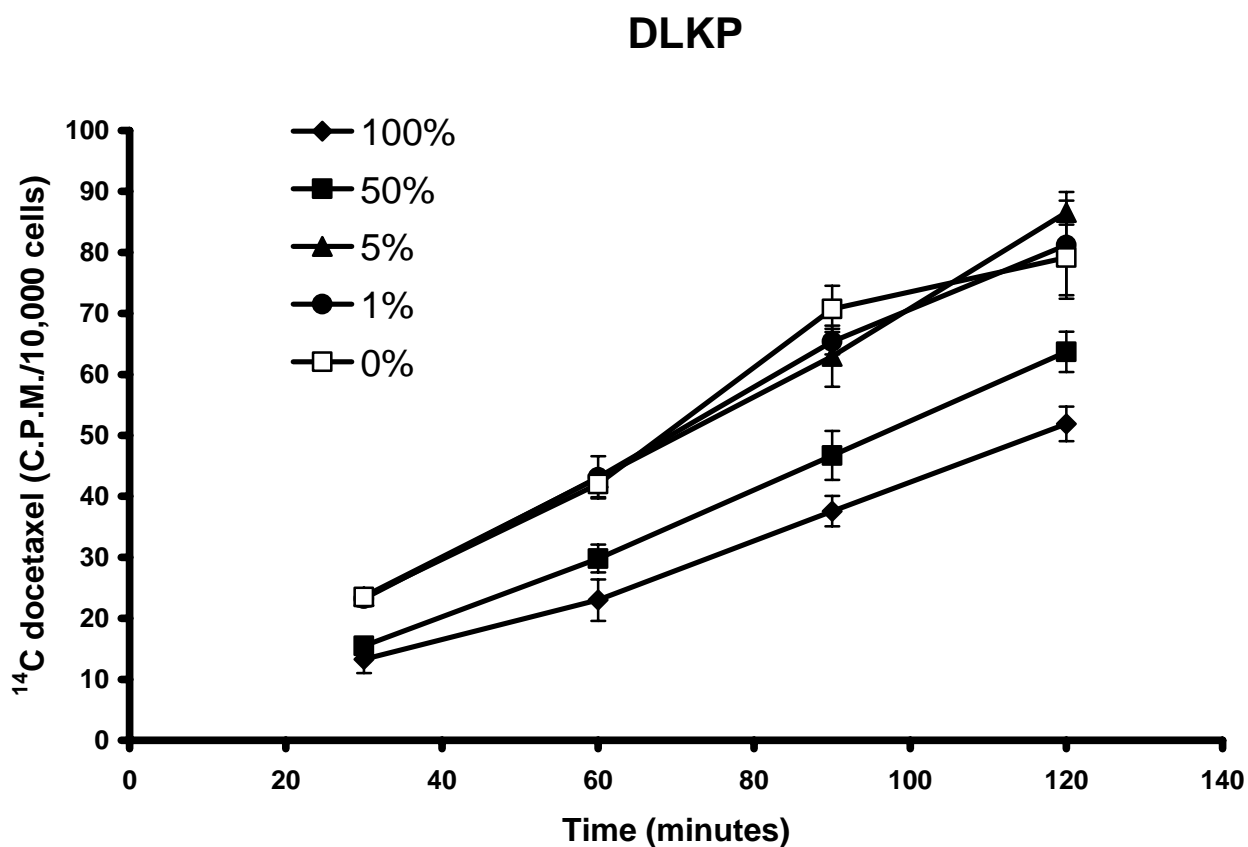


**Figure 5.2.5.2** Effect of medium serum concentration on docetaxel accumulation in DLKP. Cells were incubated with 100 nM  $^{14}\text{C}$  docetaxel in the presence of 100, 50, 5, 1 and 0% foetal calf serum in DMEM/Ham's F12.  $^{14}\text{C}$  docetaxel accumulation was measured at 30, 60, 90 and 120 minutes for each serum concentration. Data are mean  $\pm$  SD calculated on experiments performed in triplicate.

### **5.3 Comparison of radiolabelled assay and HPLC method for docetaxel measurement.**

For a direct comparison to be made between the radiolabelled assay and the HPLC method, the radiolabelled results (C.P.M.) have to be converted to mass per number of cells. Figure 5.3.1 is a standard curve generated by measuring the C.P.M. values associated with different concentrations of  $^{14}\text{C}$  docetaxel. The concentration values of  $^{14}\text{C}$  docetaxel in the presence of cell debris from Figure 5.2.3.1A were converted to mass docetaxel (250  $\mu\text{l}$  of each concentration was read) and plotted against C.P.M. The curve intercepted through zero because a blank was subtracted from all samples. The equation of this curve ( $y=0.0061x$ ) can be applied to all subsequent assays using radiolabelled drug of the same specific activity.

Figure 5.3.2 shows the docetaxel saturation assay in DLKP (Figure 5.2.4.1A) when converted to mass docetaxel per 10,000 cells. A concentration of 100 nM  $^{14}\text{C}$  docetaxel applied to DLKP in a 24 -well plate for 90 minutes results in 1 ng docetaxel per ten thousand cells being accumulated. This translates to 100 ng per million cells.

A major anomaly with the HPLC method was the ineffectiveness of cyclosporin A and particularly verapamil, in inhibiting docetaxel efflux in P-gp over-expressing cell lines, Sections 3.8 and 3.10.

500 nM  $^{14}\text{C}$  radiolabelled docetaxel was applied to DLKP-A cells in the presence of elacridar, cyclosporin A and verapamil (Figure 5.3.3). This concentration of docetaxel is 20-times less than the 10  $\mu\text{M}$  docetaxel employed in the HPLC assays. All three inhibitors increased docetaxel accumulation approximately 11-fold. The concentrations of each inhibitor used are the same as used in the HPLC-based assay (Figure 3.4.1) but in this case, cyclosporin A and verapamil exhibit P-gp reversal activity as indicated by the increased drug accumulation.

Verapamil and cyclosporin A had a minor effect on docetaxel accumulation in the docetaxel-selected DLKP variant DLKP-TXT when employing the HPLC analysis method, Section 3.10. The MRP-1 inhibitor sulindac also caused a minor increase in docetaxel accumulation. The lower concentration of  $^{14}\text{C}$  docetaxel (500 nM) applied to this cell line in a radiolabel-based assay produced the same result but the effectiveness of verapamil increased (Figure 5.3.4). Cyclosporin A increased docetaxel accumulation 1.5

times while verapamil and elacridar increased docetaxel accumulation 1.4 and 1.3 times, respectively. Interestingly, sulindac caused a 1.2 fold increase in docetaxel accumulation, although this did not prove statistically significant.

The docetaxel accumulation and efflux profiles vary greatly between cell lines, depending on the presence or absence of drug transporters. These profiles are therefore a defining characteristic for a cell line. Figure 5.3.5 shows the docetaxel accumulation profiles in the non-P-gp expressing A549 and the P-gp-expressing A549-Taxol cell lines, as measured by radiolabel assay. At 100 nM docetaxel the accumulation profiles of both cell lines are almost identical up to 190 minutes. The accumulation profile of docetaxel in A549 was previously determined using the HPLC method (Figure 3.2.1). Apart from a very different profile shape, a much larger mass of docetaxel was accumulated in 90 minutes using the HPLC assay, approximately 250 ng docetaxel per million cells. The radiolabel based assay, using 100 nM docetaxel instead of 10  $\mu$ M to determine the profile, only accumulated the equivalent of 50 ng per million cells after 90 minutes.

Differences between HPLC and radiolabel-determined results were also evident in the docetaxel efflux profile in A549 (Section 3.2). The efflux profiles of cell lines are possibly more informative than the accumulation profiles, especially in those cell lines expressing drug efflux pumps. The previous efflux profile studies in A549 utilising the HPLC method (Figure 3.2.2) and 10  $\mu$ M of docetaxel to load up the cells, showed a marked decrease in the amount of docetaxel retained within the first 50 minutes, a profile that would fit a drug transporter-expressing cell line. A similar assay carried out in A549 using the radiolabel based method can be seen in Figure 5.3.6. The efflux profiles resulting from incubation with 0.1, 1 and 10  $\mu$ M docetaxel showed a concentration related effect on docetaxel efflux. The comparison of mass docetaxel accumulated at T10 between each method in A549 showed the equivalent of 20 ng per million cells retained using the radiolabel method (incubated with 0.1  $\mu$ M  $^{14}$ C docetaxel) and approximately 60 ng per million cells using the HPLC procedure (incubated with 10  $\mu$ M docetaxel).

Figure 5.3.7 represents the docetaxel efflux profile in the non-Pgp-expressing DLKP cell line. The profile was similar to that obtained in A549 (Figure 5.3.6) with no significant decrease in the mass of docetaxel retained after 100 minutes. Approximately one third more docetaxel was retained within DLKP compared to A549, 0.32 ng/10,000 cells and 0.22 ng/10,000 cells, respectively.

An accumulation assay examining the levels of docetaxel accumulated in DLKP-A when exposed to 100 and 500 nM docetaxel in the absence and presence of cyclosporin A is shown in Figure 5.3.8. 500 nM docetaxel was chosen as the incubation concentration for radiolabelled efflux assays in DLKP-A.

**Mass Docetaxel (ng) Vs. CPM (Cells included With STDs)**

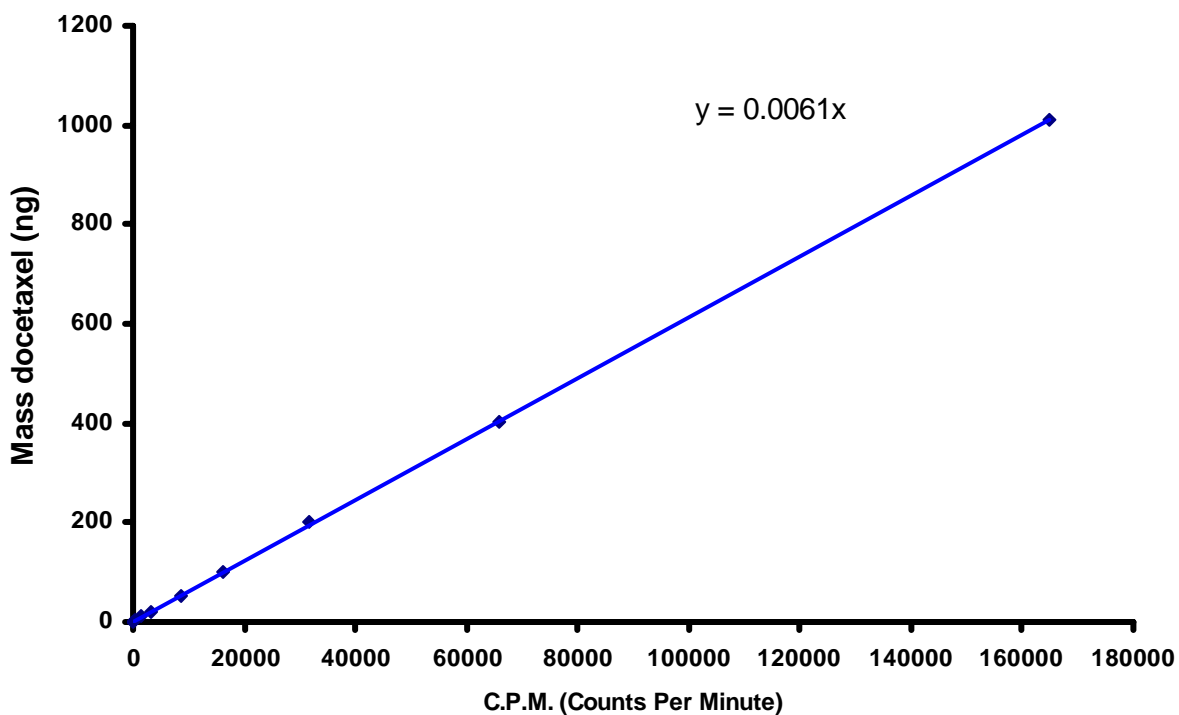


**Figure 5.3.1** The C.P.M. of the standard curve in Figure 5.3.1 was plotted against the mass of docetaxel each standard contained. The resulting plot gave the equation  $y=0.0061x$ . All data points determined in duplicate  $\pm$  SD.

## DLKP

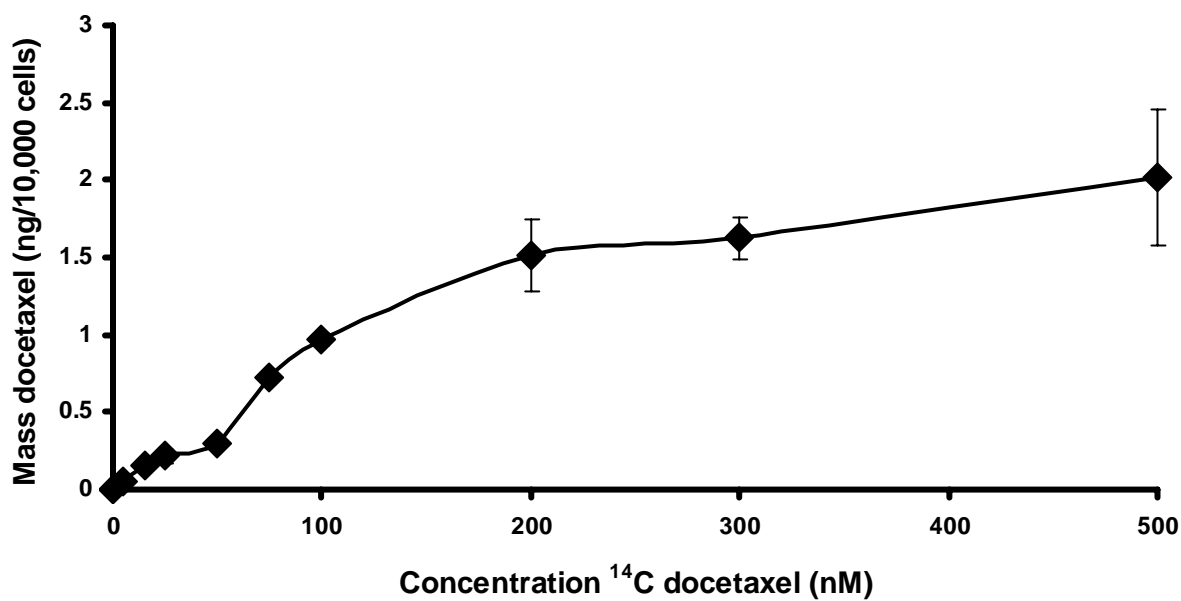


**Figure 5.3.2** The curve calculated in Figure 5.3.1 ( $y=0.0061x$ ) was used to convert C.P.M./10,000 cells to mass docetaxel/10,000 cells. The curve represents mass docetaxel accumulated. Data are mean  $\pm$  SD calculated on experiments performed in triplicate.

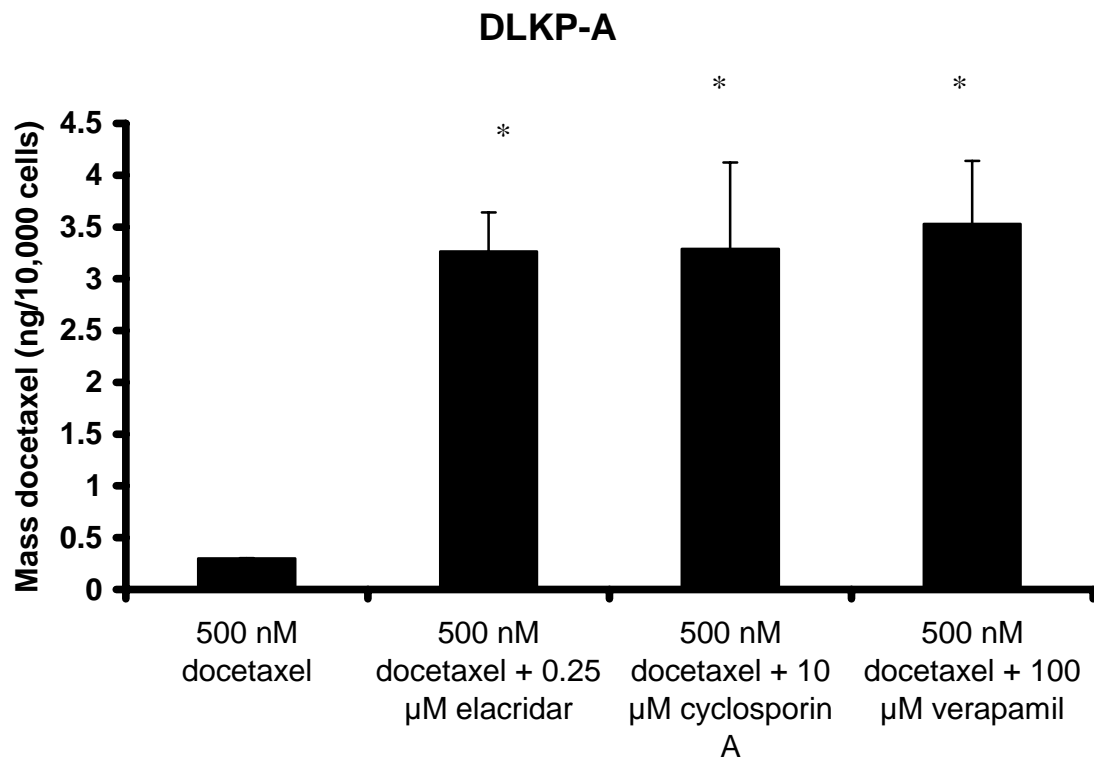


**Figure 5.3.3**  $^{14}\text{C}$  docetaxel accumulation assay in DLKP-A. Cells were incubated with 500 nM  $^{14}\text{C}$  docetaxel alone or in combination with 0.25  $\mu\text{M}$  elacridar, 10  $\mu\text{M}$  cyclosporin A or 100  $\mu\text{M}$  verapamil for 90 minutes. Data are mean  $\pm$  SD calculated on experiments performed in triplicate.

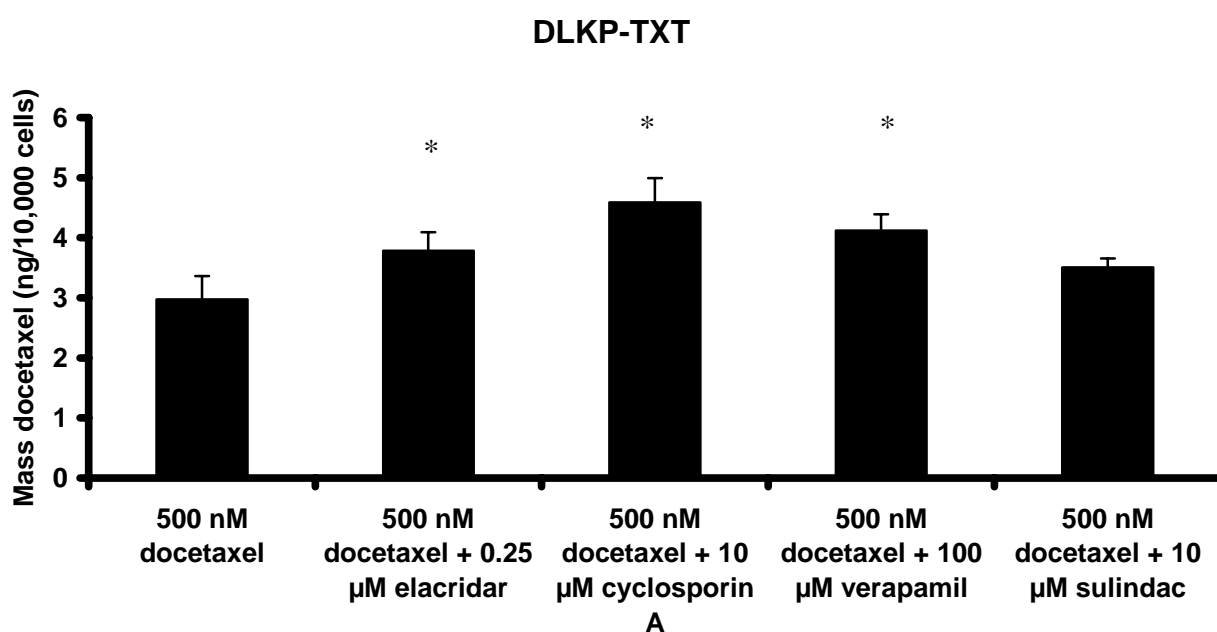


**Figure 5.3.4**  $^{14}\text{C}$  docetaxel accumulation assay in DLKP-TXT. Cells were incubated with 500 nM  $^{14}\text{C}$  docetaxel alone or in combination with 0.25  $\mu\text{M}$  elacridar, 10  $\mu\text{M}$  cyclosporin A, 100  $\mu\text{M}$  verapamil or 10  $\mu\text{M}$  sulindac for 90 minutes. Data are mean  $\pm$  SD calculated on experiments performed in triplicate. \* significant relative to 500 nM docetaxel control,  $P < 0.05$ .

### 100 nM $^{14}\text{C}$ docetaxel accumulation

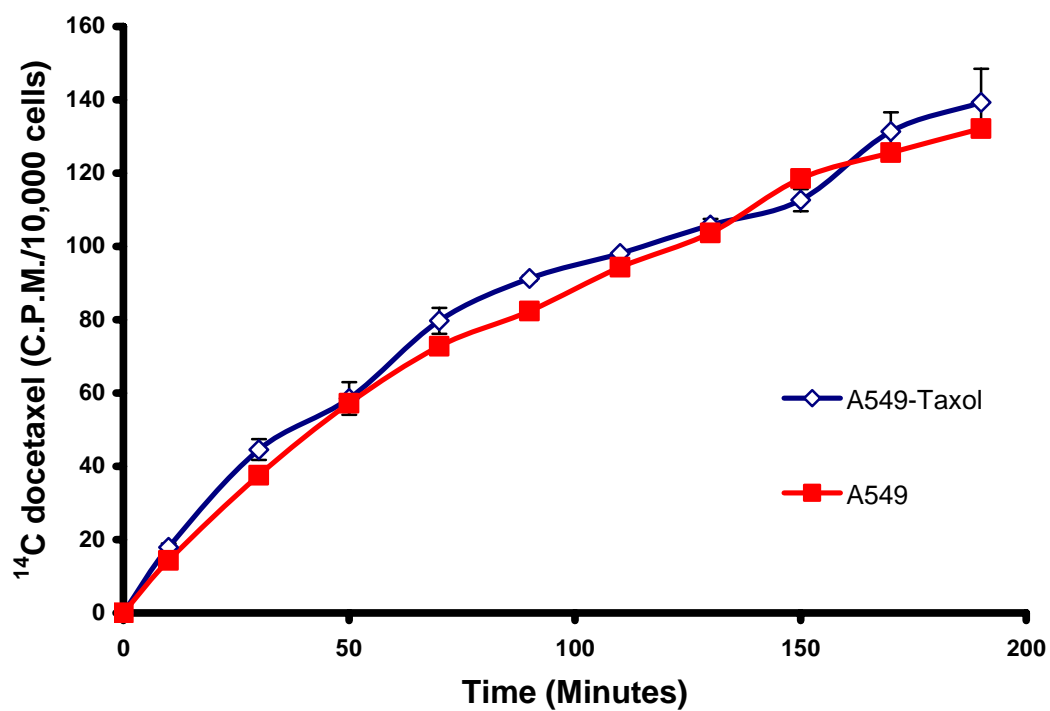


**Figure 5.3.5** Comparison of  $^{14}\text{C}$  docetaxel accumulation profiles in A549 and A549-Taxol. Cells were exposed to 100 nM  $^{14}\text{C}$  docetaxel for various timepoints up to 190 minutes. Data are mean +/- SD calculated on experiments performed in duplicate.

## A549

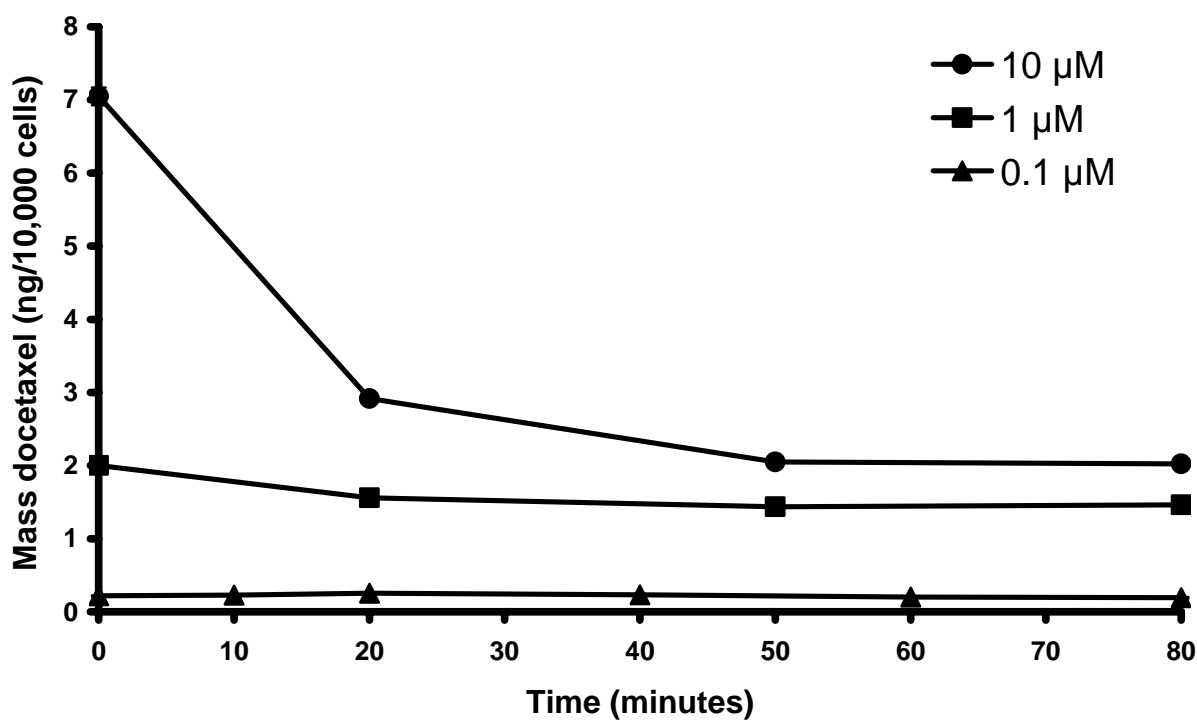


**Figure 5.3.6** <sup>14</sup>C docetaxel efflux profile in the A549 cell line. Cells were incubated with 0.1 μM, 1 μM or 10 μM <sup>14</sup>C docetaxel for 90 minutes. The drug was then removed, the cells washed and fresh drug-free medium applied. The amount of <sup>14</sup>C docetaxel retained was measured at intervals up to 80 minutes. Data are mean +/- SD calculated on experiments performed in triplicate.

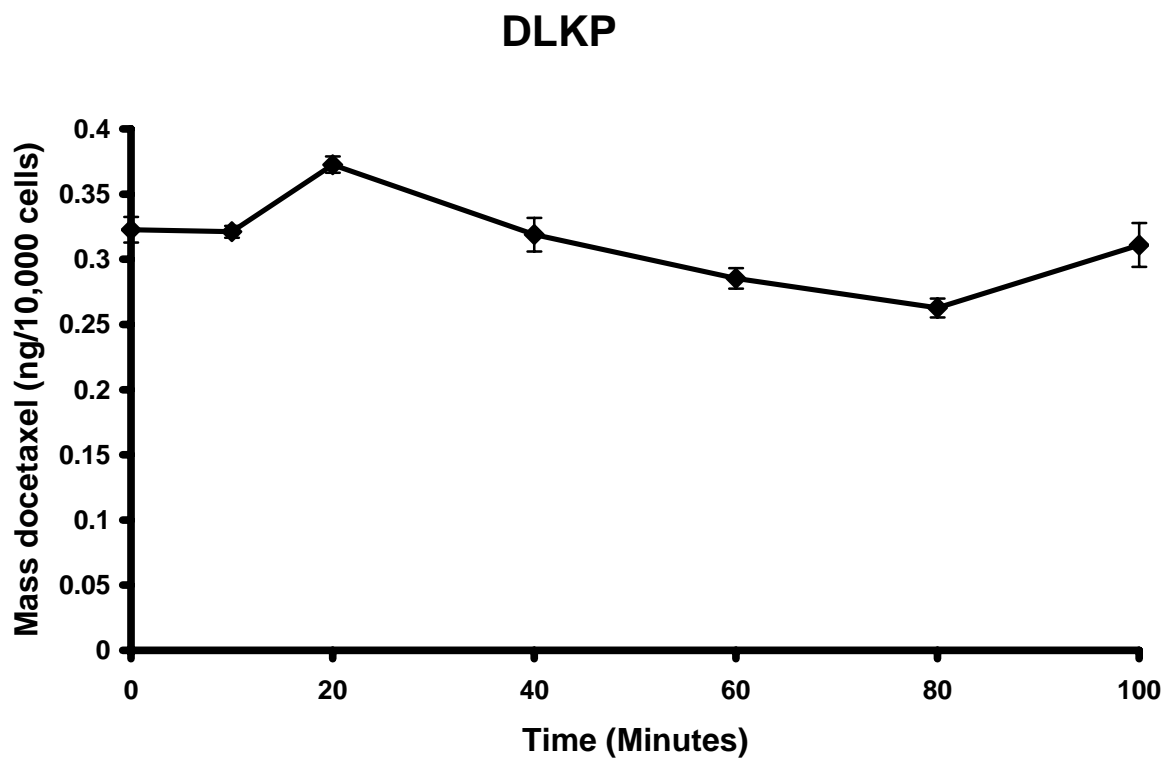


**Figure 5.3.7**  $^{14}\text{C}$  docetaxel efflux profile in the DLKP cell line. Cells were incubated with 100 nM  $^{14}\text{C}$  docetaxel for 90 minutes. The drug was then removed, the cells washed and fresh drug-free medium applied. The amount of  $^{14}\text{C}$  docetaxel retained was measured at intervals up to 100 minutes. Data are mean  $\pm$  SD calculated on experiments performed in triplicate.

## DLKP-A

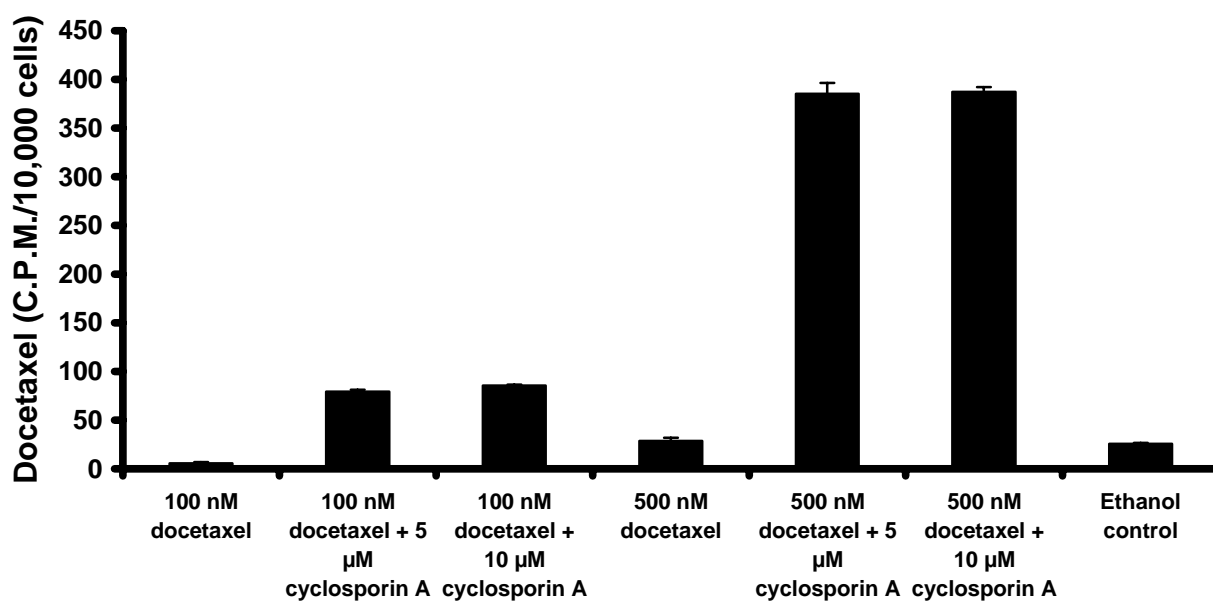


**Figure 5.3.8** Determination of loading concentration for  $^{14}\text{C}$  docetaxel efflux assays in DLKP-A. DLKP-A cells were exposed to 100 nM or 500 nM  $^{14}\text{C}$  docetaxel alone or in combination with 5  $\mu\text{M}$  or 10  $\mu\text{M}$  cyclosporin A for 90 minutes. Cyclosporin A was dissolved in ethanol. The ethanol control corresponds to the 500 nM  $^{14}\text{C}$  docetaxel and 10  $\mu\text{M}$  cyclosporin A. Data are mean  $\pm$  SD calculated on experiments performed in triplicate.

## 5.4 Summary

Optimal conditions for the  $^{14}\text{C}$  radiolabelled docetaxel assay were determined:

- Cells were seeded 24 hours prior to assay in a 24-well plate at a concentration of  $1 \times 10^5$  cells/ml.
- Assays were carried out under normal growth conditions, 5% FCS in DMEM/Ham's F12.
- 100 nM  $^{14}\text{C}$  docetaxel is sufficient for examining drug accumulation in all cell lines to be examined. 500 nM  $^{14}\text{C}$  docetaxel is required for  $^{14}\text{C}$  docetaxel efflux assays in DLKP-A.
- Direct extraction of  $^{14}\text{C}$  docetaxel using 0.1M NaOH is possible as cell debris does not cause signal quenching.

The  $^{14}\text{C}$  radiolabelled docetaxel assay proved able to address the limitations of the HPLC based method for taxane measurement:

- 100 nM  $^{14}\text{C}$  docetaxel is within the physiological exposure levels of docetaxel.
- The efflux profile of docetaxel in A549 and DLKP is consistent with a non-MDR cell line.
- Inhibition of  $^{14}\text{C}$  docetaxel transport by verapamil is detectable in the P-gp over-expressing cell lines DLKP-A and DLKP-TXT.
- The assay protocol is considerably less time consuming.

*Chapter 6. Docetaxel influx in the human lung cancer cell  
lines DLKP and A549*

## 6.1 Introduction

There are no known energy-dependent influx mechanisms for the taxanes in lung cancer cells. An energy-dependent taxane transport mechanism would be saturable, temperature-dependent and ATP-dependent. Saturation occurs when the concentration of a substrate reaches such a level that all the available transporters for that substrate are utilised and no increase in the rate of accumulation is possible. Inhibition of activity due to decreasing temperature is another characteristic of active transport-mediated movement. A reduction in the levels of cellular ATP would be expected to reduce the effectiveness of an ATP-dependent transporter. All three characteristics were examined in the DLKP and A549 lung cancer cell lines.

The OATP (SLC21, SLCO, organic anion transporter polypeptides) family of transporters have recently been implicated in the transport of taxanes in the liver. The OATP family are classified as anion exchangers that do not rely directly on ATP for functionality. The OATP1B3 (OATP8/SLC21A8) transporter has been identified as an important hepatocellular transporter of paclitaxel [192]. DNA microarray analysis carried out on the DLKP and A549 cell lines revealed RNA expression levels for many of the OATP family in A549 but not in DLKP (Appendix A, Table A1). To investigate the possible involvement of the OATP family in docetaxel accumulation in the A549 cell line, initial docetaxel accumulation assays were carried out in the presence of bromosulphothalein (BSP) and digoxin. BSP is an OATP inhibitor of broad specificity (OATP1A2 (OATP-A), OATP2B1 (OATP-B), OATP1B1 (OATP-C) and OATP1B3) while digoxin is a selective transport substrate for OATP1B3 [263]. Based on initial BSP results, other OATP inhibitors were tested including indocyanine green, OATP-1B1 specific and not transported by OATP1B3 [264] and cyclosporin A, reported to be an OATP1B1 and OATP1B3 inhibitor [265]. Digoxin, indocyanine green and cyclosporin A were examined as they interact with OATPs that are inhibited by BSP but are not necessarily OATPs that are known to be specific to lung tissue. OATP2B1 is found in lung tissue and BSP is a substrate [266]. More specific to this research, Northern blot analysis has detected OATP3A1 (OATP-D) at the mRNA level in A549 [267].

OATP2B1, -3A1 and -4A1 (OATP-E) and prostaglandin transporter (PGT) expression have been found in lung tissue by RT-PCR in a study by Tamai *et al.* [268]. OATP1A2

and OATP-1B1 were not detected in lung tissue. The most specific substrates that could potentially inhibit OATP2B1, -3A1 and -4A1 competitively are DHEAS [263], prostaglandin E<sub>2</sub> [267] and thyroid hormone (T<sub>3</sub>) [269]. The effect of these three compounds on docetaxel accumulation was also examined in A549.

## 6.2 Saturation

Saturation assays looking at the accumulation of a range of increasing docetaxel concentrations at a 90 minute timepoint were carried out in A549, DLKP, A549-Taxol and DLKP-Mitox. Saturation is a result of capacity limited drug transport. Docetaxel concentrations up to 500 nM did not reach saturation in A549 (Figure 6.2.1). Saturation of docetaxel transport occurred in DLKP within the range of drug concentrations examined (Figure 6.2.2). In the P-gp-expressing A549-Taxol, docetaxel accumulation does not reach saturation up to 400 nM but then starts to decrease at 500 nM, Figure 6.2.3. Accumulation of docetaxel does not reach saturation in DLKP-Mitox despite a decrease in rate of accumulation at 200 nM, Figure 6.1.4.

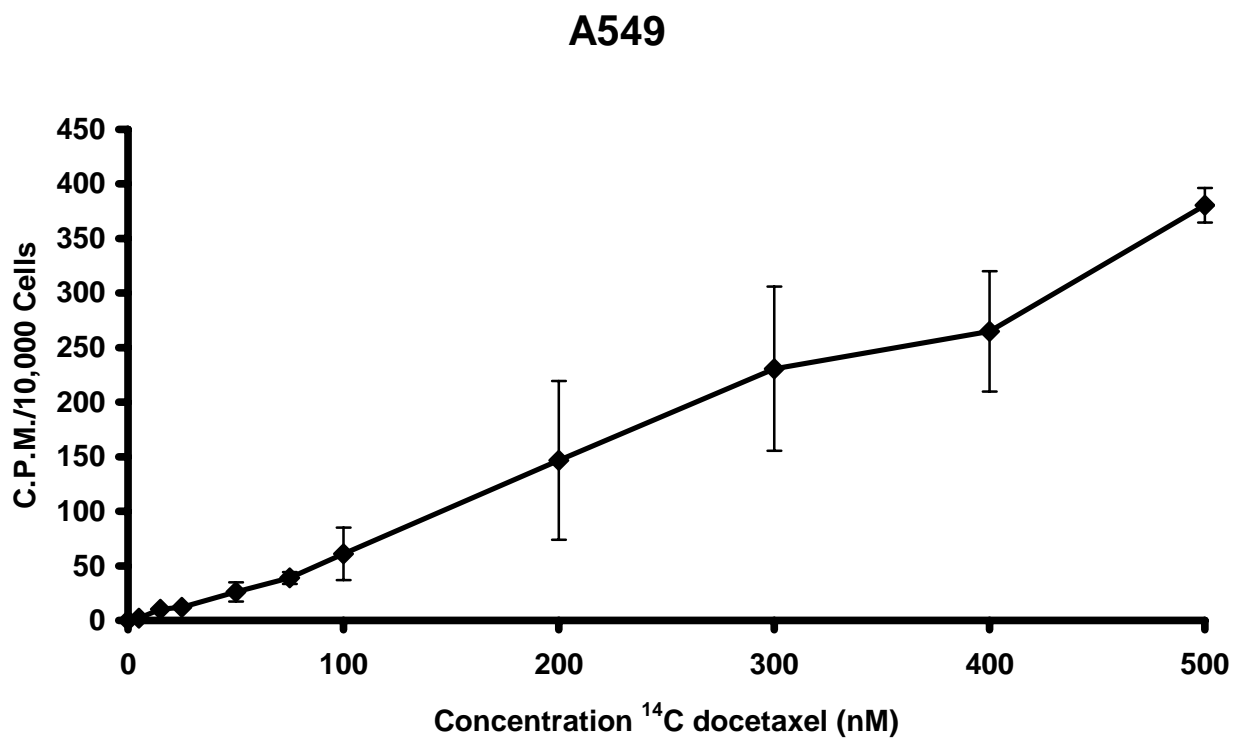


**Figure 6.2.1** <sup>14</sup>C docetaxel accumulation assay examining saturation in the A549 cell line. Cells were exposed to a range of <sup>14</sup>C docetaxel concentrations (5, 15, 25, 50, 75, 100, 200, 300, 400 and 500 nM) for 90 minutes. Data are mean +/- SD calculated on experiments performed in duplicate.

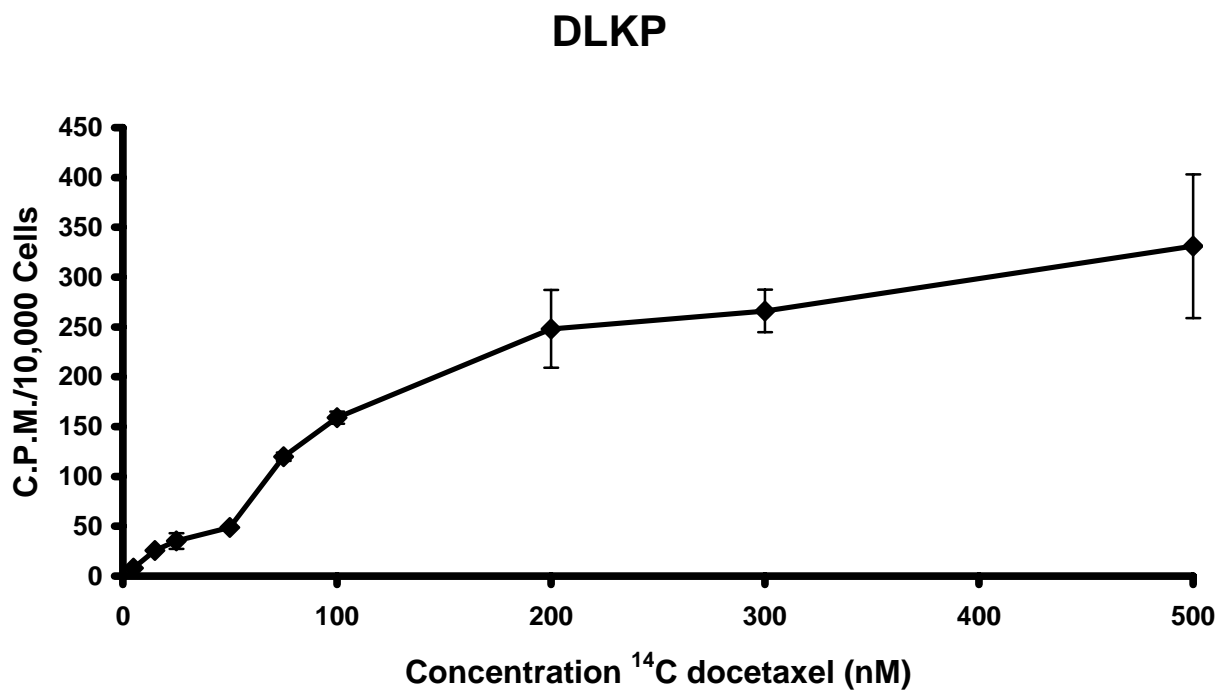


**Figure 6.2.2** <sup>14</sup>C docetaxel accumulation assay examining saturation in the DLKP cell line. Cells were exposed to a range of <sup>14</sup>C docetaxel concentrations (5, 15, 25, 50, 75, 100, 200, 300 and 500 nM) for 90 minutes. Data are mean +/- SD calculated on experiments performed in duplicate.

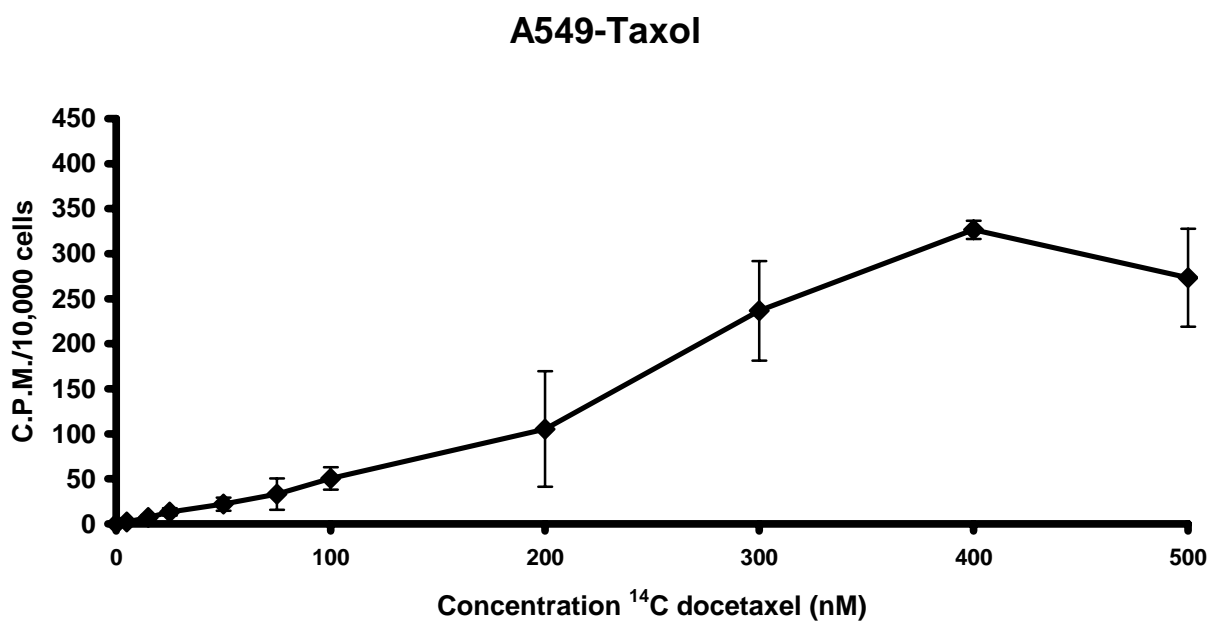


**Figure 6.2.3** <sup>14</sup>C docetaxel accumulation assay examining saturation in the A549-Taxol cell line. Cells were exposed to a range of <sup>14</sup>C docetaxel concentrations (5, 15, 25, 50, 75, 100, 200, 300, 400 and 500 nM) for 90 minutes. Data are mean +/- SD calculated on experiments performed in duplicate.

## DLKP-Mitox

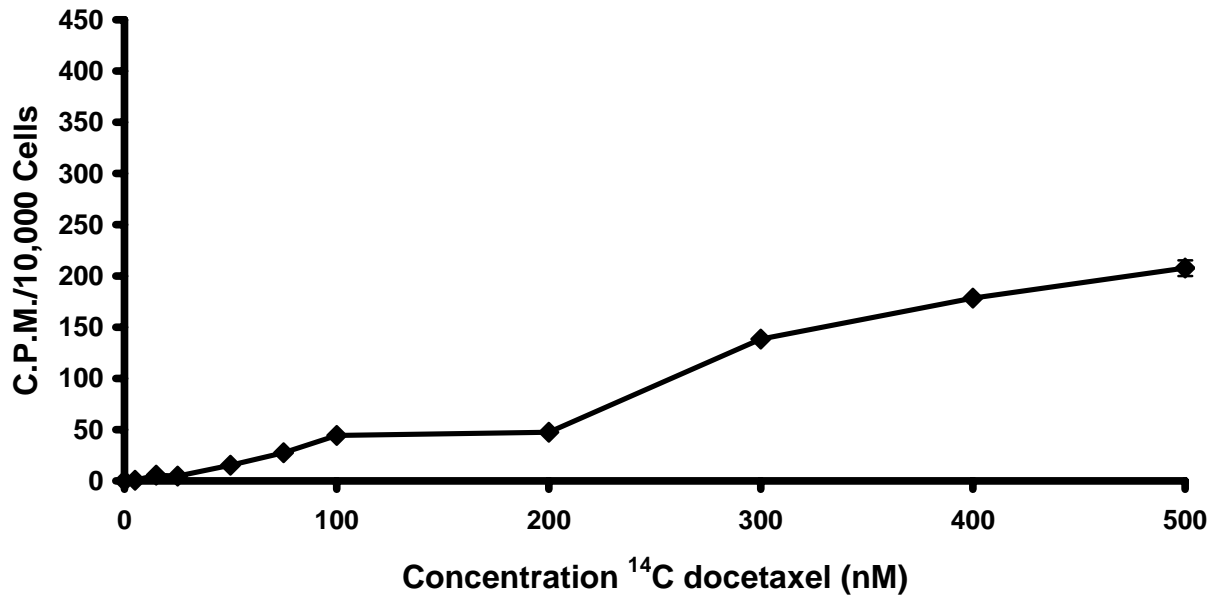


**Figure 6.2.4** <sup>14</sup>C docetaxel accumulation assay examining saturation in DLKP-Mitox. Cells were exposed to a range of <sup>14</sup>C docetaxel concentrations (5, 15, 25, 50, 75, 100, 200, 300, 400 and 500 nM) for 90 minutes. Data are mean +/- SD calculated on experiments performed in duplicate.

### 6.3 Temperature

Accumulation of 100 nM  $^{14}\text{C}$  docetaxel was examined at 30, 60, 90 and 120 minutes at a range of temperatures in A549 and DLKP.

In the A549 cell line, the transport of  $^{14}\text{C}$  docetaxel was found to be temperature-dependent, Figure 6.3.1. Reduced temperatures ( $4^{\circ}\text{C}$  and  $27^{\circ}\text{C}$ ) decreased docetaxel accumulation significantly. At  $4^{\circ}\text{C}$  accumulation was almost eliminated but at  $27^{\circ}\text{C}$  docetaxel accumulation reached equivalent levels to the mass accumulated after 120 minutes at  $37^{\circ}\text{C}$ . At  $41^{\circ}\text{C}$  drug accumulation increased and at  $46^{\circ}\text{C}$  a further increase was observable until the 60 minute timepoint when docetaxel accumulation levels then began to drop.

In the DLKP cell line (Figure 6.3.2), decreasing temperature once again reduced docetaxel accumulation but in this cell line the difference in accumulation between  $37^{\circ}\text{C}$  and  $27^{\circ}\text{C}$  was more pronounced than in A549, never attaining parity. Drug accumulation was almost eliminated at  $4^{\circ}\text{C}$ . The accumulation profile for  $^{14}\text{C}$  docetaxel at  $41^{\circ}\text{C}$  and  $46^{\circ}\text{C}$  in DLKP was similar to A549 but a complete reduction in accumulation after 60 minutes at  $46^{\circ}\text{C}$  was evident.

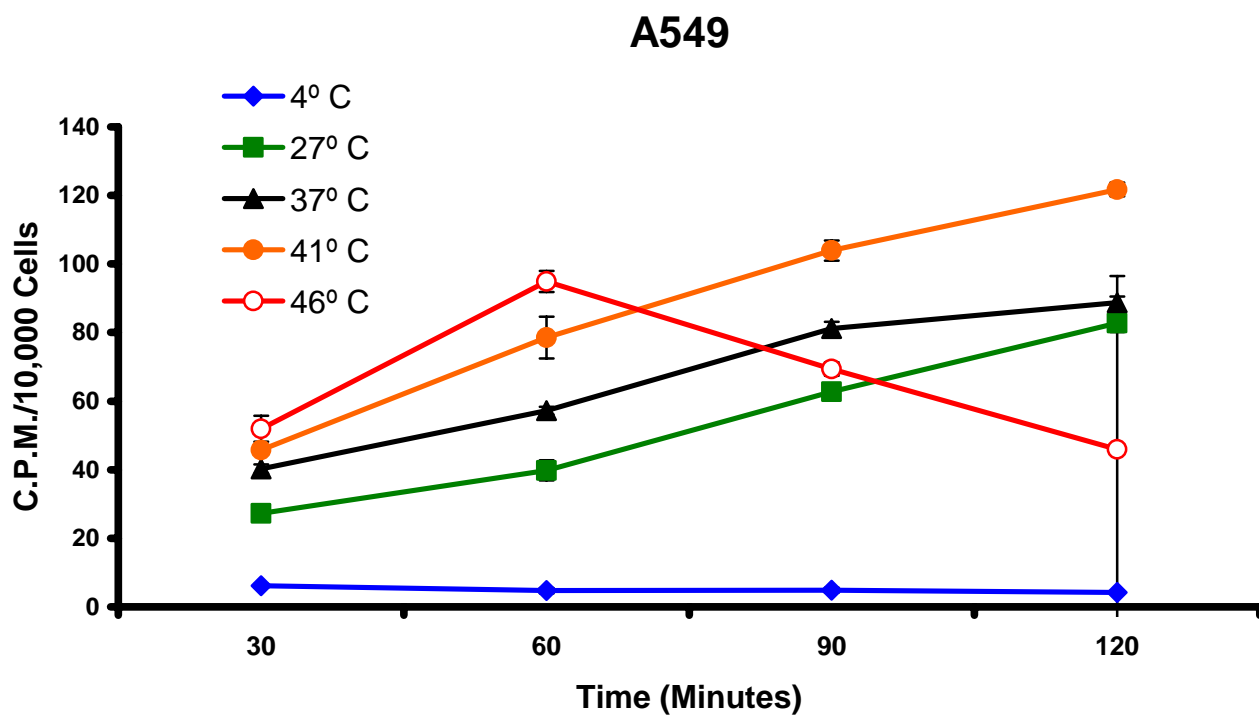


**Figure 6.3.1** The effect of temperature on accumulation of  $^{14}\text{C}$  docetaxel in A549. Cells were exposed to 100 nM  $^{14}\text{C}$  docetaxel for 30, 60, 90 and 120 minutes at 4, 27, 37, 41 and 46°C. Data are mean  $\pm$  SD calculated on an experiment performed in triplicate.

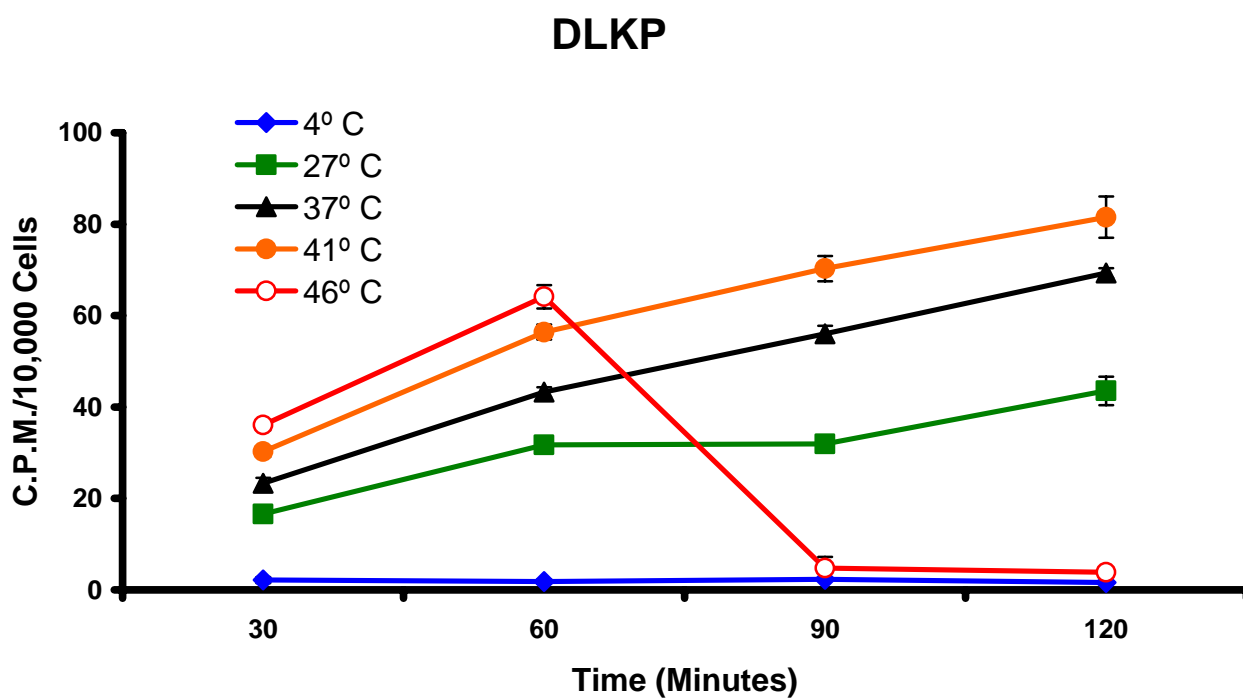


**Figure 6.3.2** The effect of temperature on accumulation of  $^{14}\text{C}$  docetaxel in DLKP. Cells were exposed to 100 nM  $^{14}\text{C}$  docetaxel for 30, 60, 90 and 120 minutes at 4, 27, 37, 41 and 46°C. Data are mean  $\pm$  SD calculated on experiments performed in triplicate.

## 6.4 ATP depletion

ATP depletion by sodium azide (mitochondrial metabolic inhibitor), 2-deoxyglucose (glycolysis inhibitor) and antimycin A (electron transport chain inhibitor) was quantified over 15, 30 and 45 minutes using a bioluminescent luciferase-based assay (Section 2.17) in the DLKP and A549 cell lines. The level of ATP in glucose-free medium containing 5% FCS was also determined at these timepoints.

In DLKP, glucose-free medium alone reduced ATP levels by 21.5% after 30 minutes and the three inhibitors reduced ATP levels further at the three concentrations studied, Figure 6.4.1. 10 mM 2-deoxyglucose proved the most effective at reducing ATP levels in DLKP. At the 30 minute timepoint, 10 mM sodium azide reduced ATP levels by 44.1%, 5 mM 2-deoxyglucose by 60.6% and 10  $\mu$ M antimycin A by 36%. Similar results were found in the A549 cell line (Figure 6.4.2). Glucose-free medium alone had a less substantial impact on ATP levels (18.6% reduction after 30 minutes) compared to 10 mM sodium azide (48.1%), 2-deoxyglucose (56.2%) and 10  $\mu$ M sodium azide (49.8%).

Two combinations of inhibitors in glucose-free medium were then tested in DLKP and A549, Figure 6.4.3. 10 mM sodium azide and 5 mM 2-deoxyglucose (treatment A) caused a 90.3% and 90.1% reduction in cellular ATP levels in DLKP and A549, respectively. 10 mM sodium azide, 5 mM 2-deoxyglucose and 10  $\mu$ M antimycin A (treatment B) depleted ATP levels by 93.5% in DLKP and 95.2% in A549. A standard curve was used to generate values for the mass of ATP (ng) per 10,000 cells for the two treatments, Table 6.4.1. DLKP contains 2.1 times the amount of ATP found in A549.

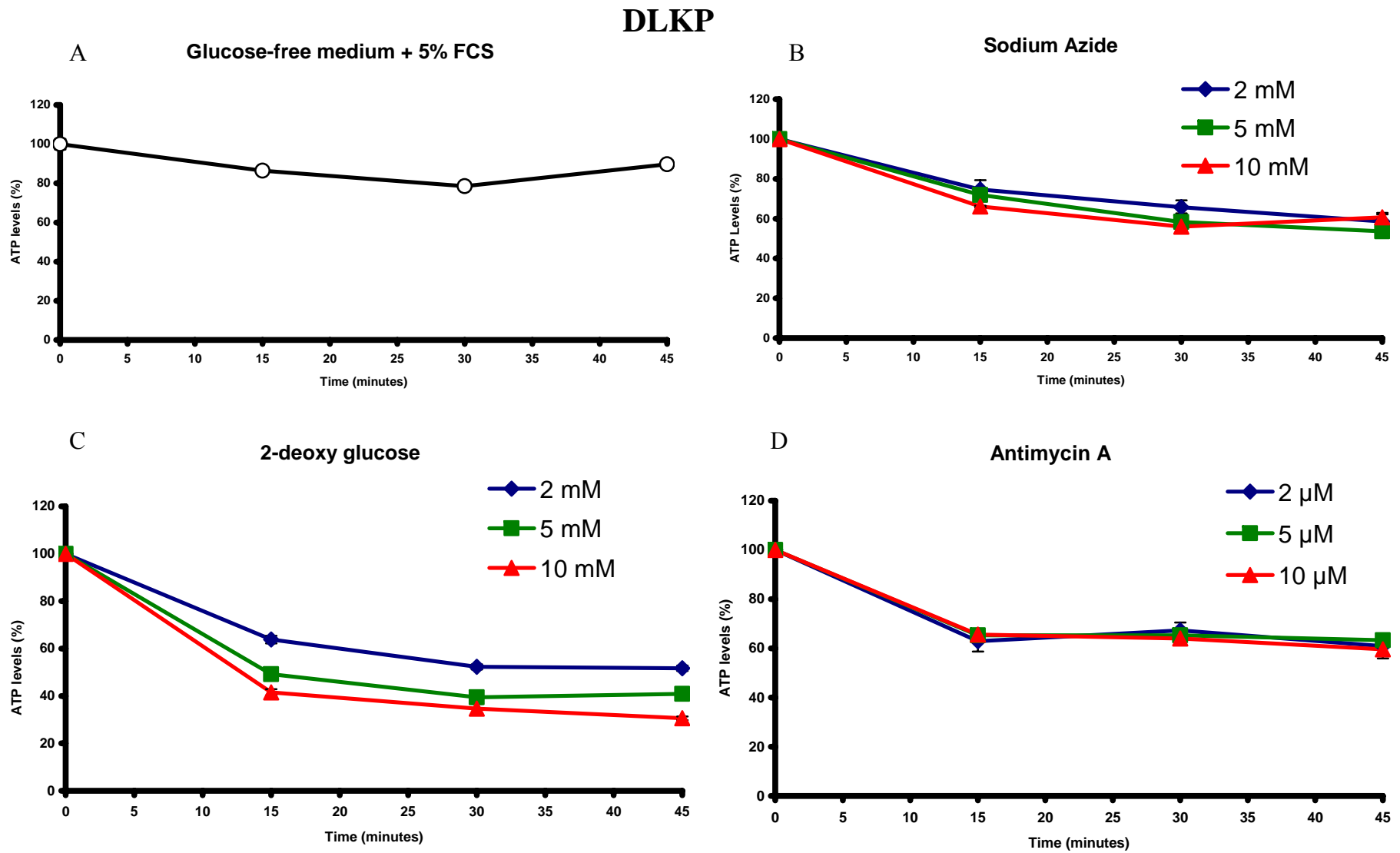


**Figure 6.4.1** The effects of glucose-free medium (DMEM/Ham's F12) supplemented with 5% FCS alone (A) and in combination with sodium azide (B), 2-deoxyglucose (C) and antimycin A (D) on ATP levels in DLKP. Results are expressed as a percentage of control. Data are mean  $\pm$  SD calculated on experiments performed in duplicate.

## A549

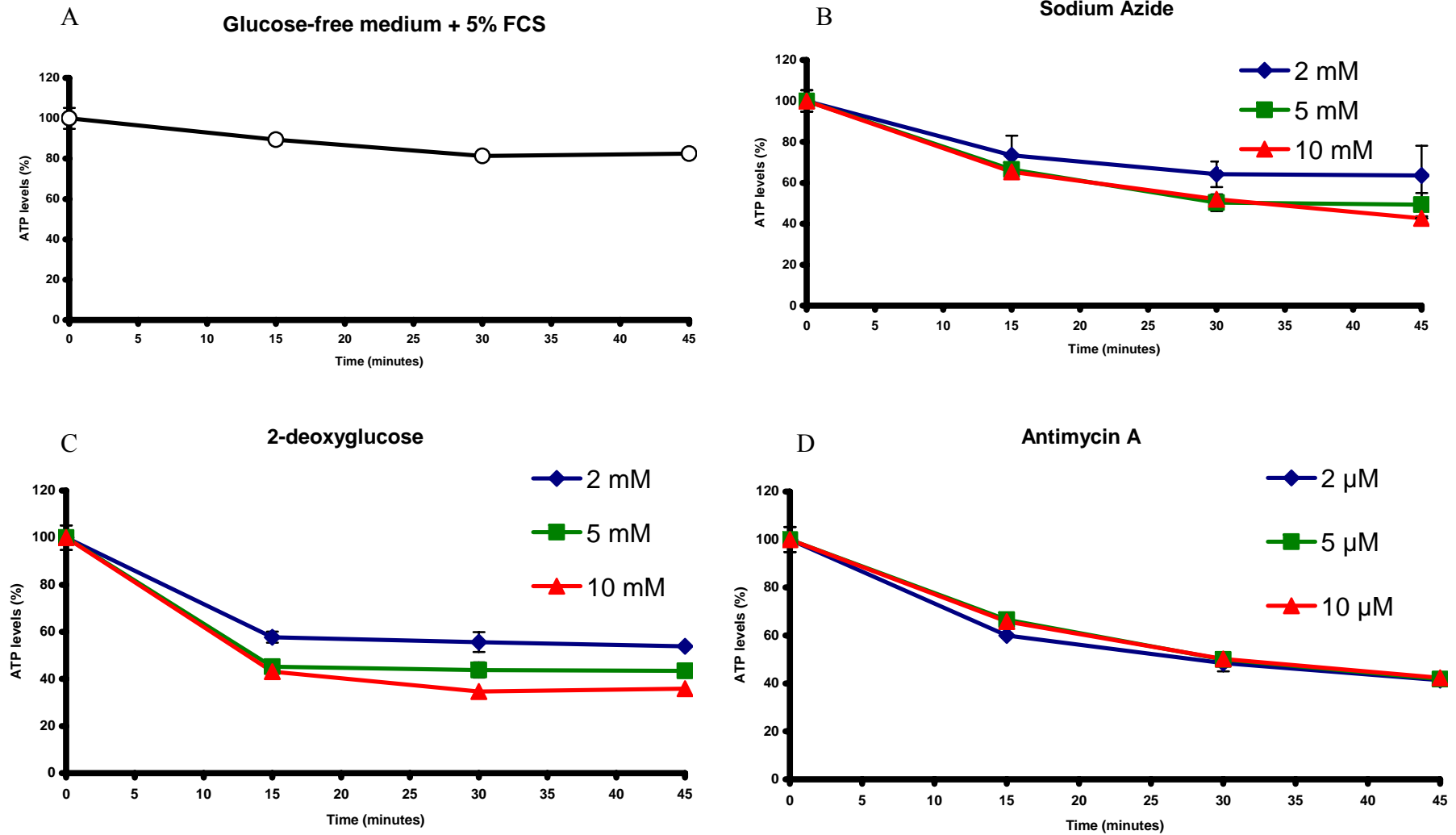


**Figure 6.4.2** The effects of glucose-free medium (DMEM/Ham's F12) supplemented with 5% FCS alone (A) and in combination with sodium azide (B), 2-deoxyglucose (C) and antimycin A (D) on ATP levels in A549. Results are expressed as a percentage of control. Data are mean  $\pm$  SD calculated on experiments performed in duplicate.

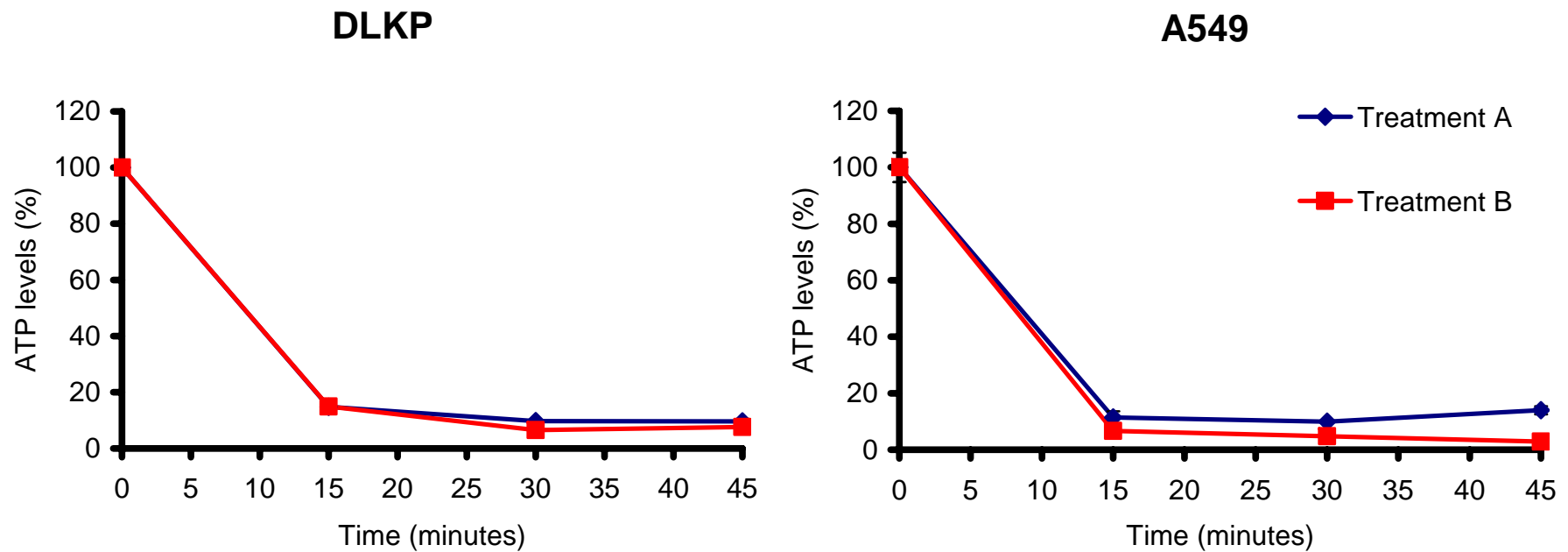


**Figure 6.4.3** The effects of two combinations of ATP-depleting agents on ATP levels in DLKP and A549. Treatment A consisted of 10 mM sodium azide and 5 mM 2-deoxyglucose. Treatment B consisted of 10 mM sodium azide, 5 mM 2-deoxyglucose and 10  $\mu$ M sodium azide. Both assays were undertaken in the presence of glucose -free medium (DMEM/Ham's F12) supplemented with 5% FCS. Results are expressed as a percentage of a control representing ATP levels under normal glucose containing conditions. Data are mean  $\pm$  SD calculated on an experiment performed in duplicate.

**Table 6.4.1** The effects of glucose-free medium (DMEM/Ham's F12) supplemented with 5% FCS (medium control), 10 mM sodium azide and 5 mM 2-deoxyglucose (treatment A) and 10 mM sodium azide, 5 mM 2-deoxyglucose and 10  $\mu$ M antimycin A (treatment B) in DLKP and A549. A standard curve was used to determine the nanograms of ATP per 10,000 cells (Section 2.17.2). Data are mean  $\pm$  SD calculated on an experiment performed in duplicate.

<b>DLKP</b>	<b>T0</b> (ng ATP/10,000 cells)	<b>T15</b> (ng ATP/10,000 cells)	<b>T30</b> (ng ATP/10,000 cells)	<b>T45</b> (ng ATP/10,000 cells)
<b>Medium control</b>	<b>8.6 <math>\pm</math> 0.27</b>	<b>7.12 <math>\pm</math> 0.02</b>	<b>7.43 <math>\pm</math> 0.25</b>	<b>8.17 <math>\pm</math> 0.52</b>
<b>Treatment A</b>	<b>8.6 <math>\pm</math> 0.27</b>	<b>1.36 <math>\pm</math> 0.08</b>	<b>0.92 <math>\pm</math> 0.03</b>	<b>0.90 <math>\pm</math> 0.05</b>
<b>Treatment B</b>	<b>8.6 <math>\pm</math> 0.27</b>	<b>1.28 <math>\pm</math> 0.12</b>	<b>0.66 <math>\pm</math> 0.08</b>	<b>0.71 <math>\pm</math> 0.03</b>
<b>A549</b>				
<b>Medium control</b>	<b>4.19 <math>\pm</math> 0.04</b>	<b>3.92 <math>\pm</math> 0.28</b>	<b>3.58 <math>\pm</math> 0.09</b>	<b>3.71 <math>\pm</math> 0.23</b>
<b>Treatment A</b>	<b>4.19 <math>\pm</math> 0.04</b>	<b>0.53 <math>\pm</math> 0.15</b>	<b>0.44 <math>\pm</math> 0.05</b>	<b>0.63 <math>\pm</math> 0.08</b>
<b>Treatment B</b>	<b>4.19 <math>\pm</math> 0.04</b>	<b>0.30 <math>\pm</math> 0.06</b>	<b>0.19 <math>\pm</math> 0.01</b>	<b>0.15 <math>\pm</math> 0.01</b>

## 6.5 The effect of ATP depletion on docetaxel accumulation

Treatment B (10mM sodium azide, 5 mM 2-deoxyglucose and 10  $\mu$ M antimycin A) was used to deplete ATP levels when examining the accumulation of 100 nM  $^{14}$ C docetaxel in DLKP and A549. A decrease in docetaxel accumulation would be indicative of an ATP-dependent influx mechanism while an increase in docetaxel levels would be suggestive of an ATP-dependent efflux mechanism. Accumulation of 100 nM  $^{14}$ C docetaxel was studied directly in the presence of normal medium (glucose-containing DMEM/Ham's F12 supplemented with 5% FCS), glucose free-medium alone (glucose-free DMEM supplemented with 5% FCS) and glucose-free medium containing ATP inhibitors (treatment B). The same assay was also carried out after cells had been pre-treated with ATP inhibitors in glucose-free medium for 30 minutes. Figure 6.5.1A shows docetaxel accumulation in DLKP cells pre-treated and not pre-treated with ATP inhibitors. In both instances accumulation in normal medium and glucose-free medium was similar. In DLKP, in the presence of ATP inhibitors, there was a significant decrease in the amount of docetaxel accumulated after 120 minutes in both pre-treated and non-pre-treated cells. Comparing the non-pre-treated and pre-treated cells under each medium condition directly revealed a strong decrease in docetaxel accumulation in pre-treated cells under all medium circumstances, Figure 6.5.1B. The decreases were significant at 60, 90 and 120 minutes under the various assay conditions.

Accumulation of 100 nM  $^{14}$ C docetaxel was also similar in the A549 cell line irrespective of ATP inhibitor pre-treatment, Figure 6.5.2 A. Converse to the DLKP results, the presence of ATP inhibitors resulted in an increase in the amount of docetaxel accumulated in both assay conditions but the trend was more prominent in the pre-treated cells. Pre-treatment did not result in differences in accumulation of docetaxel in A549 when the pre-treated and non-pre-treated conditions were compared in A549, Figure 6.5.2B.

## DLKP

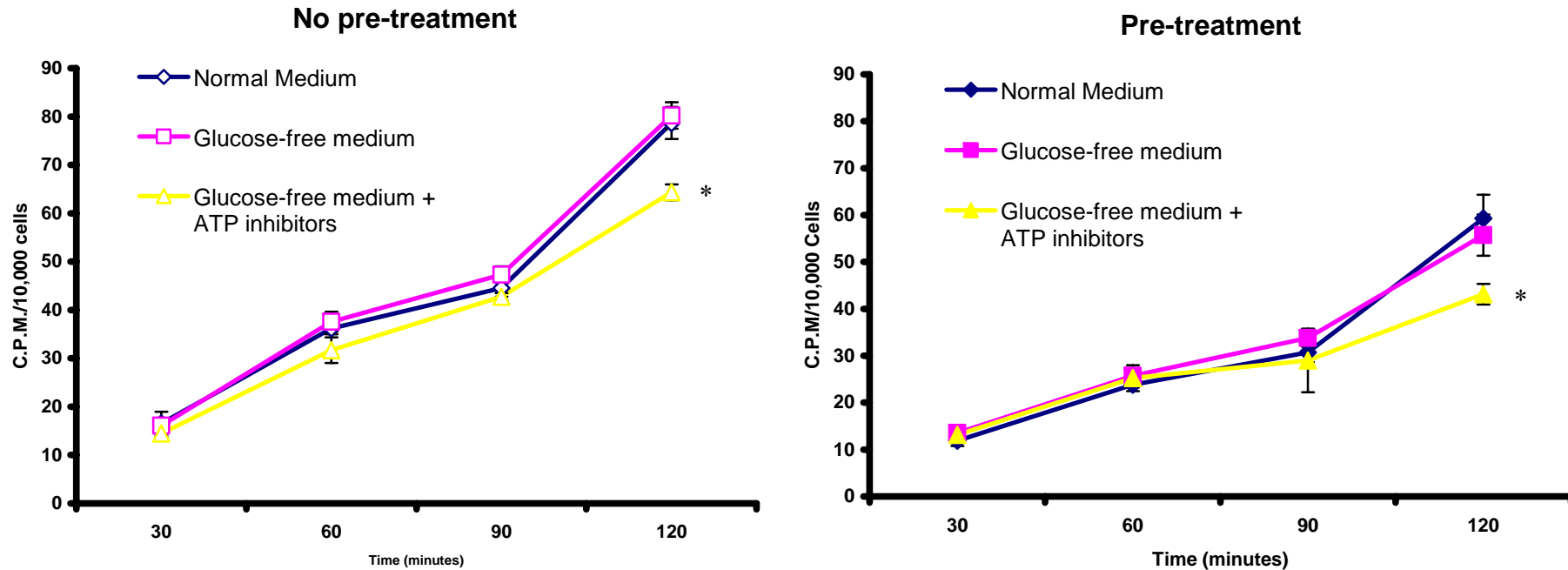


**Figure 6.5.1A** Effects of energy depletion on accumulation of 10nM  $^{14}\text{C}$  docetaxel in DLKP. Accumulation of 100 nM  $^{14}\text{C}$  docetaxel was examined in normal medium (DMEM/Ham's F12 supplemented with 5% FCS), glucose-free medium (glucose-free DMEM supplemented with 5% FCS) and glucose-free medium and ATP inhibitors (glucose-free DMEM supplemented with 5% FCS, 10 mM sodium azide, 5 mM 2-deoxyglucose and 10  $\mu\text{M}$  antimycin A). Pre-treatment involved pre-incubation of cells with 10 mM sodium azide, 5 mM 2-deoxyglucose and 10  $\mu\text{M}$  antimycin A in glucose-free medium supplemented with 5% FCS for 30 minutes. Cells were washed once with warm PBS and accumulation of 100 nM  $^{14}\text{C}$  docetaxel measured. Data are mean  $\pm$  SD calculated on an experiment performed in triplicate. \* significant,  $P < 0.05$  at 120 minutes relative to the normal medium control.

## DLKP

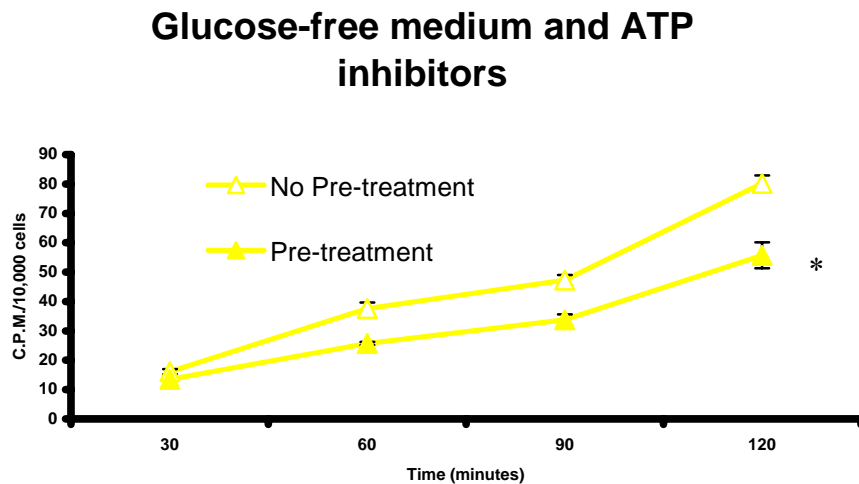
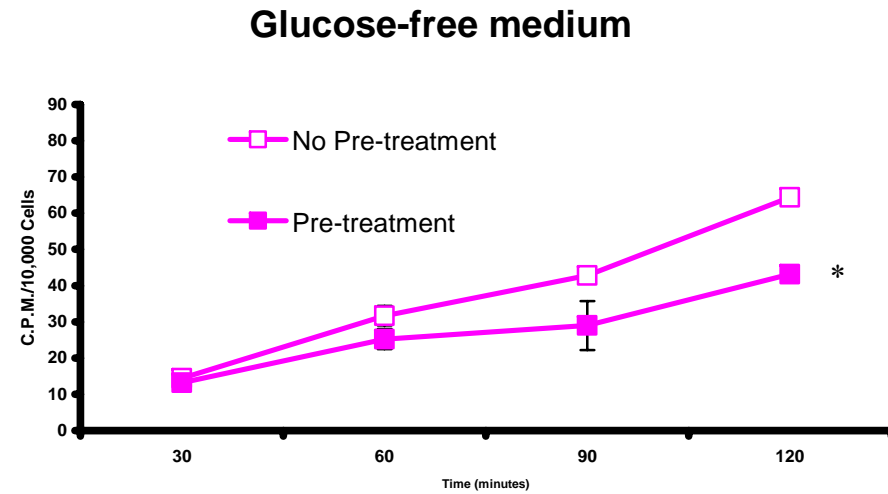
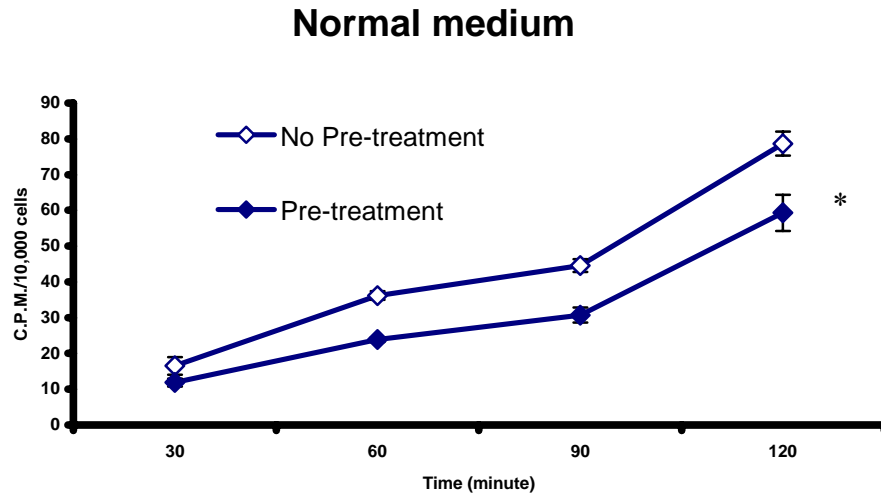


**Figure 6.5.1B** Comparison of the effects of pre-treatment and no pre-treatment on 100 nM  $^{14}\text{C}$  docetaxel accumulation in DLKP under individual assay conditions. Normal medium consisted of DMEM/Ham's F12 supplemented with 5% FCS. Glucose-free medium consisted of glucose-free DMEM supplemented with 5% FCS. ATP inhibitors utilised were 10 mM sodium azide, 5 mM 2-deoxyglucose and 10  $\mu\text{M}$  antimycin A. Data are mean  $\pm$  SD calculated on an experiment performed in triplicate. \* significant,  $P < 0.05$  at 60, 90 and 120 minutes relative to cells receiving no pre-treatment.

## A549

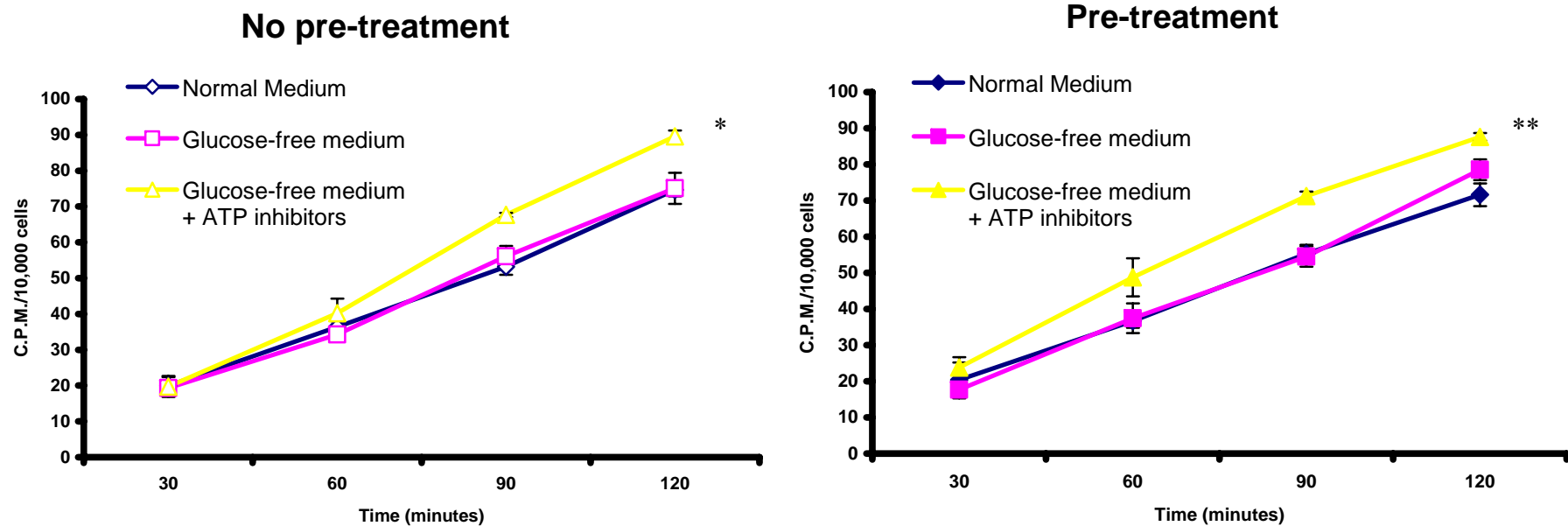


**Figure 6.5.2A** Effects of energy depletion on accumulation of 100 nM  $^{14}\text{C}$  docetaxel in A549. Accumulation of 100 nM  $^{14}\text{C}$  docetaxel was examined in normal medium (DMEM/Ham's F12 supplemented with 5% FCS), glucose-free medium (glucose-free DMEM supplemented with 5% FCS) and glucose-free medium and ATP inhibitors (glucose-free DMEM supplemented with 5% FCS, 10 mM sodium azide, 5 mM 2-deoxyglucose and 10  $\mu\text{M}$  antimycin A). Pre-treatment involved pre-incubation of cells with 10 mM sodium azide, 5 mM 2-deoxyglucose and 10  $\mu\text{M}$  antimycin A in glucose-free medium supplemented with 5% FCS for 30 minutes. Cells were washed once with warm PBS and accumulation of 100 nM  $^{14}\text{C}$  docetaxel measured. Data are mean  $\pm$  SD calculated on an experiment performed in triplicate. \* significant,  $P < 0.05$  at 90 and 120 minutes relative to the normal medium control. \*\* significant,  $P < 0.05$  at 60, 90 and 120 minutes relative to the normal medium control.

## A549

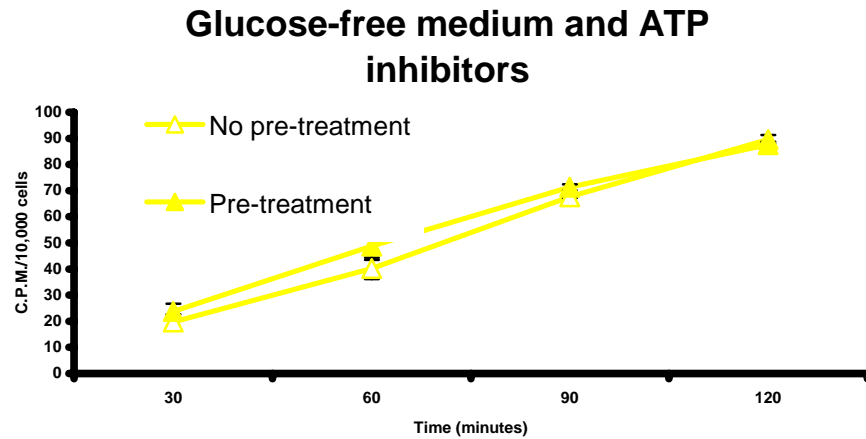
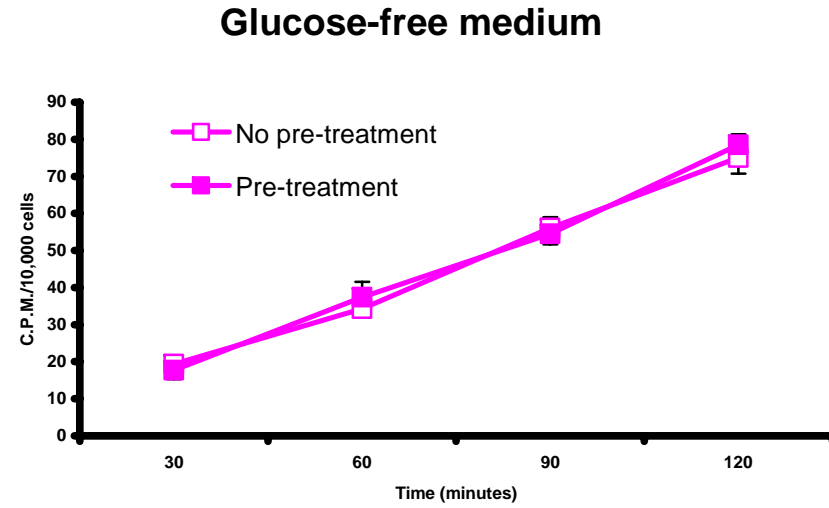
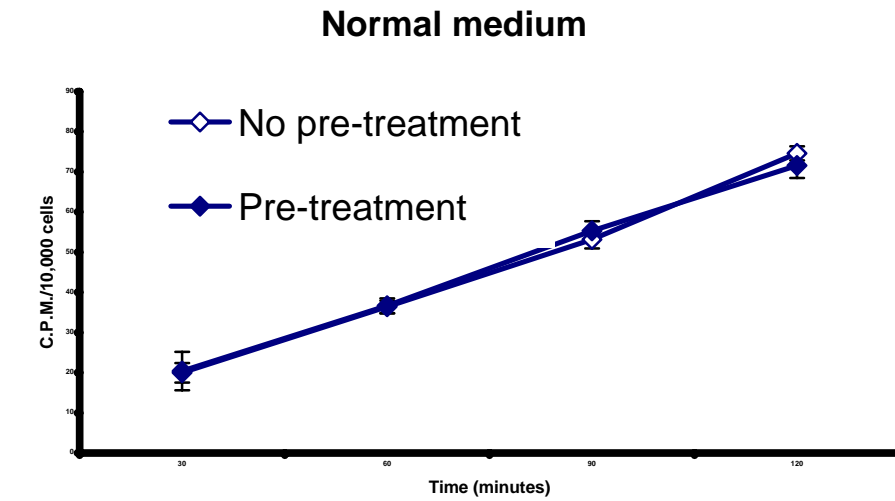


**Figure 6.5.2 B** Comparison of the effects of pre-treatment and no pre-treatment on 100 nM  $^{14}\text{C}$  docetaxel accumulation in A549 under individual assay conditions. Normal medium consisted of DMEM/Ham's F12 supplemented with 5% FCS. Glucose-free medium consisted of glucose-free DMEM supplemented with 5% FCS. ATP inhibitors utilised were 10 mM sodium azide, 5 mM 2-deoxyglucose and 10  $\mu\text{M}$  antimycin A. Data are mean  $\pm$  SD calculated on an experiment performed in triplicate.

## 6.6 OATP inhibitors

To investigate the possible involvement of OATP (organic anion transporter polypeptides) in docetaxel accumulation in the A549 and DLKP cell lines, a number of  $^{14}\text{C}$  docetaxel accumulation assays were carried out in the presence of OATP inhibitors.

The effects of bromosulfophthalein (BSP) on  $^{14}\text{C}$  docetaxel accumulation in A549 and DLKP are shown in Figure 6.6.1. BSP is an OATP inhibitor of broad specificity. BSP concentrations of 1, 5, and 10  $\mu\text{M}$  had no effect on docetaxel accumulation in A549. 50  $\mu\text{M}$  BSP, however, reduced docetaxel accumulation significantly, contrary to the increase in accumulated  $^{14}\text{C}$  docetaxel observed in A549 in the presence of ATP depleting agents (Figure 6.5.2A). BSP had no effect on docetaxel accumulation in DLKP at any of the concentrations used.

A comparison of the effects of digoxin on  $^{14}\text{C}$  docetaxel accumulation in A549 and DLKP is shown in Figure 6.6.2. Digoxin is a selective transport substrate for OATP1B3. 10, 50, and 100  $\mu\text{M}$  digoxin had no effect on docetaxel accumulation but the presence of 150  $\mu\text{M}$  digoxin produced a significant decrease in drug accumulation in the A549 cell line.

In the DLKP cell line, 50  $\mu\text{M}$  digoxin decreased docetaxel accumulation and 10  $\mu\text{M}$  had no effect on drug accumulation. The 0.8% DMSO control renders the decrease associated with 50  $\mu\text{M}$  digoxin insignificant, however.

A wide range of indocyanine green (ICG) concentrations were examined in A549, Figure 6.6.3. Unexpectedly, the highest concentrations of ICG (10-100  $\mu\text{M}$ ) increased docetaxel levels by up to 1.8 times (100  $\mu\text{M}$  for 120 minutes). The highest concentration assayed, 150  $\mu\text{M}$ , increased docetaxel accumulation but to a lesser extent than 100  $\mu\text{M}$ . The lower range of ICG concentrations examined (0.05- 1  $\mu\text{M}$ ) had no effect on  $^{14}\text{C}$  docetaxel accumulation. 10-150  $\mu\text{M}$  ICG was also studied in the DLKP cell line, Figure 6.6.4. 50  $\mu\text{M}$  ICG resulted in a 1.47 fold increase in docetaxel accumulated after 120 minutes relative to the control. 100 and 150  $\mu\text{M}$  also resulted in changes to docetaxel accumulation levels but the high levels of DMSO (up to 5.8%) countered the effects of ICG, ultimately reducing docetaxel levels.

The effect of a further four OATP inhibitors of varying specificity were examined in the A549 cell line. Dehydroepiandrosterone (DHEAS) produced significant increases in  $^{14}\text{C}$  docetaxel accumulation across all timepoints in a concentration dependent manner, Figure 6.6.5. Cyclosporin A had no major effect on  $^{14}\text{C}$  docetaxel accumulation, Figure 6.6.6.

Treatment with 150  $\mu\text{M}$  prostaglandin E<sub>2</sub> (PGE<sub>2</sub>) did result in a minor but significant decrease in docetaxel levels but this corresponded with a significant decrease associated with the DMSO control, Figure 6.6.7. 50  $\mu\text{M}$  thyroid hormone (tri-iodothyronine, T<sub>3</sub>) resulted in a significant increase in <sup>14</sup>C docetaxel accumulation up to 90 minutes in A549, Figure 6.6.8.

High DMSO concentrations decrease <sup>14</sup>C docetaxel accumulation in A549 and DLKP. DLKP was more susceptible to this effect than A549, Figures 6.6.3 and 6.6.4.

## Bromosulfophthalein

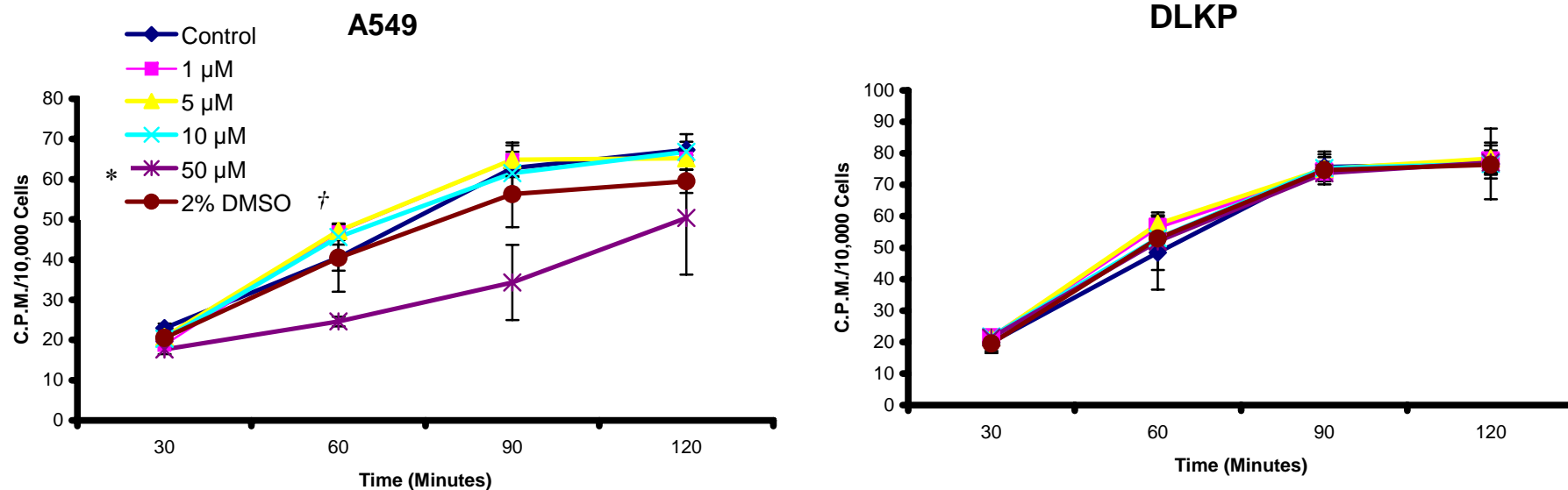


**Figure 6.6.1** The effect of bromosulfophthalein (BSP) on  $^{14}\text{C}$  docetaxel accumulation in the A549 and DLKP cell lines. Cells were incubated with 100 nM  $^{14}\text{C}$  docetaxel alone (Control) or 100 nM  $^{14}\text{C}$  docetaxel and BSP (1, 5, 10, 50  $\mu\text{M}$ ) for 30, 60, 90 and 120 minutes. A 2% DMSO control was also included that corresponded to the amount of DMSO present in 50  $\mu\text{M}$  BSP. Data are mean  $\pm$  SD calculated on experiments performed in triplicate. \* significant,  $P < 0.05$  at 30, 60 and 90 minutes relative to the control. † not significant,  $P > 0.05$  for all timepoints relative to the control.

## Digoxin

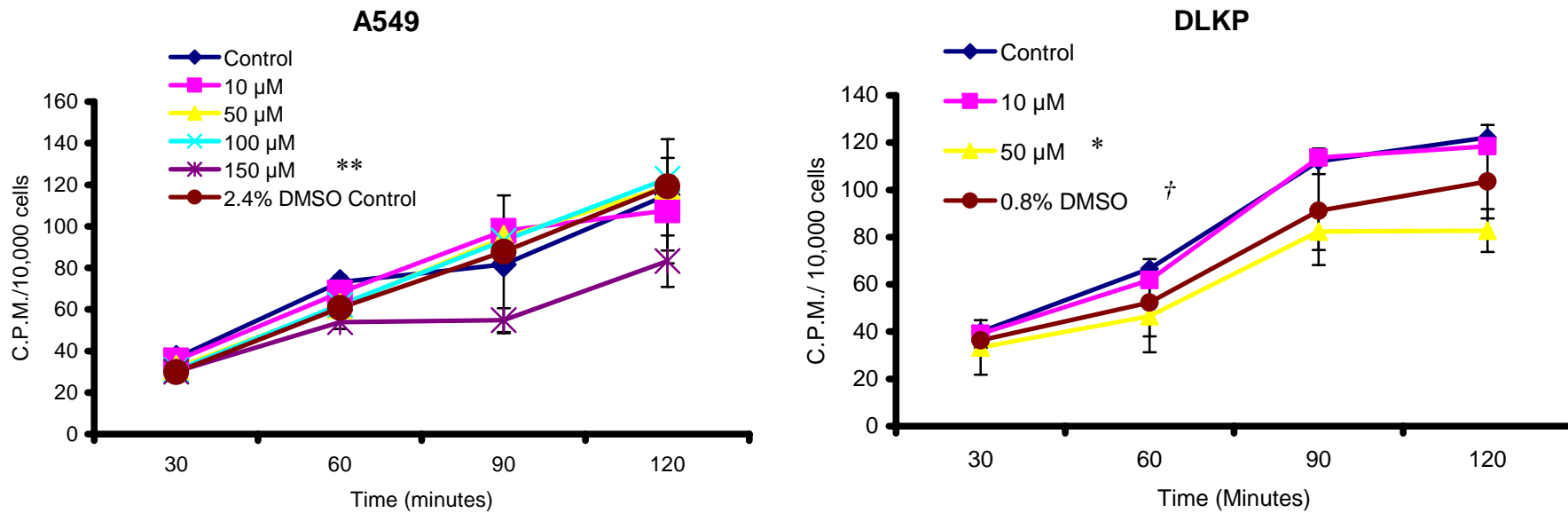


**Figure 6.6.2** The effect of digoxin on  $^{14}\text{C}$  docetaxel accumulation in the A549 and DLKP cell lines. Cells were incubated with 100 nM  $^{14}\text{C}$  docetaxel alone or 100 nM  $^{14}\text{C}$  docetaxel and digoxin (1, 5, 10, 50 $\mu\text{M}$ ) for 30, 60, 90 and 120 minutes. 2.4% and 0.8% DMSO control were also included that correspond to the amount of DMSO present in 150  $\mu\text{M}$  and 50  $\mu\text{M}$  digoxin respectively. Data are mean  $\pm$  SD calculated on experiments performed in triplicate. \* significant,  $P < 0.05$  at 90 and 120 minutes relative to the control. \*\* significant,  $P < 0.05$  at 60 minutes relative to the control. † not significant,  $P > 0.05$  for all timepoints relative to the control.

## A549- Indocyanine Green

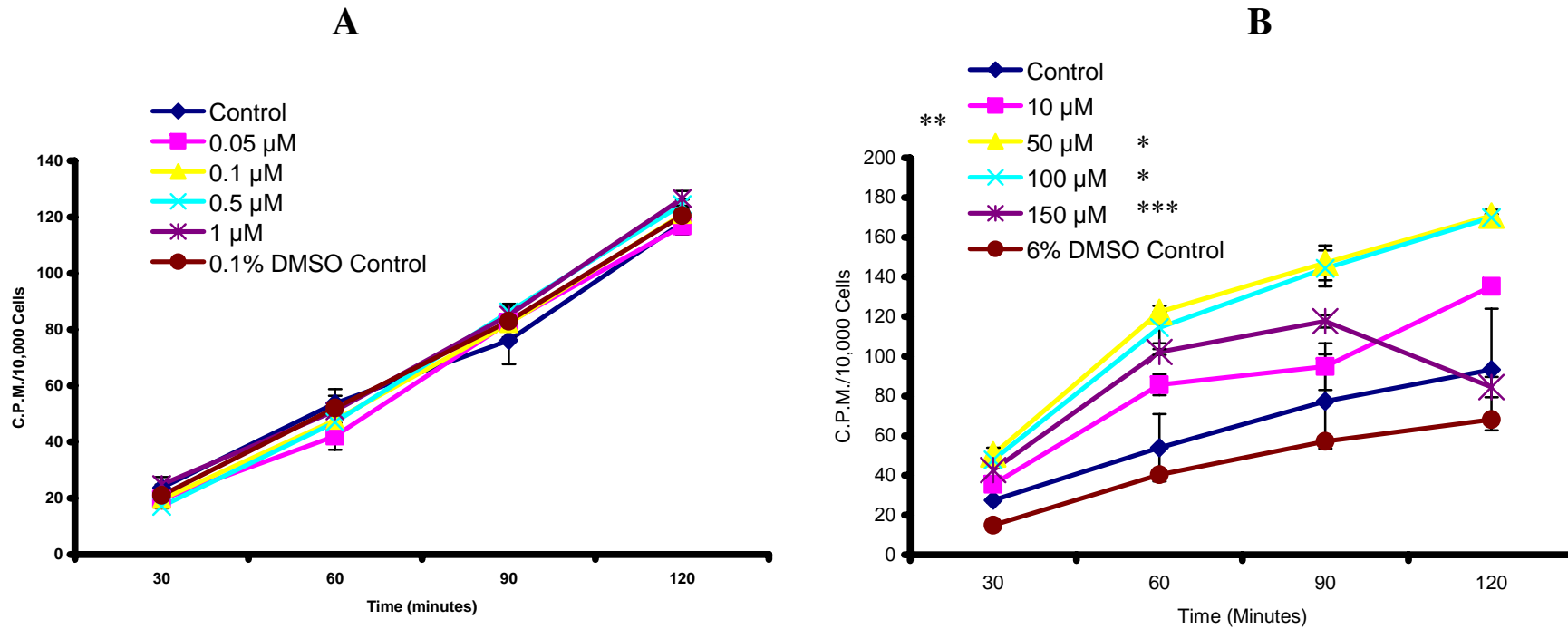


**Figure 6.6.3** The effect of indocyanine green (ICG) on  $^{14}\text{C}$  docetaxel accumulation in the A549 cell line. Cells were incubated with 100 nM  $^{14}\text{C}$  docetaxel alone (Control) or 100 nM  $^{14}\text{C}$  docetaxel and ICG (A -0.05, 0.1, 0.5, 1 and B- 10, 50, 100, 150  $\mu\text{M}$ ) for 30, 60, 90 and 120 minutes. A 2% and 0.1% DMSO control was included that correspond to the amount of DMSO present in 50  $\mu\text{M}$  and 1 $\mu\text{M}$  ICG respectively. Data are mean  $\pm$  SD calculated on experiments performed in triplicate. \* significant,  $P < 0.05$  for all timepoints relative to the control. \*\* significant,  $P < 0.05$  for 30, 60 and 120 minutes relative to the control. \*\*\* significant,  $P < 0.05$  for 30, 60 and 90 minutes relative to the control. The 6% DMSO control is significant at the 30 minute timepoint only,  $P < 0.05$ .

## DLKP

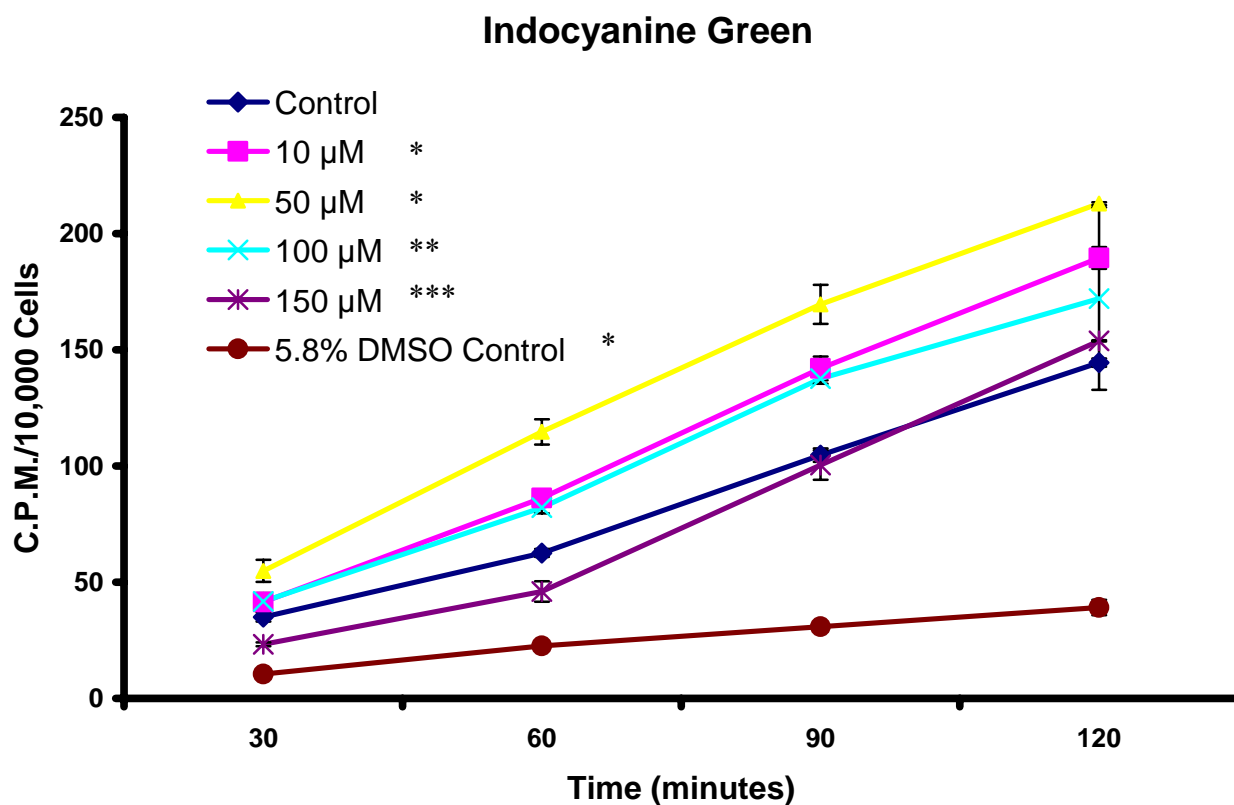


**Figure 6.6.4** The effect of indocyanine green (ICG) on  $^{14}\text{C}$  docetaxel accumulation in the DLKP cell line. Cells were incubated with 100 nM  $^{14}\text{C}$  docetaxel alone (Control) or 100 nM  $^{14}\text{C}$  docetaxel and ICG (10, 50, 100, 150  $\mu\text{M}$ ) for 30, 60, 90 and 120 minutes. A 5.8% DMSO control was included that corresponded to the amount of DMSO present in 150  $\mu\text{M}$  ICG. Data are mean  $\pm$  SD calculated on experiments performed in triplicate.

\* significant,  $P < 0.05$  for all timepoints relative to the control. \*\* significant,  $P < 0.05$  for 30, 60 and 90 minutes relative to the control. \*\*\* significant,  $P < 0.05$  for 30 and 60 minutes relative to the control.

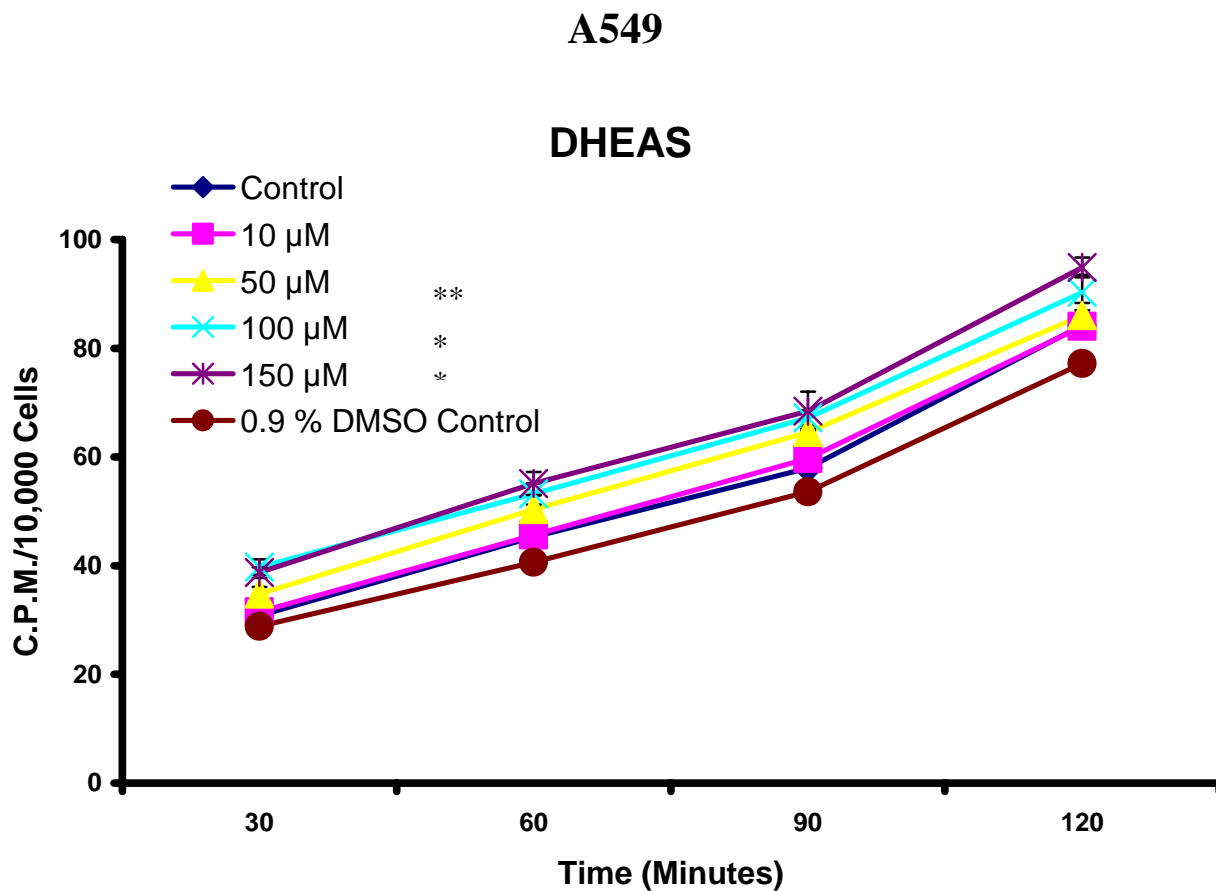


**Figure 6.6.5** The effect of dehydroepiandrosterone (DHEAS) on  $^{14}\text{C}$  docetaxel accumulation in the A549 cell line. Cells were incubated with 100 nM  $^{14}\text{C}$  docetaxel alone (Control) or 100 nM  $^{14}\text{C}$  docetaxel and DHEAS (10, 50, 100, 150  $\mu\text{M}$ ) for 30, 60, 90 and 120 minutes. A 0.9% DMSO control was included that corresponded to the amount of DMSO present in 150  $\mu\text{M}$  DHEAS. Data are mean  $\pm$  SD calculated on experiments performed in triplicate. \* significant,  $P < 0.05$  for all timepoints relative to the control. \*\* significant,  $P < 0.05$  for 30, 90 and 120 minutes relative to the control.

## A549

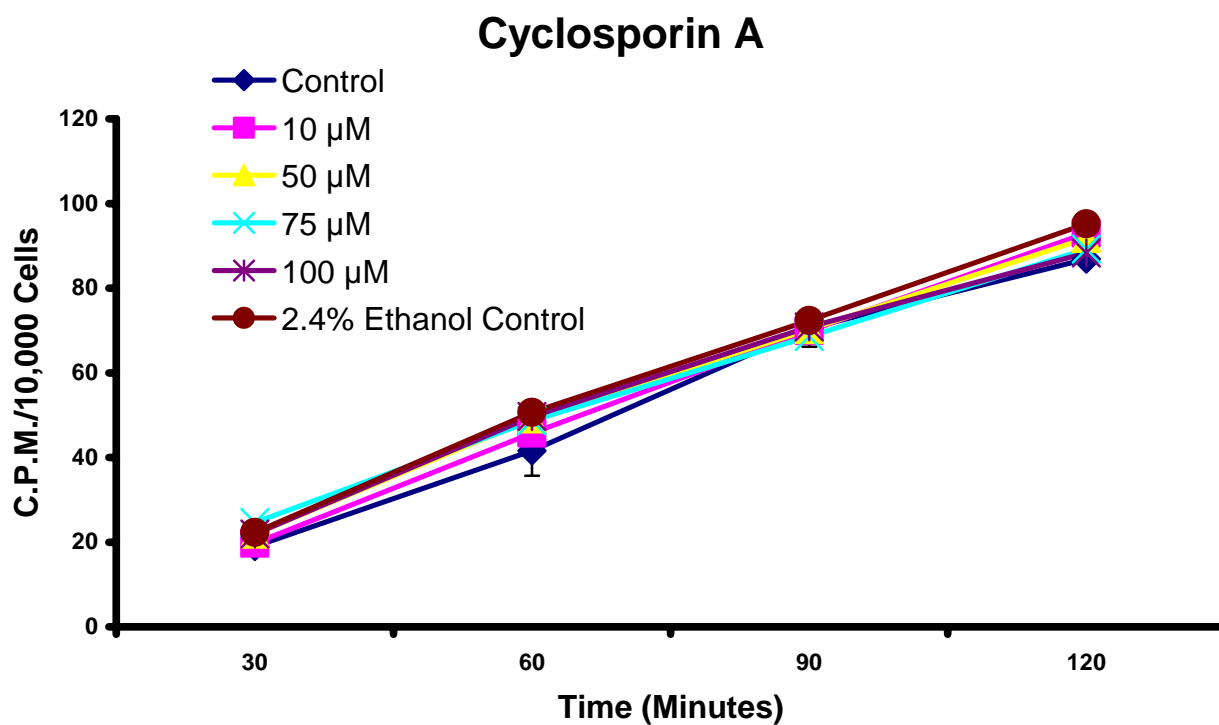


**Figure 6.6.6** The effect of cyclosporin A on  $^{14}\text{C}$  docetaxel accumulation in the A549 cell line. Cells were incubated with 100 nM  $^{14}\text{C}$  docetaxel alone (Control) or 100 nM  $^{14}\text{C}$  docetaxel and cyclosporin A (10, 50, 75, 100  $\mu\text{M}$ ) for 30, 60, 90 and 120 minutes. A 2.4% DMSO control was included that corresponded to the amount of DMSO present in 100  $\mu\text{M}$  cyclosporin A. Data are mean  $\pm$  SD calculated on experiments performed in triplicate.

## A549

### Prostaglandin E<sub>2</sub>

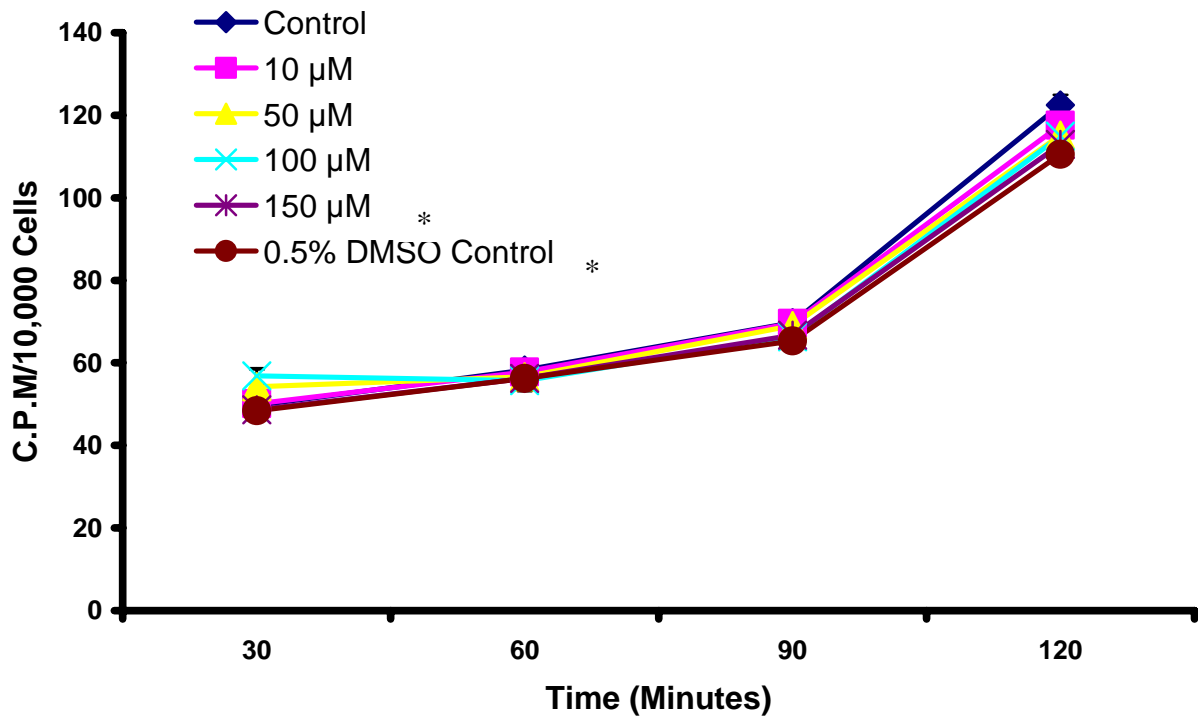


**Figure 6.6.7** The effect of prostaglandin E<sub>2</sub> on <sup>14</sup>C docetaxel accumulation in the A549 cell line. Cells were incubated with 100 nM <sup>14</sup>C docetaxel alone (Control) or 100 nM <sup>14</sup>C docetaxel and prostaglandin E<sub>2</sub> (10, 50, 100, 150 μM) for 30, 60, 90 and 120 minutes. A 0.5% DMSO control was included that corresponded to the amount of DMSO present in 150 μM prostaglandin E<sub>2</sub>. Data are mean +/- SD calculated on experiments performed in triplicate. \* significant P<0.05 at 120 minutes relative to the control.

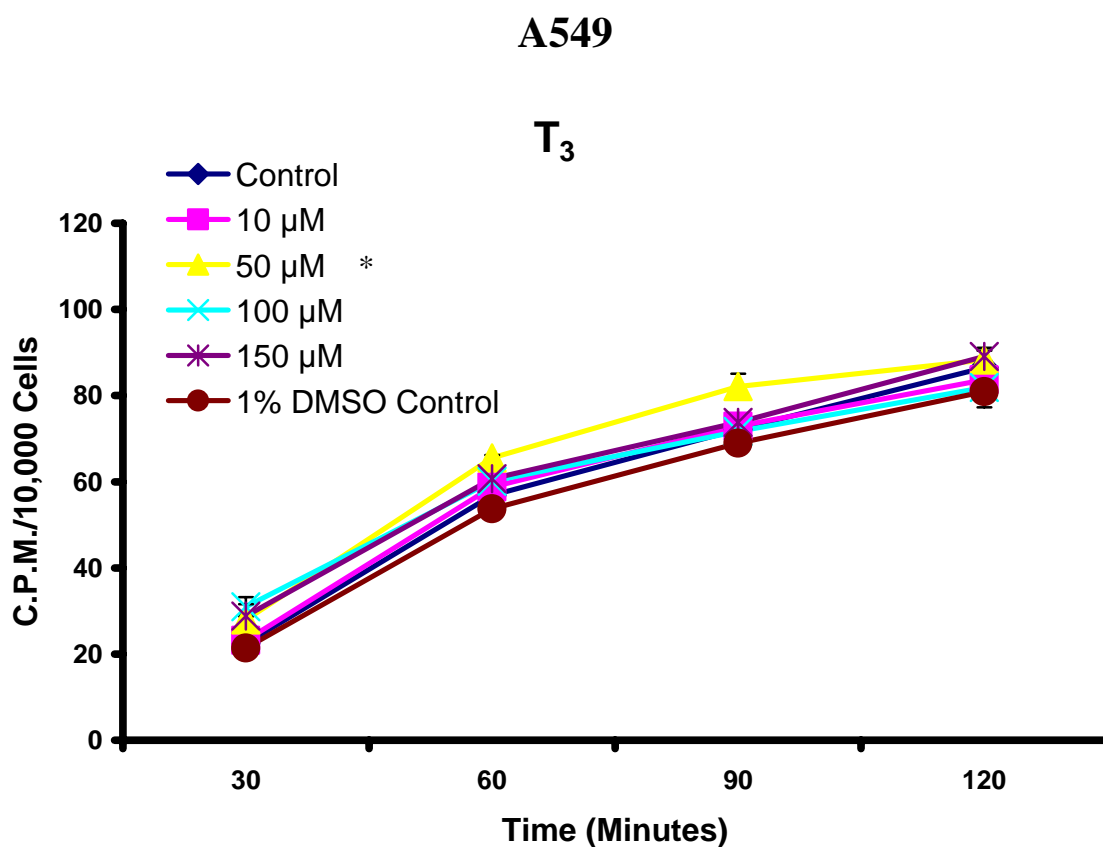


**Figure 6.6.8** The effect of tri-iodothyronine (T<sub>3</sub>) on <sup>14</sup>C docetaxel accumulation in the A549 cell line. Cells were incubated with 100 nM <sup>14</sup>C docetaxel alone (Control) or 100 nM <sup>14</sup>C docetaxel and T<sub>3</sub> (10, 50, 100, 150 μM) for 30, 60, 90 and 120 minutes. A 1% DMSO control was included that corresponded to the amount of DMSO present in 150 μM T<sub>3</sub>. Data are mean +/- SD calculated on experiments performed in triplicate.

\* significant P<0.05 at 30, 60 and 90 minutes relative to the control.

## 6.7 Summary

A number of important differences were found when comparing the transport of  $^{14}\text{C}$  docetaxel in DLKP and A549.

Accumulation of  $^{14}\text{C}$  docetaxel in DLKP was:

- Saturated at 500 nM.
- Temperature-dependent.
- Energy –dependent. ATP-depletion led to a **decrease** in  $^{14}\text{C}$  docetaxel levels in DLKP.
- Not dependent on bromosulphophthalein and digoxin.

Accumulation of  $^{14}\text{C}$  docetaxel in A549 was:

- Unsaturated at 500 nM.
- Temperature-dependent (but the accumulation levels at 27<sup>0</sup>C returned to 37<sup>0</sup>C levels with time).
- Energy –dependent. ATP-depletion led to an **increase** in  $^{14}\text{C}$  docetaxel levels in A549.
- Dependent on bromosulphophthalein and digoxin. Bromosulphophthalein and digoxin **decreased** the levels of  $^{14}\text{C}$  docetaxel accumulated.
- Dependent on DHEAS, and tri-iodothyronine (thyroid hormone, T<sub>3</sub>). DHEAS, T<sub>3</sub> **increased** the levels of  $^{14}\text{C}$  docetaxel accumulated.

Indocyanine green markedly increased docetaxel levels in A549 and DLKP. The ICG effect was concentration dependent, occurred in A549 or DLKP and was of a greater magnitude than any other of the changes in  $^{14}\text{C}$  docetaxel levels observed in this study.

High DMSO concentrations decreased  $^{14}\text{C}$  docetaxel accumulation in A549 and DLKP but DLKP was more susceptible than A549 to the DMSO-related changes in docetaxel accumulation.

***Chapter 7. TKIs as modulators of Multi-Drug Resistance***

## 7.1 Introduction

The ability of the tyrosine kinase inhibitors gefitinib and erlotinib to modulate P-gp activity has been described previously [107], [270]. This body of work endeavoured to compare and assess the ability of erlotinib, gefitinib and the dual tyrosine kinase inhibitor, lapatinib to act as P-gp modulators in lung cancer cell models with varying EGFR status. The effects of the TKIs on P-gp ATPase activity, docetaxel accumulation and efflux, epirubicin accumulation and cell proliferation were studied to provide a broad basis of evidence for the potential of these compounds as plausible MDR modulators.

An increase in P-gp levels due to TKI exposure might contribute to an increase in resistance, limiting the effectiveness of P-gp substrate cytotoxics and TKIs. Changes in EGFR levels could also affect TKI efficacy. The consequences of TKI treatment on the protein levels of P-gp and EGFR were examined by Western blot and ELISA in the EGFR- and P-gp-over-expressing, A549-Taxol cell line.

The transport proteins, MRP-1 and BCRP, are also major contributors to drug resistance in cancer. The effects of the three TKIs on MRP-1 and BCRP ATPase activity were examined. Sulindac and its metabolite sulindac sulfide were also examined for activity in the MRP-1 and BCRP ATPase assays.

## **7.2 Modulation of P-gp by TKIs**

### **7.2.1 P-gp, EGFR and Her-2 status of the cell lines**

The EGFR and Her-2 status of DLKP, DLKP-A, A549 and A549-Taxol cell lines were determined by ELISA (Figure 7.2.1.1). The parent DLKP and A549 cell lines do not express detectable levels of P-gp but the adriamycin-selected, DLKP-A, and paclitaxel (®Taxol)-selected, A549-Taxol, cell lines over-express P-gp (Figure 3.1.1). An ELISA was required to detect the low levels of EGFR and Her-2 in the lung cancer cell lines. All four cell lines expressed low Her-2 levels. DLKP was EGFR- negative while DLKP-A showed EGFR expression. A549 and A549-Taxol both expressed higher EGFR levels than DLKP-A.

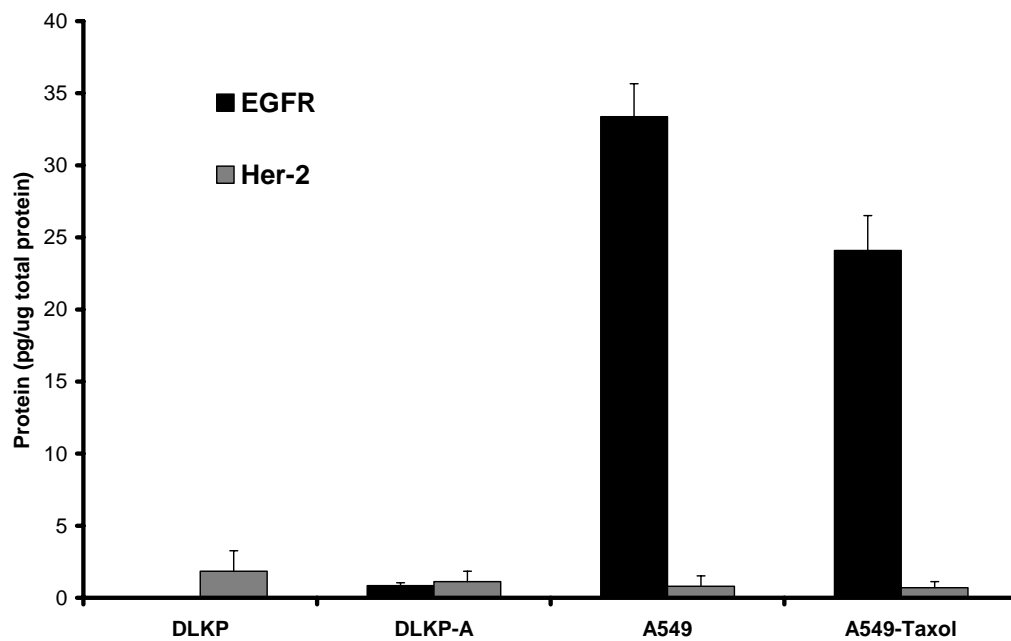


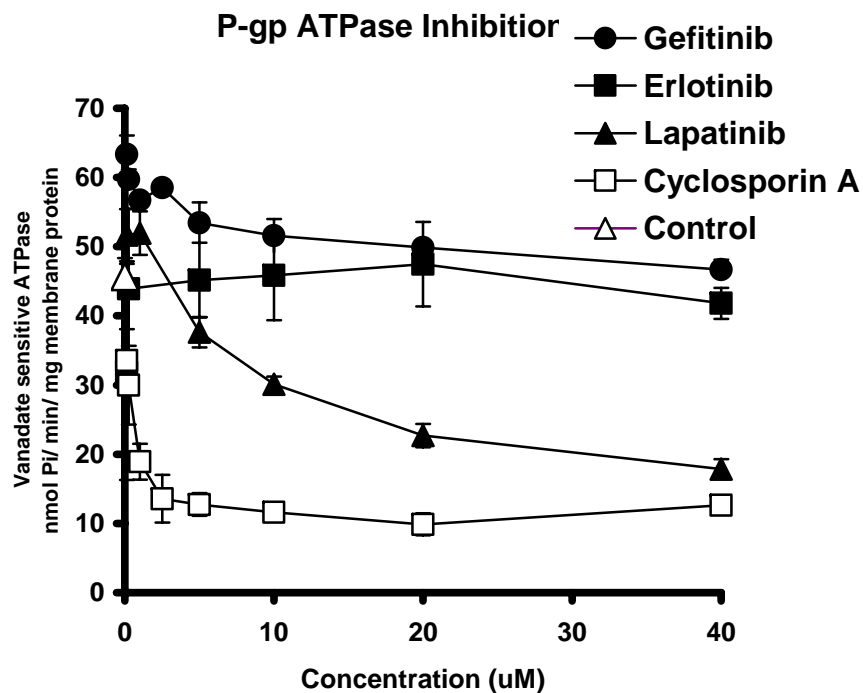
**Figure 7.2.1.1** Detection of EGFR and Her-2 by ELISA in DLKP, DLKP-A, A549 and A549-Taxol. Values were determined by two independent experiments each carried out in duplicate. Data are mean +/- SD.

## 7.2.2 Effects of TKIs on P-gp ATPase activity

We compared all three TKIs, and the classic P-gp inhibitor cyclosporin A, in P-gp ATPase inhibition (Figure 7.2.2.1A) and activation (Figure 7.2.2.1B) assays to determine the ability of lapatinib to interact with P-gp and to find the exact method of P-gp modulation employed by erlotinib and gefitinib. P-gp uses ATP as the energy source for substrate transport. The ATPase function of P-gp converts ATP to ADP and Pi in order to transport substrates. The ATPase activation assay measured the amount of Pi released by P-gp ATPase in the presence of a test compound while the inhibition ATPase assays measured the decrease a test compound produced in Pi released from fully substrate (verapamil)-activated P-gp. In the inhibition assays, lapatinib displayed direct inhibition of verapamil-activated P-gp ATPase activity at 5  $\mu\text{M}$ . Cyclosporin A demonstrated the greatest inhibitory effect at low concentrations. Erlotinib and gefitinib did not reduce verapamil-induced P-gp ATPase activity even though gefitinib stimulated P-gp ATPase activity above control levels.

All three TKIs displayed activation of P-gp ATPase activity at low concentrations. At higher concentrations (10-40  $\mu\text{M}$ ), gefitinib and erlotinib were strong activators of P-gp ATPase activity. Lapatinib activation activity did not increase above 5  $\mu\text{M}$ . Cyclosporin A was the weakest activator of P-gp. Baseline P-gp ATPase activity and the maximum verapamil-stimulated P-gp ATPase activity was within expected parameters (Section 2.18.9). These results and the implications are discussed in Section 8.6.

A)



B)

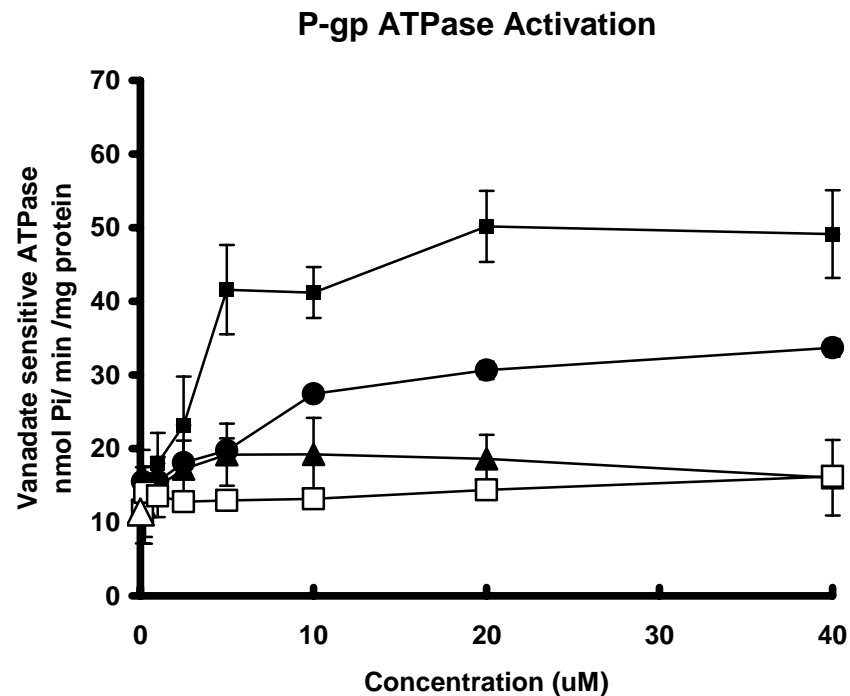


**Figure 7.2.2.1** The effects of lapatinib, gefitinib, erlotinib and cyclosporin A on vanadate-sensitive P-gp ATPase inhibition (A) and activation (B). For (A) the control represents the ATPase activity measured in the presence of 45  $\mu$ M verapamil (P-gp substrate) but in the absence of added test compounds. For (B), the control represents the ATPase activity measured in the absence of added test compounds. Each concentration was determined in duplicate. All compounds were dissolved in DMSO except cyclosporin A which was dissolved in ethanol. Each concentration was determined in duplicate. Data are mean  $\pm$  SD.

### **7.2.3 TKI-related increase in docetaxel accumulation in the P-gp-positive DLKP-A cell line**

A  $^{14}\text{C}$  docetaxel accumulation assay was employed to examine the P-gp-modulatory abilities of gefitinib, erlotinib and lapatinib compared with the classic MDR modulator cyclosporin A and the third generation P-gp inhibitor elacridar, in the P-gp over-expressing DLKP-A cell line.

Gefitinib and erlotinib increased docetaxel accumulation in a concentration-dependent manner comparable to cyclosporin A (Figure 7.2.3.1) while lapatinib proved more effective at increasing docetaxel levels than cyclosporin A. The non-competitive P-gp inhibitor, elacridar, was the most potent compound. Lapatinib, erlotinib, gefitinib, cyclosporin A and elacridar (1  $\mu\text{M}$ ) each increased docetaxel accumulation 4.2, 1.6, 1.6, 2.1, and 6.3 fold respectively.

Neither gefitinib, lapatinib nor erlotinib (10  $\mu\text{M}$ ) increased docetaxel accumulation over 90 minutes in the P-gp negative DLKP cell line, Figure 7.2.3.2. These results and their implications are discussed in Section 8.6.

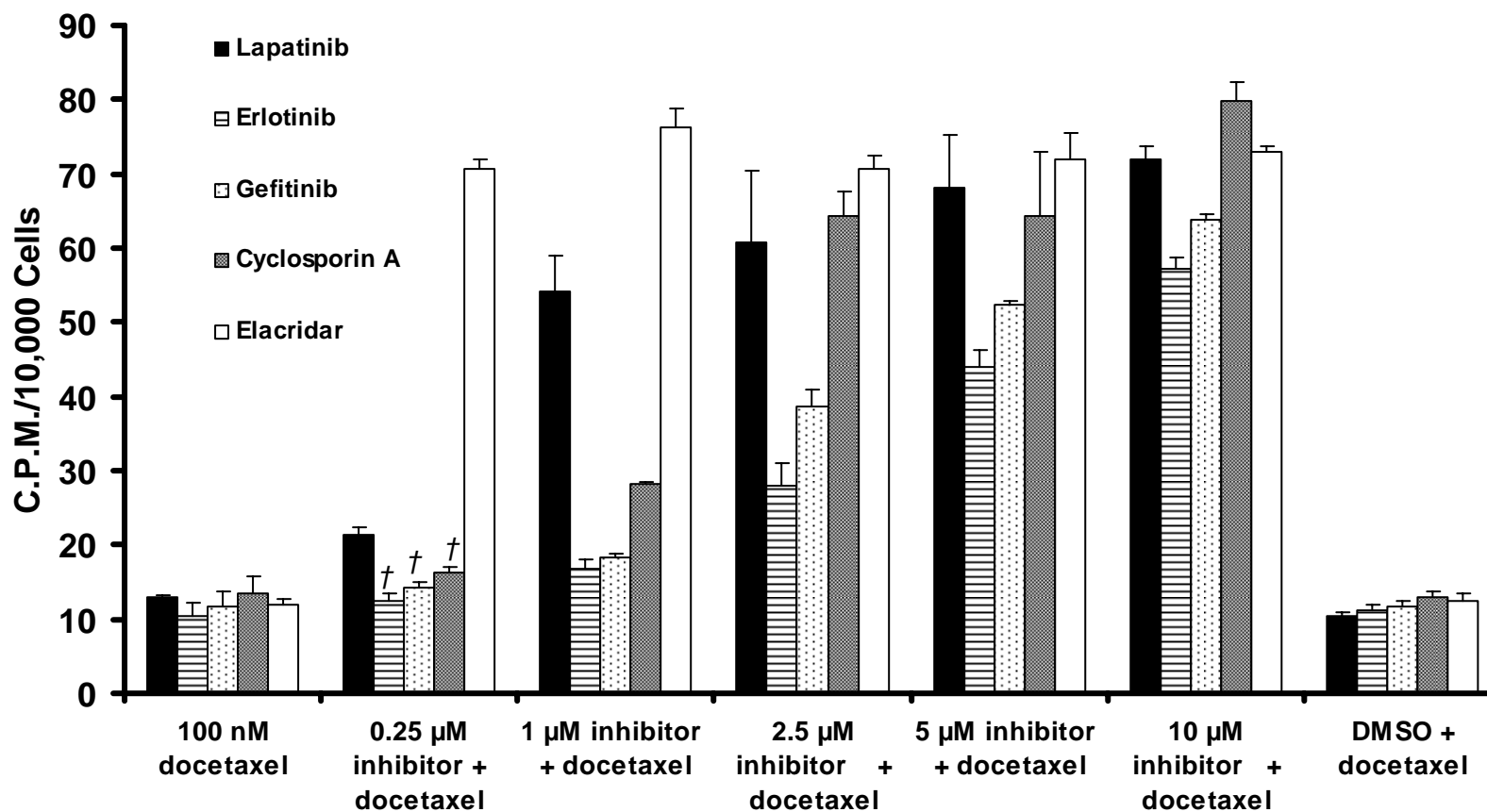


**Figure 7.2.3.1** Accumulation of 100 nM <sup>14</sup>C radio-labelled docetaxel in DLKP-A over 90 minutes. Values represent the average of three determinations. All inhibitors were dissolved in DMSO, except cyclosporin A (ethanol). Data are mean +/- SD calculated on experiments performed in triplicate. † not significant relative to control, P > 0.05

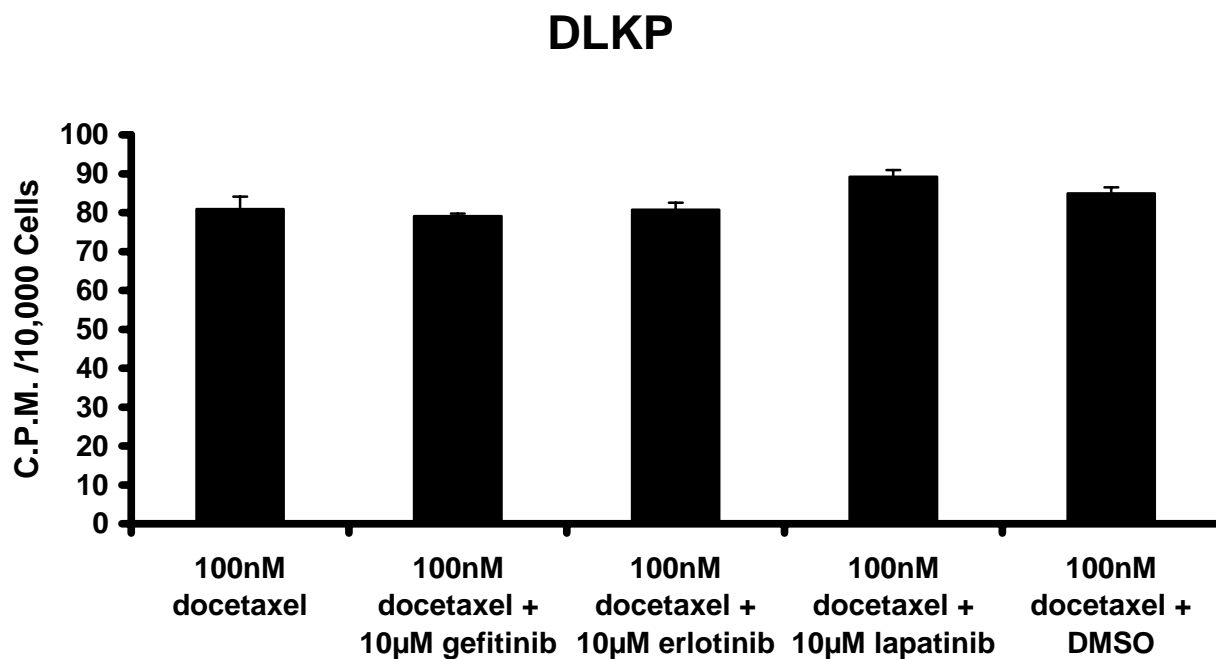


**Figure 7.2.3.2** Accumulation of 100 nM <sup>14</sup>C docetaxel in DLKP over 90 minutes. All inhibitors were dissolved in DMSO. Data are mean +/- SD calculated on experiments performed in triplicate.

#### **7.2.4 Inhibition of docetaxel efflux from the P-gp-positive DLKP-A cell line**

The accumulation studies displayed changes in docetaxel levels in the presence of continuous docetaxel influx. To isolate the effect of the TKIs on docetaxel efflux, DLKP-A cells were exposed to 500 nM docetaxel for 90 minutes. The concentration of 500 nM was determined previously in Section 5.3. Once loaded with drug, the effects of the TKIs and elacridar on docetaxel efflux were examined. Gefitinib and erlotinib effectively decreased docetaxel efflux from DLKP-A (Figure 7.2.4.1). Lapatinib and elacridar were the most potent compounds decreasing docetaxel efflux at all concentrations tested.

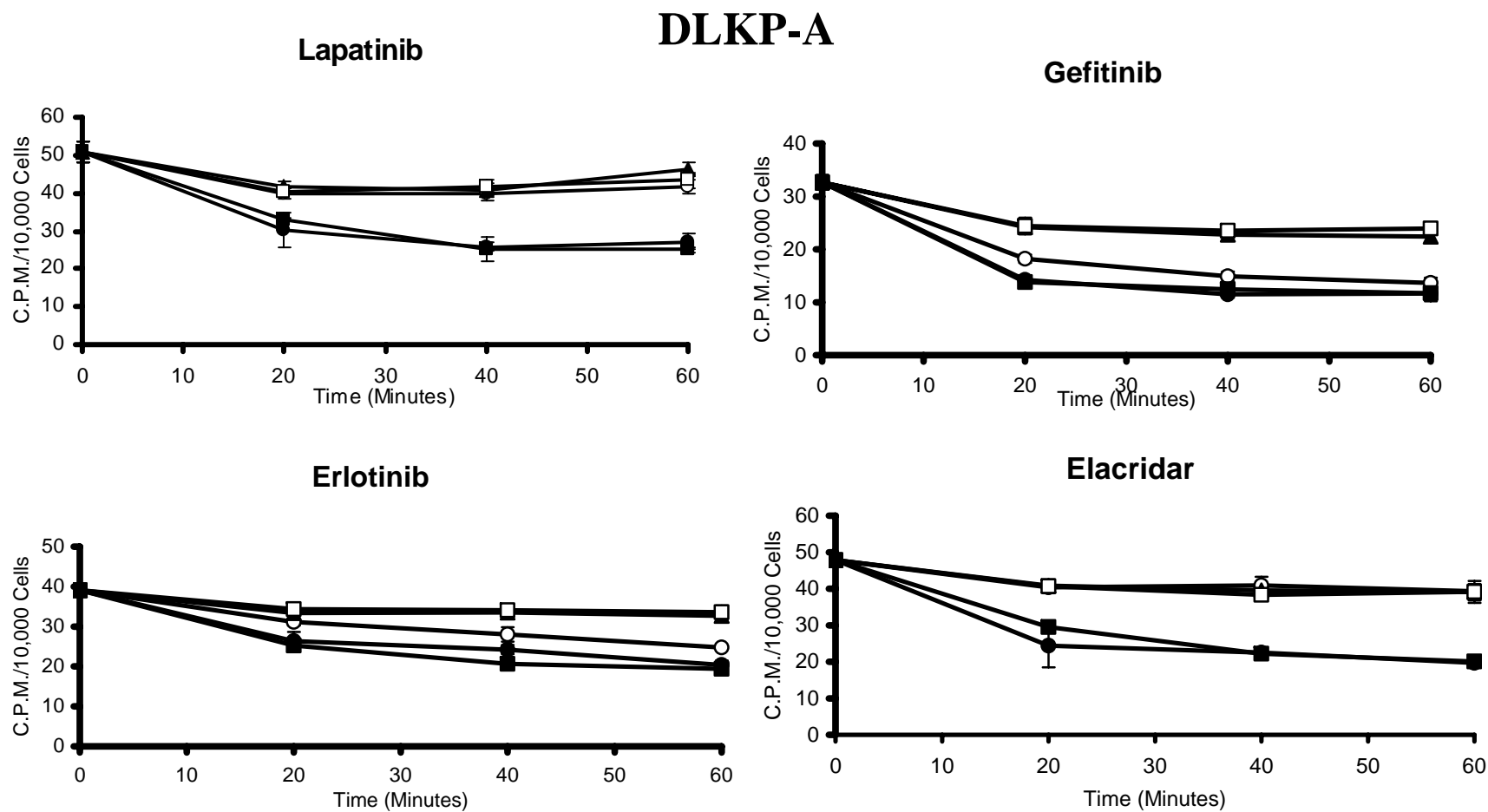


**Figure 7.2.4.1** Efflux of  $^{14}\text{C}$  docetaxel from DLKP-A. Cells were exposed to 500 nM  $^{14}\text{C}$  docetaxel for 90 minutes, the drug removed and replaced with medium or a concentration of tyrosine kinase inhibitor (TKI) or elacridar for 20, 40 and 60 minutes. (● – medium, ○ – 1  $\mu\text{M}$ , ▲ - 5  $\mu\text{M}$ , □ – 10  $\mu\text{M}$ , ■ – DMSO control). All inhibitors dissolved in DMSO. Data are mean +/- SD calculated on experiments performed in triplicate.

## 7.2.5 Increased epirubicin accumulation in the DLKP-A cell line

Accumulation of the naturally fluorescent P-gp substrate chemotherapeutic, epirubicin, was examined in DLKP-A. Quantitative analysis of the effect of lapatinib on epirubicin accumulation over 120 minutes was carried out using the mass spectrometry-based method described in Section 2.14.8 (Figure 7.2.5.1 A). Lapatinib increased the mass of epirubicin accumulated in DLKP-A in a concentration-dependent manner. Laser confocal imaging was utilised to visualise the increase in epirubicin accumulation in DLKP-A (Figure 7.2.5.1 B-G). After 120 minutes exposure to 2  $\mu\text{M}$  epirubicin, only minute cytoplasmic levels of the drug were visible (B), similar results to the DMSO control (C). Due to lapatinib-mediated P-gp inhibition, there was a dose-dependent increase in fluorescence visible in the presence of 1  $\mu\text{M}$  (E), 5  $\mu\text{M}$  (F) and 10  $\mu\text{M}$  (G) lapatinib, especially in the level of nuclear fluorescence. Mass spectrometric quantification confirmed the increased level of drug present at these concentrations.

The effects of erlotinib and gefitinib on epirubicin accumulation in DLKP-A were also examined by laser confocal microscopy at a concentration of 5  $\mu\text{M}$ , but over a 90 minute time period, Figure 7.2.5.2. Elacridar treatment resulted in epirubicin detection in all cells within the field of view (Figure 7.2.5.2B). Both gefitinib (Figure 7.2.5.2C) and erlotinib (Figure 7.2.5.2D) increased nuclear and cytoplasmic epirubicin localisation in DLKP-A by inhibition of plasma membrane and nuclear localised P-gp. Interestingly a number of the control cells displayed intercellular levels of epirubicin (Figure 7.2.5.2C) suggesting the resistance mechanism is not uniformly distributed in the cell population.

A)

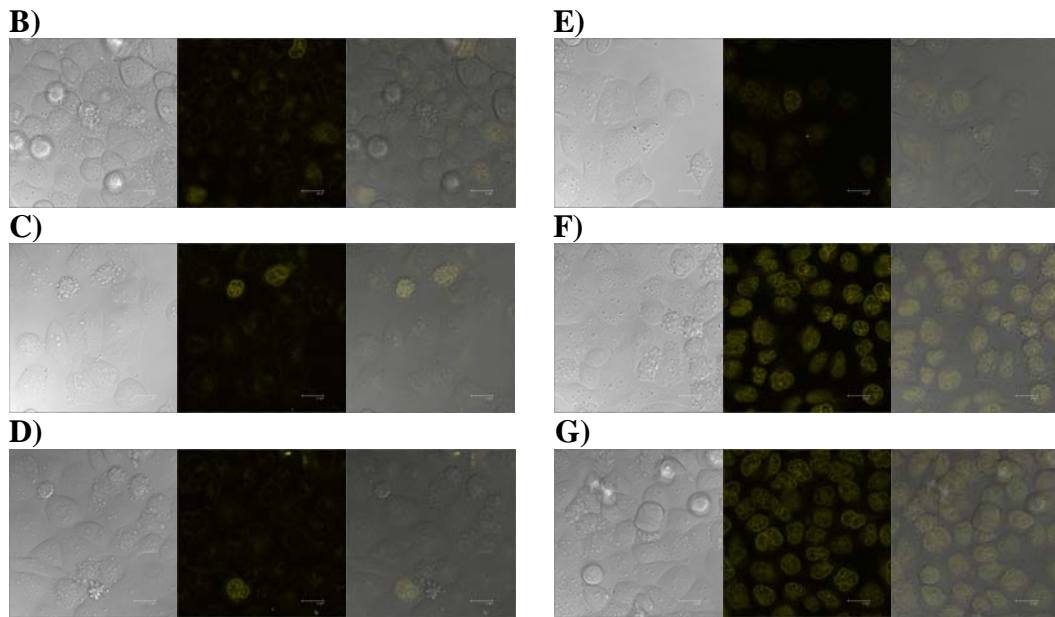
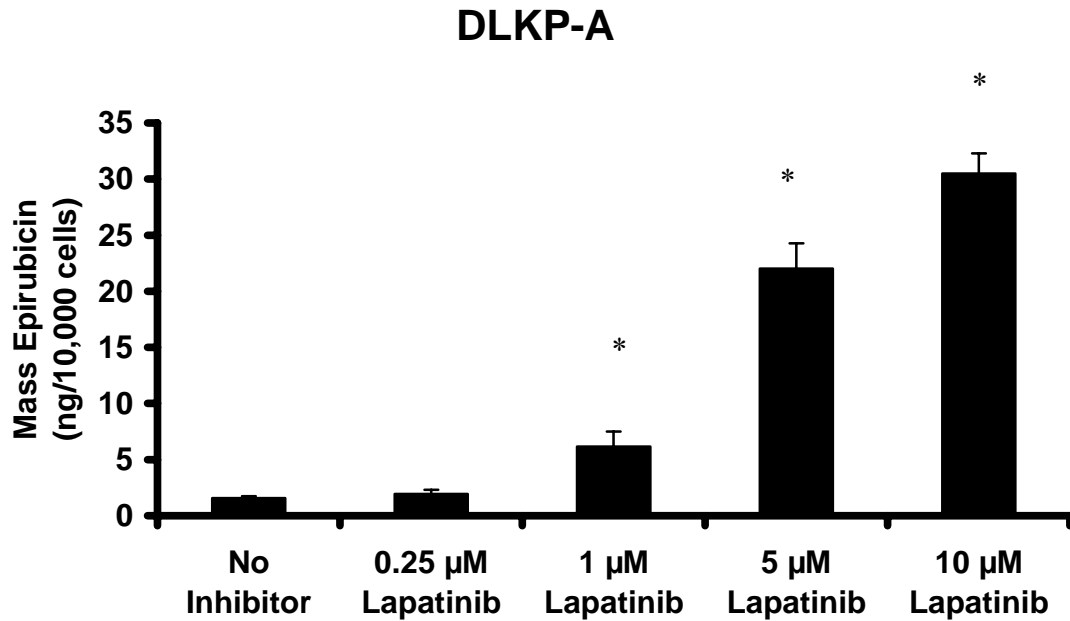
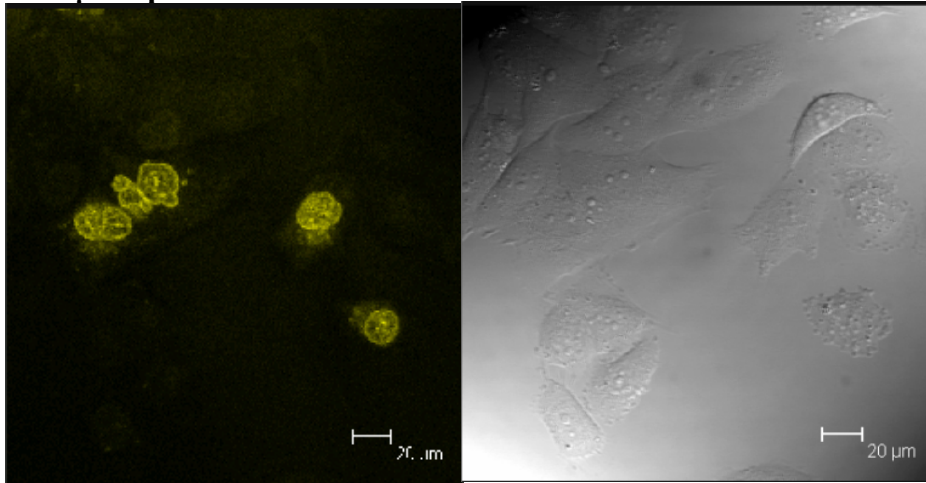


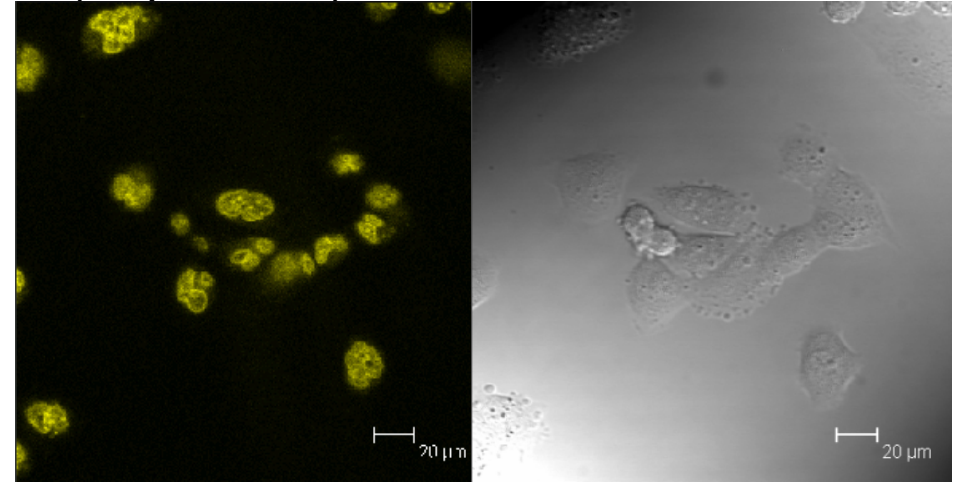
**Figure 7.2.5.1** The effect of lapatinib on epirubicin accumulation in DLKP-A. A) Epirubicin (EPI) accumulation in DLKP-A in the presence of lapatinib over 120 minutes was quantified by mass spectrometry. Data are mean  $\pm$  SD calculated on experiments performed in triplicate. Laser confocal imaging of epirubicin in DLKP-A is shown for B) 2  $\mu$ M EPI, C) 2  $\mu$ M EPI + DMSO, D) 2  $\mu$ M EPI + 0.25  $\mu$ M lapatinib, E) 2  $\mu$ M EPI + 1  $\mu$ M lapatinib, F) 2  $\mu$ M EPI + 5  $\mu$ M lapatinib, and G) 2  $\mu$ M EPI + 10  $\mu$ M lapatinib. Each panel consists of a polarised contrast image on the left, the fluorescence image in the middle and an overlay of the fluorescence on the polarised image on the right.

\* significant,  $P < 0.05$

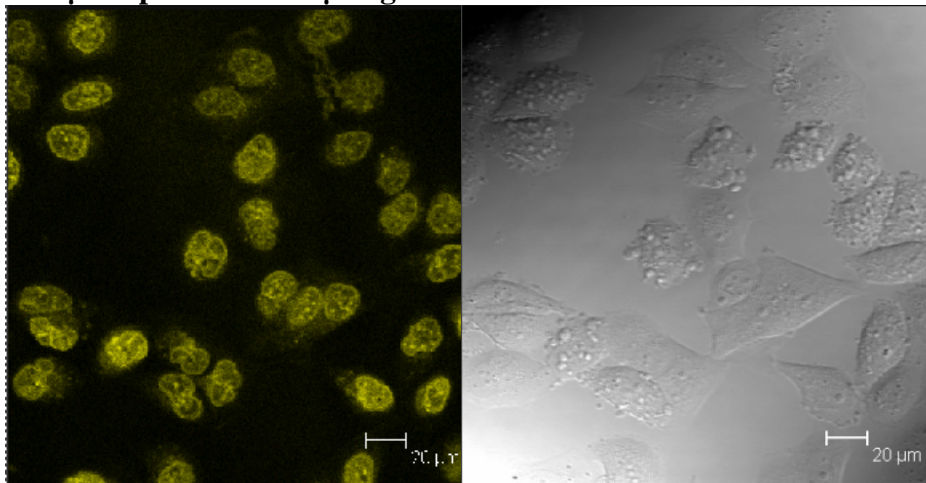
**A. 2  $\mu$ M epirubicin**



**B. 2  $\mu$ M epirubicin + 5  $\mu$ M elacridar**



**C. 2  $\mu$ M epirubicin + 5  $\mu$ M gefitinib**



**D. 2  $\mu$ M epirubicin + 5  $\mu$ M erlotinib**

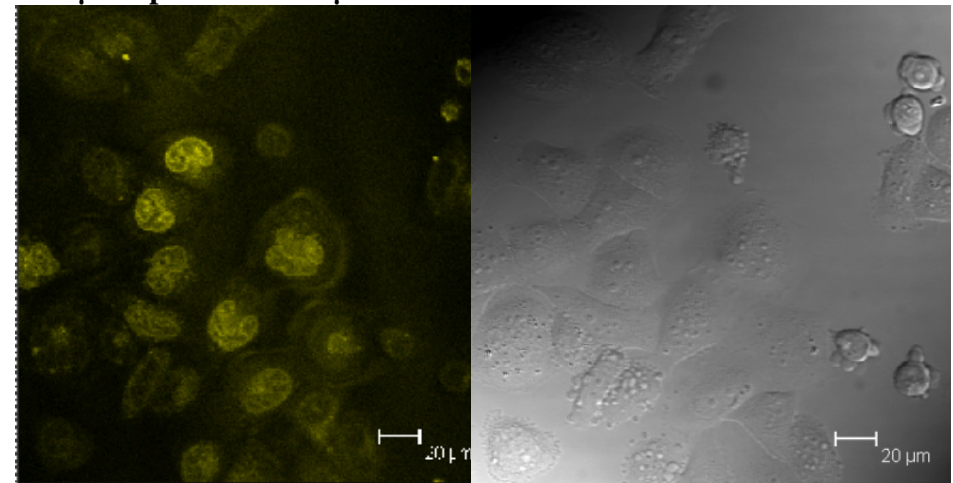


**Figure 7.2.5.2** Laser Confocal Microscope imaging of epirubicin accumulation in the P-gp over-expressing DLKP-A cell line over 90 minutes (A) and in the presence of elacridar (B), gefitinib (C) and erlotinib (D) A polarised contrast image is included on the right of each image.

### **7.2.6 The implications of P-gp modulation by TKIs on cell survival**

IC<sub>50</sub> values for the chemotherapy agents docetaxel, paclitaxel, epirubicin and cisplatin and the TKIs, lapatinib, gefitinib and erlotinib are provided in Table 7.2.6.

P-gp over-expression in DLKP-A resulted in a 228, 153 and 123-fold resistance to docetaxel, paclitaxel and epirubicin, respectively, compared to the parent cell line. Resistance to the non-P-gp substrate, cisplatin, was 1.9-fold in comparison. The lower level of P-gp expression in A549-Taxol resulted in a lower fold increases in resistance to docetaxel (5.6) and paclitaxel (3.6). Interestingly, there was no increase in epirubicin (0.8) resistance. P-gp expression in DLKP-A lead to minor resistance to the TKIs gefitinib and erlotinib compared to DLKP. There was no significant difference in sensitivity to lapatinib between the DLKP and DLKP-A cell lines. A549-Taxol exhibited minor resistance to lapatinib and erlotinib but not gefitinib compared to A549.

Drug	DLKP	DLKP-A	A549	A549-Taxol
<b>Docetaxel</b>	0.00038 +/- 0.000015	0.087 +/- 0.0067 ( <b>228</b> )	0.00025 +/- 0.000021	0.0014 +/- 0.00054 ( <b>5.6</b> )
<b>Paclitaxel</b>	0.002 +/- 0.0001	0.31 +/- 0.013 ( <b>153</b> )	0.0027 +/- 0.00057	0.0098 +/- 0.00066 ( <b>3.6</b> )
<b>Epirubicin</b>	0.017 +/- 0.0008	2.1 +/- 0.24 ( <b>123</b> )	0.038 +/- 0.0045	0.03 +/- 0.0047 ( <b>0.8<sup>†</sup></b> )
<b>Cisplatin</b>	1.1 +/- 0.24	2.0 +/- 0.17 ( <b>1.9</b> )	2.4 +/- 0.44	2.6 +/- 0.23 ( <b>1.1<sup>†</sup></b> )
<b>Lapatinib</b>	2.7 +/- 0.1	2.4 +/- 0.2 ( <b>0.9<sup>†</sup></b> )	2.8 +/- 0.1	3.7 +/- 0.1 ( <b>1.3</b> )
<b>Gefitinib</b>	6.1 +/- 0.02	8.5 +/- 0.36 ( <b>1.4</b> )	7.3 +/- 0.33	7.4 +/- 0.23 ( <b>1<sup>†</sup></b> )
<b>Erlotinib</b>	8.8 +/- 0.5	11.1 +/- 0.5 ( <b>1.3</b> )	3.1 +/- 0.2	9.3 +/- 1.8 ( <b>3</b> )

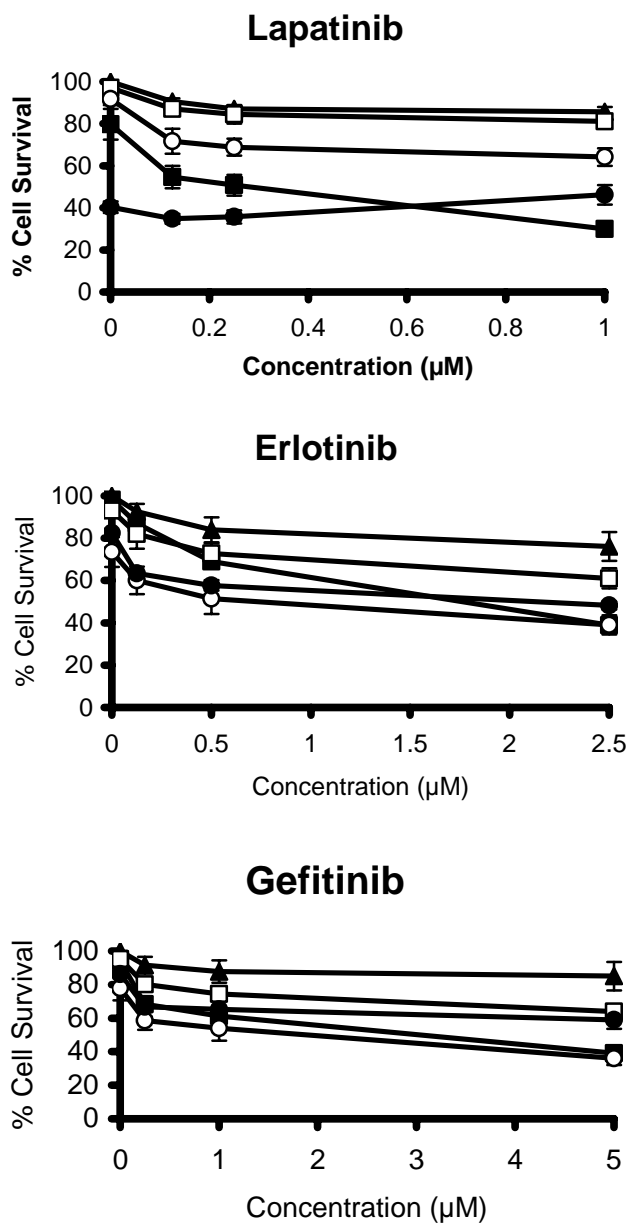
**Table 7.2.6** IC50 values ( $\mu\text{M}$ ) determined from 7-day proliferation assays. Values represent the average of three independent determinations +/- SD. Fold increase in resistance compared to the parent cell line is given in brackets. All fold increases are significant unless otherwise denoted. (<sup>†</sup> values, not significant,  $P > 0.05$ )

### 7.2.7 Combination proliferation assays

Peak serum concentration values for standard or near standard doses of gefitinib (225 mg), erlotinib (150 mg) and lapatinib (1200 mg) have been determined at approximately 0.7  $\mu$ M, 4  $\mu$ M, and 2  $\mu$ M, respectively [271], [272], [273]. TKI concentrations close to physiological levels and providing low cytotoxicity were selected for combination studies. A supra-additive decrease in cell survival resulted from co-treatment with the TKIs and the P-gp substrates docetaxel, paclitaxel and epirubicin in the P-gp positive DLKP-A (Figure 7.2.7.2) and A549-Taxol (Figure 7.2.7.1) cell lines. No potentiation of toxicity was observed when the TKIs were combined with the non-P-gp substrate cisplatin. Lapatinib exhibited the greatest potentiation of docetaxel, paclitaxel and epirubicin toxicity, followed by gefitinib and then erlotinib.

DLKP (Figure 7.2.7.2) and A549 (Figure 7.2.7.1) cells exhibited only additive potentiation of TKI- taxane toxicity due to the absence of P-gp. However, epirubicin toxicity was potentiated most notably by lapatinib and erlotinib. Of note, a minor increase in cell survival was observed when combining the TKIs with higher concentrations of cisplatin in DLKP-A (Appendix A, Figure A1).

## A549



## A549-Taxol

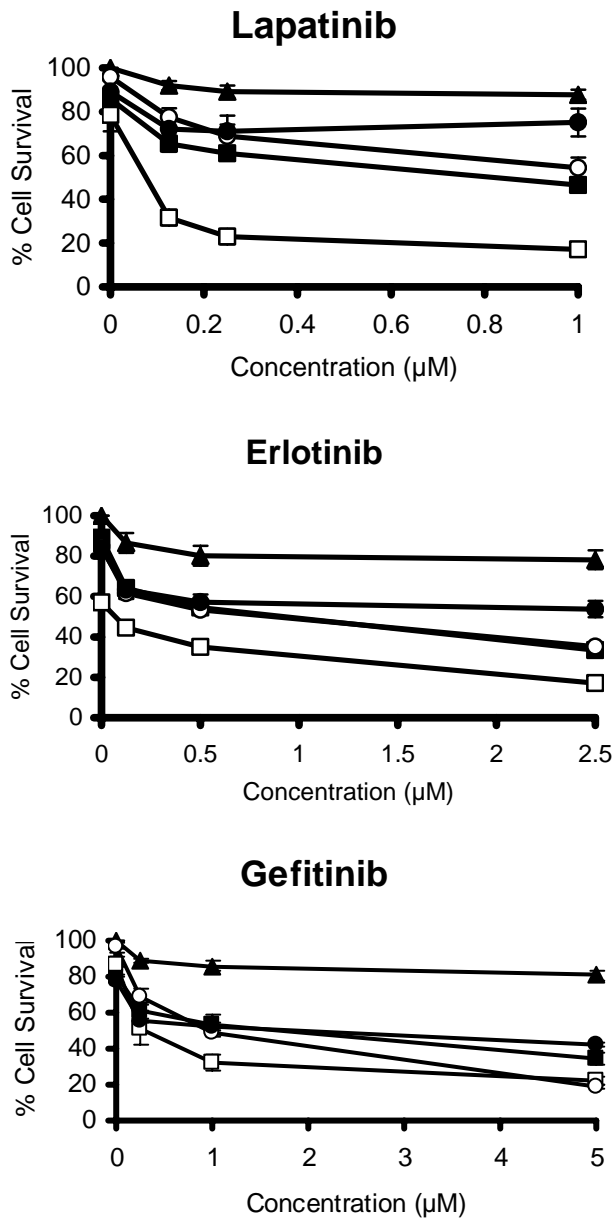


**Figure 7.2.7.1** Proliferation assays combining the TKIs lapatinib, gefitinib and erlotinib with docetaxel, paclitaxel, epirubicin and cisplatin in A549 (▲- inhibitor only, ■ - 20 nM epirubicin, □ – 0.2 nM docetaxel, ○ – 1 nM paclitaxel, ● – 1500 nM cisplatin) and A549 –Taxol (▲- inhibitor only, ■ - 30 nM epirubicin, □ – 0.75 nM docetaxel, ○ – 2 nM paclitaxel, ● – 1000 nM cisplatin). Points represent the average of three independent determinations +/- SD.

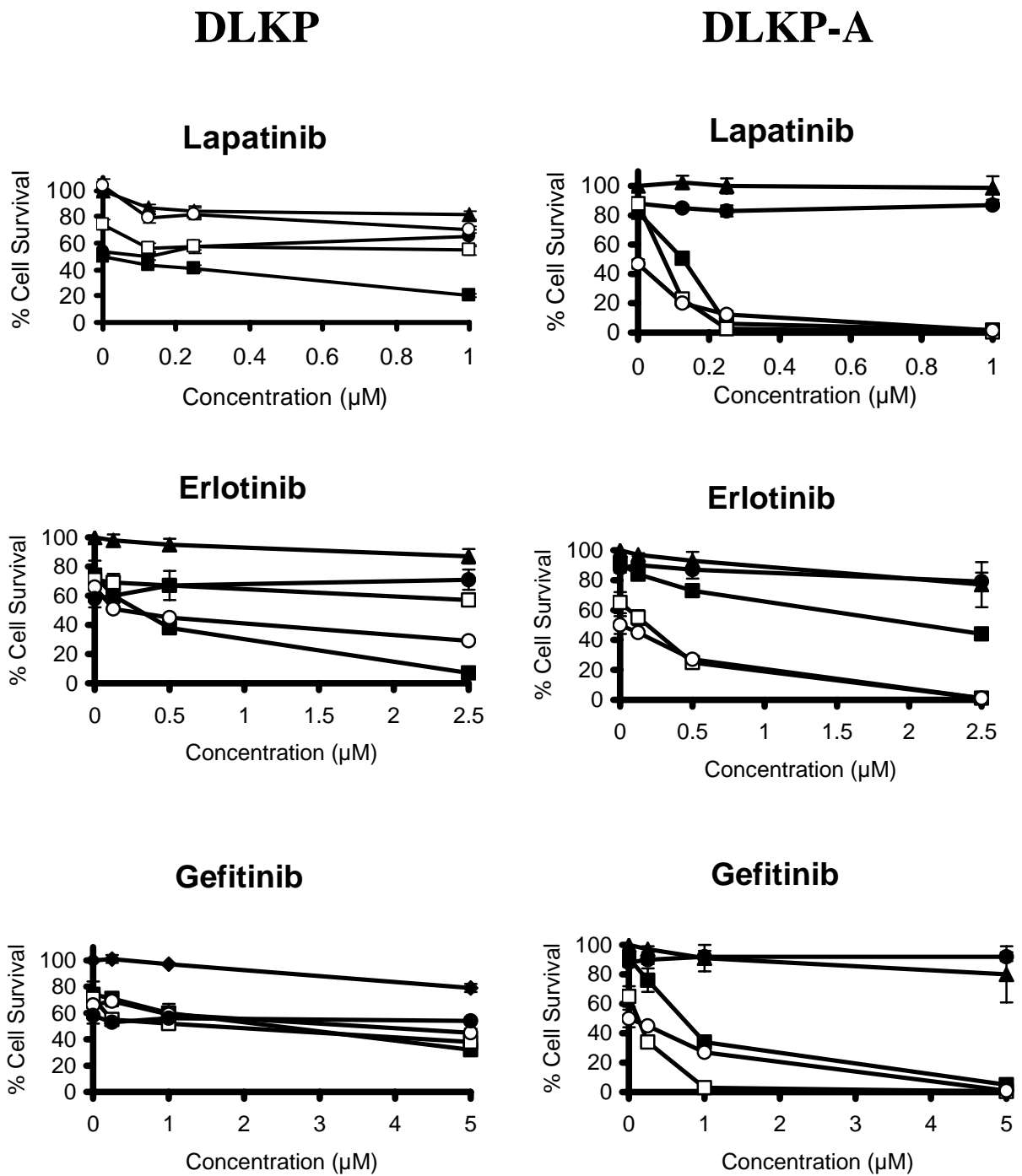
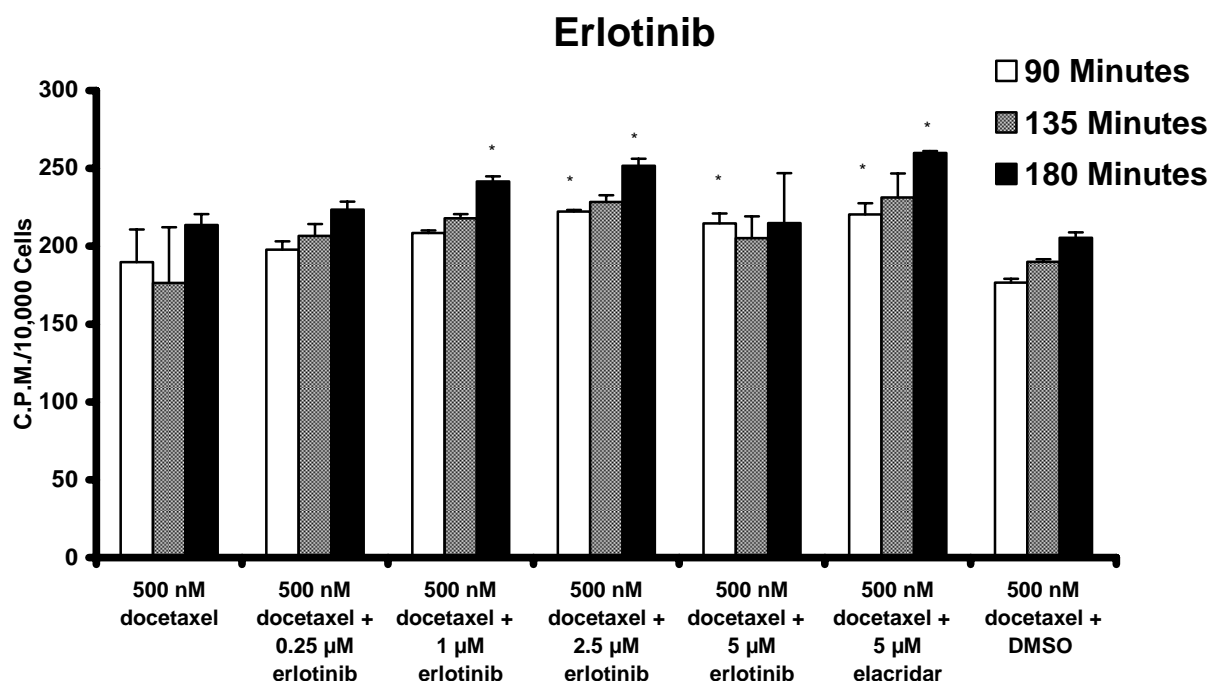


**Figure 7.2.7.2** Proliferation assays combining the TKIs lapatinib, gefitinib and erlotinib with docetaxel, paclitaxel, epirubicin and cisplatin in DLKP (▲ - inhibitor only, ■ - 15 nM epirubicin, □ - 0.25 nM docetaxel, ○ - 1 nM paclitaxel, ● - 1500 nM cisplatin) and DLKP-A (▲ - inhibitor only, ■ - 750 nM epirubicin, □ - 50 nM docetaxel, ○ - 250 nM paclitaxel, ● - 1500 nM cisplatin). Points represent the average of three independent determinations +/- SD.

## **7.2.8 Effects of the P-gp substrate erlotinib and P-gp inhibitor lapatinib on docetaxel accumulation in A549-Taxol**

In order to examine docetaxel transport in a cell line expressing levels of P-gp closer to that expected physiologically, A549-Taxol cells were exposed to 500 nM <sup>14</sup>C docetaxel in the presence of 0.25, 1, 2.5, and 5 μM erlotinib (Figure 7.2.8.1A) or lapatinib (Figure 7.2.8.1B) for 90, 135, and 180 minutes. 5 μM elacridar was included to represent maximal P-gp inhibition. Erlotinib was chosen as it displayed the highest P-gp ATPase activation and was most likely to be a transported substrate and competitive inhibitor. Lapatinib was the only TKI examined that inhibited verapamil-stimulated P-gp ATPase activity. Both TKIs increased <sup>14</sup>C docetaxel accumulation in a time- and concentration-dependent manner. 2.5 μM erlotinib was required to generate near maximal docetaxel accumulation. 0.25 μM of lapatinib produced an increased docetaxel accumulation with 1 μM generating maximum docetaxel accumulation at the 135 and 180 minute timepoints. At maximum concentrations (5 μM), lapatinib was more effective than erlotinib, significantly increasing docetaxel accumulation by 45.1, 27.9 and 30.3% over 90, 135 and 180 minutes respectively.

A)



B)

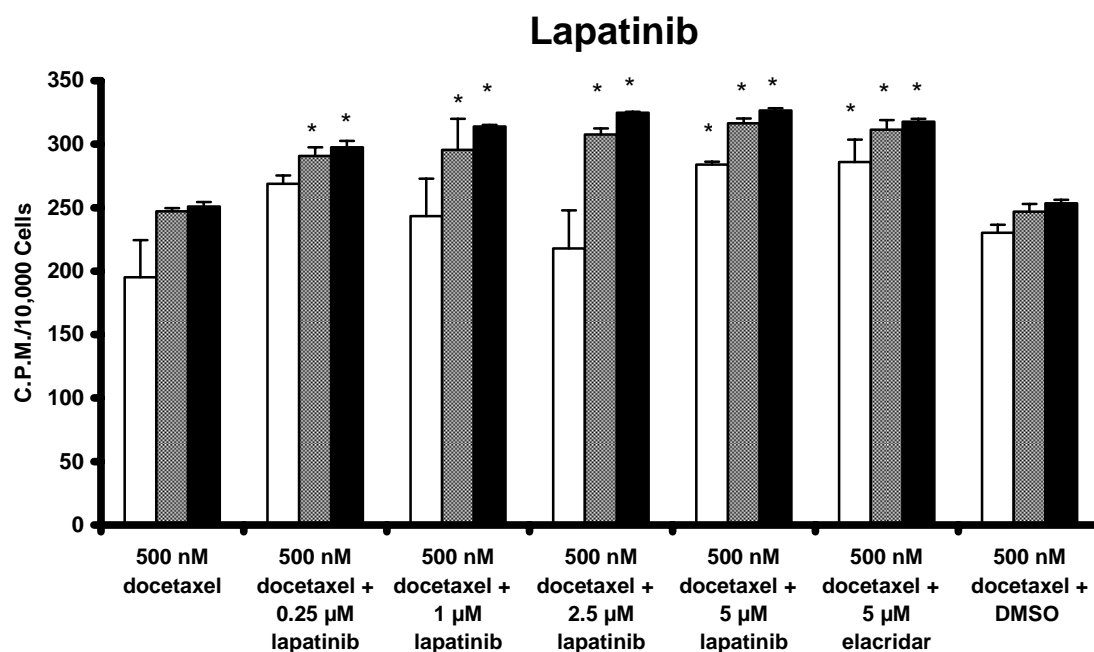


**Figure 7.2.8.1** The effects of erlotinib (A) and lapatinib (B) on accumulation of 500 nM <sup>14</sup>C docetaxel in the A549-Taxol cell line over 90, 135 and 180 minutes. A 1% DMSO control representing the amount of DMSO present in 5 μM TKI concentrations was also included. Each value represents the average of three determinations. All inhibitors dissolved in DMSO. (\* significant, P < 0.05 relative to 500 nM docetaxel control).

### **7.3 The effects of TKI exposure on P-gp expression in A549-Taxol**

The EGFR- and P-gp- over-expressing A549-Taxol cell line was utilised to examine the effects of TKI treatment on P-gp protein expression. Cells were exposed to epidermal growth factor (EGF) at concentrations of 10, 50 and 100 ng/ml and varying concentrations of lapatinib and erlotinib (2.5, 5 and 10  $\mu$ M) and gefitinib (5, 10 and 20  $\mu$ M) for 48 hours. Treatment with increasing levels of EGF resulted in a decrease in P-gp protein expression, Figure 7.3.1. Conversely, lapatinib, erlotinib and gefitinib treatment resulted in an increase in P-gp protein expression, Figure 7.3.2, Figure 7.3.3 and Figure 7.3.4, respectively.

## A549-Taxol

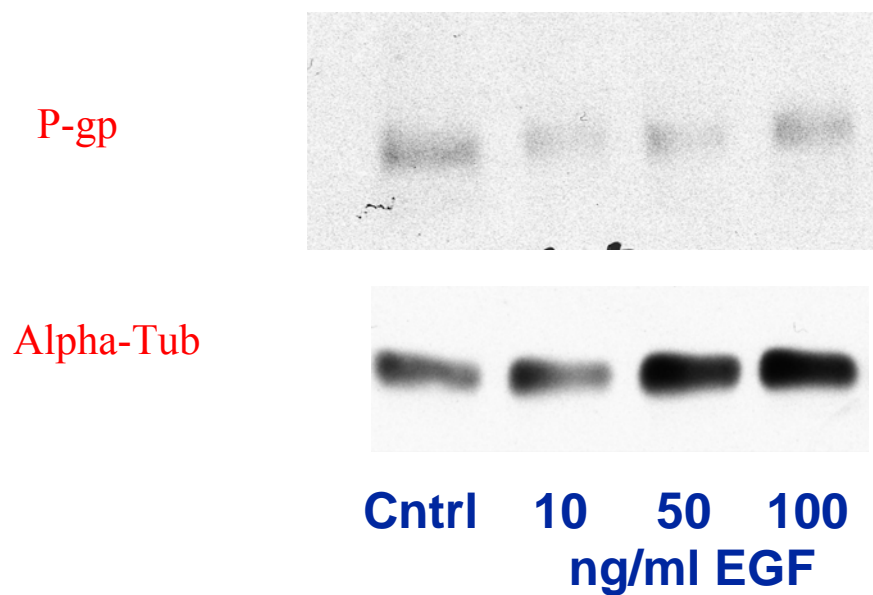


**Figure 7.3.1** Western blot showing the effect of EGF treatment on P-gp expression (170 kDa) in A549-Taxol after 48 hours. Cells were treated with 10, 50 and 100 ng/ml EGF in DMEM/Ham's F12 in serum-free conditions. The control represents P-gp expression after 48 hours in serum-free conditions.

## A549-Taxol

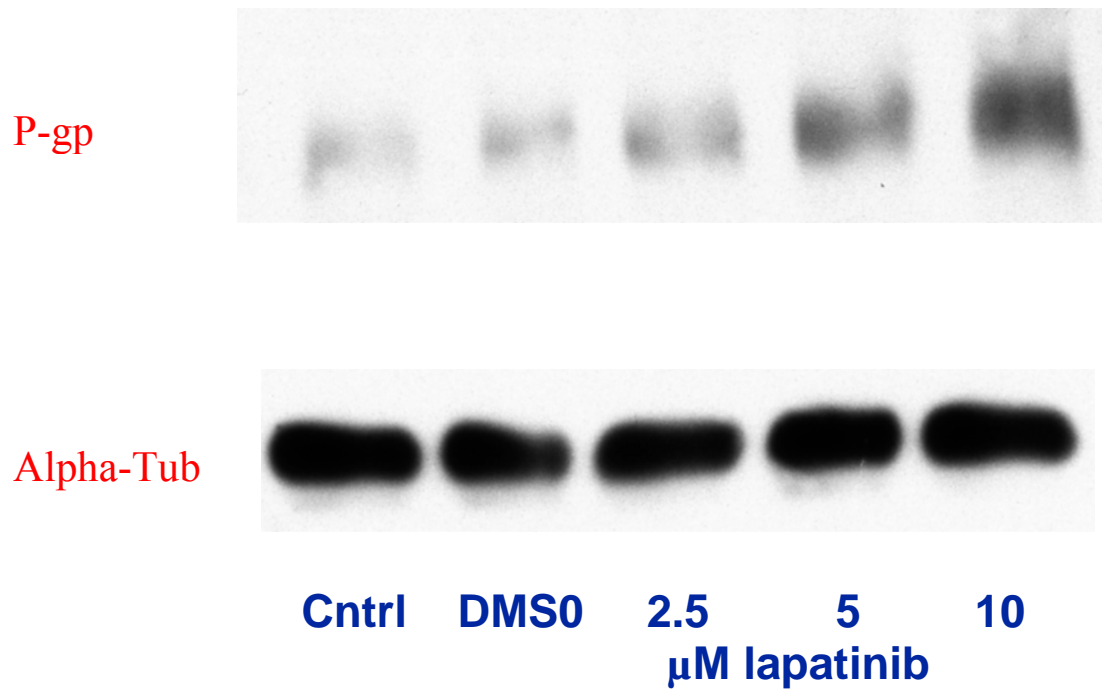


**Figure 7.3.2** Western blot showing the effect of lapatinib treatment on P-gp expression (170 kDa) in A549-Taxol after 48 hours. Cells were treated with 2.5, 5 and 10  $\mu\text{M}$  lapatinib in DMEM/Ham's F12 supplemented with 5% FCS. The control represents P-gp expression after 48 hours in DMEM/Ham's F12 supplemented with 5% FCS. DMSO represents P-gp expression after 48 hours in DMEM/Ham's F12 supplemented with 5% FCS and DMSO equivalent to the amount present in 10  $\mu\text{M}$  lapatinib.

### A549-Taxol

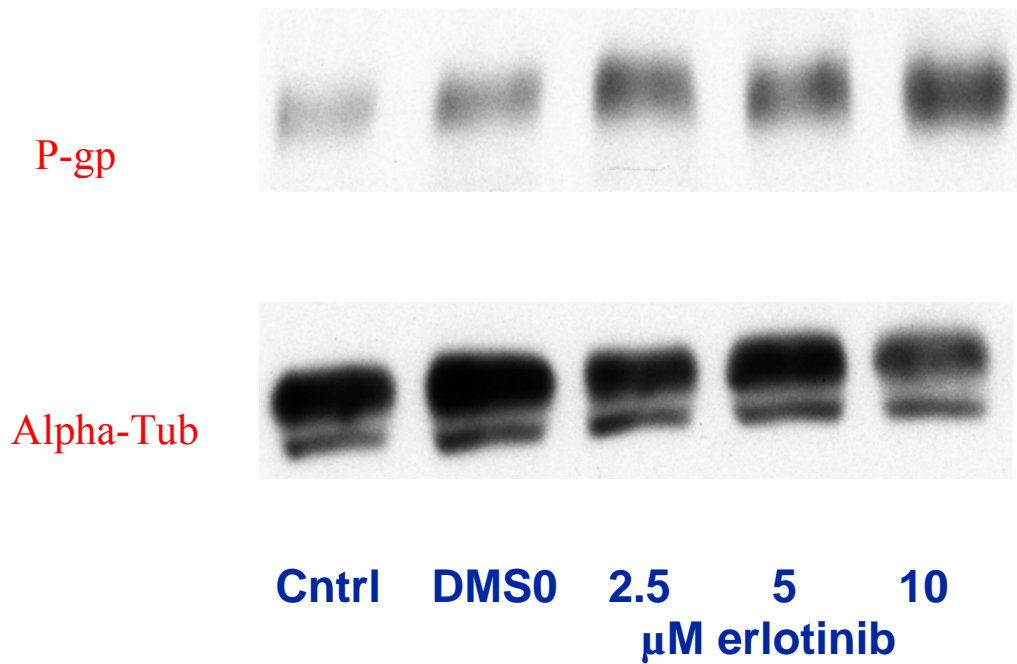


**Figure 7.3.3** Western blot showing the effect of erlotinib treatment on P-gp expression (170 kDa) in A549-Taxol after 48 hours. Cells were treated with 2.5, 5 and 10  $\mu$ M erlotinib in DMEM/Ham's F12 supplemented with 5% FCS. The control represents P-gp expression after 48 hours in DMEM/Ham's F12 supplemented with 5% FCS. DMSO represents P-gp expression after 48 hours in DMEM/Ham's F12 supplemented with 5% FCS and DMSO equivalent to the amount present in 10  $\mu$ M erlotinib.

## A549-Taxol



**Figure 7.3.4** Western blot showing the effect of gefitinib treatment on P-gp expression (170 kDa) in A549-Taxol after 48 hours. Cells were treated with 2.5, 5 and 10  $\mu\text{M}$  gefitinib in DMEM/Ham's F12 supplemented with 5% FCS. The control represents P-gp expression after 48 hours in DMEM/Ham's F12 supplemented with 5% FCS. DMSO represents P-gp expression after 48 hours in DMEM/Ham's F12 supplemented with 5% FCS and DMSO equivalent to the amount present in 10  $\mu\text{M}$  gefitinib.

## 7.4 The effects of TKIs on EGFR levels

EGFR protein levels were too low to be measured by Western blot and were instead measured through ELISA. Two ELISA kits were used to measure total EGFR in samples. One detected the extracellular domain, the other the intracellular domain. The intracellular domain is preferred as it is independent of EGFR dimerisation status. Initial experiments were carried out using the ELISA kit with an antibody developed against the extracellular domain of EGFR. The effects of EGF treatment on EGFR expression in A549-Taxol over 48 hours are shown in Figure 7.4.1. The control revealed a decrease in EGFR expression from 15.18 pg/ $\mu$ g to 5.18 pg/ $\mu$ g at the 48 hour timepoint. EGF treatment dramatically decreased EGFR expression to 2.76 pg/ $\mu$ g from 15.18 pg/ $\mu$ g after 12 hours compared to 11.2 pg/ $\mu$ g for the control. Treatment of A549-Taxol with 2.5, 5 and 10  $\mu$ M lapatinib resulted in an increase in EGFR expression at all timepoints and concentrations relative to the control, Figure 7.4.2. The largest increase in expression occurred at the 24-hour timepoint following treatment with 10  $\mu$ M lapatinib (12.3 pg/ $\mu$ g to 20.27 pg/ $\mu$ g). The 48 hour timepoint saw a decrease in EGFR expression relative to the 24 – hour timepoint for all concentrations but still remained above the 48 hour control levels.

Subsequent experiments examining the effects of the TKIs on EGFR levels utilised both ELISA protocols, detecting the intracellular domain of EGFR as well as the extracellular domain at the 48 hour timepoint. Targetting the intracellular region of the EGFR protein resulted in detection of minutely higher levels of EGFR protein than when the extracellular domain was targetted in the control, Figure 7.4.4. Treatment with 10, 50 and 100 ng/ml EGF reduced EGFR expression levels as measured by both assay systems but the reduction was more pronounced in the results obtained from detection of the EGFR intracellular domain (Figure 7.4.4). 10 ng/ml EGF reduced EGFR levels from 5.18 pg/ $\mu$ g to 4.24 pg/ $\mu$ g (extracellular domain detection) and 6.67 pg/ $\mu$ g to 3.46 pg/ $\mu$ g (detection of intracellular domain).

Treatment with each of the TKIs, lapatinib, erlotinib and gefitinib had the same effect on EGFR expression in A549-Taxol, Figures 7.4.5, 7.4.6 and 7.4.7, respectively. The TKIs increased EGFR expression. Once again, higher EGFR levels were detected using the ELISA detecting the intracellular domain of EGFR. A DMSO control was not included in the gefitinib assay as the same control was carried out in the erlotinib experiment.

### Effects Of EGF on EGFR expression in A549-Taxol

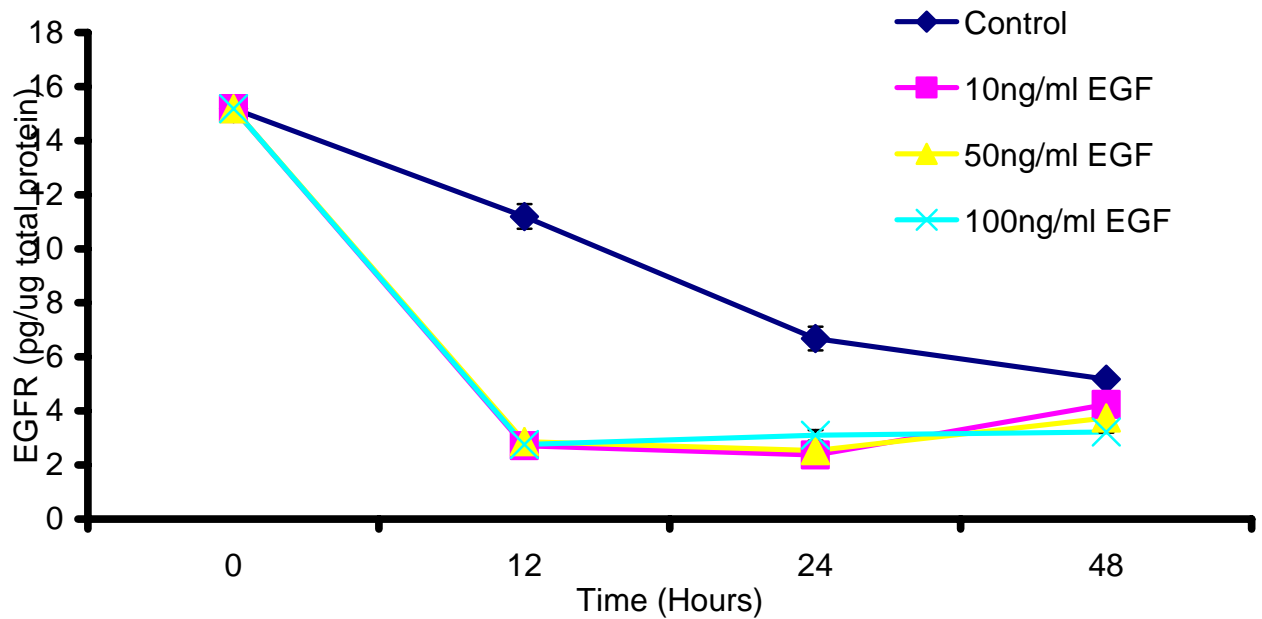


**Figure 7.4.1** The effects of EGF on EGFR protein expression in A549-Taxol over 48 hours. An ELISA recognising the extracellular domain of EGFR was utilised. Cells were treated with 10, 50 and 100 ng/ml EGF in DMEM/Ham's F12 in serum-free conditions. The control represents EGFR expression in serum-free conditions over 48 hours. Data are mean +/- SD for each concentration determined in duplicate.

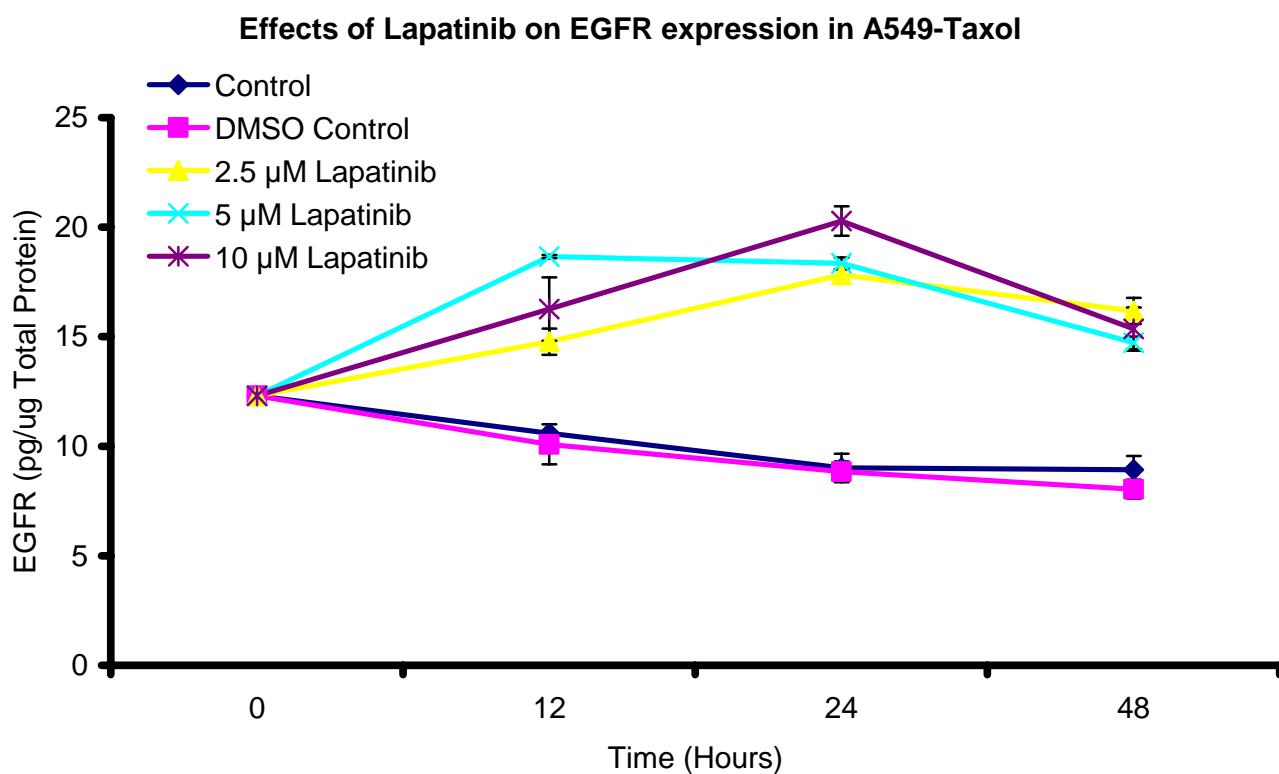


**Figure 7.4.2** The effects of lapatinib on EGFR protein expression in A549-Taxol over 48 hours. An ELISA recognising the extracellular domain of EGFR was utilised. Cells were treated with 2.5, 5 and 10  $\mu$ M lapatinib in DMEM/Ham's F12 supplemented with 5% FCS. The control represents EGFR expression in DMEM/Ham's F12 supplemented with 5% FCS. The DMSO control represents EGFR expression in DMEM/Ham's F12 supplemented with 5% FCS and DMSO equivalent to the amount present in 10  $\mu$ M lapatinib. Data are mean  $\pm$  SD for each concentration determined in duplicate.

## A549-Taxol

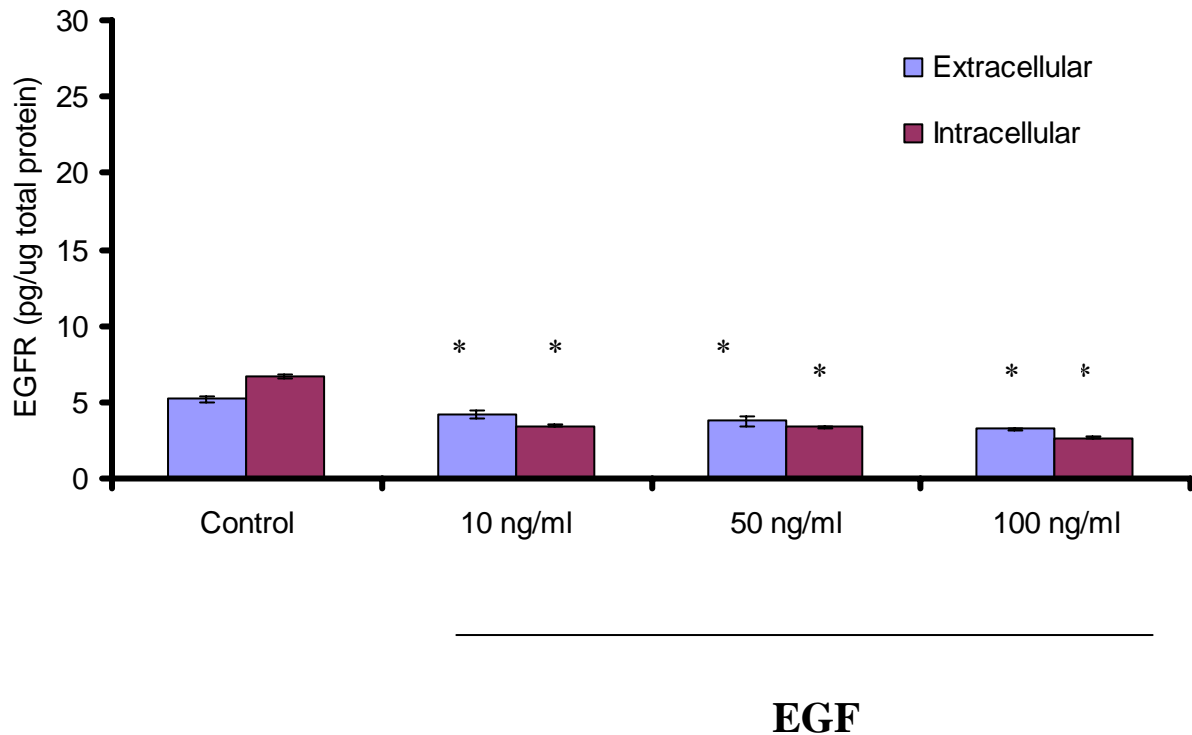


**Figure 7.4.3** The effects of EGF on EGFR protein expression in A549-Taxol at 48 hours. Two ELISA kits were utilised to determine EGFR levels. Extracellular refers to the kit that used an antibody recognising an extracellular domain of EGFR while intracellular refers to the kit that used an antibody recognising an intracellular EGFR domain. Cells were treated with 10, 50 and 100 ng/ml EGF in DMEM/Ham's F12 in serum-free conditions. The control represents EGFR expression after 48 hours in serum-free conditions. Data are mean +/- SD for each concentration determined in duplicate. \* significant,  $P < 0.05$  relative to Control.

## A549-Taxol

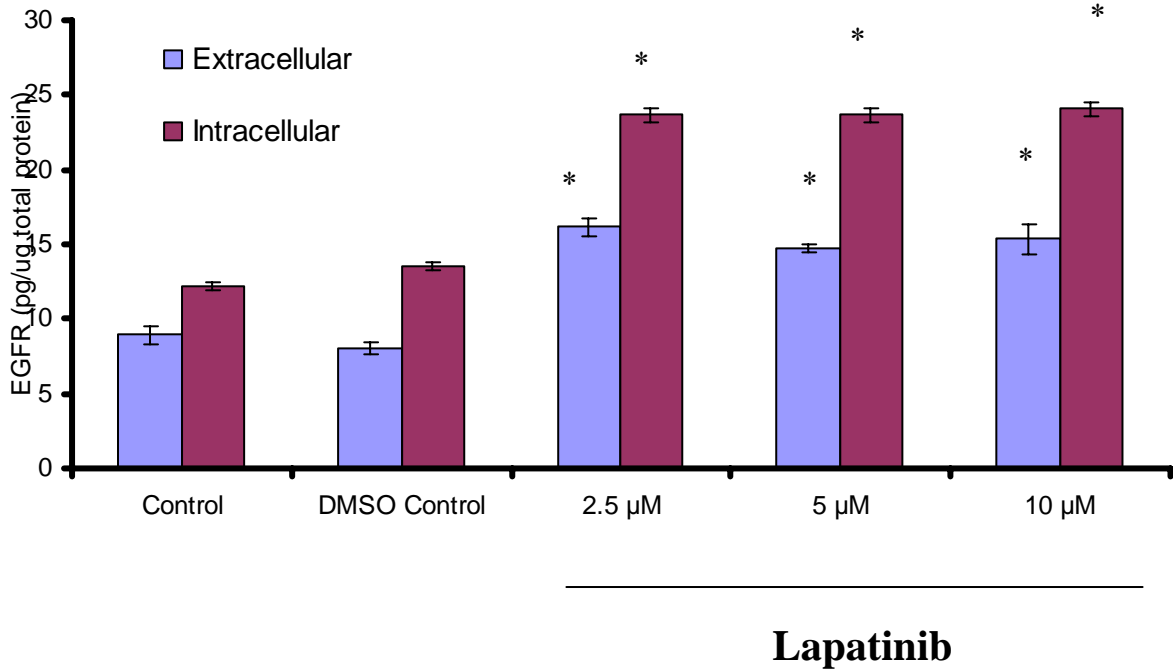


**Figure 7.4.4** The effects of lapatinib on EGFR protein expression in A549-taxol at 48 hours. Two ELISA kits were utilised to determine EGFR levels. Extracellular refers to the kit that used an antibody recognising an extracellular domain of EGFR while intracellular refers to the kit that used an antibody recognising an intracellular EGFR domain. Cells were treated with 2.5, 5 and 10  $\mu$ M lapatinib in DMEM/Ham's F12 supplemented with 5% FCS. The control represents EGFR expression after 48 hours in DMEM/Ham's F12 supplemented with 5% FCS. The DMSO control represents EGFR expression after 48 hours in DMEM/Ham's F12 supplemented with 5% FCS and DMSO equivalent to the amount present in 10  $\mu$ M lapatinib. Data are mean  $\pm$  SD for each concentration determined in duplicate. \* significant,  $P < 0.05$  relative to Control.

## A549-Taxol

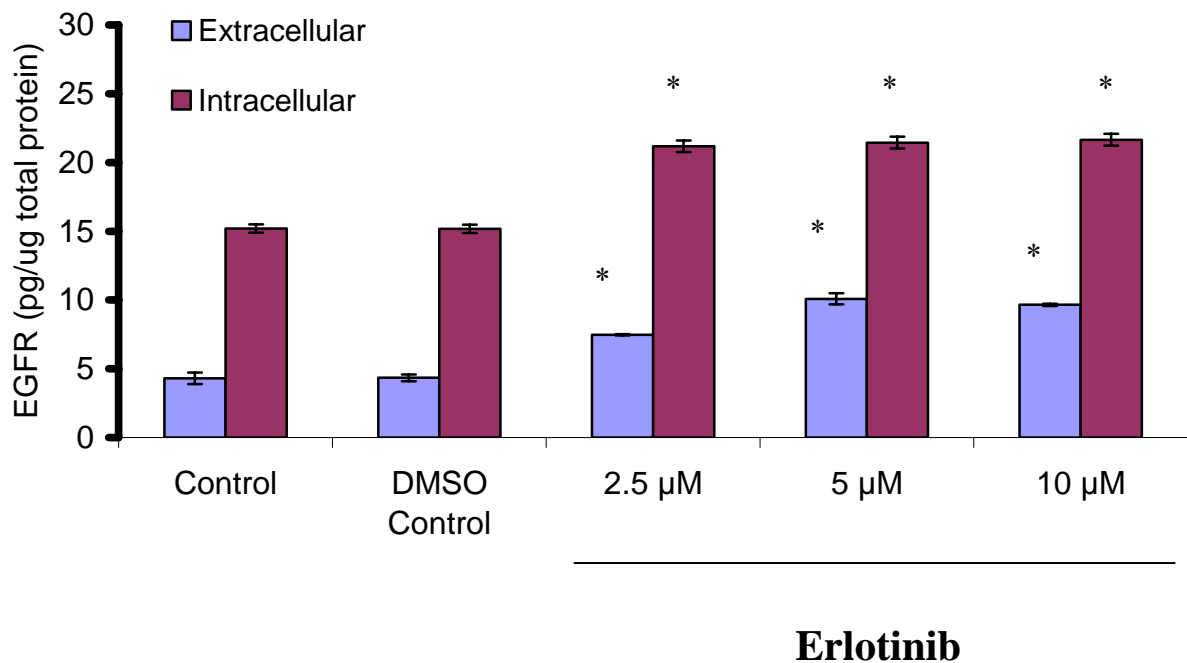


**Figure 7.4.5** The effects of erlotinib on EGFR protein expression in A549-Taxol at 48 hours. Two ELISA kits were utilised to determine EGFR levels. Extracellular refers to the kit that used an antibody recognising an extracellular domain of EGFR while intracellular refers to the kit that used an antibody recognising an intracellular EGFR domain. Cells were treated with 2.5, 5 and 10 µM erlotinib in DMEM/Ham's F12 supplemented with 5% FCS. The control represents EGFR expression after 48 hours in DMEM/Ham's F12 supplemented with 5% FCS. The DMSO control represents EGFR expression after 48 hours in DMEM/Ham's F12 supplemented with 5% FCS and DMSO equivalent to the amount present in 10 µM erlotinib. Data are mean +/- SD for each concentration determined in duplicate. \* significant,  $P < 0.05$  relative to Control

## A549-Taxol

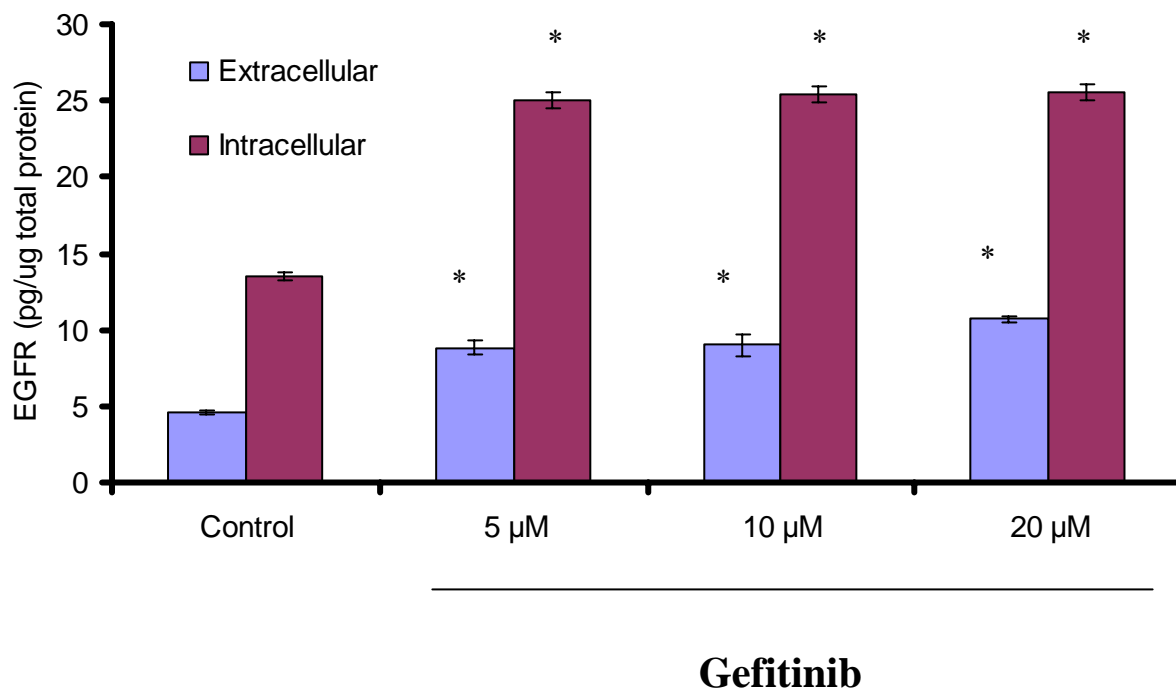


**Figure 7.4.6** The effects of gefitinib on EGFR protein expression in A549-Taxol at 48 hours. Two ELISA kits were utilised to determine EGFR levels. Extracellular refers to the kit that used an antibody recognising an extracellular domain of EGFR while intracellular refers to the kit that used an antibody recognising an intracellular EGFR domain. Cells were treated with 2.5, 5 and 10  $\mu\text{M}$  gefitinib in DMEM/Ham's F12 supplemented with 5% FCS. The control represents EGFR expression after 48 hours in DMEM/Ham's F12 supplemented with 5% FCS. The DMSO control represents EGFR expression after 48 hours in DMEM/Ham's F12 supplemented with 5% FCS and DMSO equivalent to the amount present in 10  $\mu\text{M}$  gefitinib. Data are mean  $\pm$  SD for each concentration determined in duplicate. \* significant,  $P < 0.05$  relative to Control.

## 7.5 The Effects of TKIs on MRP-1 and BCRP ATPase activity

Following examination of the effect of the three TKIs lapatinib, erlotinib and gefitinib on P-gp ATPase activity, their interaction with BCRP and MRP-1 ATPase activity was studied. The MRP-1 modulator sulindac, previously studied in taxane transport assays, Section 3, and its metabolite sulindac sulfide were also included. Classic modulators of each pump were included for reference purposes. Elacridar and mitoxantrone in the case of BCRP, and vincristine and MK571, in the case of MRP-1. The BCRP ATPase assay is based on the same principle as the P-gp ATPase activation assay (Section 7.2.2). BCRP uses ATP as the energy source for substrate transport. The ATPase function of BCRP converts ATP to ADP and Pi in order to transport substrates. The ATPase activation assay measured the amount of Pi released by BCRP ATPase in the presence of a test compound. The high activity levels of the BCRP ATPase allow both activation and inhibition to be measured directly, Figure 7.5.1. Results showed gefitinib to be the most potent stimulator of BCRP ATPase activity, followed by erlotinib and then lapatinib. All three TKIs greatly stimulated ATPase activity at low concentrations (0.25 – 5  $\mu$ M for gefitinib and erlotinib, 0.25 – 2.5  $\mu$ M for lapatinib). Above these concentrations the stimulatory effect begins to decrease and in the case of lapatinib, to inhibit ATPase activity above 5  $\mu$ M. Sulindac has a limited ability to stimulate BCRP ATPase activity above 15  $\mu$ M. Sulindac sulfide, and the BCRP-substrate mitoxantrone to a greater degree, decreased BCRP ATPase below baseline levels at all concentrations. Elacridar decreased BCRP ATPase activity below the maximal inhibited value achieved by 0.1 mM Hoechst 33342 at all concentrations examined. Baseline BCRP ATPase activity, the maximum sulfasalazine-stimulated and Hoechst 33342 inhibited BCRP ATPase activity were slightly elevated when compared to expected parameters (Section 2.18.9)

The MRP-1 ATPase assays were also based on the same principle as the P-gp ATPase activation and inhibition assays. Sulindac proved to be the tested compound that stimulated MRP-1 ATPase activity the most, followed by sulindac sulfide, Figure 7.5.2. Of the TKIs examined erlotinib exhibited most activity, continuously increasing MRP-1 ATPase activity with increasing concentration. Gefitinib followed a similar trend to erlotinib but to a lesser degree. Lapatinib stimulated MRP-1 ATPase activity at low concentrations but this effect decreases above 15  $\mu$ M. The MRP-1

substrate vincristine has a minor stimulatory effect at the lowest concentrations (0.25 and 1  $\mu\text{M}$ ) but tends towards ATPase inhibition towards higher concentrations.

Stimulation of MRP-1 ATPase activity by N-ethylmaleimide glutathione (NEM-GS) was employed to test the MRP-1 ATPase inhibitory activity of test compounds, Figure 7.5.3. The MRP-1 inhibitor MK571 proved to have the strongest ATPase inhibitory effect, followed by sulindac sulfide. Gefitinib and erlotinib had no effect on stimulated ATPase activity while lapatinib at low concentrations (0.25-15  $\mu\text{M}$ ) and sulindac at higher concentrations (5-30  $\mu\text{M}$ ) stimulated MRP-1 ATPase activity above the maximal level. Baseline MRP-1 ATPase activity and the maximum NEM-GS-stimulated MRP-1 ATPase activity was within expected parameters (Section 2.18.9).

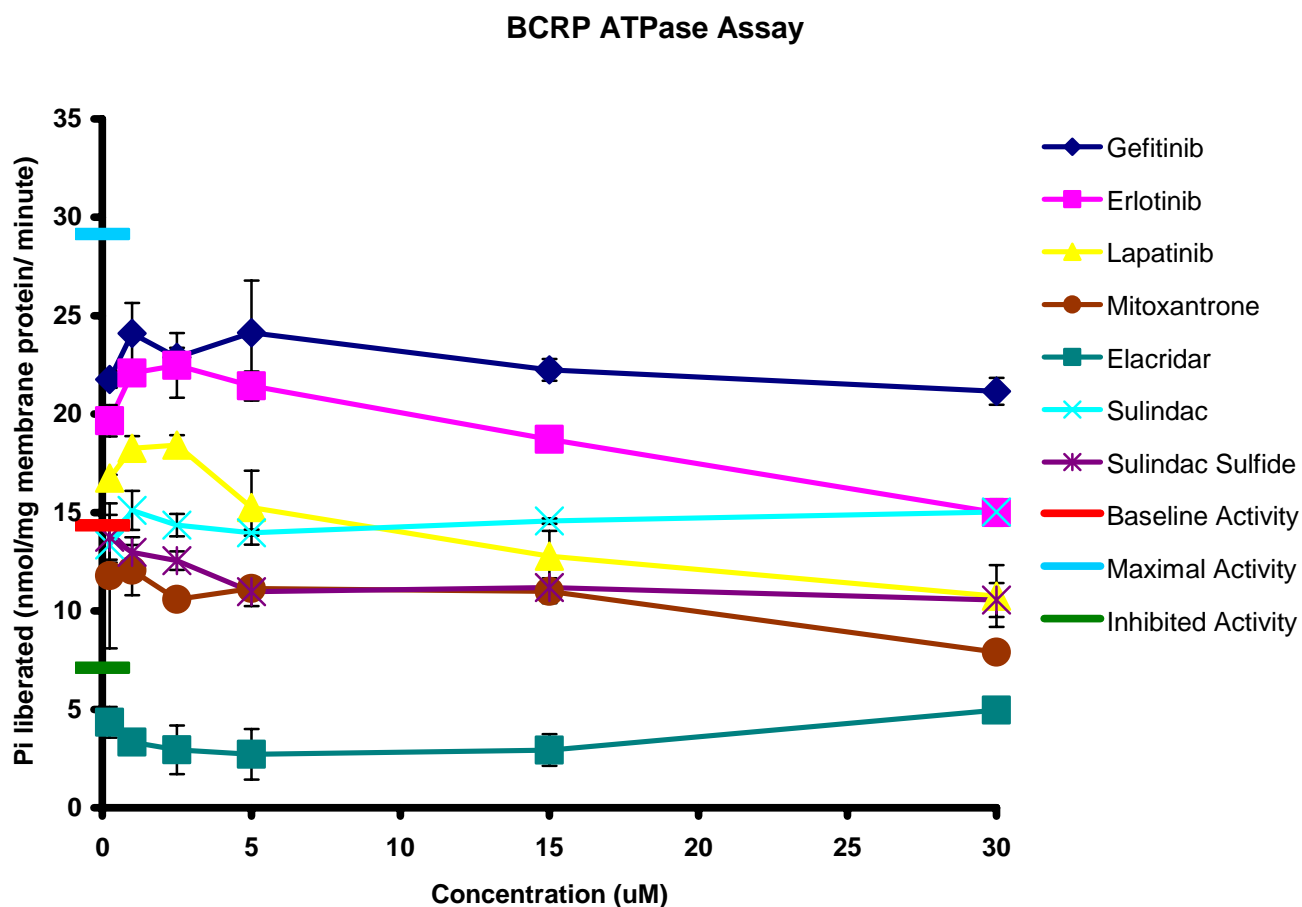


**Figure 7.5.1** The effects of a range of compounds, including the TKIs, on vanadate-sensitive BCRP ATPase activity. Compounds were tested at 0.25, 1, 2.5, 5, 15 and 30  $\mu\text{M}$ . The baseline activity represents the ATPase activity measured in the absence of added test compounds. The maximal activity represents the ATPase activity measured in the presence of 0.1 mM sulfasalazine. Inhibited activity is the BCRP ATPase activity in the presence of 0.1 mM of the BCRP inhibitor Hoechst 33342. All compounds were dissolved in DMSO. Data are mean  $\pm$  SD for each concentration determined in duplicate.

### MRP-1 ATPase Activation Assay

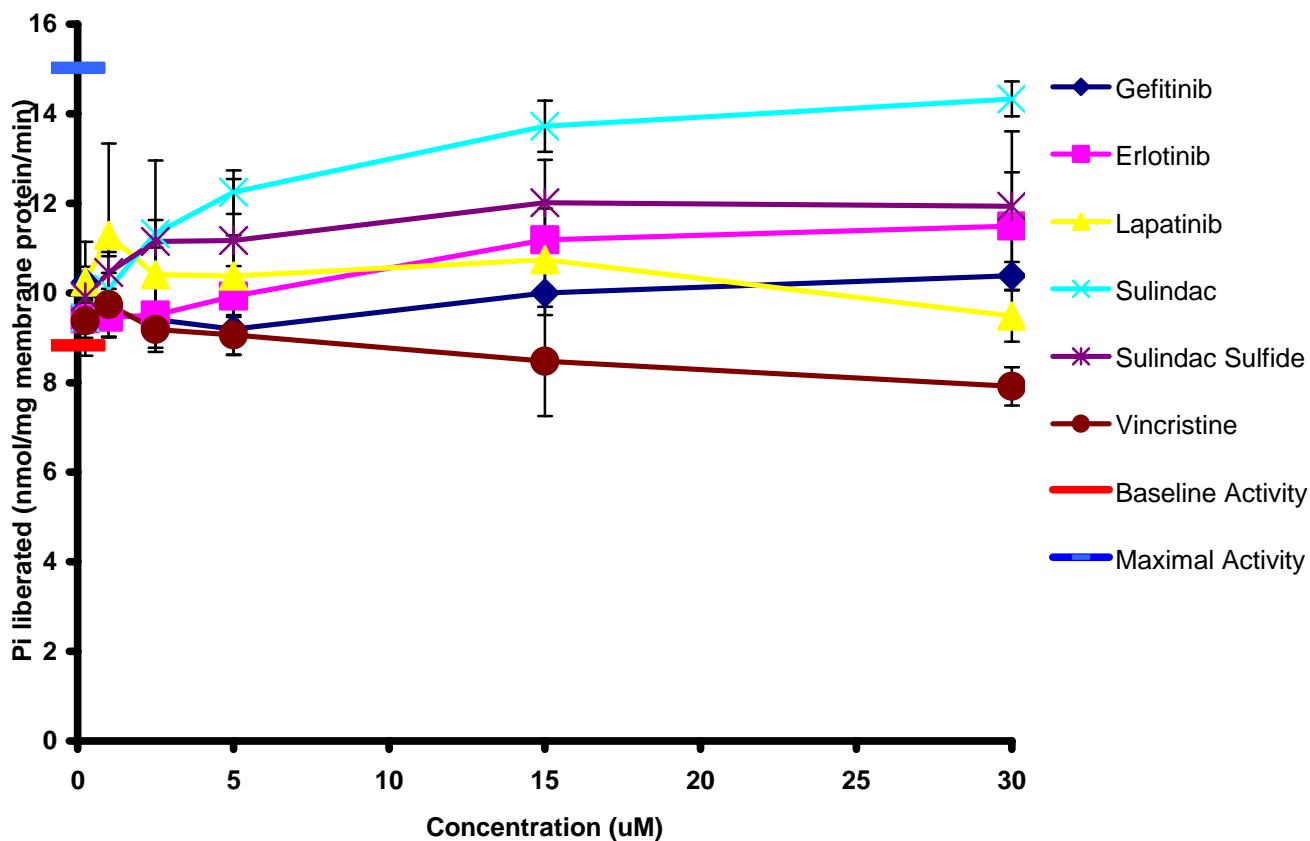


**Figure 7.5.2** The effects of a range of compounds, including the TKIs, on vanadate-sensitive MRP-1 ATPase activation. Compounds were tested at 0.25, 1, 2.5, 5, 15 and 30  $\mu\text{M}$ . The baseline activity represents the ATPase activity measured in the absence of added test compounds. The maximal activity represents the ATPase activity measured in the presence of 10 mM NEM-GS. All compounds were dissolved in DMSO. Data are mean  $\pm$  SD for each concentration determined in duplicate.

### MRP1 ATPase Inhibition Assay

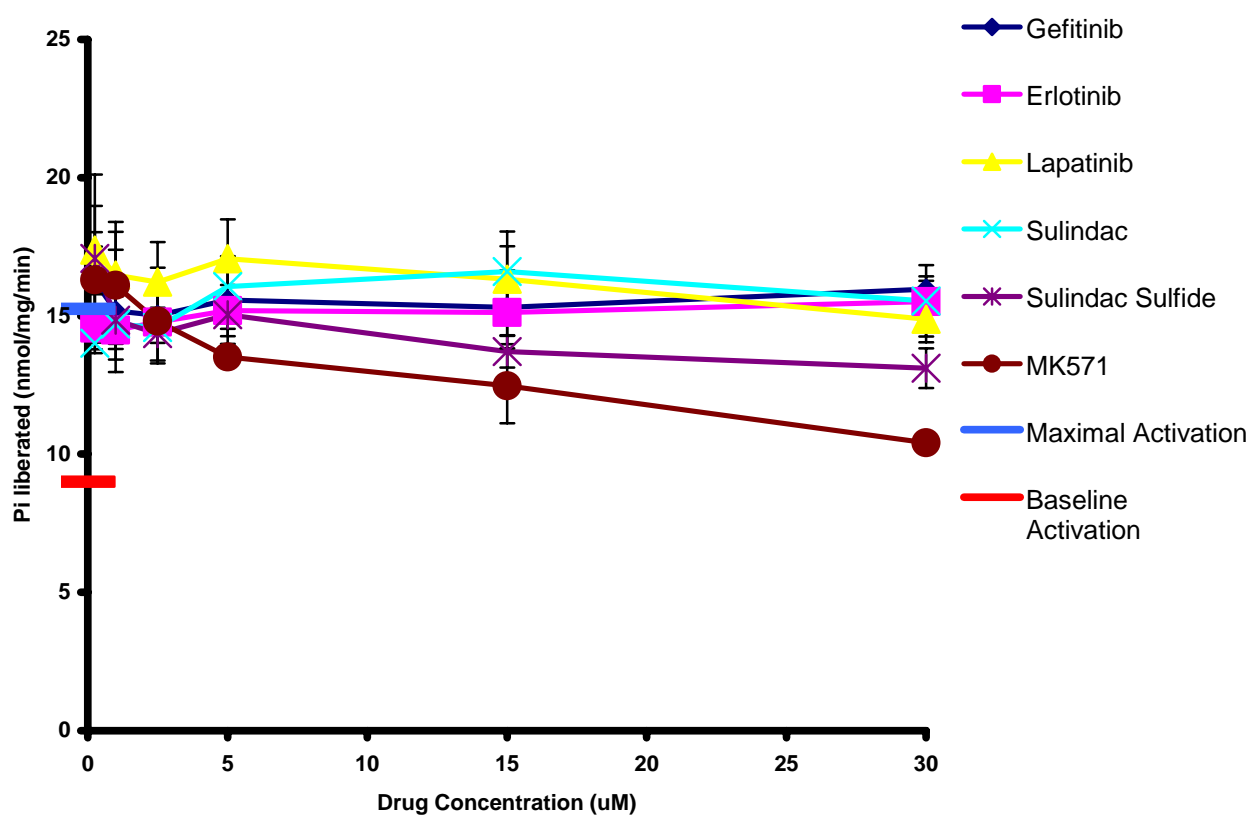


**Figure 7.5.3** The inhibitory effects of a range of compounds, including the TKIs, on activated vanadate-sensitive MRP-1 ATPase activity. Compounds were tested at 0.25, 1, 2.5, 5, 15 and 30  $\mu\text{M}$ . The compounds were assayed in the presence of 10 mM N-ethylmaleimide glutathione (NEM-GS). The baseline activity represents the ATPase activity measured in the absence of added test compounds. The maximal activity represents the ATPase activity measured in the presence of 10 mM NEM-GS only. All compounds were dissolved in DMSO. Data are mean  $\pm$  SD for each concentration determined in duplicate.

## 7.6 Summary

The ability of the tyrosine kinase inhibitors lapatinib, erlotinib and gefitinib to modulate P-gp-mediated taxane resistance in lung cancer cell models, P-gp and EGFR expression levels and MRP-1 and BCRP ATPase activity was assessed.

Lapatinib:

- Interacted with P-gp in a distinct manner to erlotinib and gefitinib.
- Was more potent than erlotinib and gefitinib at increasing docetaxel accumulation and inhibiting docetaxel efflux from the P-gp over-expressing DLKP-A cell line.
- Increased epirubicin accumulation in DLKP-A.
- Was more effective than erlotinib and gefitinib in cell proliferation studies.
- Produced synergistic potentiation of epirubicin toxicity in the absence of P-gp in DLKP and A549, along with erlotinib and gefitinib.
- Was more effective than erlotinib at increasing docetaxel accumulation at clinically relevant concentrations in the P-gp-expressing A549-Taxol cell line.

Studies in the A549-Taxol cell line showed epidermal growth factor (EGF)-treatment:

- **Reduced** P-gp protein levels.
- **Reduced** EGFR protein levels.

Conversely, lapatinib, erlotinib and gefitinib treatment in A549-Taxol:

- **Increased** P-gp protein levels.
- **Increased** EGFR protein levels.

The three TKIs proved to be poor activators and inhibitors of MRP-1 ATPase activity. Sulindac emerged as a strong activator of MRP-1 ATPase activity while its metabolite sulindac sulfide proved to be an MRP-1 ATPase activator and a weak MRP-1 ATPase inhibitor.

Studies showed gefitinib to be the most potent of the TKIs at activating BCRP ATPase activity followed by erlotinib and then lapatinib. Sulindac had no effect on basal activity but sulindac sulfide had a minor inhibitory effect.

## *Chapter 8. Discussion*

## **8.1 HPLC- determined taxane accumulation and efflux in sensitive and MDR human lung and leukemic cell lines**

To accomplish the main objectives of this project, a reproducible method of measuring changes in docetaxel transport due to drug pump inhibition was required. This method would not only have to be sufficiently sensitive to detect alterations in drug levels due to pump inhibition but also provide a range of measurement broad enough to accommodate cell types and inhibitors of varying P-gp expression and potency, respectively. The following section discusses the results presented in Chapter 3 and Chapter 4, including decisions on the cell types to be utilised, exploration of a HPLC-based method for taxane measurement and live cell laser scanning confocal microscopy of epirubicin in cells.

### **8.1.1 Cell lines**

Analysis of P-gp expression in a set of NSCLC cell lines established A549 and DLKP as P-gp negative, A549-Taxol and DLKP-TXT as P-gp over-expressing and DLKP-A as highly P-gp over-expressing (Figure 3.2.1). P-gp expression was also examined in the SK-MES-1 cell line, its taxane-selected variants, SK-Taxol and SK-Taxotere and in the DMS-53 cell line and its two taxane-selected variants, DMS-Taxol and DMS-Taxotere (Appendix A, Figure A2). While the taxane-selected variants both exhibited increased levels of P-gp expression, the parent DMS-53 cell line constitutively expressed P-gp making it unsuitable as a negative control and both cell lines exhibited slow growth rates in comparison to the A549 and DLKP cell lines. Employing A549 and DLKP as the main cell lines studied provided a variation in physiological source (adenomatous derived *vs.* squamous cell derived, respectively), and a combination of a recognised standard cell line for comparison with the in-house developed DLKP cell lines. DNA microarray data sets existed for both A549 and DLKP, a tool that was of use when searching for putative docetaxel uptake transporters. The EGFR and Her-2 status of all the lung cancer cell lines considered was also examined (Figure 7.2.1.1, Appendix A Table A6 and Appendix A Table A7). For studies involving TKIs the A549 and DLKP cell lines provided a positive and negative EGFR model,

respectively, while A549, DLKP, A549-Taxol and DLKP-A all expressed similar levels of Her-2 (Figure 7.2.1.1, Appendix A Figure A4).

### 8.1.2 Optimisation of HPLC timepoints

The HPLC method employed for docetaxel detection was adapted by Dr. Robert O'Connor from that described by Ciccolini *et al.* [274]. The same procedure was utilised for detection of paclitaxel. The accumulation and efflux timepoints for the A549 cell line were analysed (Section 3.3). 90 minutes was chosen for the docetaxel accumulation assay, a timepoint that provided sufficient accumulated drug to detect changes in transport. While accumulation increased gradually over time (Figure 3.3.1), study of the efflux profile revealed a sharp decline in docetaxel levels in the initial 40 minutes following drug removal (Figure 3.3.2). This is not consistent with a cell line that is P-gp negative (Figure 3.2.1). The 40 minute timepoint chosen for docetaxel efflux assays placed the assay stop-point at the beginning of a stable phase in the docetaxel efflux profile at which changes in efflux could readily be observed. A number of reasons for the rapid efflux of docetaxel in A549 were considered. The presence of an efflux mechanism, cell necrosis or a concentration-dependent effect related to non-specific binding was considered. MRP-2 protein expression localised to the plasma membrane has been reported in A549 [275], [276]. Huisman *et al.*, showed MRP-2 transports docetaxel in MRP-2 transduced epithelial MDCKII cells but this was examined over four hours [132]. It was unclear if the inherent level of MRP-2 expressed in A549 would be capable of such rapid docetaxel efflux within 40 minutes, a hypothesis supported by docetaxel transport studies involving sulindac (discussed in Section 8.3). A study of cell death over the chosen time periods in DLKP revealed little direct toxic insult to the cells, ruling out necrosis as a contributing factor (Table 3.7.1). The decrease in retained docetaxel was presumed to be concentration-related. It was most likely that the high docetaxel concentration saturated the high affinity intercellular binding sites leading to non-specific, low affinity docetaxel binding. The rapid decrease in retained docetaxel observed in the efflux assay (Figure 3.3.2) was likely due to dissociation of docetaxel from the low affinity binding sites. This was supported by radiolabelled <sup>14</sup>C docetaxel assays (Section 5.3) and is discussed further in Section 8.4.3.

### **8.1.3 Docetaxel accumulation and efflux in A549**

With the timepoints for monitoring drug levels characterised in A549, a set of experiments to establish accumulation and efflux assay protocols, examine the effects of sulindac on docetaxel transport in A549 and confirm the P-gp-negative status of A549 were carried out.

The docetaxel accumulation and efflux assays employed clinically relevant concentrations of sulindac, an MRP-1 inhibitor with some ability to modulate MRP-2, having been shown capable of inhibiting methotrexate transport in MRP-2-expressing membrane vesicles [277], [160], [137]. Sulindac had no effect on docetaxel transport in A549 (Figures 3.4.1. and 3.4.2). Elacridar, a compound used extensively in this project as a P-gp inhibitor, also had no effect on docetaxel accumulation in A549 (Figure 3.5.1). While Harris and Jeffery provide evidence for MRP-2 and P-gp protein expression in the A549 cell line (using a different P-gp antibody to that used in this thesis), it is clear from the docetaxel transport assays that the expression levels of P-gp and MRP-2 did not influence docetaxel transport in A549 as measured using the HPLC method [275]. Further docetaxel transport assays utilising the HPLC method in A549 can therefore be interpreted with the assumption that MRP-2 and P-gp had no influence on the outcome.

### **8.1.4 The Effects of ATP-depletion on docetaxel accumulation in A549**

A major project aim was to examine docetaxel uptake specifically to elucidate the possible existence of an energy-dependent transport mechanism. Sodium azide and 2-deoxyglucose are compounds long established and widely used as ATP-depleting agents in cell systems to compromise drug transport mechanisms such as MRP-1 [278], [156]. Depletion of ATP levels should also affect a putative energy-dependent influx mechanism. Literature-derived concentrations of sodium azide and 2-deoxyglucose were used in all ATP-depletion experiments involving the HPLC-based taxane measurement protocol as an initial exploration of the effects of such compounds on taxane transport [278], [156]. Sodium azide treatment in glucose-free

medium had no significant effect on docetaxel transport in A549 (Figure 3.6.1). Taking the 10 mM sodium azide concentration, an accumulation and efflux assay were carried out. Sulindac was included in both assays for comparative purposes with previous identical experiments in A549 carried out under normal conditions (Figures 3.6.2 and 3.6.3). The comparable nature of the docetaxel transport assays in the presence or absence of sodium azide suggest no energy-dependent taxane transport system in this cell line. However, the exact reduction in ATP levels caused by sodium azide in these assays was not quantified, a determination critical to guarantee a sufficient decrease in ATP levels to impact docetaxel transport.

### **8.1.5 Docetaxel and paclitaxel accumulation in DLKP**

The DLKP cell line was the second sensitive cell line chosen for study. Sulindac has been examined in DLKP in the past as an MRP-1 inhibitor, potentiating the toxicity of doxorubicin, vincristine and VP-16 [160]. Characterisation of the cell line by Liang *et al.* indicated that DLKP did not express P-gp (consistent with previous results discussed) or MRP-2 at the protein level but did express MRP-1 [260]. Docetaxel and paclitaxel transport was examined in DLKP to provide a control for subsequent taxane transport assays in the P-gp-expressing DLKP variants, DLKP-A and DLKP-TXT. Taxane transport assays had not previously been carried out in the DLKP cell line. The effect of three P-gp modulators on docetaxel accumulation and efflux and paclitaxel accumulation was examined in DLKP (Section 3.7). As expected, elacridar, cyclosporin A or verapamil had no influence on docetaxel or paclitaxel accumulation or efflux in this cell line due to the absence of P-gp (Figures 3.7.1, 3.7.2 and 3.7.3). Comparison of docetaxel and paclitaxel accumulation did lead to a number of interesting observations (Figure 3.7.1). The disparity observed between the mass of docetaxel and paclitaxel accumulated in DLKP was unexpected. Documented differences in lipophilicity, membrane permeability and tubulin affinity between paclitaxel and docetaxel may contribute to this effect but comparisons in the HL-60 and HL-60ADR cell lines reveal more similar levels of accumulation (Section 3.12) in these leukemic cell models [31].

The DLKP cell line accumulated higher levels of docetaxel on average than the A549 cell line, 466 +/- 110 ng/million cells *versus* 280 +/- 42 ng/million cells, respectively. When combined with the HPLC assay results in Figure 3.8.1 (sodium azide reduced

docetaxel accumulation in DLKP) and the radiolabelled docetaxel ATP-depletion assays in Section 6.4 (a combination of sodium azide, 2-deoxyglucose and antimycin A reduced docetaxel accumulation in DLKP), a strong body of evidence was mounted to suggest an ATP-dependent mechanism is responsible for docetaxel uptake in DLKP. The results in Section 6 and Section 3.4 also allude to the absence of an active influx mechanism in A549. The argument in support of this hypothesis is continued later in this discussion in Section 7.4. It will be important, and of great interest, to ascertain if the disparity in accumulation between docetaxel and paclitaxel is maintained in DLKP at lower concentrations. A comparison of the taxanes (accumulation, temperature-dependency and ATP-dependency) at pharmacological levels would determine if the putative uptake mechanism is docetaxel specific. It would also examine if the disparity in accumulation levels in DLKP and its drug-selected variants (Sections 3.7, 3.9 and 3.11) was due solely or partially to the physical properties of the compounds.

### **8.1.6 Docetaxel and paclitaxel transport in DLKP-A**

Examination of docetaxel transport in the drug-sensitive cell lines was necessary to establish experimental parameters and control conditions. A major objective for developing the HPLC-based method for taxane measurement was to establish a cell system model to compare and assess putative modulators of P-gp-mediated docetaxel transport. The adriamycin-selected DLKP-A cell line is an example of a highly resistant cell line. The resistance conferred through P-gp expression in DLKP-A is clearly illustrated in Table 7.2.6 in Section 7, presenting IC<sub>50</sub> values for docetaxel, paclitaxel and epirubicin that are 228-, 153- and 123-fold greater than the parent DLKP cell line.

There was a distinct difference between the interaction of paclitaxel and docetaxel with P-gp modulating agents at the concentrations examined in DLKP-A.

The specific potency of elacridar as an irreversible P-gp inhibitor allowed a physiologically relevant concentration of it to be employed in DLKP-A accumulation and efflux studies. Supra-physiological levels of cyclosporin A and verapamil were chosen to increase the likelihood of inhibition of taxane efflux [279]. Despite greatly reduced cellular levels of docetaxel and paclitaxel due to P-gp over-expression, a relative difference in the mass of each taxane accumulated was once again evident in

this DLKP variant (Figure 3.9.1). Taxane accumulation was greatly increased by P-gp inhibition. Elacridar proved the most effective compound for reversal of P-gp-mediated resistance in DLKP-A. Cyclosporin A had a lesser, but significant, effect on accumulation of both taxanes. This is expected as cyclosporin A, along with verapamil, is classed as a first generation P-gp inhibitor [280]. While elacridar and cyclosporin A behaved in an expected fashion, verapamil did not. Verapamil increased cellular paclitaxel accumulation to a similar extent as cyclosporin A but failed to affect docetaxel accumulation (Figure 3.9.1). The taxane efflux assays followed a similar trend. Paclitaxel levels were maintained at the 90 minute control level by cyclosporin A, verapamil and elacridar after 40 minutes in paclitaxel-free medium (Figure 3.9.2). Elacridar was the only compound to inhibit docetaxel efflux from DLKP-A (Figure 3.9.2).

### **8.1.7 Taxane and verapamil proliferation assays in DLKP-A**

The ability of verapamil to modulate P-gp activity is well documented [95]. To determine if verapamil was truly unable to modulate P-gp-mediated docetaxel transport in DLKP-A, a number of proliferation assays combining docetaxel and paclitaxel with verapamil were carried out. The drug concentrations used in the transport assays could not be used in the seven-day proliferation assays (Section 2.7.2) due to toxicity from the high taxane levels employed. Non-toxic concentrations of all drugs were chosen to emphasise any potentiation of toxicity. The P-gp inhibitory effects of verapamil were clearly evident through increased docetaxel and paclitaxel toxicity (Figures 3.9.3 and 3.9.4). A proliferation assay exposing DLKP-A to the transport assay conditions (drug concentrations and exposure time) also resulted in potentiation of docetaxel cytotoxicity. The discrepancy between transport and proliferation assays can be explained. The ratio of docetaxel to verapamil in the docetaxel accumulation assays is 1:10, while in the proliferation assays it is 1:27. The higher ratio of verapamil in the proliferation assays inhibited docetaxel transport in DLKP-A. This concentration-dependent effect suggests that docetaxel has a higher affinity for P-gp than paclitaxel. This is supported by observations made by Shirakawa *et al.*, that 100  $\mu\text{M}$  verapamil was capable of inhibiting apical to basal transport of 860 nM  $^{14}\text{C}$  docetaxel in P-gp over-expressing porcine kidney epithelial

cells [281]. This was the first indication that the HPLC-based method for taxane detection may not be sensitive enough for the ultimate purposes of the project.

### **8.1.8 Effect of ATP inhibitors on docetaxel transport in DLKP-A**

The reduced levels of docetaxel in the DLKP cell line due to treatment with ATP depletion agents was unexpected but could largely be attributed to an effect on docetaxel influx, due to the absence of major drug efflux mechanisms (Section 3.8). ATP depletion in DLKP-A would be expected to reduce P-gp efficacy and increase docetaxel accumulation levels. It should also be considered that the expression status of any energy-dependent influx mechanism is unknown in this cell line. Approximately three times more docetaxel was accumulated in the DLKP-A ATP depletion assay compared to previous DLKP-A transport experiments (Figure 3.10.1). It was intended to carry out all comparable cell-based experiments within fifteen passages of each other but even within this range a drop in resistance was observable. The docetaxel accumulation assay in Figure 3.10.1 provided tentative evidence that a putative energy-dependent mechanism may also be present in DLKP-A. The addition of sodium azide and 2-deoxyglucose in glucose-free medium reduced docetaxel accumulation to below control levels, although the reductions were not significant. One explanation of the observed results may be the inhibition of docetaxel influx in the absence of active P-gp. The failure of elacridar to restore the mass of docetaxel accumulated to control levels in the presence of sodium azide and 2-deoxyglucose supports the belief that all P-gp is inhibited and the decrease in docetaxel accumulation was attributable to inhibition of a putative energy-dependent influx mechanism (Figure 3.10.1).

### **8.1.9 Docetaxel and paclitaxel transport in DLKP-TXT**

P-gp expression in DLKP-TXT is much lower than in DLKP-A (Section 3.2). The fold-resistance of DLKP-TXT and indeed A549-Taxol to the taxanes is much lower and closer to *in vivo* levels of resistance [111]. The discrepancy between docetaxel and paclitaxel accumulation was once again evident in this cell line (Figure 3.11.1). The mass of both drugs accumulated is comparable to that accumulated in DLKP (Section 3.7), highlighting the lower resistance levels conferred by P-gp in DLKP-

TXT (Appendix A, Table A5). The presence of active P-gp was indicated by the increase in docetaxel accumulation associated with cyclosporin A and elacridar. Verapamil does not affect docetaxel levels, consistent with DLKP-A results (Section 3.9). However, proliferation assays confirmed dose-dependent potentiation of docetaxel toxicity by verapamil at higher docetaxel/verapamil ratios (Figures 3.11.2). Elacridar also potentiated docetaxel toxicity concurrent with the docetaxel accumulation results (Figures 3.11.4). The minor increases in paclitaxel accumulation due to elacridar and verapamil also translated to potentiation of toxicity in proliferation assays (Figures 3.11.3 and 3.11.5).

### **8.1.10 Docetaxel and paclitaxel transport in HL-60**

The anthracyclines are mainstay treatment for acute myeloid leukaemia (AML) [282]. Anthracycline transport has been studied in leukaemia cell lines such as the AML-derived HL-60 cell line [283]. Nagasawa *et al.*, have suggested the nucleoside transport system is involved in doxorubicin uptake in HL-60 [283]. Taxane transport, in contrast, has not been examined in the HL-60 and HL-60 ADR cell lines as the taxanes are not used in the treatment of leukaemia. The HL-60 cell line provides an ideal model for the comparison of docetaxel and paclitaxel transport as it is lacking in expression of the drug transporters P-gp, BCRP, MRP-2, MRP-3, MRP-5 with only minor expression levels of MRP-1 [284].

Contrary to previous taxane accumulation assays in DLKP, DLKP-A and DLKP-TXT, the mass of docetaxel and paclitaxel accumulated in HL-60 are similar (Figure 3.12.1). Given the number of general differences between HL-60 and the DLKP variants (size/physiological source/adherent vs. non-adherent), it would be impossible to draw any conclusions on the contribution of drug uptake mechanisms to this observation but it may be a point notable for further investigation.

Docetaxel or paclitaxel accumulation was not affected significantly by elacridar, cyclosporin A or sulindac treatment, to be expected in a cell line that does not express P-gp (Figure 3.12.1). Of most interest is the significant reduction in both docetaxel and paclitaxel accumulation evident with co-incubation with verapamil. This effect is not without precedent. Verapamil inhibited <sup>14</sup>C paclitaxel uptake in the adriamycin-selected NCI/ADR RES breast cancer cell line through suggested inhibition of active inward transport [285]. The exact mechanism was not identified. The same study also

reported that verapamil increased the efflux of  $^{14}\text{C}$  paclitaxel in the adriamycin-sensitive MDA-MB-435 breast cancer cell line [285]. The decrease in retained paclitaxel is unlikely to be accounted for by stimulation of efflux in HL-60 as verapamil had no effect on paclitaxel efflux (Figure 3.12.2). Elacridar caused a significant increase in paclitaxel efflux (Figure 3.12.2) but did not produce a corresponding decrease in paclitaxel accumulation (Figure 3.12.1) that was significant and therefore did not provide supporting evidence of an elacridar stimulated efflux mechanism. The large decrease in paclitaxel levels observed in HL-60 over 40 minutes in the absence of major taxane transporters is most likely the same effect previously seen in A549 (Figure 3.3.2) compounded by the smaller size of the HL-60 cells. This effect is discussed in greater detail in Section 8.4.3.

### **8.1.11 Docetaxel and paclitaxel transport in HL-60 ADR**

The HL-60ADR cell line over-expresses MRP-1 conferring significant resistance to MRP-1 substrate drugs including adriamycin [286] (Appendix A, Table A5). As mentioned previously, it has been reported that adriamycin selection of HL-60 cells has led to resistance to anthracyclines and vinca alkaloids but also low level cross-resistance to paclitaxel [287]. A study involving HL-60 ADR-derived MRP-1 vesicles showed little or no transport of paclitaxel [288]. Inclusion of sulindac in the HL-60 ADR taxane accumulation experiments supports the findings that the taxanes are not MRP-1 substrates (Figure 3.12.3). It also confirmed the absence of functional P-gp expression from the HL-60ADR cell line as none of the P-gp modulators tested significantly altered docetaxel or paclitaxel accumulation.

### **8.1.12 Assessment of the HPLC method for taxane quantification**

The HPLC-based method for taxane quantification is reliable and reproducible but was ultimately unsuitable for fulfilment of the project goals. The supra-physiological taxane levels required for detection meant the effects of potential competitive inhibitors could be missed, extrapolation of clinical relevancy would not be possible and changes in accumulation in cell lines expressing low levels of P-gp would be difficult. Assay logistics such as required cell number and overall experiment duration

contribute to the weaknesses of this method. However, the HPLC-based protocol did provide valuable results including identifying a disparity in docetaxel and paclitaxel accumulation, a decrease in docetaxel accumulation in DLKP and HL-60 due to sodium azide and sulindac, respectively, and a decrease in paclitaxel and epirubicin (discussed in Section 8.2.3) levels observed in DLKP-TXT related to sulindac.

## **8.2 LSCM imaging of epirubicin**

The anthracycline, epirubicin, is a P-gp and MRP-1 substrate chemotherapy drug that is naturally fluorescent, allowing it to be imaged directly through laser confocal microscopy [289]. It was initially envisaged that the laser confocal imaging of epirubicin in sensitive and drug-resistant cell lines could provide additional quantitative information on the effects of P-gp modulators on chemotherapy compounds. Direct epirubicin measurement by HPLC (Section 4.2) was deemed more advantageous than confocal methods for quantifying epirubicin because of the varied distribution of epirubicin within cells and the subjective nature of determining concentrations through fluorescence. It became apparent that confocal imaging was more useful in a qualitative capacity, defining cellular localisation and changes therein due to transporter inhibition.

### **8.2.1 LSCM imaging of epirubicin in DLKP**

Epirubicin was shown to be localised to the nucleus and plasma membrane of DLKP cells with minimal cytoplasmic presence (Figure 4.1.1). This is consistent with the slow permeability of epirubicin through the plasma membrane, the intercalation of epirubicin with DNA and previous confocal observations in non-MDR tumour cells by other groups [290], [291]. Elacridar, cyclosporin A, verapamil or sulindac treatment caused no visible change in the level of epirubicin fluorescence or localisation in the DLKP cell model (Figure 4.1.2). Sulindac treatment might have been expected to increase epirubicin levels through MRP-1 inhibition. It was unlikely, however, that increases in epirubicin mass would have been visibly detectable through microscopy given the limited exposure time and the low MRP-1 expression levels in DLKP [160]. High over-expression of drug pumps is required to detect epirubicin

changes using the confocal method. A comparison of the DLKP-TXT and DLKP-A confocal results clearly illustrates this point (Figures 4.1.3 and 4.1.4). Cyclosporin A, elacridar and verapamil increased epirubicin accumulation and fluorescence through P-gp inhibition in DLKP-A but did not produce observable changes in lower P-gp expressing DLKP-TXT.

### **8.2.2 LSCM of epirubicin in DLKP-A**

In contrast to the results obtained in DLKP, there is a complete absence of nuclear localised epirubicin in DLKP-A due to P-gp over-expression (Figure 4.1.3). This is consistent with LSCM anthracycline results in MDR bladder and myeloid cancer cell lines [291], [292]. All three P-gp modulators, elacridar, cyclosporin A and verapamil, increased intracellular epirubicin accumulation, and affect nuclear localisation through P-gp inhibition. There is no preferential increase in epirubicin levels accorded to a particular modulator implying a similar ability for each compound to modulate epirubicin transport in DLKP-A at the concentrations used. Anthracycline selection has been shown to increase cytoplasmic vesicle and nuclear membrane-localised P-gp in MCF-7/DX breast cancer cells leading to increased resistance [293]. The confocal images suggest an increase in cytoplasmic vesicle-localised P-gp may have occurred through adriamycin selection in DLKP-A. No cytoplasmic epirubicin-containing vesicles were observed in DLKP treated with P-gp modulators (Figure 4.1.2, Appendix B) but epirubicin containing cytoplasmic vesicles were clearly visible in the inhibitor-treated DLKP-A cells.

### **8.2.3 LSCM of epirubicin in DLKP-TXT**

The reduction in accumulated paclitaxel levels due to sulindac in DLKP-TXT, as measured by HPLC, was not observed with docetaxel (Figure 4.1.4). The epirubicin confocal studies show that while the three P-gp modulators do not increase epirubicin levels sufficiently to be observable within the parameters of the experiment (Figure 4.1.4), there is a decrease in nuclear epirubicin fluorescence in the presence of sulindac that is congruent with the decrease in paclitaxel accumulation seen in the HPLC accumulation assay. Further study is needed to establish if sulindac is selectively inhibiting uptake of epirubicin and paclitaxel in DLKP-TXT.

## **8.2.4 Laser confocal imaging of Oregon-green paclitaxel in DLKP and A549-Taxol**

The taxanes are not naturally fluorescent and require conjugation with fluorophores to allow visualisation by laser confocal microscopy [294]. These bulky additions (MW paclitaxel = 854 g/mol / MW Oregon-green 488 paclitaxel = 1319 g/mol) most likely alter a number of paclitaxel kinetic characteristics such as drug transport and permeability but in the case of Oregon-green-tagged paclitaxel allowed visualisation of the tubulin network in A549-Taxol and DLKP (Figures 4.1.5, 4.1.6, 4.1.7 and Appendix B). Marcus *et al.*, have recently published similar images of the tubulin structure of A549 in which they were using fluorescently-tagged paclitaxel to probe the mechanistic basis for farnesyl transferase-mediated reversal of taxane resistance [294]. By observing the levels of Oregon-green paclitaxel bound to cellular microtubules, Marcus *et al.*, found that farnesyl transferase inhibitors could reverse paclitaxel resistance by increasing the levels of paclitaxel bound to microtubules in paclitaxel-sensitive and paclitaxel-resistant cell lines [294]. This technique could be employed to examine tubulin structure after exposure to tubulin –targetted cytotoxics like the taxanes or during mitotic events in tumour cell lines as shown in Figure 4.1.8. There appears to be distinctive variations in tubulin distribution between DLKP (Figure 4.1.5) and A549-Taxol (Figure 4.1.6). The variation in uptake of Oregon-green paclitaxel in the A549-Taxol cells could be due to P-gp over-expression but a control experiment in A549 would be needed to verify this. A comparison of taxane cytotoxicity values between A549-Taxol and DLKP revealed differences in sensitivity levels to the taxanes in these cell lines (Table 7.2.6) but this is most likely due to P-gp expression levels.

## **8.2.5 HPLC-based quantification of epirubicin in DLKP-A**

The transport of epirubicin was examined to provide a quantitative result to complement the confocal studies in Section 4.2 and to compare the P-gp-mediated transport of a member of the anthracycline family with that of the taxanes, docetaxel

and paclitaxel. In addition, epirubicin/docetaxel and epirubicin/paclitaxel are used in combination for the treatment of advanced breast cancer [295], [296]. HPLC-detection of the anthracycline, doxorubicin (adriamycin), was optimised by Dr. Robert O'Connor and later adapted for epirubicin measurement [160]. The epirubicin assays employed extended accumulation (2 hours) and efflux (3 hours) timepoints compared to the taxane transport assays. This is presumably due to epirubicin requiring increased time to reach and bind its high affinity nuclear target (DNA) in contrast to the cytoplasmic microtubule target of the taxanes [25]. Unlike the taxane transport studies reported herein, the HPLC-based epirubicin measurement protocol required 2  $\mu\text{M}$  of drug for accumulation and efflux assays, a concentration that is below reported pharmacological  $C_{\text{max}}$  (peak plasma concentration) values for epirubicin (Section 2.14) [297], [298].

Elacridar, cyclosporin A and verapamil increased the mass of epirubicin accumulated in DLKP-A (Figure 4.2.1) and not only maintained levels of epirubicin in the efflux assay, they also increased drug levels after three hours in epirubicin-free medium (Figure 4.2.2). P-gp has been found localised in the nuclear membrane of doxorubicin-selected cells [293]. Although counterintuitive, the increase in epirubicin levels produced by P-gp modulators in the DLKP-A efflux assay may be due to inhibition of nuclear localised P-gp. The control set of cells were exposed to epirubicin for two hours but there was no nuclear localisation and some cytoplasmic localisation as gleaned from the confocal data (Figure 4.1.3). The cytoplasmic epirubicin could possibly be sequestered in expanded lysosomal compartments as has been shown previously for anthracyclines in the doxorubicin-selected U-937 leukemic cell line [292]. With no access to its nuclear targets, this cytoplasmic pool of epirubicin would be quickly depleted by lysosomal sequestration and extrusion by active P-gp, even in the time between assay washes. In the presence of the P-gp modulators however, with inhibited plasma membrane, vesicle and nuclear membrane localised P-gp, the cytoplasmic epirubicin pool is stabilised and allowed access to the nucleus. DNA intercalated epirubicin would not be easily effluxed leading to the higher levels of epirubicin retained than in the control cells.

### **8.3 Development of a radiolabelled-based assay for determination of docetaxel accumulation and efflux**

Radiolabelled-based drug assays have achieved levels of detection in the picomolar range [143].  $^{14}\text{C}$  radiolabelled drugs are relatively safe and extremely stable (half life  $\sim 5000$  years). As an alternative to the HPLC method of taxane detection,  $^{14}\text{C}$ -radiolabelled docetaxel was chosen as the basis for the development of a more efficient detection method. A quick throughput protocol for the detection of  $^{14}\text{C}$  docetaxel in multi-drug resistant cells was not found in the literature. Given the importance of developing an accurate and reliable assay, a number of optimisation steps were undertaken. The optimisation process resulted in a method for docetaxel measurement that was of greater sensitivity than the HPLC-based technique, which utilised lower cell numbers, less consumables, and improved results throughput.

#### **8.3.1 Scintillation counter efficiency and seeding density**

Scintillation counter efficiency remained stable over a range of  $^{14}\text{C}$  docetaxel concentrations from 0.05 to 10  $\mu\text{M}$  averaging 47.6% (Table 5.2.1.1). Counter efficiency can be used for calculation of disintegrations per minute (D.P.M.) along with background levels to calculate the actual mass of docetaxel present in a sample if required. DLKP-A were seeded at  $1 \times 10^5$  cells/ml and  $2 \times 10^5$  cells/ml for 24 hours prior to  $^{14}\text{C}$  docetaxel exposure (Figure 5.2.2.1). DLKP-A was chosen for this step as it accumulates the lowest levels of docetaxel of the cell lines being examined due to P-gp over-expression. Both seeding densities resulted in similar uptake levels at the  $^{14}\text{C}$  docetaxel concentrations examined. This supported visual evidence that  $1 \times 10^5$  cells/ml provided a confluent monolayer and the excess cells present by seeding  $2 \times 10^5$  cells/ml did not attach to the well surface but were removed at various wash steps in the procedure.

### **8.3.2 The presence of cell debris does not quench radioactivity signal**

The samples to be read on the scintillation counter would not contain pure radio-labelled drug but a mixture of  $^{14}\text{C}$  docetaxel, cell debris and 0.1 M NaOH. To quantify any cell debris-related quenching of  $^{14}\text{C}$  signal, an experiment was designed to compare the counts per minute (C.P.M.) for a range of  $^{14}\text{C}$  docetaxel concentrations in the presence or absence of cell debris. Cell debris was found to have negligible effect on detection levels (Figure 5.2.3.1A). The quantity of cell debris included with each sample was equivalent to that present in an assay sample. Assay reproducibility was increased due to the fact that cell debris does not affect readings. A representation of the scintillation count error as reported by the scintillation counter for the assay in Figure 5.2.3.1A revealed that the internal error associated with  $^{14}\text{C}$  docetaxel concentrations of 50 nM (0.05  $\mu\text{M}$ ) and above was below 5% (Figure 5.2.3.1B).

### **8.3.3 Drug adsorption has negligible effect on assay error**

The capacity of the cell culture-treated 24-well plates to adsorb drug was a potential source of assay error. Song *et al.*, have shown rapid and non-specific adsorption of paclitaxel to glass and plastic surfaces, such as glass vials and polystyrene tissue culture plates [299]. Retention of  $^{14}\text{C}$  docetaxel by 24-well tissue culture plates would lead to falsely elevated and unpredictable accumulation readings. The accumulation of a range of  $^{14}\text{C}$  docetaxel concentrations was measured in a 24-well plate containing DLKP and mirrored in an empty 24-well plate (Figure 5.2.4.1A). The readings reflecting drug adsorption in the empty 24-well plate were nominal and proved to be a negligible source of error compared to the large values recorded in the DLKP cell line. A representation of the internal scintillation counter error for this experiment reveals the higher error levels associated with lower radiation counts (Figure 5.2.4.1B). While the internal % error is not of critical importance due to replicate data sets, maintaining error levels below 5% improves confidence in the assay. The % error levelled out below 5% at 100 nM in DLKP. 100 nM was chosen as the standard concentration for accumulation assays. 100 nM (0.1  $\mu\text{M}$ ) is a hundred times lower than the 10  $\mu\text{M}$  employed previously in the HPLC based studies. 100 nM is a value

that is also within the pharmacologically relevant range of docetaxel exposure (~0.01 to 6  $\mu\text{M}$ ), therefore making findings more therapeutically relevant [300].

### **8.3.4 5% FCS has no effect on $^{14}\text{C}$ docetaxel accumulation**

The presence of plasma proteins such as those found in foetal calf serum (FCS) within transport assays could have a major impact on drug accumulation. Urien *et al.*, reported that docetaxel was extensively bound to plasma proteins (>98%) *in vivo*, the main carriers being lipoproteins, albumin and alpha 1-acid glycoprotein at clinically relevant concentrations [301]. FCS has also been shown to bind paclitaxel *in vitro* [299]. A549 and DLKP and their drug-selected variants are maintained in 5% FCS in DMEM/Ham F12. Accumulation of 100 nM  $^{14}\text{C}$  docetaxel was examined in A549 and DLKP in the presence of increasing concentrations of FCS (Section 5.2.5). Maintaining the cells in 5% FCS was deemed acceptable in all  $^{14}\text{C}$  docetaxel assays. 50 and 100% FCS lead to huge reductions in  $^{14}\text{C}$  docetaxel accumulation, highlighting the influence of FCS on drug transport due to drug binding reducing the quantity of drug available for uptake into cells.

### **8.3.5 Choice of a standard concentration of $^{14}\text{C}$ docetaxel for use in DLKP-A efflux assays**

It was established that the pharmacologically relevant 100 nM  $^{14}\text{C}$  docetaxel was the optimum concentration for accumulation assays in A549, DLKP and their variants and, by default, for efflux assays in A549 and DLKP. It remained unclear if 100 nM  $^{14}\text{C}$  docetaxel would provide sufficient accumulated  $^{14}\text{C}$  docetaxel for the purposes of an efflux assay in DLKP-A, an important factor when the effectiveness of TKIs as P-gp inhibitors was examined (Section 7). A comparison of 100 nM and 500 nM  $^{14}\text{C}$  docetaxel accumulation alone and in the presence of cyclosporin A revealed 500 nM  $^{14}\text{C}$  docetaxel provided a level of drug accumulation adequate for efflux assays in DLKP-A (Figure 5.3.8). Although 100 nM  $^{14}\text{C}$  docetaxel gave a measurable signal in DLKP-A, 500 nM  $^{14}\text{C}$  docetaxel provided a higher signal allowing detection of a wider range of potential effects. 500 nM is still within therapeutically relevant

concentrations [300]. Including cyclosporin A resulted in higher levels of drug retention but the effects of residual cyclosporin A on  $^{14}\text{C}$  docetaxel efflux in an assay would have needed further examination.

### **8.3.6 Calculation of the mass of docetaxel in cells**

To directly compare the radiolabelled  $^{14}\text{C}$  docetaxel assay to the HPLC based method for taxane measurement, C.P.M. were converted to mass docetaxel (ng). This was achieved by generating a standard curve, plotting C.P.M. against mass docetaxel (Figure 5.3.1). The  $^{14}\text{C}$  docetaxel accumulation assay in DLKP (Section 5.2.4.1A) was then converted from C.P.M. to ng docetaxel/10,000 cells (Figure 5.3.2). The standard concentration of  $^{14}\text{C}$  docetaxel chosen for accumulation studies (100 nM) resulted in 1 ng docetaxel accumulated per 10,000 cells or 100 ng docetaxel accumulated per million cells. This is lower than the mass of docetaxel retained in DLKP on average on exposure to 10  $\mu\text{M}$  docetaxel (466 +/- 110 ng/million cells) (Section 3.7).

## **8.4 Comparison of accumulation assays using radiolabel and HPLC techniques**

A major limitation of the HPLC-based method was the difficulty in identifying competitive inhibitors of P-gp-mediated docetaxel efflux because of the supraphysiological extracellular concentration employed (Section 3.13). The efflux profile of docetaxel in A549 was also inconsistent with the absence of taxane transporters (Section 3.3.2). The radiolabelled-based assay overcame these limitations.

### **8.4.1 Verapamil increased <sup>14</sup>C docetaxel accumulation in DLKP-A and DLKP-TXT**

Co-treatment of DLKP-A with verapamil and a concentration of 100 nM <sup>14</sup>C docetaxel resulted in an increase in docetaxel accumulation (Figure 5.3.3).

All three P-gp modulators produced similar levels of drug resistance reversal in DLKP-A (Figure 5.3.3). Inhibition of P-gp by verapamil resulting in an increase in docetaxel accumulation was apparent, contrary to the same experiment carried out using the HPLC method, Figure 3.9.1, in which the same concentration (100 μM) of verapamil did not affect docetaxel accumulation.

A corresponding comparison of <sup>14</sup>C docetaxel accumulation in the presence of P-gp inhibitors in DLKP-TXT also uncovered the P-gp inhibitory effects of verapamil (Figure 5.3.4), an effect absent when the HPLC-based system was used to quantify docetaxel levels (Figure 3.11.1). This showed the suitability of the <sup>14</sup>C docetaxel assay for examination of docetaxel transport in cell lines expressing lower levels of P-gp. Cyclosporin A and elacridar also elicited relatively large increases in <sup>14</sup>C docetaxel accumulation in DLKP-TXT. Sulindac was shown to have no influence on <sup>14</sup>C docetaxel accumulation in DLKP-TXT. These results confirmed the <sup>14</sup>C docetaxel assay was superior to the HPLC method for docetaxel measurement.

## **8.4.2 Comparison of the accumulation profiles of 100 nM <sup>14</sup>C docetaxel in A549 and A549-Taxol**

It was unexpected that the accumulation of 100 nM <sup>14</sup>C docetaxel was similar between the P-gp over-expressing A549-Taxol and the non-P-gp expressing A549 (Figure 5.3.5). An accumulation assay in A549-Taxol examining a range of <sup>14</sup>C docetaxel concentrations revealed that the decrease in accumulation only initiated at 400 nM <sup>14</sup>C docetaxel (Figure 6.2.3). This would suggest a minimum concentration threshold for activation and/or detection of P-gp-mediated docetaxel efflux in A549-Taxol over the 90 minute time period examined. The lipophilic nature of docetaxel may mean a higher docetaxel concentration (500 nM) is required to increase the rate of passive docetaxel influx to a rate where the influence of P-gp-mediated docetaxel efflux can be observed. Analysis of the major factors affecting the intracellular pharmacokinetics of paclitaxel (extracellular concentration, intracellular binding capacity, intracellular binding affinity and P-gp expression) by computational model analysis predicted that extracellular drug concentration was the most important factor at pharmacological drug levels (100-1000 nM) [302]. Figures 5.3.5 and 6.2.3 may be *in vitro* evidence for the complexity of the intracellular pharmacokinetics of docetaxel in low P-gp-expressing cells at pharmacologically relevant concentrations. Lapatinib and erlotinib increased the accumulation of <sup>14</sup>C docetaxel in A549-Taxol (Figure 7.2.8.1) but this occurred using a concentration of 500 nM <sup>14</sup>C docetaxel, above the threshold value observed in A549-Taxol (Figure 6.2.3). Furthermore, the TKI-related increases in <sup>14</sup>C docetaxel accumulation only became significant at later timepoints for the lower concentrations of lapatinib (Figure 7.2.8.1). These observations indicate that maximising the concentration of the chemotherapeutic agent that the tumour is exposed to is a priority if pursuing the TKI/cytotoxic combinations to circumvent MDR, as suggested in Section 8.6.8.

## **8.4.3 The effects of high extracellular concentrations of docetaxel on efflux profiles in A549 and DLKP**

The influence of the extracellular docetaxel concentration on drug binding was apparent in the HPLC-determined docetaxel efflux profile in A549 in which a

significant reduction in cellular docetaxel was evident 45 minutes after drug removal (Figure 3.3.2). The efflux profile of docetaxel was re-examined with the radiolabel-based assay at three concentrations, 0.1, 1 and 10  $\mu\text{M}$  (Figure 5.3.6). This revealed that the efflux profile was dependent on the concentration of  $^{14}\text{C}$  docetaxel employed to load the cells. Saturation of intracellular and extracellular binding sites and a constant accumulation pressure due to the extracellular/intracellular drug gradient may be an explanation for the HPLC results (Figure 3.3.2) and the docetaxel efflux profile at 10  $\mu\text{M}$  in Figure 5.3.6. Once the docetaxel containing medium is removed, the drug concentration gradient is reversed and excess docetaxel diffuses from the cell. Sang *et al.*, provide evidence of triphasic changes in intracellular to extracellular paclitaxel ratios in MCF-7 breast cancer cells [303]. They postulate that low extracellular paclitaxel concentrations (<100 nM) result in a linear increase in intracellular concentrations before saturation of the high affinity intracellular binding sites (tubulin) while the second phase, between 100 nM and a 1000 nM, exhibit a non-linear relationship between extracellular and intracellular drug concentrations as the intracellular binding sites become saturated [303]. In the third phase, above 1000nM (1  $\mu\text{M}$ ), once the high affinity binding sites are saturated, the relationship returns to a linear function as non-saturable binding becomes the major mode of intracellular drug binding [303]. Docetaxel has a higher affinity for tubulin than paclitaxel and may therefore be expected to be more effective at saturating the high affinity intracellular binding sites [31]. Exposure to 100 nM  $^{14}\text{C}$  docetaxel resulted in an A549 (Figure 5.3.6) and DLKP (Figure 5.3.7) efflux profile that would be expected in cell lines that do not express major levels of taxane efflux mechanisms and retain accumulated drug at the high affinity intracellular binding sites.

#### **8.4.4 Assessment of the radiolabel-based method for docetaxel quantification**

The radiolabel-based transport assay addressed the major disadvantages of the HPLC method:

- Pharmacological levels of docetaxel could be examined.
- The effects of competitive inhibitors are easier to detect.
- The docetaxel efflux profile in A549 and DLKP is consistent with the absence of detectable levels of P-gp.
- Improvement of assay efficiency.

Similar variations of the developed method have been used to detect other radiolabelled drugs such as tritium-labelled [<sup>3</sup>H] paclitaxel and OATP substrates like 17β-D-glucuronide [143], [304]. The extensive optimisation process should mean the developed protocol could easily be adapted for the detection of other radiolabelled drugs.

## 8.5 A docetaxel uptake mechanism in lung cancer

There are a number of reasons why a docetaxel transporter would be of interest in the treatment of lung cancer. A specific docetaxel uptake mechanism could:

- Increase sensitivity to and concentrations of substrate drugs in tissues with expression of the transporter
- Be useful in predicting chemotherapeutic drug response
- Be a potential therapeutic target
- Lead to drug:drug interactions between substrate compounds

### 8.5.1 Docetaxel influx in the human lung cancer cell lines DLKP and A549

It is widely believed that many MDR-type drugs (e.g. taxanes, anthracyclines) enter cells by passive diffusion through the plasma membrane [305]. Active systems of influx and efflux for other agents such as anti-folate therapies like methotrexate and the platinum-based drugs cisplatin, carboplatin and oxaliplatin have been described [306]. Smith *et al.*, reported that OATP1B3 (SLCO1B3, OATP8) is capable of stimulating uptake of paclitaxel and docetaxel, using oocyte injection experiments, an artificial *in vitro* method for determining transporter affinity for substrates [307]. *Xenopus laevis* oocytes were injected with OATP1B3 cRNA and incubated with radiolabelled docetaxel or paclitaxel and the intracellular taxane concentration of the oocytes determined [307]. Kobayashi *et al.*, reported similar findings for OAT2 (SLC22A7)-expressing oocytes with respect to paclitaxel [193].

The discovery that members of the SLCO and SLC22 families of transporters are involved in the hepatic transport of the taxanes has raised the possibility of the existence of further tissue-specific docetaxel transporters. OATP1B3 and OAT2 do not utilise ATP directly but do rely on the concentration gradients of co-transported compounds that may be maintained through energy-dependent means [308], [201]. A number of studies have recently shown that the SLCO family members transport a

wide range of amphipathic compounds in a sodium-independent manner accepting glutathione in exchange for an organic anion while the SLC22 family are passive diffusion organic cation transporters [308], [201].

There is no evidence in the literature for an energy-dependent docetaxel, or indeed paclitaxel, transport mechanism responsible for drug uptake in lung tissue. The study of docetaxel influx in this project was divided into exploration of two areas, energy-dependent docetaxel transport and OATP-mediated docetaxel transport. All the  $^{14}\text{C}$  docetaxel accumulation studies carried out utilised the protocol developed in Section 5.

### **8.5.2 Energy-dependent docetaxel transport**

Energy-dependent drug transport has a number of characteristics:

- Energy-dependent drug transport is saturable, that is, it reaches a maximum rate. Saturation is the point at which all transporters present are being utilised and transport is capacity limited.
- It is temperature-dependent. Changes in temperature affect the enzymatic processes, such as ATPase function, involved in active drug transport.
- It is ATP-dependent. ATPase conversion of ATP to ADP provides the energy required for drug transport.

Each of these factors were examined and compared in the adenomatous NSCLC cell-derived A549 and squamous cell-derived DLKP to determine if an energy-dependent docetaxel influx mechanism is present.

### **8.5.3 $^{14}\text{C}$ docetaxel accumulation is saturable in DLKP but not A549**

The linear trend observed for  $^{14}\text{C}$  docetaxel accumulation in A549 is indicative of transport that is not saturable up to 500 nM (Figure 6.2.1). In contrast,  $^{14}\text{C}$  docetaxel accumulation was saturable in DLKP (Figure 6.2.2). Saturation alone is not conclusive evidence of an energy-dependent transport mechanism but it does imply the presence of a rate-limiting transport step.

$^{14}\text{C}$  docetaxel saturation was also studied in A549-Taxol and DLKP-Mitox cells. The over-expression of P-gp in A549-Taxol would have been expected to reduce the accumulation of  $^{14}\text{C}$  docetaxel compared to the A549 parent cell line (Figure 6.2.3). As expected, the levels of  $^{14}\text{C}$  docetaxel accumulated were indeed lower for all concentrations measured except for 300 nM and 400 nM, but these values were within the standard deviation range for the A549 values. The  $^{14}\text{C}$  docetaxel accumulation profile in DLKP-Mitox was markedly different from the parent DLKP cell line (Figure 6.2.4). The reduced accumulation of  $^{14}\text{C}$  docetaxel relative to DLKP could be due to increased efflux due to expression of a docetaxel efflux pump other than P-gp. DLKP-Mitox does not express P-gp (Figure 3.2.1) and the BCRP it is known to express does not transport docetaxel [260]. Another possibility is decreased accumulation due to down-regulation of an unknown influx mechanism.

#### **8.5.4 $^{14}\text{C}$ docetaxel accumulation is temperature-dependent in A549 and DLKP**

The use of temperature change (0-37 $^{\circ}\text{C}$ ) to affect drug accumulation in order to demonstrate the presence of an active transport mechanism is an established technique [309], [310]. Lower temperatures would be expected to reduce the rates of reaction and catalytic activities of proteins associated with transport. Accumulation of  $^{14}\text{C}$  docetaxel was reduced at 4 $^{\circ}\text{C}$  and 27 $^{\circ}\text{C}$  in both A549 (Figure 6.3.1) and DLKP (Figure 6.3.2), indicative of a temperature-dependent accumulation rate. Temperatures above 37 $^{\circ}\text{C}$  have not generally been examined in the literature. This is presumably due to the unreliable integrity of the cell membrane above a temperature of 37.2 $^{\circ}\text{C}$ . The rapid decrease in  $^{14}\text{C}$  docetaxel accumulation occurring after 60 minutes at 46 $^{\circ}\text{C}$  was accompanied by visual changes in cell morphology, including poorly defined outlines and morphological homogenisation (observation). It could be presumed that increased levels of accumulation observed at 41 $^{\circ}\text{C}$  and in the first 60 minutes at 46 $^{\circ}\text{C}$  are similarly related to changes in membrane state but further work would be needed to confirm this. The difference between  $^{14}\text{C}$  docetaxel accumulation at 27 $^{\circ}\text{C}$  and 37 $^{\circ}\text{C}$  in DLKP is consistently greater than the difference observed in A549. This suggests  $^{14}\text{C}$  docetaxel accumulation is more temperature sensitive in DLKP than A549.

The temperature-dependent changes in  $^{14}\text{C}$  docetaxel accumulation alone are not definitive evidence of the existence of an ATP-dependent transport mechanism as anion exchangers such as the OATP family are also affected by temperature changes as well as membrane fluidity and flux. A fuller picture of the effect of temperature on  $^{14}\text{C}$  docetaxel accumulation in DLKP and A549 could be gained by examining accumulation at varying temperatures and concentrations.

### **8.5.5 Depletion of ATP levels by sodium azide, 2-deoxyglucose and antimycin A in A549 and DLKP**

A decrease in cellular ATP levels affects the efficiency of ATP-dependent transporters. Previous studies carried out involving ATP-depletion agents assumed ATP levels were reduced (Section 3). The extent of ATP depletion caused by glucose-free medium alone and in combination with sodium azide, 2-deoxyglucose and antimycin A was measured in A549 and DLKP using a bioluminescent luciferase-based assay (Figures 6.4.1 and 6.4.2). Although a source of ATP, it was decided to include 5% FCS in the assays to maintain uniformity between saturation temperature and ATP depletion assays. While none of the compounds alone completely eliminated ATP, a combination of sodium azide, 2-deoxyglucose and antimycin A in glucose-free medium achieved 92 % and 96 % reductions in ATP levels for DLKP and A549, respectively (Figure 6.4.3, Table 6.4.1). These reductions are comparable to those achieved in other breast and lung cancer cell lines [311], [312].

### **8.5.6 ATP depletion reduced $^{14}\text{C}$ docetaxel accumulation in DLKP and increased $^{14}\text{C}$ docetaxel accumulation in A549**

Pre-treatment of DLKP with the ATP inhibitors resulted in a decrease in  $^{14}\text{C}$  docetaxel accumulation (Figure 6.5.1 A). The decrease in  $^{14}\text{C}$  docetaxel accumulation was visible directly when comparing medium conditions within pre-treated and non-pre-treated cells, but only at the 120 minute timepoint (Figures 6.5.1 A). Comparison of each individual condition (normal medium, glucose-free medium and glucose-free medium and ATP inhibitors) under pre-treated and non-pre-treated conditions defined the reduced  $^{14}\text{C}$  docetaxel accumulation clearly (Figure 6.5.1 B). This representation

of the data revealed that the 30 minute pre-treatment with the ATP inhibitors in DLKP subsequently resulted in lowered levels of  $^{14}\text{C}$  docetaxel accumulated under all conditions (Figure 6.5.1 B).

The ATP inhibitor study in A549 revealed an increase in  $^{14}\text{C}$  docetaxel accumulation, concomitant with inhibition of an efflux mechanism or stimulation of a non-active uptake mechanism by one of the ATP inhibitors used. While 2-deoxyglucose is taken into the cell through the glucose uptake system, there is no evidence that sodium azide, 2-deoxyglucose or antimycin A are substrates for an influx mechanism that could be associated with docetaxel accumulation. A549 is reported to express MRP-2 and the presence of OATP family members capable of bi-directional transport cannot be discounted [276], [195]. Pre-treatment with ATP inhibitors did not affect  $^{14}\text{C}$  docetaxel accumulation in normal and glucose-free medium (Figure 6.5.2 B). Pre-treatment with ATP inhibitors produced an initial minor increase in  $^{14}\text{C}$  docetaxel accumulation compared to the non-pre-treated cells but produced comparable results at later timepoints (Figure 6.5.2 B).

The recovery rate of the ATP levels in DLKP and A549 after ATP inhibitor exposure has not been studied, so it may be that A549 has a quicker response and recovery time to ATP inhibitors than DLKP. The rate of ATP recovery could be determined experimentally by exposing cells to ATP depleting agents for a set period then incubating cells in medium, and determining ATP levels at set intervals thereafter.

In summary,  $^{14}\text{C}$  docetaxel accumulation in DLKP is saturable (Figure 6.2.2), temperature-dependent (Figure 6.3.2) and ATP-dependent (Figures 6.5.1 A and 6.5.1 B) fulfilling the criteria expected for an energy-dependent influx mechanism.

### **8.5.7 Possible docetaxel transport mechanisms in DLKP**

Speculation based on current results for possible uptake mechanisms in DLKP is difficult for a number of reasons. Saturation and temperature-dependence are characteristic of all carrier-mediated transport mechanisms. ATP-dependence may be a result of transporters being directly dependent on ATP (contain an ATPase component) or indirectly relying on ATP to maintain electrochemical gradients (secondary active transport). The ability of anion exchangers such as the OATP

transporters to translocate drugs in a bi-directional manner further complicates the situation. Bi-directional transport can be dependent on the site of protein localisation and/or changes in substrate concentrations [195].

The two available sources of information for speculation on the possible transporters in the NSCLC cell line DLKP are the literature and microarray data generated from the cell line. Studies on uptake mechanisms for the taxanes in tissues other than the liver are in short supply as it was generally assumed that taxane tumour uptake is passive in nature. Ehrlichova *et al.*, studied  $^{14}\text{C}$  paclitaxel in adriamycin-sensitive (P-gp-negative) MDA-MB-435 and adriamycin-resistant (P-gp-positive) NCI/ADR-RES breast cancer cell lines [285]. They found that  $^{14}\text{C}$  paclitaxel accumulation (20-500 nM) was saturable in MDA-MB-435. Additionally, SB-T-1214, a novel taxane analog was found to cause dose-dependent inhibition of  $^{14}\text{C}$  paclitaxel uptake in both MDA-MB-435 and NCI/ADR-RES. The authors suggested that these effects could be due to an active inward transport mechanism. It is also worth noting that  $^{14}\text{C}$  paclitaxel efflux was stimulated by high concentrations of verapamil (100 – 400  $\mu\text{M}$ ) in the MDA-MB-435 cell line. MDA-MB-435 was shown to express MRP-2 and the authors discussed the possibility that stimulation of MRP-2 could be responsible for the increased  $^{14}\text{C}$  paclitaxel efflux.

Ehrlichova *et al.*, provided circumstantial evidence for a taxane uptake mechanism in a breast cancer cell line but others have found members of the SLC superfamily of transporters that mediate taxane transport. The SLC family of transporters are the subject of intense interest at present due to advances in identification of family members and their recently appreciated importance in vectorial drug transport. Drug vectoring occurs in polarised tissues involved in drug disposition (liver, kidney) and restricted distribution to protected sites (blood-brain barrier) and so plays a vital role in drug absorption, disposition, metabolism and excretion. Polarised cells asymmetrically express a variety of drug transporters on the apical (e.g. MRP-2) and basolateral sides (e.g. SLCO1B1), resulting in transcellular drug transport in a specific direction.

Smith *et al.*, found that OATP1B3 (SLC01B3) was able to stimulate uptake of radiolabelled paclitaxel and docetaxel. OAT2 (SLC22A7) is a sodium-independent multi-specific organic anion/dimethyldicarboxylate exchanger expressed predominantly in the liver that has been shown to mediate transport of dehydroepiandrosterone sulfate (DHEAS), prostaglandin  $\text{E}_2$ , 5-fluorouracil and

paclitaxel [193]. OATP1B3 and OAT2 expression has not been reported in normal lung tissue in previous studies [203], [313].

A search of microarray data obtained from DLKP, DLKP-A, A549 and A549-Taxol and analysed by Genespring software, indicated SLC22A3 (OCT3, EMT), SLC22A5 (OCTN2) and SLC22A18 (HET, ITM, BWR1A, IMPT1, TSSC5, ORCTL2, BWSCR1A, p45-BWR1A) mRNA transcripts to be present (Appendix A, Table A2). The presence of SLC22A3 and SLC22A5 mRNA is consistent with previous studies reporting expression of these transporters in the lung [201]. SLC22A3 is a passive diffusion organic cation transporter, while SLC22A5 is a sodium-dependent carnitine co-transporter that can also function as a sodium-independent organic cation transporter [201]. SLC22A18 may be associated with tumorigenesis in Wilm's disease, breast and lung cancers as well as the transport of chloroquine- and quinidine-related compounds in the kidney [314], [315], [316]. At this point, it is important to note that the microarray data was only used as an exploratory tool to provide a starting point to indicate which SLC family members were most likely to be expressed in A549 and DLKP. mRNA levels do not necessarily correlate directly to protein expression. Protein detection techniques are the only way to positively confirm the presence of identified transporters. This applies to all references to the microarray data in this discussion.

Expression of all members of the OATP/SCLO family was absent according to the DLKP microarray data (Appendix A, Table A1). This was unusual as studies have shown expression of a number of OATP members in normal lung tissue [268]. The broad specificity OATP inhibitor bromosulphophthalein (BSP) had no effect on docetaxel accumulation in DLKP (Figure 5.5.1), offering confirmatory evidence that OATP family members were absent. Interestingly, digoxin did reduce docetaxel accumulation in DLKP, (Figure 5.5.2). It is possible that DLKP expresses a protein that transports digoxin and not BSP but there is insufficient data to provide evidence for this. The mRNA for the digoxin transporter OATP1B3 is absent from DLKP according to microarray results and there is no evidence for the ability of SLC22A3 or SLC22A18 to transport digoxin. Digoxin has been shown to have no effect on SLC22A5-mediated carnitine transport [317]. Investigation of the effects of digoxin on docetaxel accumulation in DLKP warrants further investigation.

Taking the results at face value, none of the transporters discussed fit the saturable, temperature-dependent and ATP-dependent nature of  $^{14}\text{C}$  docetaxel accumulation observed in DLKP. In order to identify the likely mechanism involved, future studies should examine putative inhibitors of ATP-dependent transporters that are known to be expressed in lung tissue. These target transporters could be prioritised according to the DLKP microarray data. The involvement of anion exchangers should also be explored by examining docetaxel transport in combination with anion exchange-associated substrates such as glutathione, carnitine, carboxylate and sodium. These assays would also function to narrow down possible candidate transporters. Rather than looking at total cellular docetaxel accumulation, the use of monolayer transport assays that distinguish between apical and basolateral transport may also be helpful in identifying transporters that may have polarised expression on one cell membrane surface.

### **8.5.8 OATP-mediated docetaxel transport in A549**

As mentioned previously, members of the OATP/SLCO transporter family are expressed in the lung (Section 6.1). With the knowledge that OATP1B3 can transport docetaxel, a study of the affects of various OATP inhibitors on  $^{14}\text{C}$  docetaxel accumulation in A549 and DLKP was designed [192]. Alterations in  $^{14}\text{C}$  docetaxel accumulation due to treatment with such inhibitors could be indicative of OATP-mediated docetaxel transport in these cell lines.

Exploratory examination of DNA microarray analysis carried out on the A549 cell line revealed RNA expression levels for OATP3A1 and OATP4A1 and particularly high levels of OATP1B3 (Appendix A, Table A1).

Initial experiments involving OATP inhibitors revealed that BSP and digoxin reduced  $^{14}\text{C}$  docetaxel accumulation in A549 (Figure 6.6.1 and Figure 6.6.2). For this reason and the absence of OATP mRNA expression in DLKP according to the microarray data, the A549 cell line was chosen for the assays involving the more specific OATP inhibitors (indocyanine green, DHEAS, prostaglandin  $\text{E}_2$ , tri-iodo thyroxine ( $\text{T}_3$ )).

### 8.5.9 Indocyanine green increases <sup>14</sup>C docetaxel accumulation in A549 and DLKP

Indocyanine green (ICG, cardiogreen) is used intravenously as a diagnostic aid in the determination of blood volume, cardiac output and hepatic function, and as a tissue stain for imaging retinal and choroidal vasculatures [318], [319]. Indocyanine green had unexpected effects on <sup>14</sup>C docetaxel accumulation in A549 and DLKP. Its uptake is mediated by OATP1B1 in the liver and BSP is also an OATP1B1 substrate [320]. The effect of ICG on <sup>14</sup>C docetaxel accumulation was examined to determine if OATP1B1 was involved in the initial BSP-related decrease in <sup>14</sup>C docetaxel accumulation levels observed in A549 (Figure 6.6.1). The increased amount of <sup>14</sup>C docetaxel accumulated in A549 due to ICG is most likely not OATP-related. A similar increase was shown in DLKP (Figure 6.6.4), a cell line in which the OATP1B1 inhibitor BSP had no effect on <sup>14</sup>C docetaxel accumulation (Figure 6.6.1). The diminished increase in drug accumulation at the highest concentrations of ICG in A549 and DLKP are most likely due to the high DMSO levels (Section 8.5.13).

The mechanism of the ICG effect may merit investigation for the possibility that ICG could have the potential to increase tumour docetaxel levels *in vivo*. ICG uptake in HaCaT keratinocytes was saturable, highly cumulative and inhibited by BSP [321]. A study to determine if the ICG <sup>14</sup>C docetaxel accumulation effect in A549 and DLKP is reversible by BSP would provide evidence for the involvement of the OATP family in the effect. ICG is amphiphilic and has been shown to interact strongly with phospholipids, the main constituent of cellular plasma membrane bi-layers [319]. There is evidence that ICG can bind both the hydrophilic and lipophilic structures of phospholipids at the same time [319]. Such interactions could alter the structure and permeability of phospholipid bi-layers and may be an explanation for the increased <sup>14</sup>C docetaxel levels observed in A549 and DLKP.

Photoactivation of ICG by irradiation has been shown to effectively kill human keratinocytes, fibroblasts and squamous cell carcinoma cells *in vitro* [321]. Identification of a possible carrier, other than OATP1B1, could further the potential of phototherapies in suitable cancers.

### 8.5.10 T<sub>3</sub> and DHEAS increase <sup>14</sup>C docetaxel accumulation in A549

The BSP and digoxin-related decrease in <sup>14</sup>C docetaxel accumulation in A549 suggested involvement of the OATP family in docetaxel uptake. The subsequent results for indocyanine green, the OATP1B1 modulator and cyclosporin A (Figure 6.6.6), a reported OATP1B1 and OATP1B3 modulator, suggest that OATP1B3 or OATP1B1 are not involved in <sup>14</sup>C docetaxel accumulation in A549 [264],[265].

Digoxin, indocyanine green and cyclosporin A interact with OATPs that are inhibited by BSP, but are not necessarily OATPs whose expression has been reported in lung tissue. OATP2B1 (OATP-B) is found in lung tissue and BSP is a substrate [266]. More specific to this research, Northern blot analysis has detected OATP3A1 (OATP-D) at the mRNA level in A549 [267]. OATP2B1, 3A1 and 4A1 (OATP-E) and prostaglandin transporter (PGT) expression has been found in lung tissue by RT-PCR in a study by Tamai *et al.* [268]. OATP1A2 (OATP-A) and OATP1B1 were not detected in lung tissue [268]. Microarray analysis reported mRNA presence for OATP1B3, 3A1 and 4A1 in A549 (Appendix A, Table A1). Although cyclosporin A had no effect on <sup>14</sup>C docetaxel accumulation in A549 (Figure 6.6.6), further examination of this transporters influence on docetaxel transport in A549 is warranted. OATP1B3 is still the only documented member of the SLCO family to transport the taxanes. BSP, a broad specificity inhibitor capable of modulating OATP1B3, reduced docetaxel accumulation in A549 (Figure 6.6.1) and the protein levels of OATP1B3 expressed in A549 are still unknown [307]. It is possible that cyclosporin A was not present at the optimum conditions necessary for inhibition of OATP1B3 transport.

The most specific substrates that could potentially inhibit OATP2B1, -3A1 and -4A1 competitively are dehydroepiandrosterone sulfate (DHEAS) [263], prostaglandin E<sub>2</sub> (PGE<sub>2</sub>) [267] and thyroid hormone (Tri-iodothyronine, T<sub>3</sub>) [269]. BSP is a substrate for both OATP2B1 and OATP4A1, and considering the decrease in <sup>14</sup>C docetaxel uptake associated with BSP, these transporters are candidates for the inhibition of docetaxel accumulation in A549. OATP3A1 has a similar drug transport profile to PGT. The fact that PGE<sub>2</sub> did not affect <sup>14</sup>C docetaxel accumulation would suggest that OATP3A1 is not involved in <sup>14</sup>C docetaxel uptake in A549 (Figure 6.6.7). DHEAS and T<sub>3</sub> did affect <sup>14</sup>C docetaxel accumulation (Figures 6.6.5 and 6.6.8). Both produced minor but significant increases in <sup>14</sup>C docetaxel accumulation. Combined with the

increase in accumulation due to ATP inhibition (Figure 6.4.2), the most plausible explanation is the existence of an ATP-dependent docetaxel efflux mechanism that can be inhibited by DHEAS and T<sub>3</sub>. The indocyanine green-related increases in <sup>14</sup>C docetaxel accumulation are most likely not due to OATP or any putative efflux mechanism. The reduction in <sup>14</sup>C docetaxel accumulation due to BSP and digoxin, however, may still be down to inhibition of an influx mechanism other than OATP. The possibility that OATP bi-directional transport is responsible is plausible given the small <sup>14</sup>C docetaxel increase observed.

### **8.5.11 ATP-dependent docetaxel transporter in A549**

MRP-2 is the best candidate to explain the ATP-dependent (Figure 6.5.2A) and DHEAS-dependent (Figure 6.6.5) increases in <sup>14</sup>C docetaxel accumulation in A549. A549 expresses detectable levels of MRP-2 protein but not P-gp (Figure 3.2.1) [276]. DNA microarray data also provides corroborative evidence of this MRP-2 expression (Appendix A, Table A3). There are conflicting reports over the ability of MRP-2 to transport DHEAS. Zelcer *et al.*, have reported no direct transport of DHEAS in membrane vesicles containing MRP-2 or MRP-3 [322]. On the other hand, Spears *et al.*, suggest that OATP1B1 and MRP-2 are mediators of DHEAS and rifampicin directional trans-epithelial transport in porcine LLC-PK1 [323]. Spears *et al.*, do acknowledge that similar work carried out in canine MDCKII-derived cell models by Sasaki *et al.*, found no increase in the basolateral to apical transport of DHEAS [323], [324]. An examination of DHEAS transport and MRP-2 ATPase activity would elucidate the involvement of MRP-2 in docetaxel transport in A549. The other compound to increase <sup>14</sup>C docetaxel accumulation in A549 was tri-iodothyroxine (T<sub>3</sub>) (Figure 6.6.8). T<sub>3</sub> has been shown to be involved in the regulation of MRP-2 protein and mRNA expression [325]. An exploration of the ability of MRP-2 to transport T<sub>3</sub> would be of interest. Future work to ascertain if MRP-2 is a mediator of <sup>14</sup>C docetaxel efflux in A549 would include the determination of MRP-2 protein levels in A549, the study of DHEAS and T<sub>3</sub> transport in A549 and MRP-2 ATPase assays and a study of the protein levels of the other known energy-dependent docetaxel transporter, MRP-7 [143]. DNA microarray data suggests the presence of MRP-7 mRNA in A549 (Appendix A, Table A3).

### **8.5.12 Future investigation of cisplatin transport by SLC family members in A549 and DLKP**

Two members of the SLC superfamily, SLC7A11 (xCT) and SLC31A (Ctr1, copper transporter 1) have been implicated in chemosensitivity to cisplatin [306]. mRNA for both these transporters was present in DLKP and A549 according to microarray data (Appendix A Table A4). Given the importance of cisplatin in NSCLC, investigation of the expression and possible involvement of these transporters in sensitivity to cisplatin and cisplatin resistance in platinum-selected variants of NSCLC cell lines (A549 and DLKP) would be of merit.

### **8.5.13 DMSO decreases <sup>14</sup>C docetaxel accumulation**

In the <sup>14</sup>C docetaxel transport assays, high DMSO concentrations were associated with decreased <sup>14</sup>C docetaxel accumulation in DLKP (Figure 6.6.2 and 6.6.4). DMSO caused no significant changes in <sup>14</sup>C docetaxel accumulation in A549 at the concentrations examined (Section 6.6). Of the two cell lines, DLKP was more sensitive to the presence of DMSO (Figure 6.6.4). DMSO increases the permeability of cell membranes, the basis for its use in the treatment of vesicant chemotherapeutic extravasation in the clinic [326]. Extravasation occurs when chemotherapeutic drug leaks from a vein or an I.V. catheter into surrounding tissue. Studies on the molecular mechanism of action of DMSO reveal that DMSO causes thinning of phospholipid membranes at low concentrations and pore formation and membrane disintegration at high concentrations [327]. The evidence suggests that increasing DMSO concentration should increase membrane fluidity and permeability and increase docetaxel accumulation. This is contrary to the observed results. Disruption of plasma membrane integrity could affect the function of a specific drug uptake mechanism. This is a possible explanation for the decrease in <sup>14</sup>C docetaxel accumulation in DLKP that is consistent with the evidence for an energy-dependent uptake mechanism in this cell line.

## 8.6 Modulation of P-gp-mediated docetaxel transport

Having considered the mediation of docetaxel uptake in NSCLC, modulators of P-gp-mediated docetaxel efflux, the second major aim of the project, was considered. The ability of a number of P-gp modulators to overcome tumour resistance has been tested *in vivo* [280]. Many of these first (cyclosporin A, verapamil) and second generation (PSC833) drugs failed in attempts to circumvent MDR due to intolerable toxicity, poor bioavailability and lack of specificity [280]. In a different strategy, that takes advantage of pharmacokinetic interactions, cyclosporin A and PSC833 have proved useful in increasing the oral bioavailability and brain penetration of the taxanes when so utilised in clinical and pre-clinical studies [328]. Tariquidar is the third generation inhibitor considered to have the most potential, having successfully completed Phase I and II trials but there is little information on its pharmacokinetic interactions with cytotoxic agents as yet [329]. Recent reports of the ability of tyrosine kinase inhibitors to interact with mediators of MDR raise new potential for this class of drug [253]. In addition to their primary function of c-ErbB inhibition, the low toxicity tyrosine kinase inhibitors, gefitinib, erlotinib and lapatinib may provide the balance between bioavailability and P-gp inhibition at pharmacologically achievable doses necessary to circumvent MDR.

### 8.6.1 Distinct manner of lapatinib's interaction with P-gp

Results indicate that lapatinib interacts with P-gp in a manner distinct from that of gefitinib and erlotinib. Lapatinib is an effective inhibitor of verapamil-stimulated P-gp ATPase activity while erlotinib and gefitinib have very little direct P-gp ATPase inhibitory activity even at elevated concentrations (Figure 7.2.2.1A). The energy released from ATP hydrolysis is used to drive drug movement. A strong substrate will stimulate P-gp ATPase activity resulting in increased levels of ATP hydrolysis. P-gp ATPase studies showed erlotinib to be a strong P-gp substrate while gefitinib was transported at a slower rate (Figure 7.2.2.1B). The gefitinib results were consistent with previous findings by Ozvegy-Laczka *et al.* [251]. In contrast to gefitinib and erlotinib, lapatinib was a poor activator of P-gp ATPase activity which suggests, when combined with the ATPase inhibition assay results, that it is a slowly transported

substrate with a high affinity for a P-gp binding site (Figure 7.2.2.1). Lapatinib may therefore be more effective at overcoming P-gp-mediated resistance to chemotherapeutic agents than erlotinib and gefitinib at equal concentrations.

ATPase assays alone do not definitively classify compounds as P-gp substrates or inhibitors. Verapamil, for instance, is a strong P-gp ATPase activator but it is not transported in monolayer efflux assays [330]. Direct measurement of compound transport using sensitive techniques such as mass spectrometry or radiolabelled drug transport assays would provide the best verification for a substrate or inhibitor. In order to evaluate the three TKIs as possible MDR modulators, the effects of the TKIs in cytotoxic drug transport and combination proliferation assays were examined to complement the ATPase findings.

### **8.6.2 Potency of lapatinib in docetaxel combination proliferation and transport assays**

*In vitro* docetaxel transport assays confirmed lapatinib as the most potent P-gp modulator of the TKIs tested. Using a physiologically-relevant concentration of radiolabelled docetaxel, it was shown that each of the TKIs increased the net accumulation of docetaxel in the P-gp-over-expressing DLKP-A cell line (Figure 7.2.3.1). Lapatinib produced near maximal P-gp inhibition and very significantly increased the accumulation of docetaxel at concentrations of 1-2.5  $\mu$ M. This observation is particularly noteworthy as lapatinib serum levels peaked at approximately 2-4  $\mu$ M when patients received a 1250 -1,600 mg dose [273].

Although cyclosporin A was a better inhibitor of verapamil-stimulated P-gp activity in the purified ATPase assay (Figure 7.2.2.1), lapatinib was more effective at increasing P-gp-mediated docetaxel accumulation in DLKP-A (Figure 7.2.3.1). This observation possibly reflects differences in transport rates between the purified insect vesicle preparation and live human cancer cell P-gp models, a point discussed in further detail later with relation to the BCRP ATPase assays (Section 8.8). A greater affinity of lapatinib over cyclosporin A for binding site of docetaxel on P-gp is another possibility. A control experiment in the parent DLKP cell line confirmed the

P-gp specific nature of the TKIs in DLKP-A (Figure 7.2.3.2). The effect of gefitinib, erlotinib and lapatinib on docetaxel efflux was also tested, with lapatinib, predictably, proving to be the most potent inhibitor of docetaxel efflux in DLKP-A at the concentrations tested (Figure 7.2.4.1).

### **8.6.3 Lapatinib potentiates epirubicin toxicity and accumulation through inhibition of P-gp**

Using direct quantitation assays and confocal microscopy in DLKP-A cells, it was found that concurrent incubation with lapatinib increased the net accumulation of another P-gp substrate, epirubicin, in a concentration-dependent manner (Figure 7.2.5.1). Concentrations of 1  $\mu$ M lapatinib and above increased the concentration of the anthracycline, particularly in the nucleus of the cells, while higher levels increased both nuclear and cytoplasmic levels of epirubicin. Erlotinib and gefitinib also proved capable of inhibiting epirubicin efflux in DLKP-A at a concentration of 5  $\mu$ M (Figure 7.2.5.2).

P-gp detected in the plasma membrane, nuclear membrane and intracellular organelles of cancer cells has been associated with acquired and intrinsic drug resistance [293], [331]. P-gp protects the cell by extruding epirubicin and lowering intracellular drug concentrations. Given the nuclear primary target of epirubicin action, inhibition of P-gp, allowing the drug to permeate to the nucleus, is likely the major source of the observed potentiation in epirubicin toxicity.

### **8.6.4 IC<sub>50</sub> Determinations in DLKP, DLKP-A, A549 and A549-Taxol**

IC<sub>50</sub> determinations in the NSCLC cell lines revealed little influence of P-gp on TKI efficacy (Table 7.2.6), consistent with previous findings by Kitazaki *et al.* [107]. The sizable taxane and anthracycline resistance conferred by P-gp over-expression in DLKP-A did not translate to similar levels of TKI resistance. This is most likely due to the low tyrosine kinase receptor levels in these cell lines. The amount of drug in the cells was of no consequence due to low level expression of target receptors. Lapatinib

proved to be the most potent TKI in all NSCLC cell lines, irrespective of EGFR and Her-2 status.

The high concentrations of TKIs that were needed to produce toxicity in these cells were also likely to be due to the low tyrosine kinase receptor expression levels (Figure 7.2.1.1). The observed toxicity at high concentrations may be generated by a more non-specific toxic effect.

Unexpectedly, P-gp expression in the taxane-selected A549-Taxol did not result in resistance to epirubicin. The existence of genetic P-gp polymorphisms may offer an explanation for this observation although the influence they have on substrate disposition is controversial [332].

### **8.6.5 Implications of combination proliferation assays**

Combination toxicity assays of cytotoxic P-gp substrates plus TKIs in the resistant A549-Taxol and DLKP-A cell lines yielded strong cytotoxic synergy (Figure 7.2.7.1 and Figure 7.2.7.2). This was not evident with the non-P-gp substrate, cisplatin. Further observations, employing higher cisplatin concentrations, suggest that all three TKIs may partially antagonise the actions of cisplatin in DLKP-A (Appendix A, Figure A1). Other pre-clinical studies of gefitinib and cisplatin have yielded conflicting observations of synergy or antagonism [333]. Two clinical studies utilising chemotherapy regimens containing cisplatin and carboplatin in combination with gefitinib, failed to meet either the primary end point of survival or the secondary end points of time to disease progression or response rates [334]. Further investigation is required to identify the cause of the cisplatin antagonism in our system and the possible clinical implications, particularly in NSCLC treatment, where the platinum drugs are a mainstay treatment. Potentiation of epirubicin toxicity by the TKIs in the non-P-gp-expressing A549 and DLKP cell lines was not anticipated (Figure 7.2.7.1 and Figure 7.2.7.2). Inhibition of other putative epirubicin efflux mechanisms and interactions between pathways associated with tyrosine kinase-mediated signalling pathways and epirubicin toxicity may play a role. The effect is unlikely to be EGFR-related due to presence of the phenomenon in the EGFR-negative DLKP cell line (Figure 7.2.1.1).

### 8.6.6 Docetaxel accumulation in A549-Taxol

While DLKP-A is an ideal model in which to study the effects of putative P-gp inhibitors, the extreme levels of P-gp present confer significant resistance to a number of important chemotherapeutic agents. The level of docetaxel resistance present in the A549-Taxol cell line may be closer to that observed *in vivo* [111] (Table 7.2.6). The ability of erlotinib and lapatinib to increase accumulation of a physiologically relevant concentration of docetaxel (500 nM) in the A549-Taxol cell line over a time period within the exposure profile of both docetaxel [300] and each TKI is indicative of a feasible therapeutic strategy for P-gp inhibition (Figure 7.2.8.1). Erlotinib and lapatinib were selected as they represented the most effective ATPase activator and inhibitor, respectively, of the three TKIs examined. Lapatinib was more effective than erlotinib at the clinically relevant concentrations of 0.25  $\mu\text{M}$  and 1  $\mu\text{M}$ .

### 8.6.7 Negative effects of TKI P-gp inhibitor

The anatomical localisation (luminal surface of intestinal epithelium, bile canalicular membrane of hepatocytes, placenta, blood-brain barrier) and its broad substrate specificity means P-gp plays a major role in drug absorption and disposition [335]. P-gp inhibitors such as cyclosporin A, PSC833, imatinib and elacridar have been shown to increase the bioavailability and central nervous system penetration of paclitaxel and docetaxel in clinical and pre-clinical studies [328]. Lapatinib-mediated P-gp inhibition could partly reduce the clearance of P-gp substrate cytotoxics to a greater degree than gefitinib and erlotinib, affecting the pharmacokinetics and pharmacodynamics of concurrently administered P-gp substrate cytotoxics. This effect would be most pronounced in compartments in the body which are especially dependent on P-gp to provide protection from the toxic effects of drugs, e.g. certain stem cell populations [336], [337]. Clinical studies of docetaxel, paclitaxel and epirubicin with lapatinib may provide a better insight. To date, no adverse interactions have been observed between the taxane, paclitaxel, and lapatinib [338], [339]. A phase I study of docetaxel and lapatinib has been completed (NCT00148902). A number of phase I, II and III trials are planned combining both docetaxel and paclitaxel with lapatinib in Her-2-positive breast cancer (NCT00450892 and NCT00356811). A Phase I clinical

study (NCT00313599) examining paclitaxel and lapatinib treatment in a broad range of tumours, including lung cancer, is currently recruiting patients. Two clinical trials involving lapatinib in the treatment of advanced metastatic breast cancer are currently recruiting in Ireland. These trials are a Phase IV trial combining lapatinib and capecitabine in patients whose breast cancer has progressed on other therapies (NCT00338247), and a phase I/II trial involving lapatinib in combination with docetaxel and trastuzumab in Her-2 overexpressing, and previously untreated, metastatic breast cancer (NCT00251433).

### **8.6.8 Applications of TKIs in combination chemotherapy regimen and as P-gp modulators in the clinic**

The results presented suggest an application for the TKIs, particularly lapatinib, as MDR modulators in P-gp-positive tumours in combination with P-gp substrate chemotherapy agents such as docetaxel and epirubicin, irrespective of EGFR and Her-2 status (Section 7). Anthracycline/TKI combinations may be capable of additional anti-cancer actions, due to potentiation of toxicity, as observed in our study, even in the cell lines with little or no P-gp. Lapatinib mono- and combination therapies may be useful in the treatment of NSCLC, where a taxane/platinum combination is a standard first line therapy for advanced NSCLC [340]. Gefitinib and erlotinib have achieved most clinical success in a sub-population of NSCLC patients with mutated forms of EGFR [341]. Lapatinib has been shown to bind the inactive form of EGFR rather than the active form bound by erlotinib [250]. A slower off-rate than gefitinib and erlotinib from bound EGFR has also been reported. Additional *in vitro* studies in mutated and wild type EGFR-over-expressing cell lines may be useful to model if there is a greater efficacy of lapatinib than erlotinib in those patients whose tumours over-express EGFR but do not contain the sensitising mutation.

Gefitinib and erlotinib most likely interact with P-gp as substrates rather than inhibitors. At high concentrations these agents can reduce the P-gp-mediated efflux of substrate cytotoxics in a competitive manner. There is a possibility that P-gp could become a resistance factor for gefitinib and erlotinib. The distinct manner of lapatinib interaction with P-gp when compared to gefitinib and erlotinib combined with the

transport and proliferation data suggest P-gp over-expression is unlikely to generate resistance to this agent. Lapatinib, at readily achievable serum concentrations, effectively inhibits P-gp-mediated efflux, leading to an increased toxicity of P-gp substrate cytotoxics. Lapatinib-mediated P-gp inhibition provides potential for A) MDR circumvention and B) drug pharmacokinetic interactions between lapatinib and potent P-gp substrate cytotoxics. These results would suggest that the combination of lapatinib with a taxane or an anthracycline warrants clinical investigation in cancer.

## **8.7 Possible link between EGFR signalling and P-gp expression**

A change in P-gp expression or activity due to inhibition of the EGFR signalling cascade would have important consequences for the efficacy of P-gp substrate EGFR-TKIs and co-administered P-gp substrate chemotherapeutic agents.

The EGFR, Her-2 and P-gp-positive, A549-Taxol cell line was the ideal candidate to investigate possible links between EGFR and P-gp (Figure 7.2.1.1).

Studies have shown a link between EGFR and P-gp activity and expression. Results published by Yang *et al.*, indicate that EGF exposure can modulate the phosphorylation and function of P-gp, suggesting that the effect may be initiated through the activation of phospholipase C (PLC) in MCF-7/AdrR drug resistant breast cancer cell lines [342]. Wartenberg *et al.*, report that EGF-mediated signal transduction pathways negatively regulate P-gp expression in a process that may involve reactive oxygen species (ROS) as second messengers in DU-145 tumour spheroids [343]. Maximum expression of P-gp was found to correlate with a number of factors including reduced ROS levels and minor activity of the MAPK members, c-JNK and the EGF-regulated ERK1, 2 and p38 MAPK. The down-regulation of P-gp expression due to EGF treatment (activation of the ERK1, 2 and p38 MAPK pathways) reported by Wartenberg *et al.* is consistent with the down-regulation of P-gp expression seen in A549-Taxol due to EGF treatment (Figure 7.3.1). Furthermore, the ROS-mediated downregulation of P-gp by buthionine sulfoximine (BSO) treatment was completely abolished upon inhibition of the Ras-mediated tyrosine kinase signalling pathway, clearly indicating that EGF-mediated signal transduction pathways are negatively regulating P-gp expression [343]. This would support the increases in P-gp expression observed in A549-Taxol on inhibition of the EGFR pathway by gefitinib, erlotinib and lapatinib (Figures 7.3.2, 7.3.3, 7.3.4). The

involvement of ROS in this up-regulation was not examined in A549-Taxol or the phosphorylation state of P-gp, two factors that would be of interest given the evidence in the literature. It is also of interest to note that the lowest concentration of erlotinib and lapatinib used (2.5  $\mu$ M) can be considered pharmacologically relevant. To further examine the link between EGFR and P-gp, measurement of total and phosphorylated EGFR was planned. Total EGFR levels were determined but unfortunately pEGFR levels remain uncharacterised because of time constraints.

To ascertain if the link between EGFR and P-gp is merely a general stress response to TKI insult or a specific connection, further studies are needed. To this purpose, analysis of pEGFR and the total and phosphorylated levels of members of the major EGFR signalling pathways (Akt, MAPK, JNK) under TKI treatment in A549-Taxol, and indeed other P-gp and EGFR-positive cell lines, is required.

### **8.7.1 EGF treatment reduced EGFR protein levels**

Endocytic removal of active ligand-receptor complexes from the cell surface is the major process that regulates the amplitude and kinetics of signal transduction by tyrosine kinase receptors [344]. Following internalisation of the activated tyrosine kinase receptor, regulation of EGFR levels is a balance between degradation, within intercellular lysosomes, and recycling to the plasma membrane. Internalised receptors are generally recycled from early endosomes back to the plasma membrane [219]. Treatment of the A549-Taxol cell line with EGF had dramatic effects on the levels of detectable EGFR protein (Figure 7.4.1). This is consistent with the knowledge that the total number of surface EGFR declines in response to EGF treatment within a short time period (30 minutes) [345]. The continuous activation and internalisation by excess EGF pushes the regulated balance towards degradation. It is possible, that similar to prolonged VEGFR exposure to VEGF in HUVEC cells, the EGFR levels remain depleted until newly synthesised receptors arrive at the surface with recovery of three quarters of the original VEGFR occurring within 5 hours [346]. The fact that EGFR levels do not start to recover within the 48 hour time frame examined may be related to the serum-free conditions. The control reveals that abrogation of all ligand stimulation initiates a slow overall reduction of detectable EGFR protein levels in the control.

### **8.7.2 TKIs increase EGFR levels in A549-Taxol**

The TKI lapatinib produces the opposite effect to treatment with EGF (Figure 7.4.2). There are a number of possibilities as to how lapatinib produces this increase in EGFR protein levels. Lapatinib binds the inactive (monomer) conformation of EGFR as opposed to the active conformation (dimer) bound by erlotinib and gefitinib. Although this has little overall consequence for signalling as gefitinib-bound EGFR dimers have been shown to exist as inactive receptor/ligand complexes, it is unknown if lapatinib bound EGFR is internalised [250], [347]. It is possible that lapatinib treatment produces a build-up of inactive EGFR at the cell surface. Gefitinib treatment has been shown to exert a strong inhibitory effect on the endocytosis of EGFR and the internalisation rate of EGFR from the plasma membrane via the early

endosomes to the late endosomes/lysosomes was delayed in the NSCLC PC-9 cell line [348]. Internalised ligand-bound and active EGFR on endosomes can continue to signal and recruit proteins [219]. Presumably such signalling contributes to regulation of degradation pathways and any TKI bound EGFR is non-active. The similar effects of lapatinib, erlotinib and gefitinib on EGFR levels (Figures 7.4.4, 7.4.5 and 7.4.6), at least at the 48 hour timepoints, would suggest that eradication of the active EGFR signal by all the TKIs increases EGFR protein levels. This process could involve an increase in recycling, an inhibition of endocytosis or an increase in newly synthesised protein. The decrease in EGFR protein observed post 24 hours of lapatinib exposure would suggest a restoration of the mechanisms of EGFR degradation or a reduction in protein synthesis. It is unlikely to be related to cell mortality as control levels of EGFR remain relatively constant between 24 and 48 hours of exposure (Figure 7.4.2). It is interesting to note that in the presence of serum, EGFR levels do not decrease as rapidly as in serum starved conditions (Figure 7.4.1). The presence of ligands is required to maintain EGFR protein levels.

An investigation to discern any differences between the effects of lapatinib, erlotinib and gefitinib on EGFR trafficking in A549 and A549-Taxol would be of interest. A549 express WT-EGFR that has been associated with constitutively impaired endocytic machinery and gefitinib resistance in NSCLC cell lines [348]. A comparison with A549-Taxol would determine any changes associated with paclitaxel resistance and P-gp expression. Her-2 interactions could also be studied, particularly in the presence of lapatinib and in Her-2 over-expressing cell lines. Shorter timepoints should be employed as EGFR trafficking events occur rapidly as approximately 40% of surface EGFR in A549 is internalised within 15 minutes of EGF exposure [349].

### **8.7.3 Comparison of ELISAs utilising detection antibodies to intercellular and extracellular EGFR epitopes**

Total EGFR protein was initially measured using an ELISA (DY231, Section 2.16.1) that utilised a detection antibody recognising an extracellular EGFR epitope (Figures 7.4.1 and 7.4.2). It was unknown if this detection antibody could detect ligand bound EGFR. A second ELISA was carried out on the 48 hour timepoints of EGF, lapatinib, gefitinib and erlotinib treatments in A549-Taxol, which employed a detection antibody raised to an intracellular region of EGFR (DYC1854, Section 2.16.1) (Figures 7.4.3, 7.4.4, 7.4.5 and 7.4.6). The intracellular ELISA detected higher levels of EGFR protein than the extracellular ELISA. This disparity is most likely due to differences in overall sensitivity of the ELISAs rather than a real increase in detected EGFR as the magnitude of the TKI-associated increase (and decrease in the case of EGF) is similar between the two ELISAs. Taking just the magnitudes of TKI-induced augmentation of EGFR protein levels, lapatinib and gefitinib produce greater increases in EGFR levels than erlotinib.

A549 has been shown to express wild-type EGFR [348]. Examination of the EGFR phenotype in A549-Taxol or the same treatments carried out in A549 would be needed to confirm that lapatinib and gefitinib produce a greater increase than erlotinib on WT-EGFR protein levels.

### **8.7.4 c-ErbB receptors and P-gp: A more direct association?**

EGFR signalling is associated with a number of processes implicated in cancer development including cell cycle control, apoptosis, angiogenesis and metastasis [350]. A number of recent studies have started to reveal connections between EGFR signalling, invasion and multi-drug resistance. Over-expression of EGFR and/or ligands, as well as several metalloproteinases (MMPs), is associated with an invasive phenotype in NSCLC lines, with EGFR levels correlated directly to invasive potential [350]. Motogenic activation by EGF has recently been shown to require the concomitant functionality of EGFR and the hyaluronan receptor, CD44, in fibroblasts [351]. This is of particular interest when considered in conjunction with two papers

that relate CD44 with P-gp and Her-2. Miletti-Gonzalez *et al.* report that A) the expression of CD44 and P-gp are coregulated, B) CD44 and P-gp co-immunoprecipitate and are co-localised in the plasma membrane and C) drugs that interfere with P-gp function (trans-flupenthixol and vinblastine) also interfere with invasion and metastasis in the drug resistant breast cancer cell line MCF-7/Adr [352]. Results obtained by Misra *et al.*, also from the MCF-7/Adr cell line, led them to propose that hyaluronan constitutively induces assembly of a Her-2-containing signalling complex that stimulates the PI3K/Akt pathway (and others) through interaction with CD44 [353]. P-gp and MRP-2 are induced by PI3K in MCF7/Adr cells [353]. These studies suggest complex interplay between motogenic and drug resistance pathways involving members of the c-ErbB family and P-gp at the plasma membrane. It would be interesting to investigate if lapatinib had any effect on the invasion levels of the NSCLC lines used in this thesis. It may provide further impetus for the use of lapatinib in P-gp expressing NSCLC.

## 8.8 TKIs and BCRP and MRP-1

The investigation of the capability of the TKIs to modulate multi-drug resistance has to this point concentrated solely on P-gp. Along with P-gp, MRP-1 and BCRP are considered the key ABC proteins involved in multi-drug resistance. A full description of these transporters and their substrates can be found in the Section 1.3.2.

The interaction of gefitinib with BCRP has been well established [354], [108], [251], [355], [255]. Results indicate that gefitinib is a BCRP substrate at low micromolar concentrations, activating ATPase activity and exhibiting decreased accumulation in BCRP-transfected SaOS2 cell lines [251], [354]. Gefitinib has been shown to inhibit BCRP ATPase activity at higher concentrations (10  $\mu\text{M}$ ) [251]. The evidence for the interaction of erlotinib with BCRP is less abundant [356], [357]. A similar situation exists for lapatinib. Lapatinib has been shown to inhibit P-gp and BCRP with  $\text{IC}_{50}$  values of 4  $\mu\text{M}$  and 1.85  $\mu\text{M}$  respectively [358]. Due to the limited information available, the nature of the interaction between erlotinib and lapatinib and BCRP is unknown.

The interaction of gefitinib with MRP-1 has not been tested extensively. Gefitinib has been found to inhibit MRP-1 ATPase activity, but not stimulate it, and inhibit calcein AM extrusion from HL-60-MRP1 cells [251]. There is no data available for the interaction of erlotinib and lapatinib with MRP-1.

There is evidence linking various elements of the EGFR signalling cascade to MRP-1 and BCRP expression levels. Garcia *et al.*, have shown that EGF treatment in the absence of other growth factors induced MRP-1, 3, 5, and 7 gene expression and lead to an increase in MRP-1 promoter activity in MCF-7 breast cancer cells [359]. The same study reported activation of ERK and Akt by EGF in MCF-7. Takada *et al.*, have found evidence that the relative expression of BCRP on the cell surface is regulated by the PI3K-Akt pathway with a positive correlation in polarised LLC-PK1 cells [360].

Considering these findings, the abrogation of EGFR signalling by MRP-1 or BCRP substrate TKIs could lead to changes in the resistance phenotype of cancer cells affecting the efficacy of chemotherapeutic cytotoxics and TKIs.

Any interaction of the TKIs with MRP-1 or BCRP would also have pharmacokinetic implications. Additionally, patients expressing naturally occurring BCRP polymorphic variants may be more sensitive to BCRP substrate TKIs. These BCRP variants have been shown to have differences in their activities and substrate recognition and it has been suggested that they may play a role in the increased sensitivity to gefitinib in the Japanese population, who express the BCRP variant Q141K with a high frequency [361].

To further investigate the scope of TKI/ABC interactions gefitinib, erlotinib and lapatinib were examined in MRP-1 and BCRP ATPase assays. Sulindac and its active metabolite sulindac sulfide were also assayed. As mentioned earlier, ATPase assays do not provide definitive answers as to the nature of drug: transporter interactions but are useful indicators of substrates or inhibitors. When a number of drugs are assayed simultaneously, they can be ranked relative to one another based on their ability to modulate ATPase activity.

### **8.8.1 BCRP ATPase activity as measured using SB-MXR-M-ATPase membrane preparations**

Test compounds were examined in membrane preparations obtained from mammalian cells expressing wild-type BCRP (WT-482R) rather than from the *Spodoptera frugiperda* ovarian (*Sf9*) cell membrane preparations used in the P-gp and MRP-1 ATPase assays. The advantages of the mammalian cell based membrane preparations were recently extolled by Glavinas *et al.*, [362]. *Sf9* membranes expressing the wild type (WT) BCRP transporter (482R) exhibit high baseline vanadate –sensitive ATPase activity that cannot be further stimulated by known BCRP substrates [363]. BCRP characterisation could still be carried out in *Sf9* membranes expressing the R482G variant of BCRP that also had very high baseline vanadate-sensitive ATPase activity but could be stimulated by a number of known BCRP substrates [364]. Glavinas *et al.*, showed that membranes prepared from human cell lines selected with cytotoxic substrates for BCRP are more suitable for the detection of WT BCRP substrates in ATPase assays. The baseline vanadate-sensitive ATPase level in the mammalian cell membrane preparations is also high enough to detect both activators

and inhibitors of BCRP ATPase activity without need of a stimulating agent like verapamil in the P-gp ATPase inhibition assays. This is of considerable advantage as it reveals direct transporter ATPase inhibition. The existence of more than one binding site for substrates and inhibitors, as reported for BCRP and P-gp, can mean complex interaction profiles when a stimulatory agent is utilised [361], [365].

It is noticeable that control BCRP ATPase activity levels (baseline, maximal and inhibited) as measured in this project using the SB-MXR-M-ATPase membrane preparations (Figure 7.5.1) are considerably lower than those reported for the MXR-M-ATPase membrane preparations by Glavinas *et al.* [362]. This is probably due to differences in protocol. BCRP ATPase activity was assayed at 32<sup>0</sup>C for this project as described in the supplied protocol (Section 2.18) but at 37<sup>0</sup>C by Glavinas *et al.* The range of SB-MXR-M-ATPase membrane preparations is still of a magnitude to distinguish activators and inhibitors of baseline BCRP ATPase activity (Figure 7.5.1).

### **8.8.2 Gefitinib, erlotinib and lapatinib stimulate BCRP ATPase activity at low, pharmacologically-relevant, levels**

The stimulation of BCRP ATPase activity by gefitinib is consistent with the results of Ozvegy-Laczka *et al.* although direct comparison is not possible due to the use of *Sf9* membranes in their work, rather those of mammalian cell origin (Figure 7.5.1) [251]. Low gefitinib concentrations stimulated BCRP ATPase activity while higher concentrations started to reduce the maximum BCRP ATPase activity achieved. There is a variation of the concentration at which gefitinib reduced ATPase activity below the baseline level between our results (not achieved at 30  $\mu$ M) and Ozvegy-Laczka *et al.* (10  $\mu$ M) but this once again could be attributable to assay parameters. The concentration at which the TKIs inhibit the baseline ATPase activity is the point they become true inhibitors of BCRP ATPase activity. Lapatinib (5  $\mu$ M) inhibits the baseline BCRP ATPase activity at lower concentrations than gefitinib and does not achieve similar levels of ATPase stimulation (Figure 7.5.1). Erlotinib may inhibit baseline BCRP ATPase activity at concentrations above 30  $\mu$ M. The analysis of BCRP ATPase activity suggests gefitinib and erlotinib have a greater affinity for BCRP at low concentrations than lapatinib (Figure 7.5.1). It is interesting to note that the maximum BCRP ATPase inhibition for each TKI, irrespective of its magnitude,

falls within the same range ( $\sim 2.5 - 5 \mu\text{M}$ ). Further work is required to confirm if the TKIs are transported substrates at low concentrations.

Sulindac had no significant effect on BCRP activity but its metabolite sulindac sulfide displayed minor inhibition of the baseline ATPase activity. It is unlikely that the inhibition levels observed could be of therapeutic benefit against BCRP-mediated drug resistance but what is of interest is its similarity to the effects of mitoxantrone, the prototypical BCRP substrate [364], [366] (Figure 7.5.1). It may be of interest to examine sulindac sulfide further as a BCRP substrate. Past studies involving *Sf9* BCRP ATPase assays showed stimulation of BCRP ATPase activity by mitoxantrone [364]. There is no comparable study of mitoxantrone in mammalian cell membranes to ascertain if this is a phenomenon associated with membrane preparations from differing origins.

Elacridar confirms that it is a better BCRP inhibitor than Hoechst 33342, the lowest concentration ( $0.25 \mu\text{M}$ ) reducing the BCRP ATPase activity below that produced by an excess of Hoechst 33342.

Results confirm that the TKIs interact with BCRP at lower concentrations than P-gp, when considering stimulation of ATPase. Direct inhibition of BCRP ATPase activity occurs at higher concentrations of the TKIs with lapatinib producing inhibition of baseline BCRP ATPase activity at  $5 \mu\text{M}$  followed by erlotinib and gefitinib. The ability of the TKIs to modulate BCRP ATPase activity in the presence of a stimulating agent was not conducted. Lapatinib is the poorest activator of BCRP ATPase activity as it was the poorest activator of P-gp ATPase activity. Although the TKIs show no direct inhibition of BCRP ATPase alone, this study is concerned with the ability of the TKIs to modulate transport of other drugs. It would be interesting to compare the capabilities of the TKIs to inhibit drug stimulated BCRP ATPase activity to see if there is a difference in the ability of lapatinib, and gefitinib and erlotinib, to modulate it, as in the verapamil stimulated P-gp ATPase inhibition assays. This also brings up another factor, the choice of stimulating agent. Future work may consider studying the effects of the TKIs on P-gp and BCRP ATPase activity when stimulated using the cytotoxic compound of interest, in the case of this project, docetaxel. The P-gp modulator cyclosporin A proved a better inhibitor of verapamil stimulated P-gp ATPase activity than lapatinib (Figure 7.2.2.1) but lapatinib increased docetaxel

levels to a greater degree than cyclosporin A *in vitro* (Figure 7.2.3.1). A comparison of lapatinib and cyclosporin A inhibition of docetaxel-stimulated P-gp ATPase activity may have provided a better prediction of the *in vitro* result.

A BCRP ATPase inhibition assay would be required to assess the TKIs as modulators of BCRP-mediated drug transport. Low TKI concentrations could be subject to BCRP-mediated resistance in tumours and the profiles of TKIs in combination with BCRP substrate cytotoxics should be studied carefully *in vitro* and *in vivo*. There are recent clinical indications that lapatinib may alter the pharmacokinetic profiles of SN-38, the active metabolite of the BCRP substrate drug irinotecan [358].

### **8.8.3 Gefitinib, erlotinib and lapatinib have a minor stimulatory effect on MRP-1 ATPase activity**

The effects of gefitinib on MRP-1 ATPase have been studied in *Sf9* cells previously by Ozvegy-Laczka *et al.* [251]. Our findings that gefitinib has a minor stimulatory effect on MRP-1 ATPase activity and no inhibitory effect on NEM-GS stimulated ATPase activity are contrary to their findings (Figures 7.5.2 and 7.5.3). MRP-1 sometimes requires the presence of free glutathione to transport uncharged or mildly cationic compounds such as vincristine and etoposide [125]. It is possible that the conflicting results may be attributable to the presence of glutathione (2 mM) in the MRP-1 ATPase activation assay carried out in this project but not in the published study. There are no comparable results for lapatinib and erlotinib. Both TKIs exhibit minor ATPase activation suggesting possible interaction with MRP-1 as weak substrates in the presence of glutathione (Figure 7.5.2).

None of the three TKIs inhibited NEM-GS stimulated MRP-1 ATPase activity up to a concentration of 30  $\mu$ M (Figure 7.5.3). Gefitinib has been shown to inhibit NEM-GS stimulated MRP-1 ATPase activity [251]. This effect occurred above 10  $\mu$ M but there were no intermediate data points between 10  $\mu$ M and 50  $\mu$ M, the next concentration assayed. It is possible that the inhibition of MRP-1 ATPase activity may have occurred at a concentration above 30  $\mu$ M in this situation. Exploration of higher gefitinib concentrations in our system would confirm this.

#### **8.8.4 The MRP-1 substrate vincristine does not stimulate MRP-1 ATPase activity**

The effect of vincristine on MRP-1 ATPase activity highlights the caution needed when extrapolating the transport characteristics of a compound from ATPase activity alone. Vincristine is a transported MRP-1 substrate but, consistent with the MRP-1 ATPase activation results in Figure 7.5.2, it does not increase MRP-1 ATPase activity [367]. In the same study, Hooijberg *et al.*, have shown that glutathione alone stimulates the ATPase activity of MRP-1 in a dose dependent manner up to 5 mM. The baseline ATPase activity of MRP-1 was not examined in the absence of glutathione in this thesis. A working hypothesis consistent with literature data and the thesis results has been suggested by Salerno *et al.* [368]. They imagine MRP-1 to be composed of two components, an active, ATP-dependent “G” unit and an inert “D” unit, dependent on the G unit for transport. Each unit has its profile substrate drugs (G-class and D-class). G-class substrates include glutathione and LTC<sub>4</sub>. Vincristine and daunorubicin are considered D-class substrates. D-class substrates are essentially co-transported in the presence of G-class substrates without additional ATP hydrolysis. Salerno *et al.*, also envisage two types of MRP-1 inhibitor, Class I and Class II. A class I inhibitor (e.g. MK571) affects the G unit, therefore abrogating transport of both G and D class substrates. A class II inhibitor (e.g. verapamil) affects the D unit only. Free of the dependent D unit, the transport of G class substrates is actually stimulated by class II inhibitors. Taking this model, it could be argued that the minor increases the TKIs and vincristine could be Class II MRP-1 inhibitors (Figure 7.5.3).

#### **8.8.5 Sulindac is an activator but not an inhibitor of MRP-1 ATPase activity**

Sulindac is a reported MRP-1 modulator and the subject of a clinical trial to determine its efficacy in this role [369], [161]. The nature of the effect of sulindac on MRP-1 ATPase activity has not been explored to date. The strong concentration-dependent increase in MRP-1 ATPase activation and little inhibitory effect on n-ethylmaleimide (NEM) stimulated MRP-1 ATPase activity would suggest that sulindac is a substrate

of MRP-1 (Figures 7.5.2 and 7.5.3). The classification of sulindac sulfide is harder to predict from the MRP-1 ATPase results. Sulindac sulfide stimulates MRP-1 ATPase activity in a concentration-dependent manner that levels off at 15  $\mu\text{M}$  but also inhibits NEM-GS stimulated MRP-1 ATPase activity from 15  $\mu\text{M}$ . This suggests that sulindac sulfide is an MRP-1 substrate at low concentrations (sub 15  $\mu\text{M}$ ) and an MRP-1 inhibitor at higher levels. To further elucidate the transport characteristics of sulindac and sulindac sulfide, it would be useful to examine the drugs in an MRP-1 ATPase activation assay in the absence of glutathione to determine if ATPase activation is glutathione dependent. In combination with a comparison with the effects of the class II inhibitor verapamil, a hypothesis based on the Salerno model could then be postulated. Transport assays involving MRP-1 substrates and ideally direct sulindac and sulindac sulfide measurement would complete the picture.

### **8.8.6 The possibility of TKI influx mechanisms**

This thesis has examined the influx characteristics of docetaxel in NSCLC lung cancer cell lines but with regard to the TKIs, has concentrated on the processes of efflux. Thomas *et al.*, have reported active transport of the TKI imatinib, in the chronic myeloid leukaemia cell line CEM, most probably mediated by human organic cation transporter 1 (hOCT1, SLC22A1) [310]. Given the similar profiles of P-gp-mediated inhibition of docetaxel by imatinib and gefitinib in DLKP-A (Appendix A, Figure A3), it may be plausible that hOCT1 or another influx mechanism could facilitate active influx of lapatinib, gefitinib and erlotinib in normal tissue and tumour cells. hOCT1 expression has been reported in normal breast and lung tissues and tumour cells [201]. Microarray data indicates low hOCT1 mRNA expression in A549 and A549-Taxol but does not indicate mRNA expression in DLKP or DLKP-A (Appendix A, Table A2). However, other members of the SLC22 family including SLC22A3, A4 and A5, do show expression in the microarray sets. Examination of TKI influx in a range of breast and lung cancer cell lines could reveal additional markers for TKI sensitivity and kinetics.

## *Chapter 9. Conclusions*

- The HPLC method for taxane measurement was insensitive. The results involving 10  $\mu\text{M}$  of taxane may bear little relevance to real pharmacological effects.
- Use of the  $^{14}\text{C}$ -labelled docetaxel permitted analysis of transport at pharmacologically achievable levels (100-500 nM).
- Docetaxel uptake was found to be saturable, temperature-dependent and ATP-dependent in DLKP. The decrease in accumulated docetaxel in the presence of ATP depleting agents is consistent with the existence of an ATP-dependent docetaxel uptake mechanism in DLKP. This is the first evidence of a docetaxel uptake mechanism in a NSCLC cell line. Further work is required to identify the docetaxel uptake mechanism involved.
- Docetaxel transport in A549 was shown to be temperature-dependent and non-saturable up to 500 nM. ATP depletion resulted in an increase in accumulated docetaxel levels. These observations suggested the existence of an energy-dependent efflux mechanism in A549. MRP-2 is the most likely candidate based on the ability of DHEAS and  $\text{T}_3$  to increase docetaxel accumulation and its reported expression levels in A549.
- A study of the involvement of the SLCO/OATP family in docetaxel uptake in A549 was not conclusive. The docetaxel accumulation studies involving bromosulphophthalein and digoxin, general modulators of the OATP family, resulted in a decrease in docetaxel accumulation in A549 but studies with more specific OATP modulators such as DHEAS and  $\text{T}_3$  led to increases in docetaxel levels, possibly through inhibition of the putative energy-dependent transport mechanism described above. The possibility that the bi-directional transport capabilities of the OATP family may be involved still has to be determined.

- The ability of the OATP1B1 substrate, indocyanine green, to increase the accumulation of docetaxel in A549 and DLKP, in a concentration-dependent manner, warrants further investigation. The effect is unlikely to be OATP-mediated given the magnitude of the increase and the fact it was not confined to A549, the cell line in which the general OATP inhibitor bromosulphthalein decreased docetaxel accumulation, unlike DLKP. Indocyanine green could be altering cell membrane permeability through phospholipid binding.
- The ability of known OATP substrates to modulate docetaxel transport in the NSCLC cell line A549 indicates that further study of the role of the OATP family in tumour cell taxane transport is warranted.
- The mechanisms of interaction between the TKIs examined and P-gp is distinctly different. Lapatinib inhibited verapamil-stimulated P-gp ATPase activity while being a poor activator of P-gp ATPase itself. Conversely, erlotinib and gefitinib displayed less verapamil-stimulated P-gp ATPase inhibitory activity but greatly increased P-gp ATPase activation. Lapatinib is most likely a slowly transported substrate with high affinity for P-gp while erlotinib and gefitinib are likely transported P-gp substrates. These results provide evidence that P-gp may contribute to resistance to gefitinib and erlotinib at low concentrations but is unlikely to impact on lapatinib resistance.
- In combination proliferation assays, gefitinib, erlotinib and lapatinib enhanced response to the P-gp substrate chemotherapy drugs, docetaxel, paclitaxel and epirubicin in our P-gp-positive MDR cell line models at low, physiologically relevant, levels. Lapatinib proved the most potent of the TKIs.
- Drug transport studies in the P-gp over-expressing cell lines A549-Taxol and DLKP-A showed lapatinib to be the most effective of the three TKIs at increasing docetaxel accumulation and decreasing P-gp-mediated docetaxel efflux in cell lines.

- Taken together, the ATPase assay, proliferation assay and docetaxel transport assay results suggest the three TKIs, particularly lapatinib, have significant potential to augment the cytotoxic activity of P-gp substrate chemotherapeutic agents, particularly docetaxel, in P-gp positive tumours.
- On a cautionary note, concurrent administration of gefitinib, erlotinib or lapatinib with P-gp substrate chemotherapeutics will require further investigation to assess if such combinations may generate possible alterations in cytotoxic pharmacokinetics.
- Preliminary results of combination proliferation assays between the TKIs and cisplatin indicate such combinations require further investigation to determine their efficacy and possible antagonism in NSCLC.
- Lapatinib and erlotinib demonstrated an ability to potentiate the action of epirubicin in cells with no P-gp activity. The potentiation of epirubicin toxicity by lapatinib occurred in the EGFR and Her-2 expressing A549 but it is all the more noteworthy as it also occurred in the DLKP cell line that does not express EGFR and only expresses minor levels of Her-2. Anthracycline/TKI combinations may be capable of additional anti-cancer actions, due to potentiation of toxicity, even in the cell lines with little or no P-gp.
- When assessed in the BCRP ATPase assays, gefitinib and erlotinib proved more effective at stimulating BCRP ATPase activity than lapatinib. A comparison of the effects of the TKIs on drug-stimulated BCRP ATPase activity is required to provide a definitive answer as to the which of the TKIs examined is the best candidate for the modulation of BCRP activity *in vivo*.

- MRP-1 ATPase studies suggest that the NSAID, sulindac and its active metabolite, sulindac sulfide, have potential as modulators of MRP-1 activity, supporting previous findings from our group. Gefitinib, erlotinib and lapatinib displayed a minor increase in MRP-1 ATPase activity but had no inhibitory effect on NEM-GS stimulated MRP-1 ATPase activity, suggesting they are weak substrates in the presence of GSH.
- A specific link between EGFR inhibition and the levels of P-gp protein expression would have important consequences for the use of TKIs in cancer treatment and the development of resistance for TKIs that are transported P-gp substrates. Although a general link between EGFR stimulation and P-gp protein expression was established in the A549-Taxol cell line, the specific mechanism involved was not elucidated.
- The EGF stimulated decrease in EGFR protein expression correlated with a decrease in P-gp protein expression while abrogation of the EGFR signal by TKIs increased EGFR and P-gp protein levels. Further work is required to explain the pathways involved in the link between EGFR signalling and P-gp expression and to determine if there is a specific relationship between TKI inhibition of EGFR and P-gp expression or if it is a general stress response.

## ***Chapter 10. Future work***

The section in which the point is discussed is presented in brackets where relevant.

## **10.1 Docetaxel transport in lung cancer cell lines**

- Perform comparative paclitaxel transport experiments in DLKP to further examine the disparity in the levels of paclitaxel and docetaxel accumulated in this cell line (Section 8.1.6).
- Examine the ability of sulindac to modulate paclitaxel and epirubicin uptake in DLKP-TXT (Section 8.2.3).
- Further explore the temperature-dependence of docetaxel uptake in A549 and DLKP by comparing uptake of different docetaxel concentrations (Section 8.5.4).
- Identification of the ATP-dependent transporter in DLKP using DNA microarray data as a starting point (Section 8.5.7). Monolayer efflux studies may be useful to determine apical/basal localisation of the transporter in DLKP.
- Examine the effects of digoxin/BSP/T<sub>3</sub> and DHEAS on taxane movement in A549 using a system that can distinguish apical to basal/basal to apical transport monolayer efflux studies. Such studies would determine the cellular localisation of transporters. Immunodetection of the putative docetaxel transporters MRP-2 and MRP-7 in A549 (Section 8.5.11).
- Immunodetection of the OATP family in A549 to determine expression levels and contribution to docetaxel uptake (Section 8.5.8).
- Examine the possibilities of carrier-mediated cisplatin transport in A549 and DLKP (Section 8.5.12).

- Expanding the studies of docetaxel uptake to a number of NSCLC cell lines would help determine the prevalence and relative importance of influx mechanisms in NSCLC.

## **10.2 Tyrosine kinase inhibitors**

- The effects of lapatinib on the ATPase activity of other drug transporters, i.e. MRP-2, 3 and 4, to develop a transporter profile.
- To get a definitive answer as to the ability of P-gp to transport the TKIs and therefore confer resistance, direct measurement of TKI transport by mass spectrometry or radiolabelled techniques (Section 8.6.1).
- Compare the ability of lapatinib to modulate P-gp-mediated paclitaxel transport to docetaxel transport in combination proliferation and transport assays.
- The ability of lapatinib to potentiate epirubicin toxicity via a non-P-gp mediated mechanism in NSCLC lung cancer cell lines warrants further investigation in all cancer cell lines of varying EGFR and Her-2 status in order to uncover the contributions of these receptors to the phenomenon (Section 8.6.5).
- The existence of antagonism between cisplatin/carboplatin and TKIs would have important implications for concurrent administration of TKIs and a taxane as part of a platinum/taxane doublet in NSCLC. The extent and mechanism of this effect requires further investigation (Section 8.6.5).
- Determine if the link between EGFR and P-gp expression found in A549-Taxol is a general stress response or a specific cell signalling pathway (Section 8.7).

- Investigation of the effects of lapatinib, gefitinib and erlotinib on EGFR trafficking in wild type and EGFR variant-expressing cell lines (Section 8.7.2).
- Examine the effects of lapatinib, in any, on the invasive properties of A549, A549-Taxol, DLKP, DLKP-A and other sensitive and drug resistant NSCLC cell lines (Section 8.7.4).
- A BCRP ATPase assay examining the effects of the TKIs on drug-stimulated BCRP ATPase activity (Section 8.8.3).
- Examination of the effects of sulindac and sulindac sulfide on MRP-1 ATPase in the absence of GSH (Section 8.8.5).
- Determine if the uptake of lapatinib, gefitinib and erlotinib is carrier-mediated in NSCLC cell lines (Section 8.8.6).

## *Appendix A*

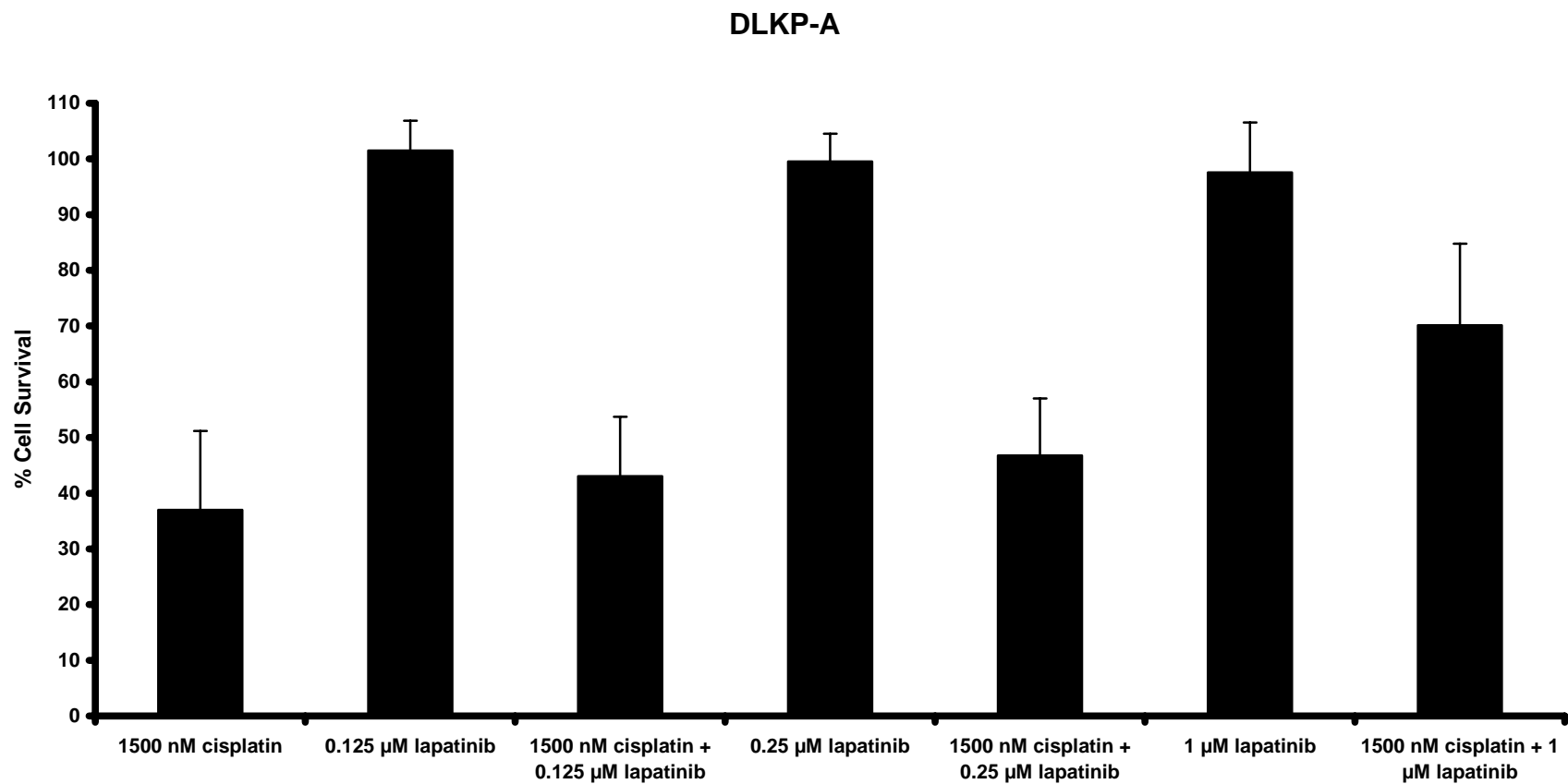
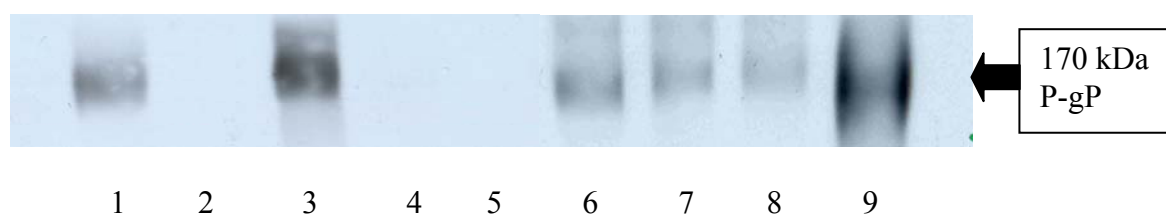


**Figure A1** Proliferation assay combining 1500 nM cisplatin and lapatinib in DLKP-A. The combination of 1500 nM cisplatin and lapatinib display antagonism. Data are mean  $\pm$  SD calculated on experiments performed in triplicate.

The NSCLC squamous cell lung carcinoma cell line SK-MES-1 (Lane 4) does not express P-gp. The taxane selected variants of this cell line, SK-MES-Taxol (Lane 3) and SK-MES-Taxotere (Lane 1) do express P-gp. The SCLC squamous cell line DMS-53 (Lane 8) does express P-gp as does its taxane selected variants DMS-Taxol (Lane 7) and DMS-Taxotere (Lane 6).

A



B



- 1 – SKMES-Taxotere
- 2 - Blank
- 3 – SKMES-Taxol
- 4 – SKMES-1
- 5 - Blank
- 6 – DMS-Taxotere
- 7 – DMS-Taxol
- 8 – DMS-53
- 9 – DLKP-A (+ control)

**Figure A2** Western blot for P-gp (A) in a NSCLC and a SCLC cell line and their drug selected variants. DMS-Taxotere and SKMES-Taxotere were selected with docetaxel while SKMES-Taxol and DMS-Taxol were selected with paclitaxel. Lanes 1-5 required a 20 minute exposure to visualise the P-gp bands while the higher P-gp levels in the DMS cell line and its variants required a five minute exposure. Samples were also blotted for alpha-tubulin expression (B)

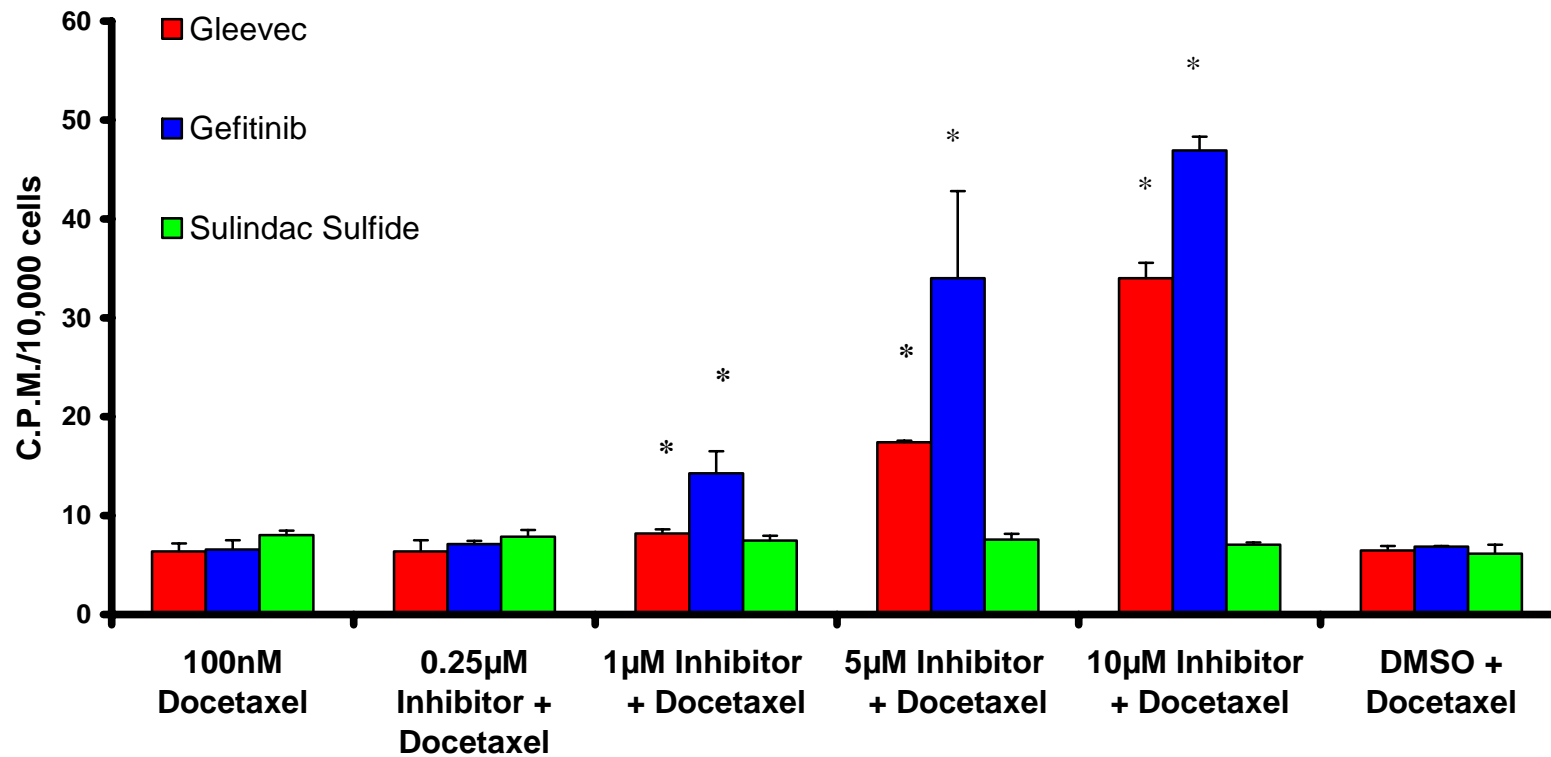


**Figure A3** Accumulation of 100 nM <sup>14</sup>C docetaxel in DLKP-A over 90 minutes. Values represent the average of three determinations. All inhibitors were dissolved in DMSO. Data are mean +/- SD calculated on experiments performed in triplicate.\* significant relative to control, P < 0.05.

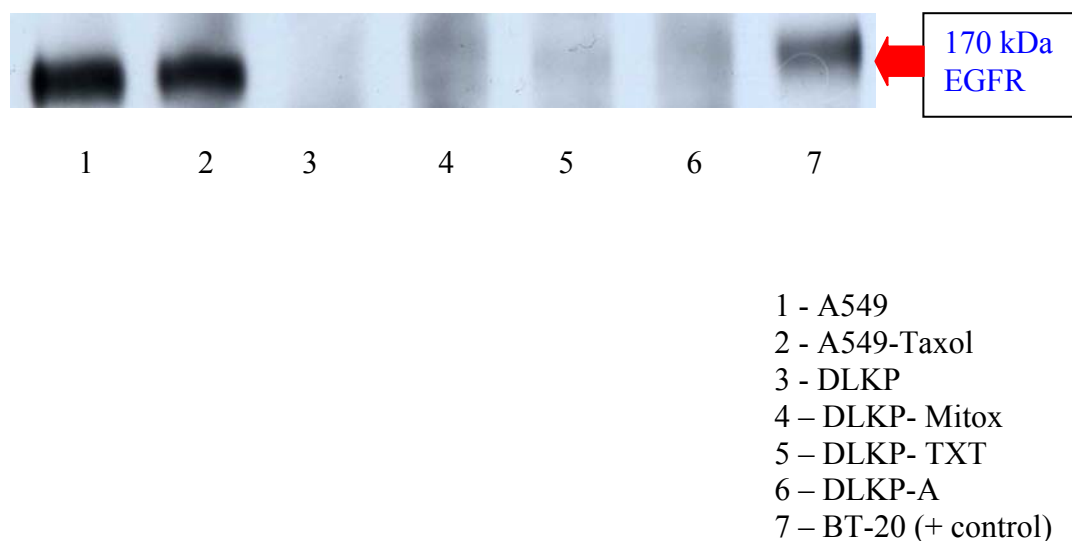


**Figure A4** EGFR immunoprecipitation in two NSCLC cell lines (A549 and DLKP) and drug selected variants. A549-Taxol was selected with paclitaxel (Taxol®), DLKP-Mitox was selected with mitoxantrone, DLKP-TXT was selected with docetaxel (Taxotere®), DLKP-A was selected with adriamycin, BT-20 was the EGFR positive control. High levels of EGFR were detected in A549 and the paclitaxel-selected A549-Taxol. DLKP show no EGFR expression. DLKP-A, DLKP-TXT and DLKP—MITOX exhibit minute expression levels.

**Table A1** DNA microarray data analysis for members of the SLCO (OATP) gene family. P = Present, A=Absent, M= Marginal, P,A=Borderline.

<b>GENE</b>	<b>EST</b>	<b>DLKP</b>	<b>DLKP-A</b>	<b>A549</b>	<b>A549-Taxol</b>
<b>SLCO</b>					
1A2	207308_at	A	A	P, A	P, A
	211480_s_at	A	M,A	A	A
	211481_at	A	A	A	P, A
1B1	210366_at	A	A	P, A	<b>P</b>
1B3	206354_at	A	A	<b>P</b>	<b>P</b>
1C1	220460_at	A	A	P, A	P, A
2A1	204368_at	A	A	A	M, A
2B1	203472_s_at	A	A	P, A	A
	203473_at	A	A	P, A	P, A
	211557_x_at	A	A	A	A
3A1	210542_s_at	A	A	<b>P</b>	<b>P</b>
	229776_at	A	A	<b>P</b>	<b>P</b>
	227367_at	P,A	P,A	<b>P</b>	<b>P</b>
	219229_at	A	A	<b>P</b>	<b>P</b>
4A1	219911_s_at	P,A	A	<b>P</b>	<b>P</b>
	229239_x_at	A	A	A	A
4C1	222071_s_at	P,A	A	P, A	P, A
5A1	220984_s_at	A	A	A	A
6A1	1552745_at	A	A	A	A

**Table A2** DNA microarray data analysis for members of the SLC22 gene family. P = Present, A=Absent, M= Marginal, P, A=Borderline.

GENE	EST	DLKP	DLKP-A	A549	A549-Taxol
<b>SLC22</b>					
A1	207201_s_at	A	A	P, A	P, A
A2	207429_at	A	A	A	A
A3	205421_at	A	A	P	P
	242578_x_at	P	P	P	P
A4	205896_at	P,A	P,A	P	P
A5	205074_at	P	P	P	P
A6	210343_s_at	A	A	A	A
	216599_x_at	A	A	A	A
A7	155553_a_at	A	A	A	A
	220554_at	A	A	A	P, A
	221661_at	A	A	A	A
	221662_s_at	A	A	A	A
	231398_at	A	A	A	A
A8	221298_s_at	A	A	A	A
	231352_at	A	A	A	A
A9	231625_at	A	A	A	A
A11	220100_at	A	A	A	A
A12	237799_at	A	A	A	A
A13	207444_at	A	A	A	A
A14	207408_at	P,M	P,A	P, M	P, A
A15	228497_at	A	P	A	P
A16	232232_s_at	A	A	A	A
	232233_at	A	A	A	A
A17	218675_at	P,M	P	P, A	A
	221106_at	A	A	A	A
A18	204981_at	P	P	P	P
A1LS	206097_at	A	A	P	P, A

**Table A3** DNA microarray data analysis for select members of the ABC gene family related to taxane resistance. P = Present, A=Absent, M= Marginal, P, A=Borderline.

<b>GENE</b>	<b>EST</b>	<b>DLKP</b>	<b>DLKP-A</b>	<b>A549</b>	<b>A549-Taxol</b>
<b>ABC</b>					
B1 (P-gp)	209994_s_at	A	P	A	P
	243951_at	A	P	A	P
	209993_at	A	P	P	P
C2 (MRP2)	206155_at	A	A	P	P
C10 (MRP7)	213485_s_at	P	P	P	P
	215873_x_at	P	P	P	P
G2(BCRP)	209735_at	A	P, A	P	P

**Table A4** DNA microarray data analysis for select members of the SLC gene family related to platinum drug resistance. P = Present, A=Absent, M= Marginal, P, A=Borderline.

<b>GENE</b>	<b>EST</b>	<b>DLKP</b>	<b>DLKP-A</b>	<b>A549</b>	<b>A549-Taxol</b>
<b>SLC</b>					
7A1 (xCT)	207528_s_at	M, A	P	P	P
	209921_at	P	P	P	P
	217678_at	P	P	P	P
31A1(CTR1)	236217_at	P	M, A	P	P
	203971_at	P	P	P	P
	235013_at	P	P	P	P

**Table A5** IC<sub>50</sub> values for docetaxel, paclitaxel, adriamycin, elacridar, verapamil and sulindac in NSCLC and human leukemic cell lines. + represents the number of 96-well plate replicates carried out. Results were calculated using Calcsyn Software.

<b>Drug</b>	<b>Cell line</b>	<b>IC50 (µM)</b>
<b>Docetaxel</b>	DLKP-TXT ++	0.0097 +/- 0.0009
	DLKP-A2B mdr 1C7 +	0.0002827
	HL-60s +++	0.0114 +/- 0.0021
	HL-60ADR +++	0.0046 +/- 0.0008
<b>Paclitaxel</b>	DLKP-TXT ++	0.018 +/- 0.0006
	HL-60s +++	0.0059 +/- 0.0012
	HL-60ADR+++	0.0064 +/- 0.0032
<b>Adriamycin</b>	HL-60s +++	0.1024 +/- 0.0056
	HL-60ADR +++	11.3 +/- 2.8
<b>Elacridar</b>	DLKP-A +++	24.8 +/- 1.5
	DLKP-TXT +++++	54.9 +/- 11.03
	DLKP-A2B mdr 1C7 +	16.3
	A549 +++	16.3 +/- 1.2
<b>Verapamil</b>	DLKP-A ++	114.5 +/- 9.9
	DLKP-TXT ++	135.7 +/- 0.1
<b>Sulindac</b>	DLKP +++	89.9
	A549 +++	Non-toxic at 40
	HL-60s +++	Non-toxic at 20
	HL-60ADR +++	Non-toxic at 15

**Table A6** EGFR levels in NSCLC cell lines. EGFR levels were quantified using two different ELISA kits, each utilising a different detection antibody that recognised an intracellular or extracellular epitope of EGFR. Values were determined in duplicate for each cell line +/- SD. DMS and taxane selected variants of DMS express no EGFR or in the case of DMS and DMS-Taxol, levels that are minute, approaching the limits of detection for these ELISAs. DLKP-Txt and DLKP-Mitox express extremely low levels of EGFR but more than the EGFR-negative DLKP parent cell line. SKMES-1 and its taxane selected variants express EGFR levels comparable to the A549 cell line (Figure 6.1.1.1)

Cell line	Extracellular	Intracellular
DLKP-TXT	1.67 +/- 0.01	1.74 +/- 0.4
DLKP-Mitox	2.8 +/- 0.003	2.78 +/- 0.04
SKMES-1	25.7 +/- 0.96	32.31 +/- 0.89
SK-Taxotere	19.16 +/- 2.27	27.24 +/- 0.5
SK-Taxol	30.1 +/- 0.29	37.44 +/- 0.09
DMS	0.42 +/- 0.024	0
DMS-Taxotere	0	0
DMS-Taxol	0.32 +/- 0.36	0

**Table A7** Her-2 levels in NSCLC cell lines. Values were determined in duplicate for each cell line +/- SD. All cell lines express extremely low levels of Her-2. The levels of Her-2 in the DLKP variants are consistent with the parent cell line (Figure 6.1.1.1).

Cell line	Her-2 (pg/ $\mu$ g total protein)
DLKP-TXT	1.12 +/- 0.01
DLKP-Mitox	0.83 +/- 0.03
SKMES-1	0.21 +/- 0.0076
SK-Taxotere	0.2 +/- 0.02
SK-Taxol	0.22 +/- 0.004
DMS	0.12 +/- 0.015
DMS-Taxotere	0.11 +/- 0.015
DMS-Taxol	0.11 +/- 0.0

## *Appendix B*

Appendix B (CD) contains additional LSCM images and 3-dimensional animations of epirubicin and Oregon-green paclitaxel localisation in NSCLC cell lines.

## **Epirubicin LSCM studies**

### **1) Appendix B\Epirubicin\A549\A54910microMepirubicinANM.avi**

A549 cells were exposed to 10  $\mu\text{M}$  epirubicin for 120 minutes and imaged as in Section 2.11. A Z-stack comprising of single scans taken at 0.24  $\mu\text{m}$  was compiled and turned into a 3-D animation. Cytoplasmic vesicles containing epirubicin were clearly visible.

### **2) Appendix B\Epirubicin\A549\A54910microMepirubicin OP.avi**

The Z-stack comprising of single scans taken at 0.24  $\mu\text{m}$  in 1) was shown in orthographic projection. Cytoplasmic vesicles containing epirubicin were clearly visible.

### **3) Appendix B\Epirubicin\DLKP\DLKP10microMepirubicinANM.avi**

DLKP cells were exposed to 10  $\mu\text{M}$  epirubicin for 120 minutes and imaged as in Section 2.11. A Z-stack comprising of single scans taken at 0.24  $\mu\text{m}$  was compiled and turned into a 3-D animation. Cytoplasmic vesicles containing epirubicin were **NOT** visible (**discussed in Section 8.2.2**).

### **4) Appendix B\Epirubicin\DLKP-A\DLKPA 2microM epirubicin Control .tif**

DLKP-A cells were exposed to 2  $\mu\text{M}$  epirubicin for 120 minutes and imaged as in Section 2.11. A single scan was obtained. There was little cytoplasmic or nuclear localisation of epirubicin.

### **5) Appendix B\Epirubicin\DLKP-A\DLKPA 2microM epirubicin 10 microM Cyclosporin A Zm.tif**

DLKP-A cells were exposed to 2  $\mu\text{M}$  epirubicin and 10  $\mu\text{M}$  cyclosporin A for 120 minutes and imaged as in Section 2.11. A single scan was obtained. Cytoplasmic and nuclear localisation of epirubicin was increased. Cytoplasmic vesicles containing epirubicin were clearly visible (**discussed in Section 8.2.2**).

### **6) Appendix B\Epirubicin\DLKP-A\DLKPA 2microM epirubicin 100 microM Verapamil Zm.tif**

DLKP-A cells were exposed to 2  $\mu\text{M}$  epirubicin and 100  $\mu\text{M}$  verapamil for 120 minutes and imaged as in Section 2.11. A single scan was obtained. Cytoplasmic and nuclear localisation of epirubicin was increased. Cytoplasmic vesicles containing epirubicin were clearly visible (**discussed in Section 8.2.2**).

## **Oregon-green paclitaxel LSCM studies**

### **7) Appendix B\Oregon green paclitaxel\DLKP\DLKP 90 min exposure to 1 microM Oregon green paclitaxel 3D ANM.avi**

DLKP cells were exposed to 1  $\mu\text{M}$  Oregon-green paclitaxel for 90 minutes and imaged as in Section 2.11. A Z-stack comprising of single scans taken at 0.24  $\mu\text{m}$  was compiled and turned into a 3-D animation.

### **8) Appendix B\Oregon green paclitaxel\DLKP\DLKP 90 min exposure to 1 microM Oregon green paclitaxel OP.avi**

The Z-stack comprising of single scans taken at 0.24  $\mu\text{m}$  in 7) was shown in orthographic projection.

### **9) Appendix B\Oregon green paclitaxel\DLKP\ DLKP 180 min exposure to 1 microM Oregon green paclitaxel 3D ANM.avi**

DLKP cells were exposed to 1  $\mu\text{M}$  Oregon-green paclitaxel for 180 minutes and imaged as in Section 2.11. A Z-stack comprising of single scans taken at 0.24  $\mu\text{m}$  was compiled and turned into a 3-D animation. **This is a 3-D animation of Figure 4.1.5 in Section 4.1.**

### **10) Appendix B\Oregon green paclitaxel\DLKP\ DLKP 180 min exposure to 1 microM Oregon green paclitaxel CS ANM.avi**

The single scans taken at 0.24  $\mu\text{m}$  intervals comprising the Z-stack in 9) were shown in sequence as an animation. **This is an animation of Figure 4.1.5 in Section 4.1.**

## *Abbreviations*

5-Fu	5-Fluorouracil
ABC	ATP-binding Cassette
ADP	Adenosine Diphosphate
ADR	Adriamycin
ATCC	American Tissue Culture Collection
ATP	Adenosine Triphosphate
BCA	Bicinchoninic Acid
BCRP	Breast Cancer Resistance Protein
BSA	Bovine Serum Albumin
BSP	Bromosulphophthalein
cDNA	Complementary DNA
C.P.M.	Counts Per Minute
CYP	Cytochrome P450
DHEAS	Dehydroepiandrosterone
DMEM	Dulbecco's Minimum Essential Medium
DMSO	Dimethyl Sulfoxide
DNA	Deoxyribonucleic Acid
DOX	Doxorubicin (adriamycin)
DTT	Dithiothreitol
E17BG	Estradiol 17- $\beta$ -D-Glucuronide
ECACC	European Collection of Animal Cell Culture
EDTA	Ethylene diamine tetracetic acid
ELISA	Enzyme-linked Immunosorbant Assay
ERK	Extracellular signal-Regulated Kinase
FCS	Fetal Calf Serum
GSH	Glutathione
HCL	Hydrochloric Acid
HEPES	4-(2-hydroxyethyl)-piperazine ethane sulphonic acid
HPLC	High Performance Liquid Chromatography
IC <sub>50</sub>	Inhibitory Concentration 50%
ICG	Indocyanine Green
IgG	Immunoglobulin
IMS	Industrial Methylated Spirits
JNK	Jun N-terminal Kinase
kDa	Kilo Daltons

MAPK	Mitogen Activated Protein Kinase
MDR	Multi-Drug Resistance
MEM	Minimum Essential Medium
MgCl <sub>2</sub>	Magnesium Chloride
Mitox	Mitoxantrone
MRP	Multidrug Resistance-associated Protein
mRNA	Messenger RNA
MW	Molecular Weight
NaCl	Sodium Chloride
NaHCO <sub>3</sub>	Sodium Bicarbonate
NaOH	Sodium Hydroxide
NEAA	Non-Essential Amino Acids
NSAID	Nonsteroidal anti-inflammatory drug
NSCLC	Non-small cell lung cancer
OATP	Organic Anion Transporting Peptide
OD	Optical Density
P450	Cytochrome P450
PAGE	Polyacrylamide Gel Electrophoresis
PBS	Phosphate Buffered Saline
PCR	Polymerase Chain Reaction
P-gp	P-glycoprotein
Pi	Inorganic Phosphate
PMSF	Phenylmethanesulphonyl Fluoride
RNA	Ribonucleic Acid
r.p.m.	Revolution(s) Per Minute
RT-PCR	Reverse Transcriptase-PCR
SCLC	Small cell lung cancer
SD	Standard Deviation
SDS	Sodium Dodecyl Sulphate
SLC	Solute Carrier
siRNA	Small interfering RNA
T <sub>3</sub>	Tri-iodo-L-thyronine
TBS	Tris Buffered Saline
TEMED	N, N, N', N'-Tetramethyl-Ethylenediamine
THF	Tetrahydrofuran
Tris	Tris(hydroxymethyl)aminomethane
UHP	Ultra high purity water

## *References*

1. Junker, K., *Prognostic factors in stage I/II non-small cell lung cancer*. Lung Cancer, 2001. **33 Suppl 1**: p. S17-24.
2. Thatcher, N., C. Faivre-Finn, and P. Lorigan, *Management of small-cell lung cancer*. Ann Oncol, 2005. **16 Suppl 2**: p. ii235-9.
3. Chrystal, K., K. Cheong, and P. Harper, *Chemotherapy of small cell lung cancer: state of the art*. Curr Opin Oncol, 2004. **16**(2): p. 136-40.
4. Hanna, N.H. and L.H. Einhorn, *Small-cell lung cancer: state of the art*. Clin Lung Cancer, 2002. **4**(2): p. 87-94.
5. Grondin, S.C. and M.J. Liptay, *Current concepts in the staging of non-small cell lung cancer*. Surg Oncol, 2002. **11**(4): p. 181-90.
6. Spiro, S.G. and G.A. Silvestri, *The treatment of advanced non-small cell lung cancer*. Curr Opin Pulm Med, 2005. **11**(4): p. 287-91.
7. Vielh, P., et al., *Molecular prognostic factors in resectable non-small cell lung cancer*. Crit Rev Oncol Hematol, 2005. **53**(3): p. 193-7.
8. Noda, K., et al., *Irinotecan plus cisplatin compared with etoposide plus cisplatin for extensive small-cell lung cancer*. N Engl J Med, 2002. **346**(2): p. 85-91.
9. Reck, M., et al., *Randomized phase III trial of paclitaxel, etoposide, and carboplatin versus carboplatin, etoposide, and vincristine in patients with small-cell lung cancer*. J Natl Cancer Inst, 2003. **95**(15): p. 1118-27.
10. Laskin, J., A. Sandler, and D.H. Johnson, *An advance in small-cell lung cancer treatment--more or less*. J Natl Cancer Inst, 2003. **95**(15): p. 1099-101.
11. Bogart, J.A. and J.N. Aronowitz, *Localized non-small cell lung cancer: adjuvant radiotherapy in the era of effective systemic therapy*. Clin Cancer Res, 2005. **11**(13 Pt 2): p. 5004s-5010s.
12. Thatcher, N., et al., *Sequential platinum-based chemotherapy-thoracic radiotherapy in early stage non-small cell lung cancer*. Clin Cancer Res, 2005. **11**(13 Pt 2): p. 5051s-5056s.
13. West, H. and K.S. Albain, *Current standards and ongoing controversies in the management of locally advanced non-small cell lung cancer*. Semin Oncol, 2005. **32**(3): p. 284-92.
14. Kelly, K., *The role of targeted agents in adjuvant therapy for non-small cell lung cancer*. Clin Cancer Res, 2005. **11**(13 Pt 2): p. 5027s-5029s.
15. Le Chevalier, T. and T. Lynch, *Adjuvant treatment of lung cancer: current status and potential applications of new regimens*. Lung Cancer, 2004. **46 Suppl 2**: p. S33-9.
16. Chu, Q., et al., *Taxanes as first-line therapy for advanced non-small cell lung cancer: A systematic review and practice guideline*. Lung Cancer, 2005.
17. Giannitto, G.C., et al., *Paclitaxel, Carboplatin and Gemcitabine Combination as Induction Chemotherapy for Stage IIIA N2 Bulky Non-Small Cell Lung Cancer*. Oncology, 2005. **69**(4): p. 295-300.
18. Hardman JG, L.L., ed. *The Pharmacological Basis of Therapeutics 10th Edition*. 10 ed. Goodman & Gilman's The Pharmacological Basis of Therapeutics, ed. G. AG. 2001, McGraw-Hill: New York.
19. Litman, T., et al., *From MDR to MXR: new understanding of multidrug resistance systems, their properties and clinical significance*. Cell Mol Life Sci, 2001. **58**(7): p. 931-59.
20. Robey, R.W., et al., *ABCG2: determining its relevance in clinical drug resistance*. Cancer Metastasis Rev, 2007. **26**(1): p. 39-57.

21. Kuo, M.T., et al., *The roles of copper transporters in cisplatin resistance*. *Cancer Metastasis Rev*, 2007. **26**(1): p. 71-83.
22. Bakos, E. and L. Homolya, *Portrait of multifaceted transporter, the multidrug resistance-associated protein 1 (MRP1/ABCC1)*. *Pflugers Arch*, 2007. **453**(5): p. 621-41.
23. Kruh, G.D., et al., *ABCC10, ABCC11, and ABCC12*. *Pflugers Arch*, 2007. **453**(5): p. 675-84.
24. Mao, Q. and J.D. Unadkat, *Role of the breast cancer resistance protein (ABCG2) in drug transport*. *Aaps J*, 2005. **7**(1): p. E118-33.
25. Nielsen, D., C. Maare, and T. Skovsgaard, *Cellular resistance to anthracyclines*. *Gen Pharmacol*, 1996. **27**(2): p. 251-5.
26. Hande, K.R., *Etoposide: four decades of development of a topoisomerase II inhibitor*. *Eur J Cancer*, 1998. **34**(10): p. 1514-21.
27. Sinha, B.K., *Topoisomerase inhibitors. A review of their therapeutic potential in cancer*. *Drugs*, 1995. **49**(1): p. 11-9.
28. Grem, J.L., *5-Fluorouracil: forty-plus and still ticking. A review of its preclinical and clinical development*. *Invest New Drugs*, 2000. **18**(4): p. 299-313.
29. Wernyj, R.P. and P.J. Morin, *Molecular mechanisms of platinum resistance: still searching for the Achilles' heel*. *Drug Resist Updat*, 2004. **7**(4-5): p. 227-32.
30. Vaishampayan, U., et al., *Taxanes: an overview of the pharmacokinetics and pharmacodynamics*. *Urology*, 1999. **54**(6A Suppl): p. 22-9.
31. Gligorov, J. and J.P. Lotz, *Preclinical pharmacology of the taxanes: implications of the differences*. *Oncologist*, 2004. **9 Suppl 2**: p. 3-8.
32. Mason, K., et al., *Enhancement of tumor radioresponse by docetaxel: Involvement of immune system*. *Int J Oncol*, 2001. **18**(3): p. 599-606.
33. Haldar, S., A. Basu, and C.M. Croce, *Bcl2 is the guardian of microtubule integrity*. *Cancer Res*, 1997. **57**(2): p. 229-33.
34. Blagosklonny, M.V., et al., *Taxol-induced apoptosis and phosphorylation of Bcl-2 protein involves c-Raf-1 and represents a novel c-Raf-1 signal transduction pathway*. *Cancer Res*, 1996. **56**(8): p. 1851-4.
35. Jones, S.E., et al., *Randomized phase III study of docetaxel compared with paclitaxel in metastatic breast cancer*. *J Clin Oncol*, 2005. **23**(24): p. 5542-51.
36. Pellegrini, F. and D.R. Budman, *Review: tubulin function, action of antitubulin drugs, and new drug development*. *Cancer Invest*, 2005. **23**(3): p. 264-73.
37. Poruchynsky, M.S., et al., *Accompanying protein alterations in malignant cells with a microtubule-polymerizing drug-resistance phenotype and a primary resistance mechanism*. *Biochem Pharmacol*, 2001. **62**(11): p. 1469-80.
38. Bhalla, K.N., *Microtubule-targeted anticancer agents and apoptosis*. *Oncogene*, 2003. **22**(56): p. 9075-86.
39. Andreu, J.M., et al., *Solution structure of Taxotere-induced microtubules to 3-nm resolution. The change in protofilament number is linked to the binding of the taxol side chain*. *J Biol Chem*, 1994. **269**(50): p. 31785-92.
40. Herbst, R.S. and F.R. Khuri, *Mode of action of docetaxel - a basis for combination with novel anticancer agents*. *Cancer Treat Rev*, 2003. **29**(5): p. 407-15.
41. Sparreboom, A., et al., *Comparative preclinical and clinical pharmacokinetics of a cremophor-free, nanoparticle albumin-bound paclitaxel (ABI-007) and paclitaxel formulated in Cremophor (Taxol)*. *Clin Cancer Res*, 2005. **11**(11): p. 4136-43.
42. Eichhorn, M.E., S. Strieth, and M. Dellian, *Anti-vascular tumor therapy: recent advances, pitfalls and clinical perspectives*. *Drug Resist Updat*, 2004. **7**(2): p. 125-38.

43. Huang, X., M. Bennett, and P.E. Thorpe, *A monoclonal antibody that binds anionic phospholipids on tumor blood vessels enhances the antitumor effect of docetaxel on human breast tumors in mice*. *Cancer Res*, 2005. **65**(10): p. 4408-16.
44. Garrett, C.R., et al., *Phase I study of a novel taxane BMS-188797 in adult patients with solid malignancies*. *Clin Cancer Res*, 2005. **11**(9): p. 3335-41.
45. Broxterman, H.J. and N.H. Georgopapadakou, *Anticancer therapeutics: "Addictive" targets, multi-targeted drugs, new drug combinations*. *Drug Resist Updat*, 2005. **8**(4): p. 183-97.
46. Baker, A.F. and R.T. Dorr, *Drug interactions with the taxanes: clinical implications*. *Cancer Treat Rev*, 2001. **27**(4): p. 221-33.
47. Vaclavikova, R., et al., *Different in vitro metabolism of paclitaxel and docetaxel in humans, rats, pigs, and minipigs*. *Drug Metab Dispos*, 2004. **32**(6): p. 666-74.
48. Sparreboom, A., et al., *Nonlinear pharmacokinetics of paclitaxel in mice results from the pharmaceutical vehicle Cremophor EL*. *Cancer Res*, 1996. **56**(9): p. 2112-5.
49. Shivapurkar, N., et al., *Apoptosis and lung cancer: a review*. *J Cell Biochem*, 2003. **88**(5): p. 885-98.
50. Perkins, C.L., et al., *The role of Apaf-1, caspase-9, and bid proteins in etoposide- or paclitaxel-induced mitochondrial events during apoptosis*. *Cancer Res*, 2000. **60**(6): p. 1645-53.
51. Liu, W., et al., *The BCL2-family of protein ligands as cancer drugs: the next generation of therapeutics*. *Curr Med Chem Anti-Canc Agents*, 2003. **3**(3): p. 217-23.
52. Martin, B., et al., *Role of Bcl-2 as a prognostic factor for survival in lung cancer: a systematic review of the literature with meta-analysis*. *Br J Cancer*, 2003. **89**(1): p. 55-64.
53. Inoue, Y., et al., *Bcl-2 overexpression enhances in vitro sensitivity against docetaxel in non-small cell lung cancer*. *Oncol Rep*, 2005. **13**(2): p. 259-64.
54. Huang, Y., et al., *Estrogen increases intracellular p26Bcl-2 to p21Bax ratios and inhibits taxol-induced apoptosis of human breast cancer MCF-7 cells*. *Breast Cancer Res Treat*, 1997. **42**(1): p. 73-81.
55. Huang, Y., et al., *Co-expression of several molecular mechanisms of multidrug resistance and their significance for paclitaxel cytotoxicity in human AML HL-60 cells*. *Leukemia*, 1997. **11**(2): p. 253-7.
56. Li, R., et al., *Apoptosis of non-small-cell lung cancer cell lines after paclitaxel treatment involves the BH3-only proapoptotic protein Bim*. *Cell Death Differ*, 2005. **12**(3): p. 292-303.
57. Hu, Y., et al., *Inhibition of mitogen-activated protein kinase/extracellular signal-regulated kinase enhances chemotherapeutic effects on H460 human non-small cell lung cancer cells through activation of apoptosis*. *Mol Cancer Ther*, 2003. **2**(7): p. 641-9.
58. Sapi, E., et al., *Resistance of ovarian carcinoma cells to docetaxel is XIAP dependent and reversible by phenoxodiol*. *Oncol Res*, 2004. **14**(11-12): p. 567-78.
59. Altieri, D.C., *Survivin and apoptosis control*. *Adv Cancer Res*, 2003. **88**: p. 31-52.
60. Zaffaroni, N., et al., *Expression of the anti-apoptotic gene survivin correlates with taxol resistance in human ovarian cancer*. *Cell Mol Life Sci*, 2002. **59**(8): p. 1406-12.
61. Shapiro, G.I., *Preclinical and clinical development of the cyclin-dependent kinase inhibitor flavopiridol*. *Clin Cancer Res*, 2004. **10**(12 Pt 2): p. 4270s-4275s.
62. Vischioni, B., et al., *Nuclear localization of survivin is a positive prognostic factor for survival in advanced non-small-cell lung cancer*. *Ann Oncol*, 2004. **15**(11): p. 1654-60.

63. Hollstein, M., et al., *Database of p53 gene somatic mutations in human tumors and cell lines*. Nucleic Acids Res, 1994. **22**(17): p. 3551-5.
64. Wang, T.H., H.S. Wang, and Y.K. Soong, *Paclitaxel-induced cell death: where the cell cycle and apoptosis come together*. Cancer, 2000. **88**(11): p. 2619-28.
65. Zaffaroni, N., et al., *Induction of apoptosis by taxol and cisplatin and effect on cell cycle-related proteins in cisplatin-sensitive and -resistant human ovarian cells*. Br J Cancer, 1998. **77**(9): p. 1378-85.
66. Murphy, M., A. Hinman, and A.J. Levine, *Wild-type p53 negatively regulates the expression of a microtubule-associated protein*. Genes Dev, 1996. **10**(23): p. 2971-80.
67. Martello, L.A., et al., *Elevated levels of microtubule destabilizing factors in a Taxol-resistant/dependent A549 cell line with an alpha-tubulin mutation*. Cancer Res, 2003. **63**(6): p. 1207-13.
68. Giannakakou, P., et al., *Paclitaxel-resistant human ovarian cancer cells have mutant beta-tubulins that exhibit impaired paclitaxel-driven polymerization*. J Biol Chem, 1997. **272**(27): p. 17118-25.
69. Monzo, M., et al., *Paclitaxel resistance in non-small-cell lung cancer associated with beta-tubulin gene mutations*. J Clin Oncol, 1999. **17**(6): p. 1786-93.
70. Goncalves, A., et al., *Resistance to Taxol in lung cancer cells associated with increased microtubule dynamics*. Proc Natl Acad Sci U S A, 2001. **98**(20): p. 11737-42.
71. Orr, G.A., et al., *Mechanisms of Taxol resistance related to microtubules*. Oncogene, 2003. **22**(47): p. 7280-95.
72. Shalli, K., et al., *Alterations of beta-tubulin isotypes in breast cancer cells resistant to docetaxel*. Faseb J, 2005. **19**(10): p. 1299-301.
73. Kavallaris, M., et al., *Taxol-resistant epithelial ovarian tumors are associated with altered expression of specific beta-tubulin isotypes*. J Clin Invest, 1997. **100**(5): p. 1282-93.
74. Kavallaris, M., C.A. Burkhart, and S.B. Horwitz, *Antisense oligonucleotides to class III beta-tubulin sensitize drug-resistant cells to Taxol*. Br J Cancer, 1999. **80**(7): p. 1020-5.
75. Dumontet, C., et al., *Expression of class III beta tubulin in non-small cell lung cancer is correlated with resistance to taxane chemotherapy*. Bull Cancer, 2005. **92**(2): p. E25-30.
76. McDaid, H.M. and S.B. Horwitz, *Selective potentiation of paclitaxel (taxol)-induced cell death by mitogen-activated protein kinase inhibition in human cancer cell lines*. Mol Pharmacol, 2001. **60**(2): p. 290-301.
77. Yamamoto, K., H. Ichijo, and S.J. Korsmeyer, *BCL-2 is phosphorylated and inactivated by an ASK1/Jun N-terminal protein kinase pathway normally activated at G(2)/M*. Mol Cell Biol, 1999. **19**(12): p. 8469-78.
78. Patel, N.M., et al., *Paclitaxel sensitivity of breast cancer cells with constitutively active NF-kappaB is enhanced by IkappaBalpha super-repressor and parthenolide*. Oncogene, 2000. **19**(36): p. 4159-69.
79. Fuino, L., et al., *Histone deacetylase inhibitor LAQ824 down-regulates Her-2 and sensitizes human breast cancer cells to trastuzumab, taxotere, gemcitabine, and epothilone B*. Mol Cancer Ther, 2003. **2**(10): p. 971-84.
80. Bentires-Alj, M., et al., *NF-kappaB transcription factor induces drug resistance through MDR1 expression in cancer cells*. Oncogene, 2003. **22**(1): p. 90-7.
81. Takada, Y., Y. Kobayashi, and B.B. Aggarwal, *Evodiamine abolishes constitutive and inducible NF-kappaB activation by inhibiting IkappaBalpha kinase activation, thereby suppressing NF-kappaB-regulated antiapoptotic and metastatic gene expression, up-regulating apoptosis, and inhibiting invasion*. J Biol Chem, 2005. **280**(17): p. 17203-12.

82. Knuefermann, C., et al., *HER2/PI-3K/Akt activation leads to a multidrug resistance in human breast adenocarcinoma cells*. *Oncogene*, 2003. **22**(21): p. 3205-12.
83. Larsen, A.K., A.E. Escargueil, and A. Skladanowski, *Resistance mechanisms associated with altered intracellular distribution of anticancer agents*. *Pharmacol Ther*, 2000. **85**(3): p. 217-29.
84. Baird, R.D. and S.B. Kaye, *Drug resistance reversal--are we getting closer?* *Eur J Cancer*, 2003. **39**(17): p. 2450-61.
85. Sparreboom, A., et al., *Pharmacogenomics of ABC transporters and its role in cancer chemotherapy*. *Drug Resist Updat*, 2003. **6**(2): p. 71-84.
86. Hyde, S.C., et al., *Structural model of ATP-binding proteins associated with cystic fibrosis, multidrug resistance and bacterial transport*. *Nature*, 1990. **346**(6282): p. 362-5.
87. Ito, K., et al., *Apical/basolateral surface expression of drug transporters and its role in vectorial drug transport*. *Pharm Res*, 2005. **22**(10): p. 1559-77.
88. Juliano, R.L. and V. Ling, *A surface glycoprotein modulating drug permeability in Chinese hamster ovary cell mutants*. *Biochim Biophys Acta*, 1976. **455**(1): p. 152-62.
89. Riordan, J.R. and V. Ling, *Genetic and biochemical characterization of multidrug resistance*. *Pharmacol Ther*, 1985. **28**(1): p. 51-75.
90. Gros, P., J. Croop, and D. Housman, *Mammalian multidrug resistance gene: complete cDNA sequence indicates strong homology to bacterial transport proteins*. *Cell*, 1986. **47**(3): p. 371-80.
91. Schinkel, A.H., et al., *Normal viability and altered pharmacokinetics in mice lacking *mdr1*-type (drug-transporting) P-glycoproteins*. *Proc Natl Acad Sci U S A*, 1997. **94**(8): p. 4028-33.
92. Schinkel, A.H., et al., *Disruption of the mouse *mdr1a* P-glycoprotein gene leads to a deficiency in the blood-brain barrier and to increased sensitivity to drugs*. *Cell*, 1994. **77**(4): p. 491-502.
93. Scheffer, G.L., et al., *Multidrug resistance related molecules in human and murine lung*. *J Clin Pathol*, 2002. **55**(5): p. 332-9.
94. Schinkel, A.H. and J.W. Jonker, *Mammalian drug efflux transporters of the ATP binding cassette (ABC) family: an overview*. *Adv Drug Deliv Rev*, 2003. **55**(1): p. 3-29.
95. Krishna, R. and L.D. Mayer, *Multidrug resistance (MDR) in cancer. Mechanisms, reversal using modulators of MDR and the role of MDR modulators in influencing the pharmacokinetics of anticancer drugs*. *Eur J Pharm Sci*, 2000. **11**(4): p. 265-83.
96. Fischer, V., et al., *The multidrug resistance modulator valsopodar (PSC 833) is metabolized by human cytochrome P450 3A. Implications for drug-drug interactions and pharmacological activity of the main metabolite*. *Drug Metab Dispos*, 1998. **26**(8): p. 802-11.
97. Hyafil, F., et al., *In vitro and in vivo reversal of multidrug resistance by GF120918, an acridonecarboxamide derivative*. *Cancer Res*, 1993. **53**(19): p. 4595-602.
98. Dantzig, A.H., et al., *Reversal of P-glycoprotein-mediated multidrug resistance by a potent cyclopropyldibenzosuberane modulator, LY335979*. *Cancer Res*, 1996. **56**(18): p. 4171-9.
99. Pusztai, L., et al., *Phase II study of tariquidar, a selective P-glycoprotein inhibitor, in patients with chemotherapy-resistant, advanced breast carcinoma*. *Cancer*, 2005. **104**(4): p. 682-91.
100. Dale, I.L., et al., *Reversal of P-glycoprotein-mediated multidrug resistance by XR9051, a novel diketopiperazine derivative*. *Br J Cancer*, 1998. **78**(7): p. 885-92.

101. Newman, M.J., et al., *Discovery and characterization of OC144-093, a novel inhibitor of P-glycoprotein-mediated multidrug resistance*. *Cancer Res*, 2000. **60**(11): p. 2964-72.
102. Germann, U.A., et al., *Chemosensitization and drug accumulation effects of VX-710, verapamil, cyclosporin A, MS-209 and GF120918 in multidrug resistant HL60/ADR cells expressing the multidrug resistance-associated protein MRP*. *Anticancer Drugs*, 1997. **8**(2): p. 141-55.
103. Mullin, S., N. Mani, and T.H. Grossman, *Inhibition of antibiotic efflux in bacteria by the novel multidrug resistance inhibitors biricodar (VX-710) and timcodar (VX-853)*. *Antimicrob Agents Chemother*, 2004. **48**(11): p. 4171-6.
104. Bardelmeijer, H.A., et al., *Efficacy of novel P-glycoprotein inhibitors to increase the oral uptake of paclitaxel in mice*. *Invest New Drugs*, 2004. **22**(3): p. 219-29.
105. Malingre, M.M., et al., *Co-administration of GF120918 significantly increases the systemic exposure to oral paclitaxel in cancer patients*. *Br J Cancer*, 2001. **84**(1): p. 42-7.
106. Fracasso, P.M., et al., *Phase I study of docetaxel in combination with the P-glycoprotein inhibitor, zosuquidar, in resistant malignancies*. *Clin Cancer Res*, 2004. **10**(21): p. 7220-8.
107. Kitazaki, T., et al., *Gefitinib, an EGFR tyrosine kinase inhibitor, directly inhibits the function of P-glycoprotein in multidrug resistant cancer cells*. *Lung Cancer*, 2005. **49**(3): p. 337-43.
108. Nakamura, Y., et al., *Gefitinib ("Iressa", ZD1839), an epidermal growth factor receptor tyrosine kinase inhibitor, reverses breast cancer resistance protein/ABCG2-mediated drug resistance*. *Cancer Res*, 2005. **65**(4): p. 1541-6.
109. Chintamani, et al., *Role of p-glycoprotein expression in predicting response to neoadjuvant chemotherapy in breast cancer--a prospective clinical study*. *World J Surg Oncol*, 2005. **3**: p. 61.
110. van den Heuvel-Eibrink, M.M., P. Sonneveld, and R. Pieters, *The prognostic significance of membrane transport-associated multidrug resistance (MDR) proteins in leukemia*. *Int J Clin Pharmacol Ther*, 2000. **38**(3): p. 94-110.
111. Leonard, G.D., T. Fojo, and S.E. Bates, *The role of ABC transporters in clinical practice*. *Oncologist*, 2003. **8**(5): p. 411-24.
112. Sukhai, M. and M. Piquette-Miller, *Regulation of the multidrug resistance genes by stress signals*. *J Pharm Pharm Sci*, 2000. **3**(2): p. 268-80.
113. Yang, J.M., A.D. Vassil, and W.N. Hait, *Activation of phospholipase C induces the expression of the multidrug resistance (MDR1) gene through the Raf-MAPK pathway*. *Mol Pharmacol*, 2001. **60**(4): p. 674-80.
114. Kyriakis, J.M., et al., *The stress-activated protein kinase subfamily of c-Jun kinases*. *Nature*, 1994. **369**(6476): p. 156-60.
115. Osborn, M.T. and T.C. Chambers, *Role of the stress-activated/c-Jun NH2-terminal protein kinase pathway in the cellular response to adriamycin and other chemotherapeutic drugs*. *J Biol Chem*, 1996. **271**(48): p. 30950-5.
116. Barancik, M., et al., *SB203580, a specific inhibitor of p38-MAPK pathway, is a new reversal agent of P-glycoprotein-mediated multidrug resistance*. *Eur J Pharm Sci*, 2001. **14**(1): p. 29-36.
117. Chan, L.M., S. Lowes, and B.H. Hirst, *The ABCs of drug transport in intestine and liver: efflux proteins limiting drug absorption and bioavailability*. *Eur J Pharm Sci*, 2004. **21**(1): p. 25-51.
118. Borst, P., M. Kool, and R. Evers, *Do cMOAT (MRP2), other MRP homologues, and LRP play a role in MDR?* *Semin Cancer Biol*, 1997. **8**(3): p. 205-13.
119. Keppler, D., J. Konig, and M. Buchler, *The canalicular multidrug resistance protein, cMRP/MRP2, a novel conjugate export pump expressed in the apical membrane of hepatocytes*. *Adv Enzyme Regul*, 1997. **37**: p. 321-33.

120. Rost, D., et al., *Expression and localization of the multidrug resistance proteins MRP2 and MRP3 in human gallbladder epithelia*. *Gastroenterology*, 2001. **121**(5): p. 1203-8.
121. Cherrington, N.J., et al., *Organ distribution of multidrug resistance proteins 1, 2, and 3 (Mrp1, 2, and 3) mRNA and hepatic induction of Mrp3 by constitutive androstane receptor activators in rats*. *J Pharmacol Exp Ther*, 2002. **300**(1): p. 97-104.
122. Oselin, K., et al., *Quantitative determination of the human MRP1 and MRP2 mRNA expression in FACS-sorted peripheral blood CD4+, CD8+, CD19+, and CD56+ cells*. *Eur J Haematol*, 2003. **71**(2): p. 119-23.
123. Paulusma, C.C., et al., *A mutation in the human canalicular multispecific organic anion transporter gene causes the Dubin-Johnson syndrome*. *Hepatology*, 1997. **25**(6): p. 1539-42.
124. Fardel, O., et al., *Physiological, pharmacological and clinical features of the multidrug resistance protein 2*. *Biomed Pharmacother*, 2005. **59**(3): p. 104-14.
125. Kruh, G.D., et al., *MRP subfamily transporters and resistance to anticancer agents*. *J Bioenerg Biomembr*, 2001. **33**(6): p. 493-501.
126. Taniguchi, K., et al., *A human canalicular multispecific organic anion transporter (cMOAT) gene is overexpressed in cisplatin-resistant human cancer cell lines with decreased drug accumulation*. *Cancer Res*, 1996. **56**(18): p. 4124-9.
127. Cantz, T., et al., *MRP2, a human conjugate export pump, is present and transports fluo 3 into apical vacuoles of Hep G2 cells*. *Am J Physiol Gastrointest Liver Physiol*, 2000. **278**(4): p. G522-31.
128. Koike, K., et al., *A canalicular multispecific organic anion transporter (cMOAT) antisense cDNA enhances drug sensitivity in human hepatic cancer cells*. *Cancer Res*, 1997. **57**(24): p. 5475-9.
129. Faneyte, I.F., P.M. Kristel, and M.J. van de Vijver, *Multidrug resistance associated genes MRP1, MRP2 and MRP3 in primary and anthracycline exposed breast cancer*. *Anticancer Res*, 2004. **24**(5A): p. 2931-9.
130. Young, L.C., et al., *Multidrug resistance proteins MRP3, MRP1, and MRP2 in lung cancer: correlation of protein levels with drug response and messenger RNA levels*. *Clin Cancer Res*, 2001. **7**(6): p. 1798-804.
131. Steinbach, D., et al., *Response to chemotherapy and expression of the genes encoding the multidrug resistance-associated proteins MRP2, MRP3, MRP4, MRP5, and SMRP in childhood acute myeloid leukemia*. *Clin Cancer Res*, 2003. **9**(3): p. 1083-6.
132. Huisman, M.T., et al., *MRP2 (ABCC2) transports taxanes and confers paclitaxel resistance and both processes are stimulated by probenecid*. *Int J Cancer*, 2005. **116**(5): p. 824-9.
133. Wang, E.J. and W.W. Johnson, *The farnesyl protein transferase inhibitor lonafarnib (SCH66336) is an inhibitor of multidrug resistance proteins 1 and 2*. *Chemotherapy*, 2003. **49**(6): p. 303-8.
134. Wang, E., et al., *The farnesyl protein transferase inhibitor SCH66336 is a potent inhibitor of MDR1 product P-glycoprotein*. *Cancer Res*, 2001. **61**(20): p. 7525-9.
135. Vavricka, S.R., et al., *Interactions of rifamycin SV and rifampicin with organic anion uptake systems of human liver*. *Hepatology*, 2002. **36**(1): p. 164-72.
136. Hooijberg, J.H., et al., *Antifolate resistance mediated by the multidrug resistance proteins MRP1 and MRP2*. *Cancer Res*, 1999. **59**(11): p. 2532-5.
137. El-Sheikh, A.A., et al., *Interaction of nonsteroidal anti-inflammatory drugs with multidrug resistance protein (MRP) 2/ABCC2- and MRP4/ABCC4-mediated methotrexate transport*. *J Pharmacol Exp Ther*, 2007. **320**(1): p. 229-35.

138. Hopper, E., et al., *Analysis of the structure and expression pattern of MRP7 (ABCC10), a new member of the MRP subfamily*. *Cancer Lett*, 2001. **162**(2): p. 181-91.
139. Kao, H.H., et al., *Genomic structure, gene expression, and promoter analysis of human multidrug resistance-associated protein 7*. *J Biomed Sci*, 2003. **10**(1): p. 98-110.
140. Dabrowska, M. and F.M. Sirotnak, *Regulation of transcription of the human MRP7 gene. Characteristics of the basal promoter and identification of tumor-derived transcripts encoding additional 5' end heterogeneity*. *Gene*, 2004. **341**: p. 129-39.
141. Maher, J.M., et al., *Tissue distribution and hepatic and renal ontogeny of the multidrug resistance-associated protein (Mrp) family in mice*. *Drug Metab Dispos*, 2005. **33**(7): p. 947-55.
142. Chen, Z.S., et al., *Transport of bile acids, sulfated steroids, estradiol 17-beta-D-glucuronide, and leukotriene C4 by human multidrug resistance protein 8 (ABCC11)*. *Mol Pharmacol*, 2005. **67**(2): p. 545-57.
143. Hopper-Borge, E., et al., *Analysis of the drug resistance profile of multidrug resistance protein 7 (ABCC10): resistance to docetaxel*. *Cancer Res*, 2004. **64**(14): p. 4927-30.
144. Cole, S.P., et al., *Overexpression of a transporter gene in a multidrug-resistant human lung cancer cell line*. *Science*, 1992. **258**(5088): p. 1650-4.
145. Leslie, E.M., R.G. Deeley, and S.P. Cole, *Toxicological relevance of the multidrug resistance protein 1, MRP1 (ABCC1) and related transporters*. *Toxicology*, 2001. **167**(1): p. 3-23.
146. Borst, P., et al., *A family of drug transporters: the multidrug resistance-associated proteins*. *J Natl Cancer Inst*, 2000. **92**(16): p. 1295-302.
147. Borst, P., et al., *The multidrug resistance protein family*. *Biochim Biophys Acta*, 1999. **1461**(2): p. 347-57.
148. Kruh, G.D. and M.G. Belinsky, *The MRP family of drug efflux pumps*. *Oncogene*, 2003. **22**(47): p. 7537-52.
149. Loe, D.W., R.G. Deeley, and S.P. Cole, *Characterization of vincristine transport by the M(r) 190,000 multidrug resistance protein (MRP): evidence for cotransport with reduced glutathione*. *Cancer Res*, 1998. **58**(22): p. 5130-6.
150. Cole, S.P. and R.G. Deeley, *Multidrug resistance mediated by the ATP-binding cassette transporter protein MRP*. *Bioessays*, 1998. **20**(11): p. 931-40.
151. Rappa, G., et al., *New insights into the biology and pharmacology of the multidrug resistance protein (MRP) from gene knockout models*. *Biochem Pharmacol*, 1999. **58**(4): p. 557-62.
152. Jedlitschky, G., et al., *Transport of glutathione, glucuronate, and sulfate conjugates by the MRP gene-encoded conjugate export pump*. *Cancer Res*, 1996. **56**(5): p. 988-94.
153. Loe, D.W., et al., *ATP-dependent transport of aflatoxin B1 and its glutathione conjugates by the product of the multidrug resistance protein (MRP) gene*. *Mol Pharmacol*, 1997. **51**(6): p. 1034-41.
154. Versantvoort, C.H., et al., *On the relationship between the probenecid-sensitive transport of daunorubicin or calcein and the glutathione status of cells overexpressing the multidrug resistance-associated protein (MRP)*. *Int J Cancer*, 1995. **63**(6): p. 855-62.
155. Zaman, G.J., et al., *Role of glutathione in the export of compounds from cells by the multidrug-resistance-associated protein*. *Proc Natl Acad Sci U S A*, 1995. **92**(17): p. 7690-4.

156. Feller, N., et al., *ATP-dependent efflux of calcein by the multidrug resistance protein (MRP): no inhibition by intracellular glutathione depletion*. FEBS Lett, 1995. **368**(2): p. 385-8.
157. Keppler, D., et al., *ATP-dependent transport of glutathione S-conjugates by the multidrug resistance protein MRP1 and its apical isoform MRP2*. Chem Biol Interact, 1998. **111-112**: p. 153-61.
158. Loe, D.W., et al., *Multidrug resistance protein (MRP)-mediated transport of leukotriene C4 and chemotherapeutic agents in membrane vesicles. Demonstration of glutathione-dependent vincristine transport*. J Biol Chem, 1996. **271**(16): p. 9675-82.
159. Evers, R., et al., *Drug export activity of the human canalicular multispecific organic anion transporter in polarized kidney MDCK cells expressing cMOAT (MRP2) cDNA*. J Clin Invest, 1998. **101**(7): p. 1310-9.
160. Duffy, C.P., et al., *Enhancement of chemotherapeutic drug toxicity to human tumour cells in vitro by a subset of non-steroidal anti-inflammatory drugs (NSAIDs)*. Eur J Cancer, 1998. **34**(8): p. 1250-9.
161. O'Connor, R., et al., *A phase I clinical and pharmacokinetic study of the multidrug resistance protein-1 (MRP-1) inhibitor sulindac, in combination with epirubicin in patients with advanced cancer*. Cancer Chemother Pharmacol, 2007. **59**(1): p. 79-87.
162. Kool, M., et al., *MRP3, an organic anion transporter able to transport anti-cancer drugs*. Proc Natl Acad Sci U S A, 1999. **96**(12): p. 6914-9.
163. Hirohashi, T., H. Suzuki, and Y. Sugiyama, *Characterization of the transport properties of cloned rat multidrug resistance-associated protein 3 (MRP3)*. J Biol Chem, 1999. **274**(21): p. 15181-5.
164. Zelcer, N., et al., *Characterization of drug transport by the human multidrug resistance protein 3 (ABCC3)*. J Biol Chem, 2001. **276**(49): p. 46400-7.
165. Ambudkar, S.V., et al., *P-glycoprotein: from genomics to mechanism*. Oncogene, 2003. **22**(47): p. 7468-85.
166. Chen, Z.S., K. Lee, and G.D. Kruh, *Transport of cyclic nucleotides and estradiol 17-beta-D-glucuronide by multidrug resistance protein 4. Resistance to 6-mercaptopurine and 6-thioguanine*. J Biol Chem, 2001. **276**(36): p. 33747-54.
167. Sauna, Z.E., K. Nandigama, and S.V. Ambudkar, *Multidrug resistance protein 4 (ABCC4)-mediated ATP hydrolysis: effect of transport substrates and characterization of the post-hydrolysis transition state*. J Biol Chem, 2004. **279**(47): p. 48855-64.
168. Schuetz, J.D., et al., *MRP4: A previously unidentified factor in resistance to nucleoside-based antiviral drugs*. Nat Med, 1999. **5**(9): p. 1048-51.
169. Pratt, S., et al., *Kinetic validation of the use of carboxydichlorofluorescein as a drug surrogate for MRP5-mediated transport*. Eur J Pharm Sci, 2006. **27**(5): p. 524-32.
170. Wijnholds, J., et al., *Multidrug-resistance protein 5 is a multispecific organic anion transporter able to transport nucleotide analogs*. Proc Natl Acad Sci U S A, 2000. **97**(13): p. 7476-81.
171. Hendig, D., et al., *New ABCC6 gene mutations in German pseudoxanthoma elasticum patients*. J Mol Med, 2005. **83**(2): p. 140-7.
172. Belinsky, M.G., et al., *Characterization of the drug resistance and transport properties of multidrug resistance protein 6 (MRP6, ABCC6)*. Cancer Res, 2002. **62**(21): p. 6172-7.
173. Guo, Y., et al., *MRP8, ATP-binding cassette C11 (ABCC11), is a cyclic nucleotide efflux pump and a resistance factor for fluoropyrimidines 2',3'-dideoxycytidine and 9'-(2'-phosphonylmethoxyethyl)adenine*. J Biol Chem, 2003. **278**(32): p. 29509-14.

174. Doyle, L.A., et al., *A multidrug resistance transporter from human MCF-7 breast cancer cells*. Proc Natl Acad Sci U S A, 1998. **95**(26): p. 15665-70.
175. Allikmets, R., et al., *A human placenta-specific ATP-binding cassette gene (ABCP) on chromosome 4q22 that is involved in multidrug resistance*. Cancer Res, 1998. **58**(23): p. 5337-9.
176. Rocchi, E., et al., *The product of the ABC half-transporter gene ABCG2 (BCRP/MXR/ABCP) is expressed in the plasma membrane*. Biochem Biophys Res Commun, 2000. **271**(1): p. 42-6.
177. Stein, U., et al., *Impact of BCRP/MXR, MRP1 and MDRI/P-Glycoprotein on thermoresistant variants of atypical and classical multidrug resistant cancer cells*. Int J Cancer, 2002. **97**(6): p. 751-60.
178. Dietel, M., et al., *Membrane vesicle formation due to acquired mitoxantrone resistance in human gastric carcinoma cell line EPG85-257*. Cancer Res, 1990. **50**(18): p. 6100-6.
179. Lage, H. and M. Dietel, *Effect of the breast-cancer resistance protein on atypical multidrug resistance*. Lancet Oncol, 2000. **1**: p. 169-75.
180. Ross, D.D., *Novel mechanisms of drug resistance in leukemia*. Leukemia, 2000. **14**(3): p. 467-73.
181. Maliepaard, M., et al., *Subcellular localization and distribution of the breast cancer resistance protein transporter in normal human tissues*. Cancer Res, 2001. **61**(8): p. 3458-64.
182. Hardwick, L.J., S. Velamakanni, and H.W. van Veen, *The emerging pharmacotherapeutic significance of the breast cancer resistance protein (ABCG2)*. Br J Pharmacol, 2007. **151**(2): p. 163-74.
183. Rabindran, S.K., et al., *Fumitremorgin C reverses multidrug resistance in cells transfected with the breast cancer resistance protein*. Cancer Res, 2000. **60**(1): p. 47-50.
184. Rabindran, S.K., et al., *Reversal of a novel multidrug resistance mechanism in human colon carcinoma cells by fumitremorgin C*. Cancer Res, 1998. **58**(24): p. 5850-8.
185. de Bruin, M., et al., *Reversal of resistance by GF120918 in cell lines expressing the ABC half-transporter, MXR*. Cancer Lett, 1999. **146**(2): p. 117-26.
186. Maliepaard, M., et al., *Circumvention of breast cancer resistance protein (BCRP)-mediated resistance to camptothecins in vitro using non-substrate drugs or the BCRP inhibitor GF120918*. Clin Cancer Res, 2001. **7**(4): p. 935-41.
187. van der Deen, M., et al., *ATP-binding cassette (ABC) transporters in normal and pathological lung*. Respir Res, 2005. **6**: p. 59.
188. Moscow, J.A., C.A. Swanson, and K.H. Cowan, *Decreased melphalan accumulation in a human breast cancer cell line selected for resistance to melphalan*. Br J Cancer, 1993. **68**(4): p. 732-7.
189. Safaei, R. and S.B. Howell, *Copper transporters regulate the cellular pharmacology and sensitivity to Pt drugs*. Crit Rev Oncol Hematol, 2005. **53**(1): p. 13-23.
190. Moscow, J.A., *Methotrexate transport and resistance*. Leuk Lymphoma, 1998. **30**(3-4): p. 215-24.
191. Kong, W., K. Engel, and J. Wang, *Mammalian nucleoside transporters*. Curr Drug Metab, 2004. **5**(1): p. 63-84.
192. Smith, N.F., et al., *Identification of OATP1B3 as a High-Affinity Hepatocellular Transporter of Paclitaxel*. Cancer Biol Ther, 2005. **4**(8).
193. Kobayashi, Y., et al., *Transport mechanism and substrate specificity of human organic anion transporter 2 (hOat2 [SLC22A7])*. J Pharm Pharmacol, 2005. **57**(5): p. 573-8.

194. Hediger, M.A., et al., *The ABCs of solute carriers: physiological, pathological and therapeutic implications of human membrane transport proteins* Introduction. *Pflugers Arch*, 2004. **447**(5): p. 465-8.
195. Hagenbuch, B. and P.J. Meier, *Organic anion transporting polypeptides of the OATP/SLC21 family: phylogenetic classification as OATP/SLCO superfamily, new nomenclature and molecular/functional properties*. *Pflugers Arch*, 2004. **447**(5): p. 653-65.
196. Hagenbuch, B. and P.J. Meier, *The superfamily of organic anion transporting polypeptides*. *Biochim Biophys Acta*, 2003. **1609**(1): p. 1-18.
197. Ballatori, N., et al., *Molecular mechanisms of reduced glutathione transport: role of the MRP/CFTR/ABCC and OATP/SLC21A families of membrane proteins*. *Toxicol Appl Pharmacol*, 2005. **204**(3): p. 238-55.
198. Abe, T., et al., *LST-2, a human liver-specific organic anion transporter, determines methotrexate sensitivity in gastrointestinal cancers*. *Gastroenterology*, 2001. **120**(7): p. 1689-99.
199. Cvetkovic, M., et al., *OATP and P-glycoprotein transporters mediate the cellular uptake and excretion of fexofenadine*. *Drug Metab Dispos*, 1999. **27**(8): p. 866-71.
200. Wang, X., A.W. Wolkoff, and M.E. Morris, *Flavonoids as a novel class of human organic anion-transporting polypeptide OATP1B1 (OATP-C) modulators*. *Drug Metab Dispos*, 2005. **33**(11): p. 1666-72.
201. Koepsell, H., K. Lips, and C. Volk, *Polyspecific organic cation transporters: structure, function, physiological roles, and biopharmaceutical implications*. *Pharm Res*, 2007. **24**(7): p. 1227-51.
202. Chen, R. and J.A. Nelson, *Role of organic cation transporters in the renal secretion of nucleosides*. *Biochem Pharmacol*, 2000. **60**(2): p. 215-9.
203. Sekine, T., H. Miyazaki, and H. Endou, *Molecular physiology of renal organic anion transporters*. *Am J Physiol Renal Physiol*, 2006. **290**(2): p. F251-61.
204. Anzai, N., Y. Kanai, and H. Endou, *Organic anion transporter family: current knowledge*. *J Pharmacol Sci*, 2006. **100**(5): p. 411-26.
205. Olayioye, M.A., et al., *The ErbB signaling network: receptor heterodimerization in development and cancer*. *Embo J*, 2000. **19**(13): p. 3159-67.
206. Blume-Jensen, P. and T. Hunter, *Oncogenic kinase signalling*. *Nature*, 2001. **411**(6835): p. 355-65.
207. Salomon, D.S., et al., *Epidermal growth factor-related peptides and their receptors in human malignancies*. *Crit Rev Oncol Hematol*, 1995. **19**(3): p. 183-232.
208. Yarden, Y. and M.X. Sliwkowski, *Untangling the ErbB signalling network*. *Nat Rev Mol Cell Biol*, 2001. **2**(2): p. 127-37.
209. Kamath, S. and J.K. Buolamwini, *Targeting EGFR and HER-2 receptor tyrosine kinases for cancer drug discovery and development*. *Med Res Rev*, 2006. **26**(5): p. 569-94.
210. Prenzel, N., et al., *The epidermal growth factor receptor family as a central element for cellular signal transduction and diversification*. *Endocr Relat Cancer*, 2001. **8**(1): p. 11-31.
211. Way, T.D. and J.K. Lin, *Role of HER2/HER3 co-receptor in breast carcinogenesis*. *Fut Oncol*, 2005. **1**(6): p. 841-9.
212. Roskoski, R., Jr., *The ErbB/HER receptor protein-tyrosine kinases and cancer*. *Biochem Biophys Res Commun*, 2004. **319**(1): p. 1-11.
213. Klapper, L.N., et al., *Tumor-inhibitory antibodies to HER-2/ErbB-2 may act by recruiting c-Cbl and enhancing ubiquitination of HER-2*. *Cancer Res*, 2000. **60**(13): p. 3384-8.

214. Bost, F., et al., *The Jun kinase 2 isoform is preferentially required for epidermal growth factor-induced transformation of human A549 lung carcinoma cells*. Mol Cell Biol, 1999. **19**(3): p. 1938-49.
215. Mishima, K., K. Inoue, and Y. Hayashi, *Overexpression of extracellular-signal regulated kinases on oral squamous cell carcinoma*. Oral Oncol, 2002. **38**(5): p. 468-74.
216. Matsuda, K., et al., *Multiple mitogenic pathways in pancreatic cancer cells are blocked by a truncated epidermal growth factor receptor*. Cancer Res, 2002. **62**(19): p. 5611-7.
217. Tikhomirov, O. and G. Carpenter, *Ligand-induced, p38-dependent apoptosis in cells expressing high levels of epidermal growth factor receptor and ErbB-2*. J Biol Chem, 2004. **279**(13): p. 12988-96.
218. Aguirre-Ghiso, J.A., et al., *ERK(MAPK) activity as a determinant of tumor growth and dormancy; regulation by p38(SAPK)*. Cancer Res, 2003. **63**(7): p. 1684-95.
219. Mukherjee, S., M. Tessema, and A. Wandinger-Ness, *Vesicular trafficking of tyrosine kinase receptors and associated proteins in the regulation of signaling and vascular function*. Circ Res, 2006. **98**(6): p. 743-56.
220. Razani, B., S.E. Woodman, and M.P. Lisanti, *Caveolae: from cell biology to animal physiology*. Pharmacol Rev, 2002. **54**(3): p. 431-67.
221. Downward, J., et al., *Close similarity of epidermal growth factor receptor and v-erb-B oncogene protein sequences*. Nature, 1984. **307**(5951): p. 521-7.
222. Bargmann, C.I., M.C. Hung, and R.A. Weinberg, *The neu oncogene encodes an epidermal growth factor receptor-related protein*. Nature, 1986. **319**(6050): p. 226-30.
223. Lee, S.M., *Is EGFR expression important in non-small cell lung cancer?* Thorax, 2006. **61**(2): p. 98-9.
224. Witton, C.J., et al., *Expression of the HER1-4 family of receptor tyrosine kinases in breast cancer*. J Pathol, 2003. **200**(3): p. 290-7.
225. Sweeney, C., et al., *ErbB receptor negative regulatory mechanisms: implications in cancer*. J Mammary Gland Biol Neoplasia, 2006. **11**(1): p. 89-99.
226. Sharma, S.V., et al., *Epidermal growth factor receptor mutations in lung cancer*. Nat Rev Cancer, 2007. **7**(3): p. 169-81.
227. Ross, J.S., et al., *The Her-2/neu gene and protein in breast cancer 2003: biomarker and target of therapy*. Oncologist, 2003. **8**(4): p. 307-25.
228. Slamon, D.J., et al., *Use of chemotherapy plus a monoclonal antibody against HER2 for metastatic breast cancer that overexpresses HER2*. N Engl J Med, 2001. **344**(11): p. 783-92.
229. Andre, F., T. Le Chevalier, and J.C. Soria, *Her2-neu: a target in lung cancer?* Ann Oncol, 2004. **15**(1): p. 3-4.
230. Gatzemeier, U., et al., *Randomized phase II trial of gemcitabine-cisplatin with or without trastuzumab in HER2-positive non-small-cell lung cancer*. Ann Oncol, 2004. **15**(1): p. 19-27.
231. Arteaga, C.L., *HER3 and mutant EGFR meet MET*. Nat Med, 2007. **13**(6): p. 675-7.
232. Roberts, P.J. and C.J. Der, *Targeting the Raf-MEK-ERK mitogen-activated protein kinase cascade for the treatment of cancer*. Oncogene, 2007. **26**(22): p. 3291-310.
233. Peng, D., et al., *Anti-epidermal growth factor receptor monoclonal antibody 225 up-regulates p27KIP1 and induces G1 arrest in prostatic cancer cell line DU145*. Cancer Res, 1996. **56**(16): p. 3666-9.
234. Dubey, S. and J.H. Schiller, *Three emerging new drugs for NSCLC: pemetrexed, bortezomib, and cetuximab*. Oncologist, 2005. **10**(4): p. 282-91.

235. Hirata, A., et al., *HER2 overexpression increases sensitivity to gefitinib, an epidermal growth factor receptor tyrosine kinase inhibitor, through inhibition of HER2/HER3 heterodimer formation in lung cancer cells.* *Cancer Res*, 2005. **65**(10): p. 4253-60.
236. Kelly, K. and S. Averbuch, *Gefitinib: phase II and III results in advanced non-small cell lung cancer.* *Semin Oncol*, 2004. **31**(1 Suppl 1): p. 93-9.
237. Miller, V.A., et al., *Bronchioloalveolar pathologic subtype and smoking history predict sensitivity to gefitinib in advanced non-small-cell lung cancer.* *J Clin Oncol*, 2004. **22**(6): p. 1103-9.
238. Paez, J.G., et al., *EGFR mutations in lung cancer: correlation with clinical response to gefitinib therapy.* *Science*, 2004. **304**(5676): p. 1497-500.
239. Lynch, T.J., et al., *Activating mutations in the epidermal growth factor receptor underlying responsiveness of non-small-cell lung cancer to gefitinib.* *N Engl J Med*, 2004. **350**(21): p. 2129-39.
240. Kris, M.G., *How Today's Developments in the Treatment of Non-Small Cell Lung Cancer Will Change Tomorrow's Standards of Care.* *Oncologist*, 2005. **10 Suppl 2**: p. 23-9.
241. Han, S.W., et al., *Predictive and prognostic impact of epidermal growth factor receptor mutation in non-small-cell lung cancer patients treated with gefitinib.* *J Clin Oncol*, 2005. **23**(11): p. 2493-501.
242. Pao, W., et al., *EGF receptor gene mutations are common in lung cancers from "never smokers" and are associated with sensitivity of tumors to gefitinib and erlotinib.* *Proc Natl Acad Sci U S A*, 2004. **101**(36): p. 13306-11.
243. Giaccone, G., et al., *Gefitinib in combination with gemcitabine and cisplatin in advanced non-small-cell lung cancer: a phase III trial--INTACT 1.* *J Clin Oncol*, 2004. **22**(5): p. 777-84.
244. Dancey, J.E. and B. Freidlin, *Targeting epidermal growth factor receptor--are we missing the mark?* *Lancet*, 2003. **362**(9377): p. 62-4.
245. Moyer, J.D., et al., *Induction of apoptosis and cell cycle arrest by CP-358,774, an inhibitor of epidermal growth factor receptor tyrosine kinase.* *Cancer Res*, 1997. **57**(21): p. 4838-48.
246. Rusnak, D.W., et al., *The characterization of novel, dual ErbB-2/EGFR, tyrosine kinase inhibitors: potential therapy for cancer.* *Cancer Res*, 2001. **61**(19): p. 7196-203.
247. Coleman, R., *CLiMB/EGF100151 - Capecitabine and Lapatinib in Metastatic Breast cancer. A Phase III, Randomized, Open-Label, Multicenter Study Comparing GW572016 and Capecitabine (Xeloda) versus Capecitabine in Women with Refractory Advanced or Metastatic Breast Cancer.*
248. Rusnak, D.W., et al., *The effects of the novel, reversible epidermal growth factor receptor/ErbB-2 tyrosine kinase inhibitor, GW2016, on the growth of human normal and tumor-derived cell lines in vitro and in vivo.* *Mol Cancer Ther*, 2001. **1**(2): p. 85-94.
249. Spector, N.L., et al., *Study of the biologic effects of lapatinib, a reversible inhibitor of ErbB1 and ErbB2 tyrosine kinases, on tumor growth and survival pathways in patients with advanced malignancies.* *J Clin Oncol*, 2005. **23**(11): p. 2502-12.
250. Wood, E.R., et al., *A unique structure for epidermal growth factor receptor bound to GW572016 (Lapatinib): relationships among protein conformation, inhibitor off-rate, and receptor activity in tumor cells.* *Cancer Res*, 2004. **64**(18): p. 6652-9.
251. Ozvegy-Laczka, C., et al., *High-affinity interaction of tyrosine kinase inhibitors with the ABCG2 multidrug transporter.* *Mol Pharmacol*, 2004. **65**(6): p. 1485-95.

252. Yang, C.H., et al., *Gefitinib reverses chemotherapy resistance in gefitinib-insensitive multidrug resistant cancer cells expressing ATP-binding cassette family protein*. *Cancer Res*, 2005. **65**(15): p. 6943-9.
253. Ozvegy-Laczka, C., et al., *Tyrosine kinase inhibitor resistance in cancer: role of ABC multidrug transporters*. *Drug Resist Updat*, 2005. **8**(1-2): p. 15-26.
254. Li, J., et al., *Association of variant ABCG2 and the pharmacokinetics of epidermal growth factor receptor tyrosine kinase inhibitors in cancer patients*. *Cancer Biol Ther*, 2007. **6**(3): p. 432-8.
255. Stewart, C.F., et al., *Gefitinib enhances the antitumor activity and oral bioavailability of irinotecan in mice*. *Cancer Res*, 2004. **64**(20): p. 7491-9.
256. Cusatis, G., et al., *Pharmacogenetics of ABCG2 and adverse reactions to gefitinib*. *J Natl Cancer Inst*, 2006. **98**(23): p. 1739-42.
257. Wall R, M.G., Crown J, Clynes M, O'Connor R., *Rapid and sensitive liquid chromatography-tandem mass spectrometry for the quantitation of epirubicin and identification of metabolites in biological samples*. *Talanta*, In Press, 2006.
258. Sarkadi, B., et al., *Expression of the human multidrug resistance cDNA in insect cells generates a high activity drug-stimulated membrane ATPase*. *J Biol Chem*, 1992. **267**(7): p. 4854-8.
259. Heenan, M., et al., *Absence of correlation between chemo- and radioresistance in a range of human tumour cell lines*. *Cytotechnology*, 1996. **19**(3): p. 237-42.
260. Liang, Y., et al., *Enhanced in vitro invasiveness and drug resistance with altered gene expression patterns in a human lung carcinoma cell line after pulse selection with anticancer drugs*. *Int J Cancer*, 2004. **111**(4): p. 484-93.
261. Collins, S.J., R.C. Gallo, and R.E. Gallagher, *Continuous growth and differentiation of human myeloid leukaemic cells in suspension culture*. *Nature*, 1977. **270**(5635): p. 347-9.
262. Connolly, L., et al., *A new monoclonal antibody, P2A8(6), that specifically recognizes a novel epitope on the multidrug resistance-associated protein 1 (MRP1), but not on MRP2 nor MRP3*. *Hybrid Hybridomics*, 2001. **20**(5-6): p. 333-41.
263. Kullak-Ublick, G.A., et al., *Organic anion-transporting polypeptide B (OATP-B) and its functional comparison with three other OATPs of human liver*. *Gastroenterology*, 2001. **120**(2): p. 525-33.
264. Cui, Y., et al., *Hepatic uptake of bilirubin and its conjugates by the human organic anion transporter SLC21A6*. *J Biol Chem*, 2001. **276**(13): p. 9626-30.
265. Yamaguchi, H., et al., *Transport of fluorescent chenodeoxycholic acid via the human organic anion transporters OATP1B1 and OATP1B3*. *J Lipid Res*, 2006. **47**(6): p. 1196-202.
266. Kim, R.B., *Organic anion-transporting polypeptide (OATP) transporter family and drug disposition*. *Eur J Clin Invest*, 2003. **33 Suppl 2**: p. 1-5.
267. Adachi, H., et al., *Molecular characterization of human and rat organic anion transporter OATP-D*. *Am J Physiol Renal Physiol*, 2003. **285**(6): p. F1188-97.
268. Tamai, I., et al., *Molecular identification and characterization of novel members of the human organic anion transporter (OATP) family*. *Biochem Biophys Res Commun*, 2000. **273**(1): p. 251-60.
269. Fujiwara, K., et al., *Identification of thyroid hormone transporters in humans: different molecules are involved in a tissue-specific manner*. *Endocrinology*, 2001. **142**(5): p. 2005-12.
270. Li, J., et al., *Association of Variant ABCG2 and the Pharmacokinetics of Epidermal Growth factor Receptor Tyrosine Kinase Inhibitors in Cancer Patients*. *Cancer Biol Ther*, 2007. **6**(3).
271. Herbst, R.S., et al., *Selective oral epidermal growth factor receptor tyrosine kinase inhibitor ZD1839 is generally well-tolerated and has activity in non-small-*

- cell lung cancer and other solid tumors: results of a phase I trial.* J Clin Oncol, 2002. **20**(18): p. 3815-25.
272. Hidalgo, M., et al., *Phase I and pharmacologic study of OSI-774, an epidermal growth factor receptor tyrosine kinase inhibitor, in patients with advanced solid malignancies.* J Clin Oncol, 2001. **19**(13): p. 3267-79.
273. Burris, H.A., 3rd, et al., *Phase I safety, pharmacokinetics, and clinical activity study of lapatinib (GW572016), a reversible dual inhibitor of epidermal growth factor receptor tyrosine kinases, in heavily pretreated patients with metastatic carcinomas.* J Clin Oncol, 2005. **23**(23): p. 5305-13.
274. Ciccolini, J., et al., *Rapid high-performance liquid chromatographic determination of docetaxel (Taxotere) in plasma using liquid-liquid extraction.* J Chromatogr B Biomed Sci Appl, 2001. **759**(2): p. 299-306.
275. Torkey, A.R., et al., *Immuno-histochemical detection of MRPs in human lung cells in culture.* Toxicology, 2005. **207**(3): p. 437-50.
276. Harris, K.E. and E.H. Jeffery, *Sulforaphane and erucin increase MRP1 and MRP2 in human carcinoma cell lines.* J Nutr Biochem, 2007.
277. Klassen, D.K., et al., *Sulindac kinetics and effects on renal function and prostaglandin excretion in renal insufficiency.* J Clin Pharmacol, 1989. **29**(11): p. 1037-42.
278. Versantvoort, C.H., et al., *Energy-dependent processes involved in reduced drug accumulation in multidrug-resistant human lung cancer cell lines without P-glycoprotein expression.* Cancer Res, 1992. **52**(1): p. 17-23.
279. Cantarovich, F., et al., *Cyclosporine plasma levels six hours after oral administration. A useful tool for monitoring therapy.* Transplantation, 1988. **45**(2): p. 389-94.
280. Thomas, H. and H.M. Coley, *Overcoming multidrug resistance in cancer: an update on the clinical strategy of inhibiting p-glycoprotein.* Cancer Control, 2003. **10**(2): p. 159-65.
281. Shirakawa, K., et al., *Interaction of docetaxel ("Taxotere") with human P-glycoprotein.* Jpn J Cancer Res, 1999. **90**(12): p. 1380-6.
282. Stone, R.M., *Treatment of acute myeloid leukemia: state-of-the-art and future directions.* Semin Hematol, 2002. **39**(3 Suppl 2): p. 4-10.
283. Nagasawa, K., et al., *Contribution of specific transport systems to anthracycline transport in tumor and normal cells.* Curr Drug Metab, 2001. **2**(4): p. 355-66.
284. Benderra, Z., et al., *MRP3, BCRP, and P-glycoprotein activities are prognostic factors in adult acute myeloid leukemia.* Clin Cancer Res, 2005. **11**(21): p. 7764-72.
285. Ehrlichova, M., et al., *Transport and cytotoxicity of paclitaxel, docetaxel, and novel taxanes in human breast cancer cells.* Naunyn Schmiedebergs Arch Pharmacol, 2005. **372**(1): p. 95-105.
286. Zhu, Q. and M.S. Center, *Cloning and sequence analysis of the promoter region of the MRP gene of HL60 cells isolated for resistance to adriamycin.* Cancer Res, 1994. **54**(16): p. 4488-92.
287. O'Brien, M.L., et al., *Glutathione peptidomimetic drug modulator of multidrug resistance-associated protein.* J Pharmacol Exp Ther, 1999. **291**(3): p. 1348-55.
288. Paul, S., et al., *ATP-dependent uptake of natural product cytotoxic drugs by membrane vesicles establishes MRP as a broad specificity transporter.* Proc Natl Acad Sci U S A, 1996. **93**(14): p. 6929-34.
289. Liu, S., et al., *Resonance Rayleigh scattering spectra for studying the interaction of anthracycline antineoplastic antibiotics with some anionic surfactants and their analytical applications.* Anal Chim Acta, 2007. **601**(1): p. 101-7.

290. Wielinga, P.R., H.V. Westerhoff, and J. Lankelma, *The relative importance of passive and P-glycoprotein mediated anthracycline efflux from multidrug-resistant cells*. Eur J Biochem, 2000. **267**(3): p. 649-57.
291. Featherstone, J.M., et al., *The nuclear membrane in multidrug resistance: microinjection of epirubicin into bladder cancer cell lines*. BJU Int, 2005. **95**(7): p. 1091-8.
292. Hurwitz, S.J., et al., *Vesicular anthracycline accumulation in doxorubicin-selected U-937 cells: participation of lysosomes*. Blood, 1997. **89**(10): p. 3745-54.
293. Calcabrini, A., et al., *Detection of P-glycoprotein in the nuclear envelope of multidrug resistant cells*. Histochem J, 2000. **32**(10): p. 599-606.
294. Marcus, A.I., et al., *Farnesyltransferase inhibitors reverse taxane resistance*. Cancer Res, 2006. **66**(17): p. 8838-46.
295. Sessa, C. and O. Pagani, *Docetaxel and epirubicin in advanced breast cancer*. Oncologist, 2001. **6 Suppl 3**: p. 13-6.
296. Gennari, A., et al., *Cardiotoxicity of epirubicin/paclitaxel-containing regimens: role of cardiac risk factors*. J Clin Oncol, 1999. **17**(11): p. 3596-602.
297. Fogli, S., et al., *Gemcitabine, epirubicin and paclitaxel: pharmacokinetic and pharmacodynamic interactions in advanced breast cancer*. Ann Oncol, 2002. **13**(6): p. 919-27.
298. Lunardi, G., et al., *Influence of trastuzumab on epirubicin pharmacokinetics in metastatic breast cancer patients*. Ann Oncol, 2003. **14**(8): p. 1222-6.
299. Song, D., L.F. Hsu, and J.L. Au, *Binding of taxol to plastic and glass containers and protein under in vitro conditions*. J Pharm Sci, 1996. **85**(1): p. 29-31.
300. Clarke, S.J. and L.P. Rivory, *Clinical pharmacokinetics of docetaxel*. Clin Pharmacokinet, 1999. **36**(2): p. 99-114.
301. Urien, S., et al., *Docetaxel serum protein binding with high affinity to alpha 1-acid glycoprotein*. Invest New Drugs, 1996. **14**(2): p. 147-51.
302. Jang, S.H., M.G. Wientjes, and J.L. Au, *Interdependent effect of P-glycoprotein-mediated drug efflux and intracellular drug binding on intracellular paclitaxel pharmacokinetics: application of computational modeling*. J Pharmacol Exp Ther, 2003. **304**(2): p. 773-80.
303. Jang, S.H., M.G. Wientjes, and J.L. Au, *Determinants of paclitaxel uptake, accumulation and retention in solid tumors*. Invest New Drugs, 2001. **19**(2): p. 113-23.
304. Schiffer, R., et al., *Active influx transport is mediated by members of the organic anion transporting polypeptide family in human epidermal keratinocytes*. J Invest Dermatol, 2003. **120**(2): p. 285-91.
305. Eytan, G.D., et al., *The role of passive transbilayer drug movement in multidrug resistance and its modulation*. J Biol Chem, 1996. **271**(22): p. 12897-902.
306. Huang, Y. and W. Sadee, *Membrane transporters and channels in chemoresistance and -sensitivity of tumor cells*. Cancer Lett, 2006. **239**(2): p. 168-82.
307. Smith, N.F., et al., *Identification of OATP1B3 as a high-affinity hepatocellular transporter of paclitaxel*. Cancer Biol Ther, 2005. **4**(8): p. 815-8.
308. Franco, R. and J.A. Cidlowski, *SLCO/OATP-like transport of glutathione in FasL-induced apoptosis: glutathione efflux is coupled to an organic anion exchange and is necessary for the progression of the execution phase of apoptosis*. J Biol Chem, 2006. **281**(40): p. 29542-57.
309. Kamath, A.V., I.M. Darling, and M.E. Morris, *Choline uptake in human intestinal Caco-2 cells is carrier-mediated*. J Nutr, 2003. **133**(8): p. 2607-11.
310. Thomas, J., et al., *Active transport of imatinib into and out of cells: implications for drug resistance*. Blood, 2004. **104**(12): p. 3739-45.

311. Diah, S.K., et al., *Resistance to mitoxantrone in multidrug-resistant MCF7 breast cancer cells: evaluation of mitoxantrone transport and the role of multidrug resistance protein family proteins*. *Cancer Res*, 2001. **61**(14): p. 5461-7.
312. Sorensen, M., M. Sehested, and P.B. Jensen, *Effect of cellular ATP depletion on topoisomerase II poisons. Abrogation Of cleavable-complex formation by etoposide but not by amsacrine*. *Mol Pharmacol*, 1999. **55**(3): p. 424-31.
313. Konig, J., et al., *Pharmacogenomics of human OATP transporters*. *Naunyn Schmiedebergs Arch Pharmacol*, 2006. **372**(6): p. 432-43.
314. Schwienbacher, C., et al., *Transcriptional map of 170-kb region at chromosome 11p15.5: identification and mutational analysis of the BWR1A gene reveals the presence of mutations in tumor samples*. *Proc Natl Acad Sci U S A*, 1998. **95**(7): p. 3873-8.
315. Lee, M.P., et al., *Somatic mutation of TSSC5, a novel imprinted gene from human chromosome 11p15.5*. *Cancer Res*, 1998. **58**(18): p. 4155-9.
316. Reece, M., et al., *Functional characterization of ORCTL2--an organic cation transporter expressed in the renal proximal tubules*. *FEBS Lett*, 1998. **433**(3): p. 245-50.
317. Grube, M., et al., *Uptake of cardiovascular drugs into the human heart: expression, regulation, and function of the carnitine transporter OCTN2 (SLC22A5)*. *Circulation*, 2006. **113**(8): p. 1114-22.
318. Reynolds, J.E.F., ed. *Martindale The Extra Pharmacopoeia*. 29th ed ed. Martindale The Extra Pharmacopoeia, ed. J.E.F. Reynolds. 1989, The Pharmaceutical Press: London, England. pp. 941-942.
319. Desmettre, T., J.M. Devoisselle, and S. Mordon, *[Fluorescence properties and metabolic features of fluorescein]*. *J Fr Ophtalmol*, 2000. **23**(9): p. 821-33.
320. Campbell, S.D., S.M. de Morais, and J.J. Xu, *Inhibition of human organic anion transporting polypeptide OATP 1B1 as a mechanism of drug-induced hyperbilirubinemia*. *Chem Biol Interact*, 2004. **150**(2): p. 179-87.
321. Abels, C., et al., *Indocyanine green (ICG) and laser irradiation induce photooxidation*. *Arch Dermatol Res*, 2000. **292**(8): p. 404-11.
322. Zelcer, N., et al., *Steroid and bile acid conjugates are substrates of human multidrug-resistance protein (MRP) 4 (ATP-binding cassette C4)*. *Biochem J*, 2003. **371**(Pt 2): p. 361-7.
323. Spears, K.J., et al., *Directional trans-epithelial transport of organic anions in porcine LLC-PK1 cells that co-express human OATP1B1 (OATP-C) and MRP2*. *Biochem Pharmacol*, 2005. **69**(3): p. 415-23.
324. Sasaki, M., et al., *Transcellular transport of organic anions across a double-transfected Madin-Darby canine kidney II cell monolayer expressing both human organic anion-transporting polypeptide (OATP2/SLC21A6) and Multidrug resistance-associated protein 2 (MRP2/ABCC2)*. *J Biol Chem*, 2002. **277**(8): p. 6497-503.
325. Simon, F.R., et al., *Hormonal regulation of hepatic multidrug resistance-associated protein 2 (Abcc2) primarily involves the pattern of growth hormone secretion*. *Am J Physiol Gastrointest Liver Physiol*, 2006. **290**(4): p. G595-608.
326. Ener, R.A., S.B. Meglathery, and M. Styler, *Extravasation of systemic hematological therapies*. *Ann Oncol*, 2004. **15**(6): p. 858-62.
327. Gurtovenko, A.A. and J. Anwar, *Modulating the structure and properties of cell membranes: the molecular mechanism of action of dimethyl sulfoxide*. *J Phys Chem B*, 2007. **111**(35): p. 10453-60.
328. Breedveld, P., J.H. Beijnen, and J.H. Schellens, *Use of P-glycoprotein and BCRP inhibitors to improve oral bioavailability and CNS penetration of anticancer drugs*. *Trends Pharmacol Sci*, 2006. **27**(1): p. 17-24.

329. Modok, S., H.R. Mellor, and R. Callaghan, *Modulation of multidrug resistance efflux pump activity to overcome chemoresistance in cancer*. *Curr Opin Pharmacol*, 2006. **6**(4): p. 350-4.
330. Polli, J.W., et al., *Rational use of in vitro P-glycoprotein assays in drug discovery*. *J Pharmacol Exp Ther*, 2001. **299**(2): p. 620-8.
331. Meschini, S., et al., *Intracellular P-glycoprotein expression is associated with the intrinsic multidrug resistance phenotype in human colon adenocarcinoma cells*. *Int J Cancer*, 2000. **87**(5): p. 615-28.
332. Yi, S.Y., et al., *A variant 2677A allele of the MDR1 gene affects fexofenadine disposition*. *Clin Pharmacol Ther*, 2004. **76**(5): p. 418-27.
333. Normanno, N., *Gefitinib and cisplatin-based chemotherapy in non-small-cell lung cancer: simply a bad combination?* *J Clin Oncol*, 2005. **23**(4): p. 928-30; author reply 930-1.
334. Baselga, J., *Combining the anti-EGFR agent gefitinib with chemotherapy in non-small-cell lung cancer: how do we go from INTACT to impact?* *J Clin Oncol*, 2004. **22**(5): p. 759-61.
335. Endres, C.J., et al., *The role of transporters in drug interactions*. *Eur J Pharm Sci*, 2006. **27**(5): p. 501-17.
336. Licht, T., et al., *P-glycoprotein-mediated multidrug resistance in normal and neoplastic hematopoietic cells*. *Ann Hematol*, 1994. **69**(4): p. 159-71.
337. Chen, Z., et al., *Multidrug resistance P-glycoprotein function of bone marrow hematopoietic cells and the reversal agent effect*. *J Tongji Med Univ*, 1999. **19**(4): p. 260-3.
338. Cristofanilli M, B.H., Baselga J, Lluch A, Ben Ayed F, Friaha M, Ben Ahmed S, Hurley J, Johnston S, Kaufman B, Findlay M, Olopade O, Shannon C, Harris J, Stein S, Spector N.. *A phase II combination study of lapatinib and paclitaxel as a neoadjuvant therapy in patients with newly diagnosed inflammatory breast cancer (IBC)*. in *San Antonio Breast Cancer Symposium*. 2006. San Antonio, Texas.
339. S. F. Jones, J.D.H., D. R. Spigel, N. W. Peacock, N. T. Willcutt, L. N. Pandite, M. J. Versola, K. M. Koch, F. Greco, H. A. Burris. *A phase I study of the dual kinase inhibitor GW572016 in combination with paclitaxel (EGF10009)*. in *2004 ASCO Annual Meeting*. 2004: *Journal of Clinical Oncology*, 2004 ASCO Annual Meeting Proceedings (Post-Meeting Edition).
340. Chu, Q., et al., *Taxanes as first-line therapy for advanced non-small cell lung cancer: a systematic review and practice guideline*. *Lung Cancer*, 2005. **50**(3): p. 355-74.
341. Janne, P.A., J.A. Engelman, and B.E. Johnson, *Epidermal growth factor receptor mutations in non-small-cell lung cancer: implications for treatment and tumor biology*. *J Clin Oncol*, 2005. **23**(14): p. 3227-34.
342. Yang, J.M., G.F. Sullivan, and W.N. Hait, *Regulation of the function of P-glycoprotein by epidermal growth factor through phospholipase C*. *Biochem Pharmacol*, 1997. **53**(11): p. 1597-604.
343. Wartenberg, M., et al., *Down-regulation of intrinsic P-glycoprotein expression in multicellular prostate tumor spheroids by reactive oxygen species*. *J Biol Chem*, 2001. **276**(20): p. 17420-8.
344. Waterman, H. and Y. Yarden, *Molecular mechanisms underlying endocytosis and sorting of ErbB receptor tyrosine kinases*. *FEBS Lett*, 2001. **490**(3): p. 142-52.
345. Mineo, C., et al., *Localization of epidermal growth factor-stimulated Ras/Raf-1 interaction to caveolae membrane*. *J Biol Chem*, 1996. **271**(20): p. 11930-5.
346. Wang, D., D.B. Donner, and R.S. Warren, *Homeostatic modulation of cell surface KDR and Flt1 expression and expression of the vascular endothelial cell growth factor (VEGF) receptor mRNAs by VEGF*. *J Biol Chem*, 2000. **275**(21): p. 15905-11.

347. Lichtner, R.B., et al., *Signaling-inactive epidermal growth factor receptor/ligand complexes in intact carcinoma cells by quinazoline tyrosine kinase inhibitors*. *Cancer Res*, 2001. **61**(15): p. 5790-5.
348. Nishimura, Y., B. Berezky, and M. Ono, *The EGFR inhibitor gefitinib suppresses ligand-stimulated endocytosis of EGFR via the early/late endocytic pathway in non-small cell lung cancer cell lines*. *Histochem Cell Biol*, 2007. **127**(5): p. 541-53.
349. Ono, M., et al., *Sensitivity to gefitinib (Iressa, ZD1839) in non-small cell lung cancer cell lines correlates with dependence on the epidermal growth factor (EGF) receptor/extracellular signal-regulated kinase 1/2 and EGF receptor/Akt pathway for proliferation*. *Mol Cancer Ther*, 2004. **3**(4): p. 465-72.
350. Harari, P.M., G.W. Allen, and J.A. Bonner, *Biology of interactions: anti-epidermal growth factor receptor agents*. *J Clin Oncol*, 2007. **25**(26): p. 4057-65.
351. Ellis, I.R., A.M. Schor, and S.L. Schor, *EGF AND TGF- $\alpha$  motogenic activities are mediated by the EGF receptor via distinct matrix-dependent mechanisms*. *Exp Cell Res*, 2007. **313**(4): p. 732-41.
352. Miletti-Gonzalez, K.E., et al., *The CD44 receptor interacts with P-glycoprotein to promote cell migration and invasion in cancer*. *Cancer Res*, 2005. **65**(15): p. 6660-7.
353. Misra, S., S. Ghatak, and B.P. Toole, *Regulation of MDR1 expression and drug resistance by a positive feedback loop involving hyaluronan, phosphoinositide 3-kinase, and ErbB2*. *J Biol Chem*, 2005. **280**(21): p. 20310-5.
354. Leggas, M., et al., *Gefitinib modulates the function of multiple ATP-binding cassette transporters in vivo*. *Cancer Res*, 2006. **66**(9): p. 4802-7.
355. Elkind, N.B., et al., *Multidrug transporter ABCG2 prevents tumor cell death induced by the epidermal growth factor receptor inhibitor Iressa (ZD1839, Gefitinib)*. *Cancer Res*, 2005. **65**(5): p. 1770-7.
356. Matsson, P., et al., *A Global Drug Inhibition Pattern for the Human ATP-Binding Cassette Transporter Breast Cancer Resistance Protein (ABCG2)*. *J Pharmacol Exp Ther*, 2007. **323**(1): p. 19-30.
357. Li, J., et al., *Gefitinib and erlotinib, epidermal growth factor receptor (EGFR) tyrosine kinase inhibitors, are substrates for the breast cancer resistance protein (BCRP)/ABCG2 transporter*. *Clinical Cancer Research*, 2005. **11S**: p. 120.
358. Midgley, R., et al., *A phase I and pharmacokinetic study of lapatinib in combination with infusional 5-fluorouracil, leucovorin and irinotecan*. *Ann Oncol*, 2007.
359. Garcia, R., R.A. Franklin, and J.A. McCubrey, *EGF induces cell motility and multi-drug resistance gene expression in breast cancer cells*. *Cell Cycle*, 2006. **5**(23): p. 2820-6.
360. Takada, T., et al., *Regulation of the cell surface expression of human BCRP/ABCG2 by the phosphorylation state of Akt in polarized cells*. *Drug Metab Dispos*, 2005. **33**(7): p. 905-9.
361. Ozvegy-Laczka, C., et al., *Single amino acid (482) variants of the ABCG2 multidrug transporter: major differences in transport capacity and substrate recognition*. *Biochim Biophys Acta*, 2005. **1668**(1): p. 53-63.
362. Glavinas, H., et al., *ABCG2 (breast cancer resistance protein/mitoxantrone resistance-associated protein) ATPase assay: a useful tool to detect drug-transporter interactions*. *Drug Metab Dispos*, 2007. **35**(9): p. 1533-42.
363. Ozvegy, C., A. Varadi, and B. Sarkadi, *Characterization of drug transport, ATP hydrolysis, and nucleotide trapping by the human ABCG2 multidrug transporter. Modulation of substrate specificity by a point mutation*. *J Biol Chem*, 2002. **277**(50): p. 47980-90.

364. Ozvegy, C., et al., *Functional characterization of the human multidrug transporter, ABCG2, expressed in insect cells*. Biochem Biophys Res Commun, 2001. **285**(1): p. 111-7.
365. Loo, T.W. and D.M. Clarke, *Recent progress in understanding the mechanism of P-glycoprotein-mediated drug efflux*. J Membr Biol, 2005. **206**(3): p. 173-85.
366. Pan, G., N. Giri, and W.F. Elmquist, *Abcg2/Bcrp1 mediates the polarized transport of antiretroviral nucleosides abacavir and zidovudine*. Drug Metab Dispos, 2007. **35**(7): p. 1165-73.
367. Hooijberg, J.H., et al., *The effect of glutathione on the ATPase activity of MRP1 in its natural membranes*. FEBS Lett, 2000. **469**(1): p. 47-51.
368. Salerno, M., et al., *Relation between the ability of some compounds to modulate the MRP1-mediated efflux of glutathione and to inhibit the MRP1-mediated efflux of daunorubicin*. Biochem Pharmacol, 2004. **68**(11): p. 2159-65.
369. O'Connor, R., et al., *Increased anti-tumour efficacy of doxorubicin when combined with sulindac in a xenograft model of an MRP-1-positive human lung cancer*. Anticancer Res, 2004. **24**(2A): p. 457-64.